University of Southampton
Faculty of Natural and Environmental Sciences

Design of polymer systems and surface-active agents for the improvement of cell attachment for treatment of ocular diseases

By

DARREN WILLIAM PITT

Thesis for the degree of Doctor of Philosophy
November 2014

UNIVERSITY OF SOUTHAMPTON

ABSTRACT

FACULTY OF NATURAL AND ENVIRONMENTAL SCIENCES

Chemistry

Doctor of Philosophy

DESIGN OF POLYMER SYSTEMS AND SURFACE-ACTIVE AGENTS FOR IMPROVING CELL ATTACHMENT FOR TREATMENT OF OCULAR DISEASES

By Darren William Pitt

The degradation of eyesight is a frightening experience for individuals and unfortunately gradual loss of vision with old age is commonplace. One of the most common forms of eye disease which effects vision is Age-Related Macular Degeneration (AMD). AMD is the leading cause of blindness in the developed world and there is currently no cure for the disease. One treatment option available for the neovascular form of AMD is the injection of Bevacizumab [an anti-vascular endothelial growth factor (VEGF) drug] into the eye on a monthly basis.

Investigation into the biodegradable polymers poly(L-lactic acid) (PLLA) and poly(D,L-lactic-co-glycolic acid) (PLGA) as a possible drug delivery system with highly uniform and reproducible microspheres was developed. Under optimised parameters Bevacizumab-encapsulated PLLA:PLGA microspheres were successfully prepared with a steady release of Bevacizumab being obtained.

Additionally, fibrous scaffolds of methyl methacrylate (MMA) and poly(ethylene glycol) methacrylate (PEGM) were prepared by an electrospinning process. These MMA:PEGM co-polymers were investigated as a possible Bruchs membrane replacement and as the support for retinal pigment epithelium (RPE) transplantation. The MMA:PEGM co-polymers were functionalised with *N*-succinimidyl which resulted in the fibres forming a gel *in vitro.* Gel formation was examined further and successful RPE cell attachment and growth onto these gels was observed. Further work on surface active agents was undertaken to improve the cell adhesion, proliferation and growth of RPE cells onto these methacrylate based frameworks. An arginine-glycine-aspartic acid (RGD) peptidomimetic was prepared and reacted onto the surface of the MMA:PEGM co-polymers, however, the peptidomimetic-attached MMA:PEGM fibres offered little improvement in cell growth in comparison with *N*-succinimidyl–activated MMA:PEGM co-polymer fibres.

Additional attachment of the natural proteins laminin, collagen and fibronectin onto the microspheres was achieved. Attachment of these proteins prolonged the release of the dye from the microspheres and showed no cytotoxic effects when examined *in-vitro.*

Table of Contents

Table of figures

Table of tables

Table of schemes

Declaration of authorship

I, Darren William Pitt, declare that the thesis entitled "Design of polymer systems and surface-active agents for improving cell attachment for treatment of Ocular diseases" and the work presented in the thesis are both my own, and have been generated by me as the result of my own original research.

I confirm that:

- this work was done wholly or mainly while in candidature for a research degree at this University;
- where any part of this thesis has previously been submitted for a degree or any other qualification at this University or any other institution, this has been clearly stated;
- where I have consulted the published work of others, this is always clearly attributed;
- where I have quoted from the work of others, the source is always given. With the exception of such quotations, this thesis is entirely my own work;
- I have acknowledged all main sources of help;
- where the thesis is based on work done by myself jointly with others, I have made clear exactly what was done by others and what I have contributed myself;

Parts of this work have been published in the following publications:

- D. W. Pitt, A. J. Treharne, H. A. Thomson, J. A. Scott, A. J. Lotery and M. C. Grossel, *J. Mater. Chem. B*, 2013, **1**, 6627-6633.

In addition this work has been presented at 4 conferences.

Signed: ……..

Date: June 2015

Acknowledgements

An enormous thank you to all that have supported me throughout my PhD. I have received excellent guidance from my supervisor Dr Martin Grossel who I owe a great debt of gratitude. A thank you to all the Grossel group members (Andrew T, Nick, Adam "Fish", Francesco, Richard, Nick, Dom, Gareth, Gavin, Mike, Nicco, James, Andrew H and Hassan). Additionally I would like to thank, Dr Heather Thomson, Dr Phillip Alexander, Dr Chris Hughes and Prof Andrew Lotery for their help and biological expertise. Although the work has not been included within this thesis I would like to thank Prof David Roberts and Isabel Diez-Sevilla for their collaboration and work with enucleated cells.

I would like to thank Dr Neil Wells, Julie Herniman and Dr G John Langley form the University of Southampton NMR and mass spectroscopy service. I would like to thank Dr Mark Light and Dr Peter Horton from the University of Southampton crystallography department. Thank you to Karl, Clive and Keith with all their assistance in chemistry stores.

I would like to acknowledge financial support from European Regional Development Fund (ERDF), ISCE-Chem INTERREG IV A France-(channel)-England project no. 4061. for making this project possible.

I have been lucky enough to have been supported by a fantastic group of friends and would like to thank Lisa Powell for her support and patience with me throughout my PhD.

Abbreviations

ACI	Autologous chondrocyte implantation
AIBN	Azobisisobutyronitrile
AIDS	Acquired immunodeficiency syndrome
AMD	Age-Related Macular Degeneration
ANOVA	Analysis of variance
ARPE-19	Human Retinal Pigment Epithelial cell line
ATR	Attenuated Total Reflection
ATRP	Atom transfer radical polymerization
CMV	Cytomegalovirus retinitis
CNV	Choroidal neovascularisation
CROP	Cationic ring-opening polymerisation
DAPI	4,6-diamidino-2-phenylindole
DCC	Dicyclohexylcarbodiimide
DCC	*N*,*N*-dicyclohexyl carbodiimide
DCM	Dichloromethane
DEM	2-(Dimethylamino)ethyl methacrylate
DEM	2-(Dimethylamino)ethyl methacrylate
DIC	*N*,*N*-Diisopropylcarbodiimide
DIPEA	*N*,*N*-Diisopropylethylamine
DMF	Dimethylformamide
DSA	Drop Shape Analyser
EBiB	Ethyl α-bromoisobutyrate
ECM	Extracellular matrix
EDCI	1-ethyl-3-(3-dimethylaminopropyl)carbodiimide
ELISA	Enzyme-linked immunosorbent assay
FDA	Food and Drug Administration
FITC	Fluorescein isothiocyanate
G	Gauge
GDNF	Glial cell-derived neurotrophic factor
GPC	Gel permeation chromatography
HEMA	Poly-2-hydroxyethyl methacrylate
HRP	Horseradish peroxidase
IKVAV	Ile-Lys-Val-Ala-Val peptide sequence
INT	Iodonitrotetrazolium chloride
IPA	Isopropyl alcohol
LCST	Lower critical solution temperature
LDH	Lactate dehydrogenase
MACI	Matrix applied characterised autologous cultured chondrocytes

MEK	Methyl ethyl ketone
MMA	Methyl methacrylate
MTT	3-(4,5-Dimethylthiazol-2-yl)-2,5-diphenyltetrazolium bromide
n =	Number of samples run
NHS	*N*-hydroxysuccinimide
NMR	Nuclear magnetic resonance
NVP	*N*-Vinyl-2-Pyrrolidone
OD	Optical density
PAGE	Polyacrylamide gel electrophoresis
PBS	phosphate buffered saline
PEG	Poly(ethylene glycol)
PEGM	Poly(ethylene glycol) methacrylate
PLGA	Poly(D,L-lactic-co-glycolic acid)
PLGA	Poly(lactic-*co*-glycolic acid)
PLLA	Poly(L-lactic acid)
PLLA	Poly(L-lactic acid)
PVA	Polyvinyl alcohol
PVP	Poly(vinyl pyrrolidone)
PyBOP	benzotriazol-1-yl-oxytripyrrolidinophosphonium hexafluorophosphate
RGD	Arginine-Glycine-Aspartic acid peptide sequence
RGDS	Arg-Gly-Asp-Ser peptide sequence
RPE	Retinal pigment epithelium
RMM	Relative molecular mass
S.D.	Standard deviation
SDS	Sodium dodecyl sulfate
SEM	Scanning electron micrograph
TEA	Triethylamine
TEOS	Tetraethyl orthosilicate
TFA	Trifluoroacetic acid
THF	Tetrahydrofuran
TMEDA	Tetramethylethylenediamine
VEGF	Vascular endothelial growth factor
XPS	X-ray photoelectron spectroscopy
YIGSR	Tyr-Ile-Gly-Ser-Arg peptide sequence

1. Introduction

1.1 Introduction

Degradation of eyesight is a frightening experience for individuals and unfortunately gradual loss of vision with old age is commonplace. One of the most common forms of eye disease which affects vision as people get older is Age-Related Macular Degeneration (AMD). AMD is the leading cause of blindness in the developed world[1], with an estimated 510 000 people in the UK having advanced AMD[2]. As the name suggests it only affects the macular region of the eye and results in the loss of central vision, whilst the peripheral vision remains intact (Figure 1.1).

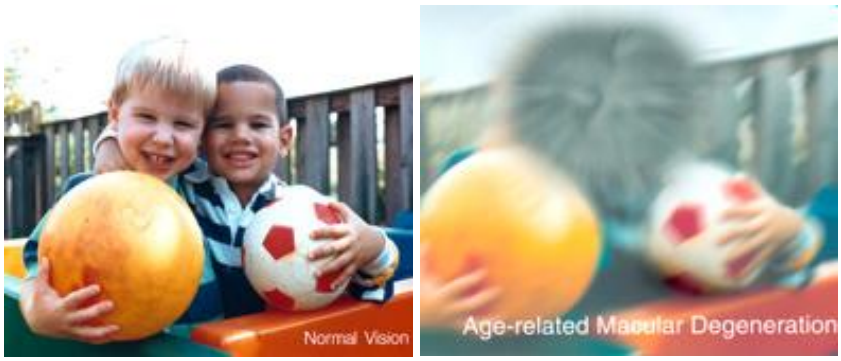

Figure 1.1 - The effect of AMD on central vision. Image courtesy of National Eye Institute.

The macular is a small region in the centre of the eye. At its centre there is the highest concentration of cone cells which are responsible for the highly defined and central vision (Figure 1.2).

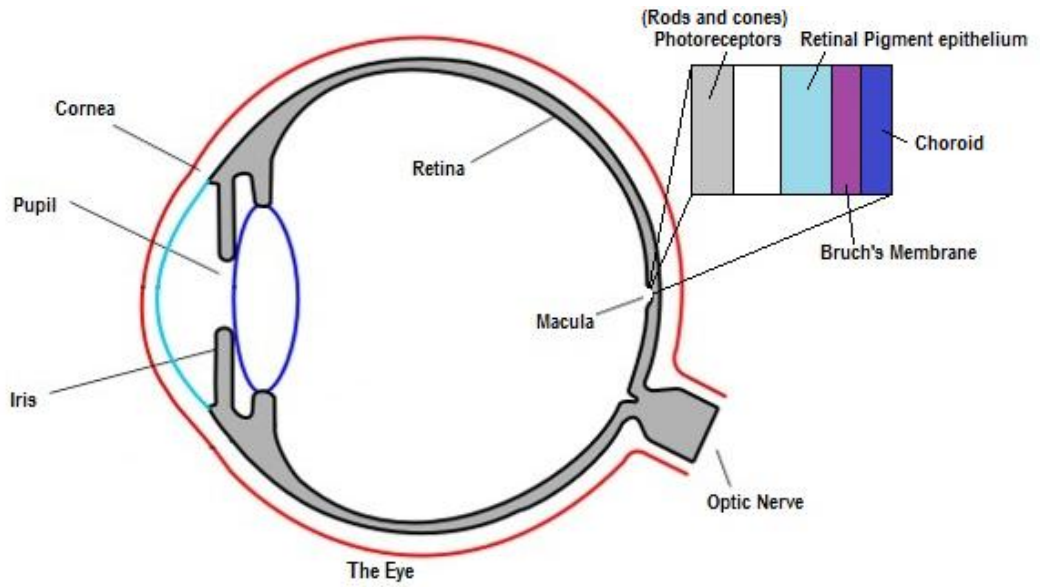

Figure 1.2 - Cross-section of the eye with the layers of the macular highlighted. The photoreceptors and retinal pigment epithelium (RPE) cell layer make up the retina which is supported by the Bruchs membrane. The choroid provides the blood supply to the cells.

There is currently no cure for AMD although some treatments are available to halt progression of the disease, but this is only effective on the most advanced forms of AMD. The development of improved treatments to halt the progression of AMD and work into improving cell attachment leading to a possible cure to AMD have been investigated within this thesis.

1.2 Age-related macular degeneration.

AMD exists in two forms, the "wet" and the "dry" form. The wet form of the disease is always preceded by the dry form and occurs in about 10-15% of patients who suffer from AMD[3]. The wet form is also known as neovascular or exudative AMD, which occurs as a result of new blood vessels beginning to grow into the macular (neovascularisation) causing swelling and bleeding within the macula. The growth of additional blood vessels leads to damage of the supportive tissue and loss of the light-sensing photoreceptor cells within the macular resulting in subsequent loss in vision. As this growth of blood vessels occurs from the choroid it is known as choroidal neovascularisation (CNV). The wet form is more severe than the dry form of the disease with blood vessels haemorrhaging leading to scar tissue formation.

This can result in permanent loss of central vision. Loss of sight can occur over a very short period of time for neovascular AMD whereas in the dry form of the disease loss of sight occurs over a number of months or years. The wet form, although more serious than dry AMD, is currently more treatable and progression of the disease can be halted. Loss to vision which has already occurred however, cannot currently be reversed.

The dry form of the disease occurs as a result of waste build up at the back of the macular and can be observed as yellow deposits (Figure 1.3). These waste deposits are known as Drusen and result in alteration of the photoreceptor layers leading to distorted vision. The Drusen number and size has an effect on sight and as dry macular degeneration progresses cell atrophy can occur causing blind spots and loss of vision. This is the most common type of the disease and is encountered by over 85% of people who have AMD[4].

Figure 1.3 – Retinal image of a patient with wet AMD. The dry form of AMD can be observed by the yellow spots on the left of the image. The dark red/black patch is the result of increased blood vessel growth and bleeding below the cell layer. The bright circular shape on the right of the image is the choroid. (Image courtesy of International Centre for Eye Health).

1.3 Treatment for age-related macular degeneration.

As it has already been noted there is no treatment available for dry AMD, however the wet form can be treated using a number of methods to halt further progression of the disease. One method is the use of photodynamic therapy with drugs such as Verteporfin[5] which have been shown to slow progression of the disease. This, however, is only effective for a small proportion of AMD sufferers and reoccurrence occurs in 50% of patients[11]. Laser photocoagulation is also used in more severe cases of neovascular AMD to help control the bleeding and atypical blood vessel growth. However not every patient is suitable for laser photocoagulation therapy[6]. The most commonly employed approach is use of anti-vascular endothelial growth factor (VEGF) drugs and this has almost completely replaced photodynamic therapy for treatment of wet AMD. Anti-VEGF drugs prevent angiogenesis (growth of new blood vessels) when VEGF is overexpressed[7]. Current anti-VEGF marketed drugs are EYLEA™ (Aflibercept)[8], Lucentis® (Ranibizumab)[9] and Macugen® (Pegaptanib)[10]. Anti-VEGF drugs bind to VEGF preventing the induction of increased blood vessel permeability and growth[12]. Another anti-VEGF drug is Avastin® (Bevacizumab) which is currently used treat various cancers; it is not currently Food and Drug Administration (FDA) approved for use for AMD but it is very frequently used "off-label" to treat AMD[14-17]. Bevacizumab is commonly used because of its lower cost compared to other anti-VEGF drugs and has been shown to be as effective as Ranibizumab for treatment of AMD. The first randomised trial showed no significant difference in treatment between the two drugs[13,16].

Bevacizumab is a monoclonal antibody with a half-life of around 6-10 days *in vivo*[26]. Currently injections of around 1.25 mg of Bevacizumab into the vitreous cavity in the eye are required every 4-6 weeks and it has been found to be an effective treatment for 'wet' AMD[18,19]. Ranibizumab, a monoclonal antibody fragment, is also required monthly while Pegaptanib is injected on a 10 day basis[27,28]. The intravitreal injection of an anti-VEGF drug is the treatment required for the rest of the patient's life and low patient compliance can be an issue. The use of a clean room is required and associated high costs can be a problem. Repeated injections of Bevacizumab can lead to other retinal issues such as endophthalmitis, increased intraocular pressure and uveitis[20].

1.4 Drug delivery for AMD.

Drug delivery encompasses a huge range of materials, designs and targets for use within the human body. Some of the approaches taken utilise liposomes or micelles[21], microspheres[25], gels[24], cyclodextrins[23], dendrimers[22] and the list continues. Using a drug-delivery approach can improve the therapeutic effect of drugs, lowering side effects and increasing the exposure or concentration of a drug to a desired target. This approach can also improve administration routes and improve the safety of the drug.

Research into drug delivery methodology and feasibility for ocular targets has been investigated in order to improve treatment outcomes and patient compliance. Over 90% of current drugs for ocular delivery are administered as drops with 95% of the active component being lost through tear drainage[29]. For a drug to maintain a therapeutic range within the posterior segment of the eye this topical treatment would be unsuccessful because of the poor diffusion through the cornea and lens of the eye. Ocular drug delivery has added difficulties because of the defenses which prevent drugs entering the inner eye. Trying to bypass these with invasive methods direct into the eye can lead to more complications as a result of scar tissue formation. Intravitreous delivery is required and this can be aided by drug delivery methodology.

1.4.1 Ocular implants.

Non-degradable implants can be used to deliver drugs in a predictable manner, however added complications are observed because of the large incision size required and the need to remove or replace the implant. The non-degradable insert Vitrasert® is used to treat Cytomegalovirus retinitis (CMV) over 5-8 months. Vitrasert® delivers Ganciclovir (an antiviral drug) via intravitreal implantation using a polyvinyl alcohol (PVA)/ethylene vinyl acetate polymer matrix. The implant requires a 5 mm insertion into the eye and also needs to be removed post treatment[42]. Retisert® uses the same technology to deliver dexamethasone (an anti-inflammatory steroid) to treat uvetitis[35]. Retisert® gained FDA approval in 2005 and can deliver dexamethasone over a three year period, but as with other implants surgical complications can arise. Ozurdex® another implant is currently under Phase II trials for treatment of AMD, again delivering dexamethasone[139]. Another implant

currently on the market is Iluvien™ used to treat diabetic macular oedema (the formation of protein deposits which cause the macular to swell) which employs the corticosteroid Fluocinolone acetonite in order to reduce inflammation[34]. Using a PVA/Polyimide matrix Fluocinolone acetonite delivery can be obtained over three years. Several other implants are available or in Phase II trials, however there are none which target AMD[40,46]. Complications with non-degradable implants are common and over 10% of patients receiving implants have complications post implant, such as vitreous hemorrhaging, retinal detachment and infection[36]. As a result of these added complications other drug delivery methods have been investigated using injectable and biodegradable systems. Such methods aim to reduce the size of any incision and avoid the need to remove any implants post treatment.

1.4.2 Injectable and biodegradable treatments.

Biodegradable drug delivery systems have the intrinsic advantage that there is no need to remove the delivery system once the treatment has been administered. The biodegradable properties themselves are also a key part of the functioning of these delivery systems since, as the device degrades, the medication is slowly released. The packaging degrades into harmless byproducts which are then excreted from the human body as waste. Ocular drug delivery into the outer eye is easy, however diffusion into the eye itself has proved challenging. Cyclodextrins have been used to overcome the external barrier of the eye and increase permeability into the cornea for drugs such as dexamethasone[37]. Liposomes have been used to aid Lidocaine (a local anesthetic) diffusion into the eye over 8 days[29]. The liposomes have been loaded onto poly-2-hydroxyethyl methacrylate (HEMA) which was then used as an additional drug delivery method. HEMA has been used in contact lens materials and the authors envision possible liposome-infused contact lenses to deliver the drug.

To avoid the barriers of the outer eye, intravitreal drug delivery has been investigated with a less invasive approach compared to that of implants, however an injection is still required. Foscarnet an anti-viral drug for treatment of CMV was encapsulated within liposomes and successfully injected intravitreally showing no intraocular toxicity within rabbits[38]. The immunosuppressive drug Tacrolimus (for treatment of autoimmune diseases) has also taken advantage of liposomes for intravitreal

delivery[39]. Using this method no derogatory effects were observed in rats and an decreased inflammation was observed compared to the unencapsulated drug. The drug was still present after 2 weeks and the authors noted that using this approach involving drug-encapsulated liposomes was more effective than a simple Tacrolimus injection.

More traditional approaches using poly(lactic-*co*-glycolic acid) (PLGA) biodegradable microspheres have been utilised for delivery of dexamethasone for treatment of Uvetitis. Uvetitis is inflammation of the middle of the eye (including the retina) and, using PLGA microspheres, delivery of dexamethasone has been shown to continue for 45 days in rabbit studies[30]. Microspheres have also been used for treatment of CMV, a common infection in patients with acquired immunodeficiency syndrome (AIDS) which can result in blindness. Again using the biodegradable polymer PLGA, delivery of ganciclovir could be continued for over 40 days in rabbits[31]. PLGA-based microspheres have also been used to deliver proteins for the treatment of glaucoma[32]. Using glial cell-derived neurotrophic factor (GDNF), a protein which promotes the survival of neurons, release could be observed over 11 weeks. GDNF was first lyophilised then using a water-in oil-in water emulsion could be encapsulated within the microspheres successfully and with no adverse effects noted during rat studies *in vivo*. Biodegradable implants using PLGA have also been investigated in rabbits[33]. A 5 mm implant was used to deliver ganciclovir over 24 weeks but, although no retrieval of the implant is required, the added complications of the initial large incision size can be problematic. Several other novel treatments are available or currently under various Phase trials for delivering a range of drugs for retinal and ocular diseases[42,43,4].

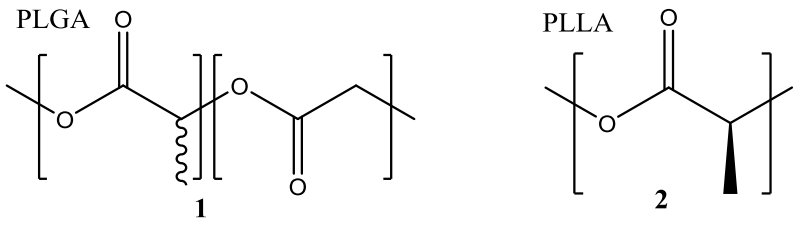

Figure 1.4 – Chemical structures of poly(L-lactic acid) (PLLA) and poly(DL-lactic-co-glycolic acid) (PLGA) biodegradable polymers.

1.4.3 Drug delivery treatments for AMD.

Currently only intravitreal injections of an anti-VEFG drug are available for treatment of AMD. There are no drug delivery methods which utilise anti-VEGF to treat neovascular AMD which are FDA approved[46]. Work on delivery systems to improve treatment of AMD by reducing the number of injections and maintaining a high therapeutic level within the eye have been investigated. Although no products are currently "on the shelf", initial work and *in vivo* studies have begun to be undertaken to investigate if drug delivery methodology could improve treatment of AMD[44]. One method of interest for treatment of AMD is the use of the polysaccharide chitosan to form a hydrogel infused with Bevacizumab[47]. Although the authors developed the treatment with glaucoma as the target they showed that 20% of Bevacizumab was released after 53 hours and it can be envisaged that a similar approach could be undertaken for treatment of AMD. *In vivo* assessment in rabbits showed that the hydrogels were non-toxic although large incisions were required for placement of the hydrogel. Bevacizumab infused nanospheres have been investigated for extended treatment of AMD utilising PLGA[48]. Nanospheres below 1 μm were prepared with sustained release, however a repeatable release profile proved difficult. Abrishami *et. al.* used liposomes to encapsulate Bevacizumab and showed that after 42 days Bevacizumab concentration was 5 times higher within the vitreous of the eye compared to a simple injection of Bevacizumab into the vitreous[49]. Liposome formation was achieved by dehydration/rehydration of egg phosphatidylcholine and cholesterol with Bevacizumab present. A Phase I trial in 20 patients has shown results comparable to monthly injections of Ranibizumab using a refillable reservoir technology, however side effects due to surgeries were noted[50]. Further work is required to obtain a beneficial anti-VEGF drug delivery system which will be effective, safe and long lasting for treatment of AMD. Any system devised would need to be cost effective and offer a sufficient time delay between treatments with a steady release of drug within the therapeutic range to be implemented as the "go to" treatment by clinicians.

1.5 PLLA/PLGA biodegradable systems.

Poly(L-lactic acid) (PLLA) and poly(DL-lactic-co-glycolic acid) (PLGA) are ideal candidates to develop a drug delivery system for anti-VEGF drugs (Figure 1.4). The

FDA-approved polymers PLLA and PLGA are widely known for their uses in medical devices (Zoladex®, Eligard®, Enantone®, Profact®)[51,52] because of their biodegradability, excretion mechanisms, cost and ease of manufacture. PLLA and PLGA polymers degrade via hydrolysis to form the lactic and glycolic acid counterparts. It has been shown that enzymes do not play a role in the degradation rate when studied *in vivo*[61]. The lactic acid is removed via the citric acid cycle within the body and is lost as carbon dioxide and water. Glycolic acid is also removed by the citric acid cycle but can also be directly excreted via the kidneys. Within the eye drugs are cleared through the hyaloid face (front of the eye behind the lens) or through the retina into the systemic circulation where they will be excreted via the typical route[53,54].

The rate of hydrolysis and degradation of PLLA and PLGA depends on a number of factors. Polymer molecular weight, polymer end group, crystallinity, and ratio of lactic to glycolic acid within the polymer all affect degradation. Other parameters such as the temperature, pH, size, shape and surface area of the polymer within the medium also influence degradation rates[55]. This results in PLLA degradation being far longer than that of PLGA, mainly due to the crystallinity of the polymer. PLLA is more crystalline in comparison with PLGA and this is a major factor as the crystalline region has decreased permeability compared to more amorphous regions[56]. This can be problematic when using polymer blends as the semi-crystalline polymers degrade via the more amorphous regions initially leaving behind a more crystalline polymer than the original and therefore degradation slows down at this point and is not uniform. Slight racemisation or impurities in PLLA can result in the degradation rate being increased as such these defects disrupt the crystallisation. PLLA is more hydrophobic compared to PLGA and therefore absorbs less water and this increases degradation times[57]. Importantly it has been observed that the polymers degrade faster *in vivo* in comparison with buffer solutions[58]. Insertion into different areas of the body also changes the rate of degradation and therefore using one polymer system to deliver drugs within may not result in the same effect as observed previously in another[59]. The drug encapsulated within PLLA/PLGA polymers also plays an important role in polymer degradation and it cannot be predicted to what extent this will occur[60]. The polymers have been

investigated for various areas of biomedicine because of their solubility in a range of solvents and having been already approved for use within the body. The polymer's degradation can however change in different environments and with different drug types encapsulated. Therefore their use within other areas of the body for other applications must be investigated fully. Problems of "dose dumping" or inconsistent release can occur and formulation needs to be fully understood before full application of these polymers can be achieved.

1.6 Microspheres and nanospheres.

Devices of various sizes and shapes have been designed for drug delivery within the body, however use within the eye limits some of these designs. The problems associated with surgical implants previously discussed suggest that injectable biodegradable systems are preferential. The use of microspheres and nanospheres has been investigated for use within the eye for a number of conditions and this methodology could prove fruitful for treatment of AMD. There are several ways to prepare microspheres[62], however the solvent evaporation method is the most commonly used[64]. By preparing an emulsion of a drug and polymer mixture dissolved in a volatile oil layer (such as dichloromethane, chloroform, ethyl acetate) and adding it into an aqueous layer an emulsion can be formed. As the volatile solvent evaporates small microparticles with encapsulated drug remain. Another approach is the solvent displacement method where a drug and polymer are dissolved in a water miscible solvent and gradually the solvent is extracted into the aqueous layer so that the polymer solidifies forming micro or nanoparticles[63]. Variations on both techniques such as spray drying, dialysis and phase separation can be used to improve encapsulation for the desired drug[65]. For ocular delivery the final microspheres should be below 50 µm in order not to scatter light therefore impeding vision[66]. It has also been shown that microspheres above 10 µm do not undergo phagocytosis within the body[67]. The stability of prepared microspheres and nanospheres in solution will determine whether the suspension will be colloidal or not. If the attractive forces between the microspheres are greater than the repulsive forces then the microspheres will not form a colloid in solution. The zeta potential of the microspheres is a useful indication as the zeta potential can be related to colloidal stability[70]. The zeta potential can be used to understand colloid stability as it is a

measure of electrical potential difference across the ionic layers surrounding a charged particle, in this case a microsphere. The higher the potential in mV (either positive of negative) the more stable the colloid solution will be. A value of ± 25 mV or greater is generally considered to form a stable colloid in solution, with values of 40 to 60 mV forming a very stable colloid and above 60 mV extremely stable systems are observed[71]. Degradation rates of PLLA and PLGA have been shown to be dependent on the surface area of the formulation, however it has been shown that microspheres below 300 µm degrade homogenously, meaning that the centre of the microsphere degrades at the same rate as the surface[68].

1.7 Bruchs membrane.

The use of anti-VEGF drugs as a treatment for neovascular AMD only halts the progression of the disease. The anti-VEGF treatment slows choroidal neovascularisation within the eye and growth of additional blood vessels. Another major contributor to photoreceptor cell death is geographic atrophy, which is caused by the Bruchs membrane distorting. Currently untreatable, geographic atrophy is the most advanced form of dry AMD and can lead to blind spots within the central vision[73,74]. For a permanent cure, replacement of the Bruchs membrane and replacement of the lost or damaged photoreceptors is required.

The Bruchs membrane is a supportive layer for the photoreceptor cells within the macular (Figure 1.2) and can itself be separated into 5 layers; that are the RPE basal lamina, inner collagenous layer, elastic layer, outer collagenous layer and the choriocapillaris layer[75]. The layers are made up from various fibre types (collagen for collagenous layers, elastin for elastic layer) providing structural support and flexibility for the retinal cells. The membrane not only has to be strong enough to support the photoreceptor cells but also flexible enough to allow for stretching of the eye as intraocular pressure changes during eye movement. The Youngs modulus of the Bruchs membrane has been calculated at 2 MPa in the human eye[76, 82]. The Bruchs membrane not only provides support for the anchorage-dependent RPE cells[86] but also provides the transport of nutrients and removal of waste products from the photoreceptor cell layer to the choroid[77].

As the eye ages, the Bruchs membrane increases in depth (typically 2-4 μm in a healthy adult eye) and can double in size[78]. This increase in size is due to waste product build up (Drusen formation) resulting in geographic atrophy for the most advanced cases. These waste deposits are made up from lipid residues, calcium deposits, keratin deposits and protein glycation[79-81]. Crosslinking can occur also leading to oxidative stress and inflammation[82]. The Youngs modulus increases within the older Bruchs membranes and the hydrolytic conductivity decreases due to this crosslinking and blockage arising from Drusen formation[83]. The structural dislodgment because of Drusen formation results in photoreceptor cell death and loss in vision without choroidal neovascularisation occurring[84]. The nutrient barrier permeability is reduced because of crosslinking and waste build up additionally contributes to cell apoptosis[85]. Geographic atrophy can then lead to choroidal neovascularisation and full wet AMD resulting in full central vision loss.

1.8 Tissue engineering.

There is currently no cure for geographic atrophy and the dry form of AMD, however current research in tissue engineering has shown positive results for the treatment of AMD. Tissue engineering utilises a combination of cells and scaffolds to replace or repair damaged body tissues. Tissue engineering is slightly different from transplants where whole tissue from the patient (autograft) or from a donor (allograft) is transplanted to replace the damaged area. These approaches are limited by donor tissue availability, cost and possible rejection. Tissue engineering falls into a third category where the damaged tissue is regenerated instead of replaced and which, in theory, could be scaled up to become the standard treatment.

Tissue engineering is approached in three ways; 1) using isolated cells; 2) introducing tissue-inducing substances and; 3) implanting cells prepared on supports[88]. A majority of cells within the human body are anchorage dependent, meaning that they need some form of support to initiate growth and proliferation[89]. A simple injection of replacement cells as a suspension will not attach and cultivate without incentive. Degradable or permanent replacements can be prepared to replace the lost biological function with the aim that the body's healthy cells will replace and encompass the scaffold. To date most biomaterial scaffolds have utilised ceramics for hard tissue repair such as bone[89,90]. Soft tissue engineering has proven slightly

more difficult and although some treatments for ligament damage such as autologous chondrocyte implantation (ACI)[91] and matrix applied characterised autologous cultured chondrocytes (MACI)[167] are available, more work is still required. ACI is an approved treatment option in Europe and is currently used by clinicians for treatment of ligament damage[91]. In ACI, cartilage from the patient is surgically obtained and the cells are removed then grown *in-vitro* to increase their numbers. The cells are seeded on a scaffold and then transplanted into the damaged area of the knee or ankle. This is a good example of tissue engineering, where healthy cells are expanded before being seeded onto a scaffold and inserted into the affected area for regeneration to occur.

Two approaches can be used for soft tissue repair, using natural or synthetic polymers. Natural polymers or proteins provide an optimum structure to promote growth and adhesion of cells[92]. However they have poor mechanical properties, are limited in quantity and are difficult to scale up. Synthetic polymers may have a reduced effect or invoke an immune response, however they can be tailored for specific cell types and targets. They have a long shelf-life, are highly reproducible, with better mechanical properties and a lower cost[93]. For tissue engineering to become the common treatment of choice for clinicians these criteria will need to be met and research into synthetic polymers for tissue engineering has increased dramatically.

Clearly synthetic polymers would need to be non-cytotoxic, biocompatible and promote cell adhesion. Importantly the synthetic polymers would also need to mimic the damaged tissue, with porosity, mechanical strength and topography for tissue regrowth to occur[94,95]. Current approaches for tissue engineering have utilised cell sheets[96], hydrogels[97], porous scaffolds[98], electrospun fibres[99] and microspheres[100]. An excellent review with comprehensive details of the polymer, method and application for each of the approaches undertaken for cells growth for tissue engineering has been prepared by Kumar *et. al.*[101]. For treatment of AMD the Bruchs membrane would have to be mimicked accurately and because of the fibrous nature of the Bruchs membrane, logical focus would be placed on electrospun fibres. Natural scaffolds derived from other areas of the body have been utilised for RPE

growth, however because of limited supply, limited mass production opportunities and risk of rejection an effective synthetic scaffold is desired[102].

1.9 Electrospinning.

A suspension of RPE cells has been shown to be ineffective for treatment of AMD on a damaged Bruchs membrane. Transplantation of an RPE monolayer shows greater promise, but growth onto a surface is required before transplantation of the monolayer can occur[102]. A large surface area is desired for attachment and good porosity is needed to allow for nutrient and waste exchange[101]. Microfibres display these features and mimic the Bruchs membrane well, with a similar topography and fibrous construction[171] (Figure 1.5).

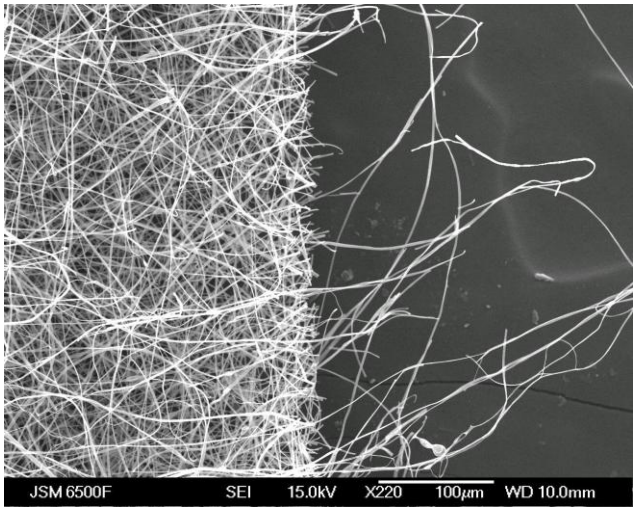

Figure 1.5 – Scanning electron micrograph (SEM) of an electrospun mat, showing the individual fibres formed. Original magnification x 220.

Electrospinning results in polymer fibre formation with fibre width ranging between 1 nm and 100 µm. For fibre formation, a polymer solution is pumped through a needle or capillary and elongates as an electric field is applied (known as a Taylor cone)[103]. When the electric field reaches the threshold and electrostatic repulsion overcomes surface tension of the polymer solution, the Taylor cone lengthens and fibres are ejected (Figure 1.6)[104]. As the solvent evaporates fibres are formed on a collector plate forming a fibrous polymer mat.

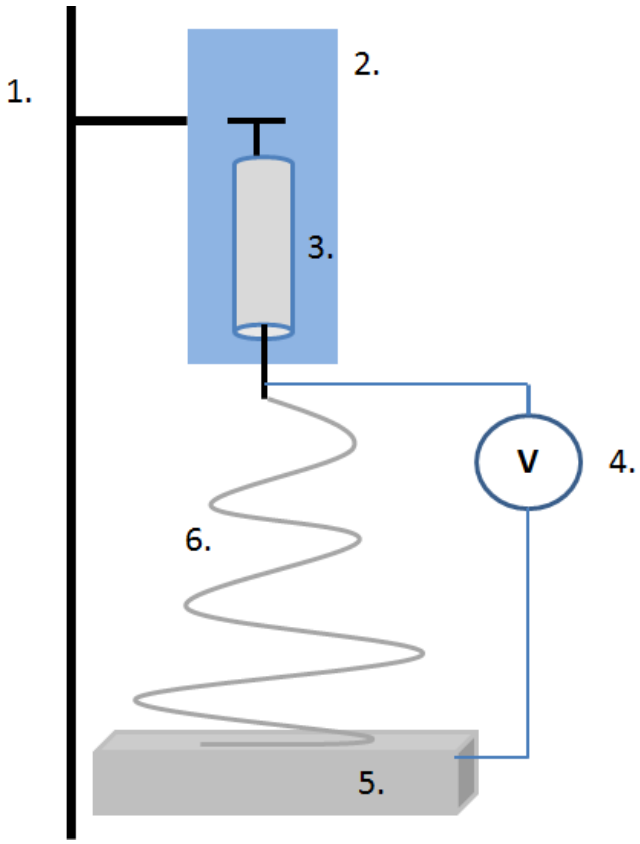

Figure 1.6 – Schematic representation of the electrospinning process. 1) Stand. 2) Syringe pump. 3) Syringe filled with polymer solution. 4) Electric potential applied on needle tip. 5) Conductive collector plate. 6) Fibre formation.

Electrospinning is a useful technique as several parameters can be changed, therefore offering control over polymer matt thickness and fibre width. To optimise the electrospinning process, both the system and the process parameters can be changed. The polymer concentration plays an important role, with use of a dilute solution resulting electrospraying instead of electrospinning and poor optimisation can result in beading within the fibres[105]. The system parameters such as molecular weight of the polymer also affects the fibres formed as the molecular weight affects their entanglement and therefore the viscosity of a solution[106]. The viscosity which is related to polymer molecular weight and polymer concentration understandably has an effect on fibre formation[106]. It has been observed that the choice of solvent is also important because of surface tension, smoother fibres being formed when the surface tension is lower[107]. The conductivity of the solution has shown to affect the width of fibres formed with increased conductivity forming thinner fibres, however natural polymers (polysaccharides) with a high conductivity are difficult to spin into

fibres[108]. The process parameters can also be tuned by varying the voltage, flow rate and distance between the needle and collector plate[109]. Once the voltage reaches the threshold value, fibre formation can occur. However there are contradicting studies on what effect increasing the voltage has on fibre widthand shape[110,111]. Ambient parameters such as humidity and temperature all affect the electrospinning process by varying drying time and solution viscosity[109]. All these factors and processes affect the electrospinning process with reproducible and controllable fibre formation being difficult to obtain. Defects such as pores or a large variation in fibre width can occur from batch to batch[112].

Despite some difficulty in spinning natural polymers, many different polymer types have been electrospun, selected examples include nylon, polyurethanes, PVA, PLLA, collagen, polystyrene, cellulose acetate and PLGA[108,116]. It has been shown that the use of scaffolds seeded with cells into the sub-retinal space increases the viable cells delivered[113]. Examples of poly(caprolactone) electrospun fibres transplanted into pig retinas have shown that they are tolerated well within the back of the eye[114]. PLGA electrospun fibres have also shown excellent RPE cell growth *in-vitro.* When these PLGA fibres were transplanted into the eyes of rabbits, highly desirable retina growth and native RPE cell growth onto the implant was observed[117]. Electrospun fibres for treatment of AMD has been investigated using methyl methacrylate (MMA) and poly(ethylene glycol) methacrylate (PEGM) copolymers[115]. MMA and PEG are both FDA approved and have been extensively used within the body[16,104]. They provide an alternative approach to treatment of AMD as they are non-degradable and could be used as a permanent transplant. It was shown human RPE cells could successfully attach and develop on the surface of the MMA:PEGM fibres. Interestingly modification of these fibres with a succinimidyl group resulted in statistically improved cell adhesion and proliferation. Tissue engineering approaches using scaffolds such as electrospun meshes show promising results and could be used for treatment of AMD. Interestingly functionalisation of the scaffolds can improve cell adhesion and growth and many frameworks utilise natural or synthetic biomolecules to increase cell attachment[118].

1.10 Surface attachment.

As stated previously, it has been shown that the cellular environment needs to be closely mimicked before high cell evolution can occur. Tissues and cells are interconnected and supported by the extracellular matrix (ECM). The ECM not only provides structure but is also critical in cell signalling, nutrient delivery, cell adhesion, migration and proliferation[119]. The ideal mimetic scaffold for cell growth would fully mimic the ECM and understanding the ECM has helped researchers to develop frameworks for cellular growth[120]. The ECM consists of a network of proteins, polysaccharides, macromolecules and biomolecules used for signalling[118]. For scaffold development, cell adhesion is the initial requirement for success. If the cells do not attach, further growth cannot be achieved and cell death will occur[121].

To improve cell adhesion, the biological processes within the ECM have been investigated and a number of biomolecules have been implicated in cell adhesion[120]. Macromolecules within the ECM such as collagen, laminin and fibronectin have binding sites recognised by cell integrin receptors[122]. These ECM macromolecules (collagen, laminin etc.) can be used to coat scaffold surfaces to improve cell adhesion[123]. Coating implants with ECM proteins is a common practice to improve cell adhesion[118], however there are some potential drawbacks. The difficulty and cost of obtaining pure proteins makes scale up for "off the shelf" treatment unlikely. Difficulty in controlling orientation during attachment and possible denaturing of the protein both in reaction and during storage are proven complications[124]. In 1984 the peptide sequence Arginine-Glycine-Aspartic acid (RGD) in fibronectin was discovered to be an essential recognition sequence for cell adhesion[125] (Figure 1.7). This small peptide sequence is found on several ECM proteins associated with cell attachment (including laminin and collagen type IV) and use of this may overcome the problems associated with whole protein use[126,127]. This RGD sequence is common throughout the body and targets various receptors, with the neighbouring amino acids being responsible for specific targeting or increased activity within the receptors[135].

Use of a short peptide sequence can overcome problems of immune responses and it has been shown that peptides of less than 6 repeat units did not invoke immune defences compared to the whole protein[128]. Small peptides require a much smaller

space and therefore can be packed with a much higher density on the surface of a scaffold[135]. Other small peptide sequences have been shown to facilitate different cellular responses such as the sequences Tyr-Ile-Gly-Ser-Arg (YIGSR) and Ile-Lys-Val-Ala-Val (IKVAV)[129]. YIGSR is also found to bind to integrin receptors in laminin and can aid adhesion with cells when used in conjunction with the RGD sequence[130].

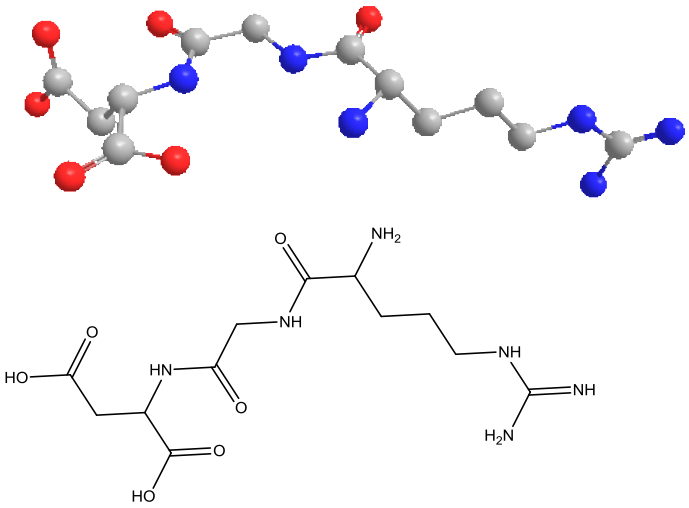

Figure 1.7 – Arginine-Glycine-Aspartic acid (RGD) peptide which is found to be a key sequence involved in the adhesion of cells.

Synthetic RGD mimics (peptidomimetics) which mimic the functional groups of the RGD peptide have also been utilised to improve cell adhesion. These synthetic mimics are less likely to contain impurities and attachment routes can be designed into the peptidomimetics which will result in fewer batch-to-batch differences[121]. The peptidomimetics can be tailored to target specific receptors with increased efficacy[131]. Peptidomimetics design falls into one of three groups[133]: firstly, the peptide core remains unchanged except that the mimic is altered with a stereochemical change; secondly the peptide mimic functional groups undergo slight change and/or a non-peptide structure is used; finally a completely novel template is used, which can be based on computational design[136]. Computation design can be used for the the integrin $\alpha_v\beta_3$ which is expressed in the RPE cell type[137]. A crystal structure of the active site of integrin $\alpha_v\beta_3$ bound to the RGD peptide has been obtained which could allow for systemic design of a stronger binding peptidomimetic[138]. It is important how the RGD peptide is displayed from the

surface of a biomaterial and not all the surface active agent (peptide/protein) will be accessible to receptors[132]. In RGD mimics, the distance between the arginine and aspartic acid groups is ideally between 8-12 bonds to give greatest activity[133]. The conformation of the peptide is not the only factor to consider but a linker between the biomaterial and the peptide has been shown to improve activity. This is because the linker increases the exposure of the peptide and a calculated length of 3.5 nm or greater is required to increase binding[134]. Surface distribution is another important factor to consider and this can be tailored in the biomaterial or the surface design.

There are many aspects in tissue engineering which need to be considered for good cell adhesion, growth and proliferation to occur. Careful design is required for successful treatment of AMD using tissue engineering methodology. Positive results within other tissues in the body demonstrate that this could be an effective approach for treating AMD. To deliver a treatment for AMD which could be readily used by clinicians frequently several barriers such as short self-life of proteins, cost, scalability and absence of immune triggers must be overcome. This is a problem with all tissue engineering applications, however the use synthetic polymers for scaffold design and use of small molecule peptidomimetics to improve adhesion could provide a solution.

1.11 Aims of research.

There is currently no cure for neovascular (wet) AMD and no treatment for geographic atrophy or the dry form of the disease. Within this thesis one aim was to extend time between intravitreal injection times for current neovascular drug treatment. By investigating biodegradable microspheres as a drug delivery vehicle it was aimed that improved drug release rates, improved times between dosing and an improved dose received by the patient could be obtained. In addition to treating neovascular AMD, possible solutions to dry AMD, were also investigated. Finding a treatment or cure for AMD, permanent scaffolds were investigated aiming to act as a replacement for the Bruchs membrane. Furthermore investigation into current scaffolds and use of biomimetic compounds was undertaken with an aim to improve cell adhesion, growth and survival on the scaffolds designed within this work.

2. Microspheres

2.1 Introduction

Traditional routes of drug administration can have potential disadvantages such as, migration away from the site of action, the need for frequent administration and cytotoxic side effects[140]. Drug delivery systems can be employed to improve the therapeutic properties of a drug by tailoring release, lowering the peak concentration in the body and protect the drugs which can degrade within the body, increasing lifetime[69]. Drug administration for ocular diseases, particularly to the posterior of the eye is especially difficult because of the defences and barriers of the eye. Because of these natural barriers, incision or injections into the eye are required. Microspheres have several advantages for ocular drug delivery because of their size and ease of manufacture. Another advantage of microspheres are they have been shown that blends below 300 µm degrade homogenously and therefore reliable release of the entrapped compound can be obtained[40]. The microspheres developed must be extremely reproducible, should have a high yield and encapsulation rate to avoid losses of the drug whilst not affecting drug activity[141]. Obtaining these three properties in combination with good release rates, a long shelf life and at a low cost has proven challenging.

Various techniques to prepare microspheres are available, however the solvent evaporation method is most commonly used[65]. The solvent evaporation method can be easily optimised, resulting in excellent control over the diameter and shape of the microspheres formed. Other methods such as spray drying, dialysis and phase separation can also be used to form microparticles. Difficulties with limited options for scale up, wide microsphere diameter distribution, and harsh physical burdens can diminish the activity of the drugs using these methods in comparison with the fairly mild solvent evaporation method. In the solvent evaporation method, an emulsion is formed by dissolving a polymer into volatile organic solvent (oil layer). This is then added to an aqueous layer with vigorous agitation to form an emulsion. As the volatile solvent evaporates small microparticles are prepared (Figure 2.1). A

component (such as, drug, dye or protein) can be encapsulated by addition into the polymer oil mixture. In order to improve encapsulation, double emulsions can be prepared. Double emulsions are prepared by adding an initial emulsion into another phase. Most commonly to increase solubility of water soluble drugs, water/oil/water double emulsions are prepared. The first water in oil emulsion is prepared before being added into a larger water phase creating a water/oil/water double emulsion[63].

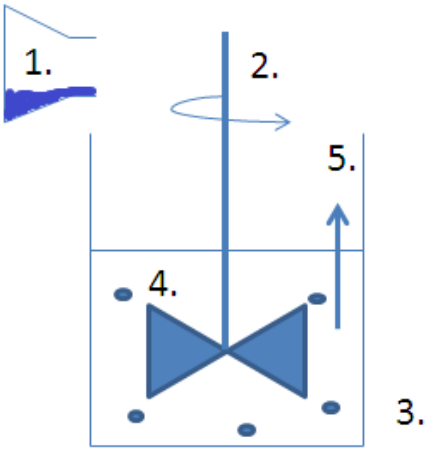

Figure 2.1 - Preparation of microspheres by the solvent evaporation technique. 1) Polymer dissolved in oil layer. 2) Agitation or mixing is required to split the oil droplets when in solution. 3) Water layer. 4) Oil/polymer droplets in solution. 5) Solvent evaporation occurs resulting in solid microspheres remaining.

PLLA and PLGA are commonly investigated as possible drug delivery systems due to their biodegradability and biocompatibility[142,143]. These biodegradable polymers have regulatory approval for human clinical use[144] and have the advantage that their degradation can be tuned based on the ratio of different monomer units present[55]. PLGA is more commonly used on its own for sustained release of drugs rather than a PLGA:PLLA blend[145,146,55]. Sustained retinal drug delivery using PLGA has been investigated for CMV[31] and AMD previously[48,49]. A need for better defined microspheres with prolonged release profiles and with a high encapsulation efficiency of active compound is still required.

2.1.1 Aim of microsphere drug delivery.

Within this chapter the aim was to develop a drug delivery system which could be used to treat age-related macular degeneration. Using microspheres as the delivery vehicle, the initial aim was to optimise the microspheres to allow repeatable production of microspheres with consistent shape and diameter. After optimisation, the encapsulation and release of dyes and drugs was investigated. The aim was to attain high encapsulation and long release times of any incorporated compound. A target goal was to encapsulate and release the drug Bevacizumab without affecting the potency of the drug over an extended period of time. Finally, surface activation of the microspheres was attempted with the intent to increase delivery times of any incorporated drug and improve the physical properties of the microspheres.

2.2 Optimisation of microspheres for intravitreal injection into the eye.

2.2.1 Factors affecting microsphere diameter and morphology.

The first area within the microsphere work was to establish what effect different polymers, molecular weights, solvent concentrations, stabilisers, polymer concentrations and use of salts had on the microspheres and if this behaviour was consistent with previous literature. Using the solvent evaporation technique, microspheres consisting of 100% PLLA, 100% PLGA and 50:50 PLLA:PLGA were prepared in order to examine what factors influenced the properties of the final microspheres. Microsphere optimisation has been undertaken before, however the work focussed on improvement of cell attachment[100]. Within this current project, we had a specific remit that microspheres needed to be below 30 µm for intravitreal injection using a 31 gauge (G) needle. From previous work[100], the optimised general preparative procedures via the solvent evaporation technique used a 5% polymer in dichloromethane (DCM) solution. Initially, the polymer concentrations were re-examined as this is the dominant factor in controlling microsphere diameter using the solvent evaporation technique for microsphere preparation. It was observed that, as polymer concentration decreased, so did the average microsphere diameter (Table 2.1), as a result of the reduced viscosity of the solution. Significantly, the surface structure of the microspheres was different between the three blends (Figure 2.2). The PLLA microspheres produced a coarser surface structure in comparison with the

smooth and highly spherical PLGA microspheres, with the 50:50 blend being an intermediate between the two. PLLA produced slightly larger spheres at all concentrations compared to PLGA which probably reflected the increased viscosity of the PLLA polymer solution.

Table 2.1 - The effect of polymer composition and concentration on microsphere diameter.

Polymer blend	% polymer concentration (w/v)	Mean diameter (µm)	S.D.[a] ±
PLLA	10	199	65
PLLA	5	139	44
PLLA	2.5	50	21
PLLA	1	43	25
PLGA	10	102	61
PLGA	5	82	53
PLGA	2.5	46	34
PLGA	1	40	30
50:50 PLLA:PLGA	10	105	49
50:50 PLLA:PLGA	5	79	55
50:50 PLLA:PLGA	2.5	41	29
50:50 PLLA:PLGA	1	35	27

[a] S.D. (n = 3; three sets of data corresponds to three separately synthesised batches of microspheres).

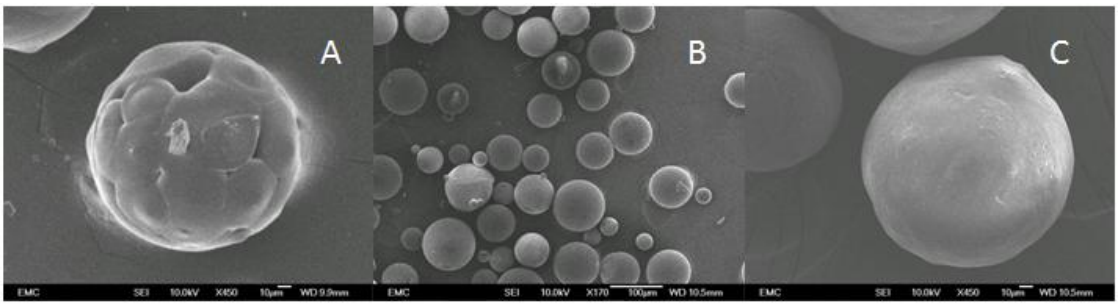

Figure 2.2 - Scanning electron micrographs of three microsphere blends obtained with polymer concentration of 10% in DCM, using the solvent evaporation technique: (A) 100% PLLA, original magnification x 450; (B) 100% PLGA, original magnification x 170; (C) 50:50 PLLA:PLGA microsphere blend, original magnification x 450.

Although smaller microspheres were produced using 1% concentration of polymer solution (Table 2.1), the yield was greatly decreased. Using 250 mg of polymer in a 2.5% polymer solution would return around 220-250 mg of microspheres, however using a 1% solution concentration would only return around 100-150 mg. Some of

the polymer would clump around the overhead stirrer blade or stick to the side of the flask to form a thin film when using a 1% polymer solution and this was where the loss in mass occurred. It was decided that, with this inconsistency, use of the lower concentration polymer solution would not be sufficiently reproducible and could be problematic in future work, especially for applications such as encapsulation of drugs.

Linked with the viscosity was the solvent that was employed, therefore the consequences of using ethyl acetate and chloroform were investigated. The change in solvent would not only change the viscosity of the solution but due to differences in volatilities would vary the rate of solvent evaporation. By increasing or decreasing the evaporation time, the microsphere diameter and morphology would be affected since the shear forces would have more or less time to split the oil droplets whilst in the emulsion. The solvent evaporation time would also affect the microsphere diameter by preventing the oil droplets in the emulsion recombining. Using ethyl acetate as the solvent produced slightly larger microspheres on average (44.9 μm ± 25.3) for 100% PLGA at 1% polymer concentration. Ethyl acetate resulted in larger microspheres formation because the solvent readily mixes into the water layer[150]. The ethyl acetate goes into the water quicker than the DCM or chloroform solvents, resulting in the microspheres drying quicker. The ethyl acetate would not dissolve the PLLA and therefore would not allow us to exploit the different degradation profiles of both PLLA and PLGA in future work. Chloroform produced similar results to DCM, with a mean average diameter of 38.5 μm for the 50:50 blend. From these results, it appeared that solvent viscosity has a greater role in microsphere diameter than solvent volatility (Table 2.2).

Table 2.2 - The effect of solvent on microsphere diameter**.**

Polymer blend	**Solvent**	**Boiling Point (°C)[200]**	**Viscosity (cP) at 20°C[200]**	**Solubility in water (g 100mL^{-1}) at 20°C[200]**	**Mean** diameter **(µm)**	**S.D.[a] ±**
50:50 PLLA:PLGA	Ethyl acetate	72.1	0.426[b]	8.3[b]	44.9	25.3
50:50 PLLA:PLGA	DCM	39.6	0.44	1.75[b]	34.5	27.1
50:50 PLLA:PLGA	Chloroform	61.2	0.563	0.809	38.5	31.6

[a] S.D. (n = 3; three sets of data corresponds to three separately synthesised batches of microspheres). [b] Measurement at 25°C.

The maximum sphere diameter would need to be below 30 µm for intravitreal injection using a 31 gauge needle, even one larger sphere could cause a blockage and therefore an incorrect dose being injected into the patients eye. In an attempt to reduce the microsphere diameter, each component in microsphere preparation was re-examined using the optimised 2.5% polymer solution concentration. The surfactant polymer added to stabilise the emulsion was scrutinised. From previous work[99], the optimised procedures using the solvent evaporation technique used 0.5% PVA, (RMM 31 000–50 000, Sigma-Aldrich) in water as the stabilising solution. In the present study, PVA concentrations of 4%, 2%, 1%, 0.5%, 0.1% and 0.05% were utilised to form 50:50 PLLA:PLGA microspheres and to see what, if any, improvement in microsphere diameter could be obtained (Table 2.3).

Increasing the PVA concentration resulted in larger microspheres forming, although the distribution range was slightly narrower. At 4% PVA concentration, the average sphere diameter was 56.7 µm but the standard deviation was only ± 25.8 µm. This is may reflect the increased kinetic stability of the oil droplets in the emulsion which the presence of extra PVA surfactant offers as a result of which, greater shear forces are required to split the oil droplets into smaller drops. Lowering the PVA concentration to 0.1% improved microsphere diameter, with a similar distribution (34.0 µm ± 27.9 µm). In an attempt to improve this further, 0.05% PVA solution was used as the water phase, however in this case larger and misshapen microspheres were produced (Figure 2.3A). A decrease in the number of surfactant molecules available to stabilise the contact between the two liquid phases leads to a decrease in

the stability of the emulsion which disfavours formation of smaller droplets within the emulsion.

Table 2.3 - The effect of surfactant on microsphere diameter.

Polymer	Concentration surfactant w:v (%)	Mean diameter[a]
50:50 PLLA:PLGA	4	56.7 ± 25.8
50:50 PLLA:PLGA	2	40.4± 32.5
50:50 PLLA:PLGA	1	41.6 ± 22.1
50:50 PLLA:PLGA	0.5	44.6 ± 18.9
50:50 PLLA:PLGA	0.1	34.0 ± 27.9
50:50 PLLA:PLGA	0.05	112.8 ± 60.6

[a] S.D. (n = 2; three sets of data corresponds to three separately synthesised batches of microspheres)

Changing the relative molecular mass (RMM) of the PVA surfactant was also investigated to understand what affect this would have on the microsphere morphology. 1%, 0.5% and 0.1% PVA (RMM 85 000–124 000, Sigma-Aldrich) was used keeping the conditions the same as the lower molecular weight PVA. This resulted in the yield of the microspheres being greatly reduced and more importantly, the microspheres were of a lower quality. The microspheres were far larger and highly deformed, showing that use of this larger molecular weight PVA offered very little benefit in lowering the surface tension between the two phases and hence is a poor surfactant for microsphere formation (Figure 2.3B).

Finally Poly(vinyl pyrrolidone) (PVP, average RMM 40 000) was used at 0.1% w:v concentration to explore the effect of changing the surfactant. Although PVP gave improved microsphere diameters compared to that of RMM 85,000–124,000 PVA, the microspheres were far larger than the current optimised conditions using the lower molecular weight PVA (Fig 2.3C), showing that PVP was less favourable in stabilising the emulsion.

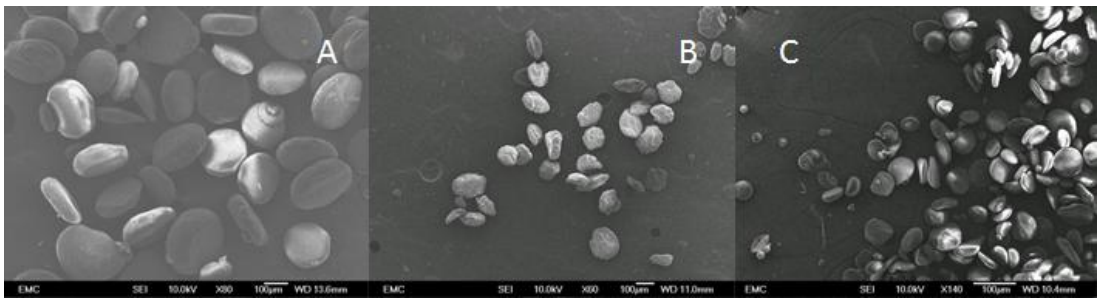

Figure 2.3 - Scanning electron micrographs of three 50:50 PLLA:PLGA blend microsphere preparations using different surfactants: (A) 0.05% PVA stabilising solution, original magnification x 80; (B) PVA RMM 85 000–124 000 as stabilising solution, original magnification x 60; (C) PVP as stabilising solution, original magnification x 140.

Shear forces seem to be a key feature in determining microsphere diameter. As viscosity was reduced and therefore the force required tosplit up the oil droplets in solution decreased, smaller microspheres were obtained. To increase the shear force, the stirring speed was increased from 900 rpm to 2500 rpm and a noticeable reduction in microsphere diameter was observed. Using the optimised conditions [0.1% PVA (RMM 31,000–50,000, Sigma-Aldrich) and 2.5% w:v polymer solution in DCM] 50:50 PLLA:PLGA microspheres could be obtained below 30 µm. In addition to obtaining smaller microspheres, the distribution range was also narrower, with all spheres being below 30 µm for the 50:50 PLLA:PLGA blend (Figure 2.4). Using these optimised parameters various other blends were tried in an attempt to create microspheres below 30 µm (Table 2.4). Apart from 100% PLLA microspheres, all blends had a mean diameter below 30 µm with a small distribution. The greater percentage PLGA present, the smaller are the microspheres that are produced.

Table 2.4 - The average diameter **of microspheres prepared using the optimised parameters with different ratios of PLLA:PLGA.**

Polymer blend	Mean Diameter (µm) [a]
100 PLLA	33.7 ± 10.1
80:20 PLLA:PLGA	28.3 ± 7.7
50:50 PLLA:PLGA	23.2 ± 8.2
20:80 PLLA:PLGA	22.9 ± 6.4
100 PLGA	20.5 ± 8.8

[a] Standard deviation (n = 3; three sets of data corresponds to three separately synthesised batches of microspheres).

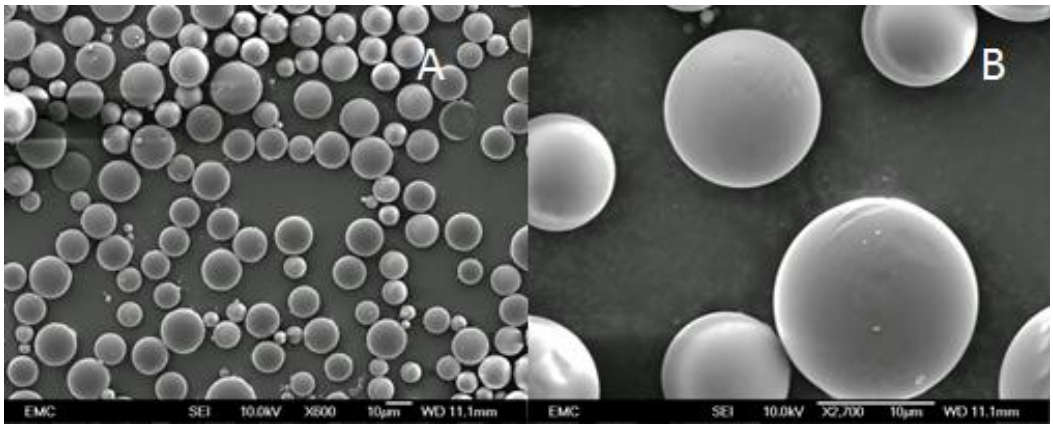

Figure 2.4 - Scanning electron micrographs of 50:50 PLLA:PLGA microspheres prepared using the solvent evaporation technique with optimised parameters (PLLA Resomer L 206S, PLGA Resomer RG 755 S, 0.1% Poly(vinyl alcohol) (RMM 31,000–50,000, Sigma-Aldrich), 2.5% w:v polymer solution in DCM stirring at 2500 rpm): (A) Original magnification x 600; (B) Original magnification x 2700.

In previous work the polymers used were PLLA (Resomer L 207S, i.v. 1.5–2.0 dL g^{-1}, 0.1% in chloroform, 25°C, RMM ~150,000 obtained from Boehringer Ingelheim) and PLGA (Resomer RG 755 S, i.v. 0.5–0.7 dL g^{-1}, 0.1% in chloroform, 25°C, RMM ~20,000-80,000 obtained from Boehringer Ingelheim). The PLGA Resomer® was changed from RG 755 S to RG 756 S (i.v. 0.71–1.0 dL g^{-1}, 0.1% in chloroform, 25°C, RMM ~76,000-150,000 obtained from Boehringer Ingelheim). For the 50:50 PLLA:PLGA microspheres it was found that the mean diameter of the microspheres increased by 1.2 µm to 24.4 µm, however the size distribution was smaller with a standard deviation of only ± 7.0. The biggest effect, however, was observed when the PLLA Resomer L 207S was changed to Resomer L 206S (i.v. 0.8–1.2 dL g^{-1},

0.1% in chloroform, 25°C, RMM ~100,000 obtained from Boehringer Ingelheim). In this case the average microsphere diameter for the 50:50 PLLA:PLGA blend was reduced to 9.1 μm with a standard deviation of just ± 4.1. Use of PLLA Resomer L 209 (i.v. 2.6–3.2 dL g^{-1}, 0.1% in chloroform, 25°C, obtained from Boehringer Ingelheim) resulted in the formation of very large microspheres (< 300 μm) reflecting the large increase in viscosity.

2.2.2 Preparation and characterisation of porous microspheres.

In future work, drug encapsulation and release are going to be the key factors in dictating the size and morphology of the microspheres used, therefore in order to understand microsphere formation better, the porosity of microspheres has been investigated using the adjusted microsphere formation conditions.

Previously, the polymer has been dissolved in a DCM layer (also known as the oil layer) before being added into a water PVA solution (known as the water layer). This creates an oil in water emulsion (w/o), however, other possible emulsions are possible. One example is by dissolving a compound in which encapsulation is desired in water solution before adding into the DCM (oil) layer, creating a water/oil emulsion (w/o). Finally by adding this water/DCM (w/o) solution into the water PVA stabilising solution creates a water/oil/water (w/o/w) emulsion. A 3%, 10%, 20%, or 40% w/v solution of ammonium hydrogen carbonate was added to the DCM/polymer solution (4 mL) and this was then emulsified with water (0.5 mL) before being added to the PVA water solution, creating a w/o/w mixture. During microsphere formation the ammonium hydrogen carbonate decomposes to form carbon dioxide and ammonia gas, creating the porous structure. The resulting microspheres were clearly porous when viewed by SEM (Figure 2.5), however they were far larger than their non-porous counterparts (mean diameter for 20% w/v solution of ammonium hydrogen carbonate 198.6 μm ± 80.5) (Table 2.5). From the SEM images of the resulting microspheres, differences in the porosity can be observed depending on the concentration of ammonium hydrogen carbonate added. At 40% ammonium hydrogen carbonate, microspheres can be seen having a greater number of pores and openings (Figure 2.5B) when compared with those obtained from the 10% ammonium hydrogen carbonate preparation (Figure 2.5C). In order to measure the porosity of the spheres, the BET method (Brunauer, Emmett and

Teller)[147] was investigated but the results were inconclusive. Normally the sample is placed under high vacuum, at a high temperature (240^{o}C) to remove any gas molecules adsorbed in the sample. At this temperature the microspheres melt, therefore, they were just held under high vacuum however some gas molecules may have remained entrapped within the microspheres producing the inconclusive results. There was a very large variation between identically prepared microspheres and the results were not reproducible.

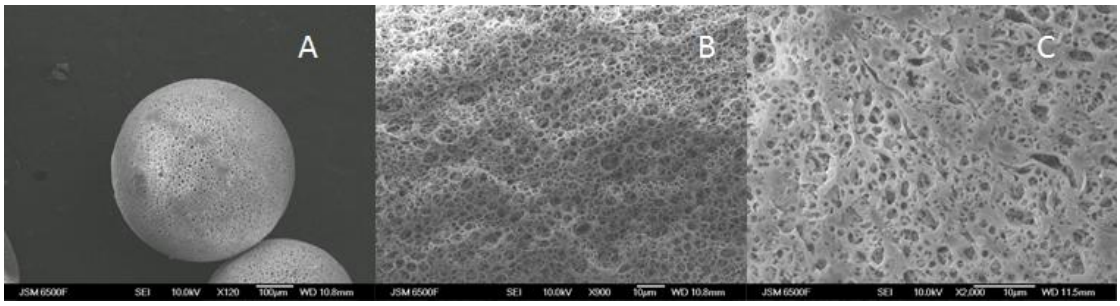

Figure 2.5 - Scanning electron micrographs of 50:50 PLLA:PLGA porous microspheres: (A) For 20% ammonium hydrogen carbonate, original magnification x 120; (B) For 40% ammonium hydrogen carbonate, original magnification x 900; (C) For 10% ammonium hydrogen carbonate, original magnification x 2000.

An indirect way to measure microsphere porosity was by immersion of a known mass of the microspheres in deionized water for 48 hours at room temperature with gentle agitation. After this time the microspheres were filtered off using a steel mesh and any excess water was allowed to drain. The microspheres were then weighed and the water absorption of the microspheres (used as an indirect measurement of porosity) was calculated as follows:

$$\textit{Water absorption} = \frac{W_s - W_d}{W_d}$$

Where W_s is the weight of the swollen microspheres after 48 hours in water and W_d is the weight of the microspheres when dry.

As would be expected, the higher the concentration at ammonium hydrogen carbonate in the w/o emulsion, the greater the porosity of the resulting microspheres. The 40% ammonium hydrogen carbonate microspheres however, were not twice as

porous as the 20% microspheres or 4 times more porous than the 10%. This might be expected as the diameters of the microspheres are not dissimilar between the different concentrations (Table 2.5). This could be due to the concentration ammonium hydrogen carbonate within the oil droplets being at saturation point in each of the experiments and when the gas molecules are released no additional pores are being formed. Another reason could be due to incomplete water absorption when immersed in deionised water. Despite the higher porosity of the microspheres, water may not be able to reach every space within the microsphere giving a lower reading than would be expected.

Another approach for increasing porosity of the surface is via the salt leaching process[148,149]. As the name suggests, a salt or water soluble molecule is added into the oil layer which will leach out during microsphere formation creating porosity[92]. 10% calcium carbonate, 10% and 20% sodium oleate, and 10% sucrose were all used to see if porosity could be obtained by this method. All three additives however, created misshapen and large microspheres with little or no porosity (Figure 2.6).

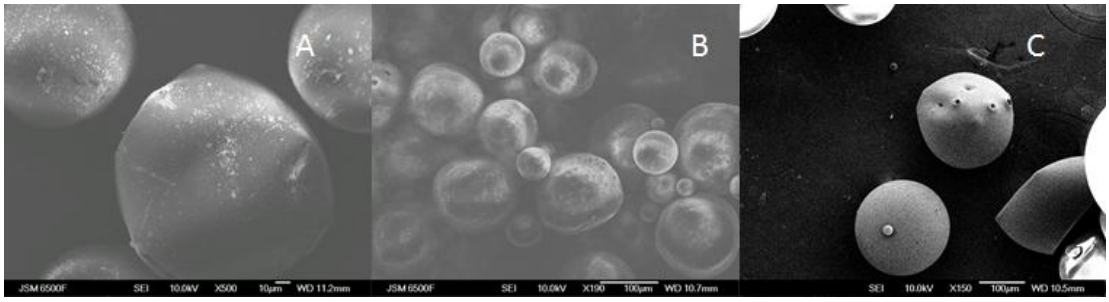

Figure 2.6 - Scanning electron micrographs of 50:50 PLLA:PLGA porous microspheres prepared via the salt leaching method: (A) 10% calcium carbonate, original magnification x 500; (B) 20% sodium oleate, original magnification x 190; (C) 10% sucrose, original magnification x 150.

Table 2.5 - The average diameter and water absorptivity of porous microspheres as a function of additive concentration.

Additive to 50:50 PLLA:PLGA microspheres	Mean diameter (μm) ± S.D.[a]	Water absorption ratio
10% ammonium hydrogen carbonate	185.8 ± 99.5	1.27
20% ammonium hydrogen carbonate	198.6 ± 80.5	1.45
40% ammonium hydrogen carbonate	190.1 ± 110.2	1.61
10% calcium carbonate	126.3 ± 55.2	0
10% sodium oleate	106.6 ± 76.4	0
20% sodium oleate	141.7 ± 95.1	0
10% sucrose	119.5 ± 84.9	0

[a] Standard deviation (n = 2; two sets of data corresponds to two separately synthesised batches of microspheres).

2.3 Investigating encapsulation and release properties of PLLA:PLGA microspheres.

2.3.1 Encapsulation and release of Rhodamine B and Fluorescein dyes.

For microspheres below 30 μm, injection into the eye is feasible and therefore provides a possible drug delivery system. In order to explore this option, organic dyes were incorporated into the microsphere synthesis with a view to monitoring their subsequent release. Rhodamine B and Fluorescein were selected as drug mimics (Appendix 7.9). Initially, the 50:50 PLLA:PLGA blends were used to investigate the encapsulation of these dye compounds. In order to measure initial encapsulation, the concentration of the dyes encapsulated was determined by collecting the washings during the preparation of the microspheres. The concentration of the residual, un-encapsulated dye present in these washings was measured using UV spectrophotometry (Shimadzu UV-1601 spectrophotometer). The concentration encapsulated was determined from the collecting the washings of the microspheres and then deducted from the total concentration of dye used in the microsphere preparation. The percentage of dye not encapsulated within the microspheres was then calculated (Table 2.6). In later work, encapsulation was also calculated by dissolving the dye or drug-encapsulated microspheres in DCM and measuring the concentration of the dye or drug released using a UV spectrophotometer against a calibration curve. This method was used to corroborate the encapsulation results after optimisation had been completed (Table 2.9).

To see how encapsulation affected the diameter and morphology of the microspheres, Rhodamine B (20 mg) and Fluorescein sodium salt (20 mg) were separately encapsulated in a 50:50 PLLA:PLGA blend. The Rhodamine B-encapsulated microspheres were of similar diameter to the non-encapsulated 50:50 PLLA:PLGA microspheres, however, some pores were present within the microspheres, most likely due to the salt leaching process (Figure 2.7A).

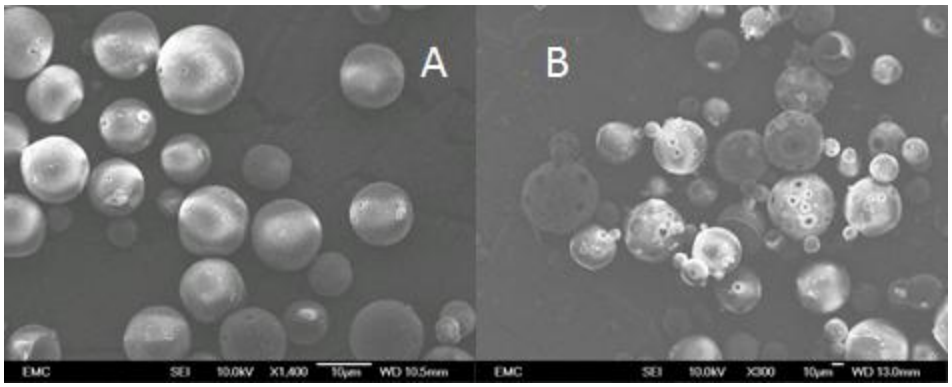

Figure 2.7 - Scanning electron micrographs of 50:50 PLLA:PLGA microspheres. (A) Rhodamine B encapsulated, original magnification x 1400; (B) Fluorescein sodium salt encapsulated, original magnification x 300.

The Fluorescein sodium salt-encapsulated microspheres were far larger than the complementary non-encapsulated microspheres. There were many pores and defects present in the Fluorescein-encapsulated microspheres and this was reflected in the amount of Fluorescein encapsulated within the microspheres. The loading efficiency of Rhodamine B was 78.2% while Fluorescein encapsulated within the microspheres was only 40.1%. As noted in the Introduction, it is known that the chemical compound or biological molecule encapsulated[55] has an effect on the microspheres and this can clearly be seen between the two different dyes.

2.3.2 Optimising encapsulation of dyes with PLLA:PLGA microspheres.

Different encapsulation methods were investigated to see the effect on microsphere morphology and whether improvements in encapsulation efficiency could be obtained[151]. Using the 50:50 PLLA:PLGA microsphere blend, different initial emulsions were attempted to create the microspheres using both the Rhodamine and Fluorescein dyes. Up until this point, only 78% and 40.1% of dye-encapsulated microspheres could be obtained using a water/oil/water (w/o/w) emulsion. These

were prepared by dissolving the Rhodamine or Fluorescein dye in a drop of water and adding it to the DCM/polymer solution (w/o) after which the resulting mixture was added to the water/PVA solution to create the final w/o/w emulsion. Other methods were investigated to improve encapsulation; a solid/oil/water (s/o/w) emulsion where the dye is directly added to the oil (DCM) layer before addition into the water/PVA solution. The water/oil/water method was attempted again for comparison and different amounts of dye were used to investigate the saturation point of the dye. A water/oil/water emulsion was repeated again but with sodium chloride (1% w:v) added to the water/PVA solution to see if this had an effect by reducing salt leaching. Finally an oil/oil/water (o/o/w) emulsion was created using cyclohexane as the primary oil layer.

Table 2.6 - The encapsulation efficiency of 50:50 PLLA:PLGA microspheres prepared using different emulsions preparation.

Dye	Mass of dye added during preparation (mg)	Preparation Method [a]	Loading efficiency (%)
Rhodamine B	5	s/o/w	89
Rhodamine B	10	s/o/w	65
Rhodamine B	5	w/o/w	90
Rhodamine B	10	w/o/w	89
Rhodamine B	20	w/o/w	78
Rhodamine B	5	w/o/w with 1% NaCl	79
Rhodamine B	5	o/o/w	50
Fluorescein sodium salt	5	s/o/w	79
Fluorescein sodium salt	10	s/o/w	75
Fluorescein sodium salt	5	w/o/w	90
Fluorescein sodium salt	10	w/o/w	85
Fluorescein sodium salt	20	w/o/w	40
Fluorescein sodium salt	5	w/o/w with 1% NaCl	86
Fluorescein sodium salt	5	o/o/w	267

[a] s/o/w, solid/oil/water emulsion; w/o/w, water/oil/water emulsion; o/o/w, oil/oil/water emulsion

As shown in Table 2.6 the loading efficiencies were highest when the w/o/w emulsions were used and that the addition of sodium chloride to the PVA solution offers no improvement to the loading efficiencies of the microspheres. For both the Rhodamine and Fluorescein microspheres, some pores are present within the

microspheres (Figure 2.8A), however, no pores are evident on the Rhodamine encapsulated microspheres prepared with the addition of sodium chloride (Figure 2.8B). The microspheres prepared using s/o/w conditions gave reasonable loading efficiencies, however, the diameter distribution of the microspheres was affected and some malformed microspheres were present (Figure 2.8C). Between 5 mg and 10 mg of dye (per 50 mg of polymer used to form the microspheres) was the saturation point at which greatest loading efficiency was obtained. Microspheres produced using the o/o/w conditions gave the lowest encapsulation for both dyes and viewing of the SEM micrographs shows a possible reason why this is the case (Figure 2.8D). The initial oil droplets seem to deform the microspheres resulting in increased dye release. As Fluorescein is only water soluble this o/o/w method hinders encapsulation as would be expected. Rhodamine B is soluble in both oil and water and this could explain the differences between Rhodamine and Fluorescein encapsulation efficiencies. A general trend of encapsulation efficiencies however, is seen for both dyes with the w/o/w emulsion being the most effective methodology.

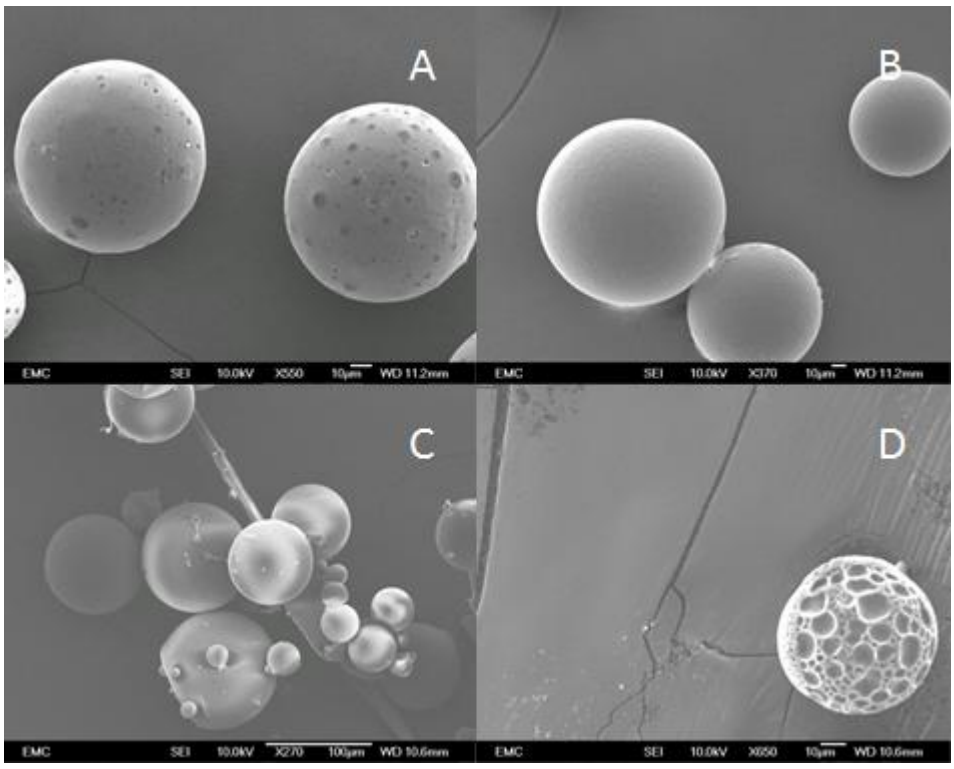

Figure 2.8 - Scanning electron micrographs of 50:50 PLLA:PLGA microspheres created by different emulsions: (A) Fluorescein sodium salt-encapsulated microspheres using a w/o/w emulsion, original magnification x 550; (B) Rhodamine B-encapsulated microspheres using the w/o/w 1% sodium chloride emulsion, original magnification x 370; (C) Rhodamine B-encapsulated microspheres using a s/o/w emulsion, original magnification x 270; (D) Rhodamine B-encapsulated microspheres using a o/o/w emulsion, original magnification x 650.

Earlier work within this project showed that increasing the PVA concentration affects microsphere diameter and this parameter was reinvestigated to see the effect on encapsulation efficiency. When the concentration of PVA was increased from 0.5% to 1% and 4% (w/v), no significant change in encapsulation efficiency was observed.

Different Resomer types were used to investigate the effect this would have on encapsulation. The previous Rhodamine B and Fluorescein experiments have utilised the PLLA Resomer L 206S and PLGA Resomer RG 755S. Using a w/o/w emulsion encapsulating Rhodamine B (5 mg), 100% blends of the polymers were used to measure encapsulation (Table 2.7). When the PLLA resomer was changed to Resomer 209 with a higher molecular weight, the encapsulation efficiency increased

by around 10 %, although the diameter of the microspheres increased to above 80 µm. Using PLLA resomer 207S resulted in a slight increase in Rhodamine encapsulation with microsphere diameter remaining below 30 µm. This increase in encapsulation is likely to arise from the increased hydrophobicity of the higher molecular weight PLLA. This pattern is also observed with the PLGA; as the hydrophobicity is increased, the encapsulation efficiency is improved.

Table 2.7 - The encapsulation efficiency of various 100% blend PLLA and PLGA Resomers®.

Resomer	Loading efficiency (%)
PLGA RG 755S	66
PLGA RG 756S	79
PLLA 206	86
PLLA 207	90
PLLA 209	96

The final parameter to be studied within the encapsulation investigation was how various PLLA:PLGA ratios affected the encapsulation efficiency. Keeping the Resomers® constant by using PLLA Resomer L 206S and PLGA Resomer RG 755S, different blend ratios were used with both Rhodamine B and Fluorescein (Table 2.8). Fluorescein encapsulation was greater when a higher percentage of PLGA was present and this is likely to be due to PLGA being more hydrophilic than PLLA. These microspheres were then used to investigate the release of the dyes in solution. The dye-encapsulated microspheres were added into centrifuge tubes (Fisher Scientific) with 1 mL of phosphate buffered saline (PBS 0.01 M, pH 7.4, Sigma-Aldrich). The sealed tubes were kept at 37^{o}C and at set intervals, the microspheres were centrifuged and the supernatant was collected for sampling after filtration through a 0.45 µm syringe filter (Fisher Scientific). The concentration of the dye was then determined by measuring the UV absorbance against a calibration curve. Fresh PBS (1 mL) was then added to the centrifuge tubes which were then placed back at 37^{o}C.

Table 2.8 - The encapsulation efficiency of various PLLA:PLGA microsphere blends.

Blend ratio PLLA:PLGA	Dye used	Encapsulation %
100:0	Rhodamine B	93
75:25	Rhodamine B	93
50:50	Rhodamine B	88
25:75	Rhodamine B	80
0:100	Rhodamine B	75
100:0	Fluorescein sodium salt	70
75:25	Fluorescein sodium salt	85
50:50	Fluorescein sodium salt	86
25:75	Fluorescein sodium salt	89
0:100	Fluorescein sodium salt	91

For both dyes, the longest release profile was given using the 100% PLLA microspheres. The release profile was reasonably steady for both the 100% and 50:50 blends of the microspheres when Rhodamine was encapsulated. The 25:75 blends gave a delayed response before rapid release, a burst type effect (Figure 2.9). When Fluorescein was encapsulated the release profiles were steady for all blends except the 50:50 blend which gave a delayed release (Fig. 2.10). The profile of the release curves is typical to literature observations, with the PLLA giving the longest release profile[55].

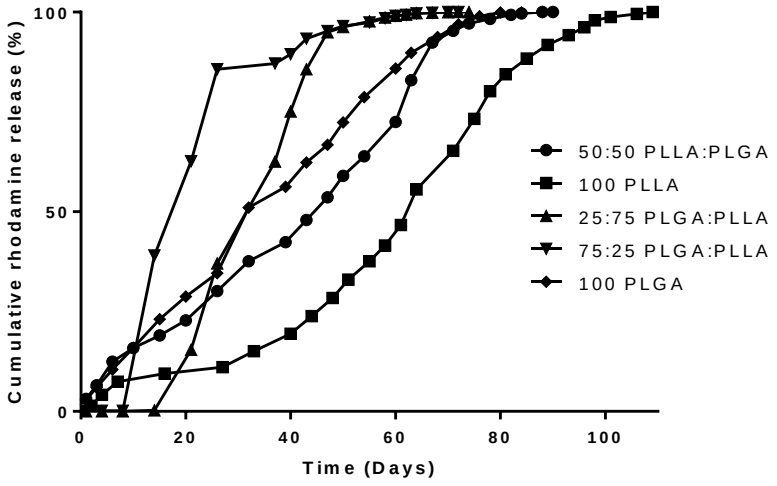

Figure 2.9 - The accumulated Rhodamine B released for different blends of microspheres as a percentage of the total Rhodamine encapsulated.

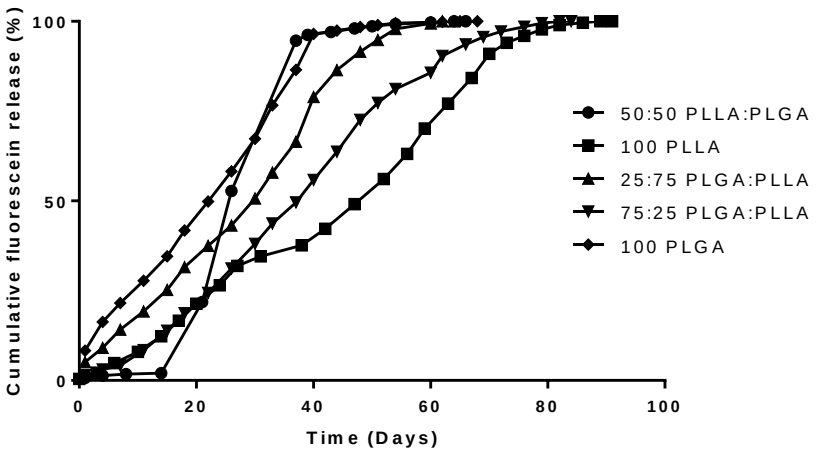

Figure 2.10 - The accumulated Fluorescein released for different blends of microspheres as a percentage of the total Rhodamine encapsulated.

To further investigate dye release using this PLLA:PLGA microsphere strategy, nanospheres and porous microspheres were used to encapsulate Rhodamine B. The preparation of the Rhodamine B-encapsulated porous microspheres and nanospheres are provided in the Experimental Section. Briefly, the nanospheres were prepared by loading the polymer and dye in dimethylformamide (DMF, 5 mL) within dialysis tubing (either 8 kDa or 12 kDa) and then adding this to 5 L of water. As the water displaces the DMF the nanospheres are formed with a diameter range of 100-800 nm (Figure 2.11).

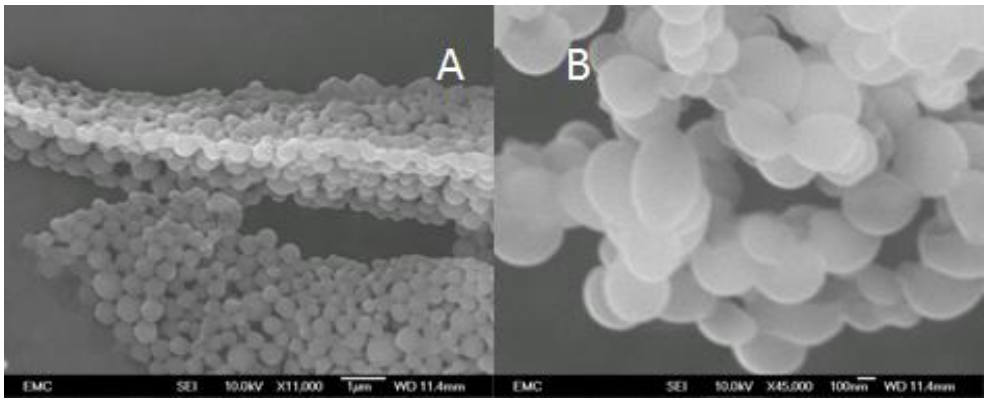

Figure 2.11 - Scanning electron micrographs of 50:50 PLLA:PLGA nanospheres created by the dialysis method. (A) original magnification x 11, 000; (B) original magnification x 45, 000.

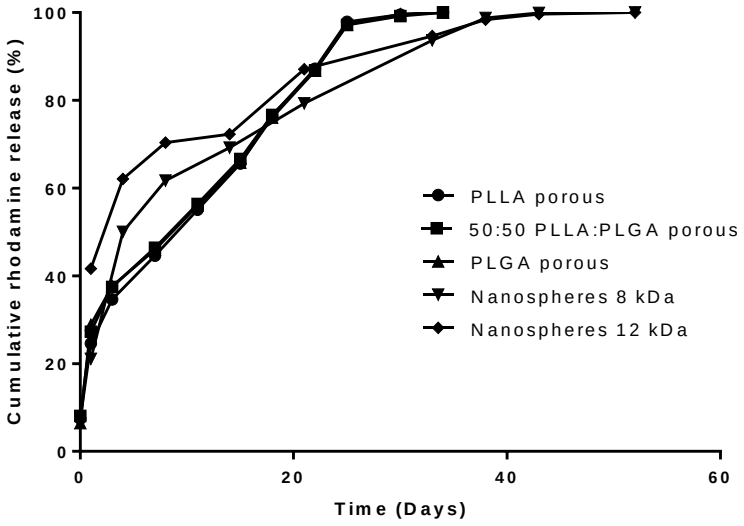

Figure 2.12 - The accumulated Rhodamine B released from different porous microspheres and nanospheres.

Full release of the dye was achieved far quicker for both the porous microspheres and nanospheres when compared with the standard microsphere blends. Both the porous microspheres and nanospheres have a higher burst effect initially over the first few days (Figure 2.12**)**. The burst effect is larger with the nanospheres, however, the porous microspheres have a constant high release rate and complete release is achieved around 8 days before the nanospheres. The burst effect and shorter release times are probably due to the increased surface area with both these samples. The use of different sized dialysis tubing to form the nanospheres resulted in very little difference between the release rates of the two samples and this is likely to be because the nanospheres formed are of similar diameterss for both methods.

2.3.3 Encapsulation of the anti-VEGF drug Bevacizumab.

Having developed a greater understanding of these microsphere systems, the next area of investigation was encapsulation of the antibody Bevacizumab (Avastin®, Genentech). Bevacizumab is an anti-VEGF drug which is currently used "off label" for treatment of AMD[15,16,17]. Intravitreal injection of the Bevacizumab is a whole of life procedure and low patient compliance and high costs can be a problem. Repeated injections of Bevacizumab can lead to other retinal issues such as endophthalmitis, increased intraocular pressure and uveitis[20]. Using the PLLA:PLGA microspheres, it was hoped that high encapsulation efficiency, sustained drug release and retention of

Bevacizumab activity could be obtained once encapsulated, therefore offering this as a potentially improved delivery method within the eye. Although the degradation of PLLA:PLGA has been previously investigated, difference in blend ratios, microsphere sizes, polymer molecular weight and the drug encapsulated[55,152-155] all have an effect on the release rate and therefore previous reaction methods needed to be re-investigated. With an improved understanding from previous experiments using dyes, the Bevacizumab-loaded microspheres were investigated. Two initial targets which the Bevacizumab-loaded microspheres would need to meet would be a microsphere diameter being below 30μm to allow for injection into the eye and a prolonged release rate to increase the time between treatments for patients. Initially, Fluorescein isothiocyanate (FITC) was attached to the Bevacizumab to improve detection via UV-Vis spectrometry (Scheme 2.1). Using a calibration at 494 nm (Appendix D) the concentration of Bevacizumab could be calculated in solution; however, encapsulation was unsuccessful when attempted using this dye attached Bevacizumab. It was then found that measuring the UV spectra at 280 nm Bevacizumab could be detected directly and a calibration graph could be produced for Bevacizumab without the need of an additional fluorescence attachment step. Encapsulation and microsphere morphologies were first investigated with pure Bevacizumab microspheres (no FITC attached). The diameter of the microsphere particles was affected by the various blend ratios used. When a greater percentage of PLLA was used, a larger average diameter of the microspheres was observed, which is consistent with the previous findings (Figure 2.13). Smaller microspheres and nanoparticles would allow the use of a 34 gauge needle, however previous results using the dye showed that the quicker release profile due to the increased surface area of these particles would be insufficient for an extended release period.

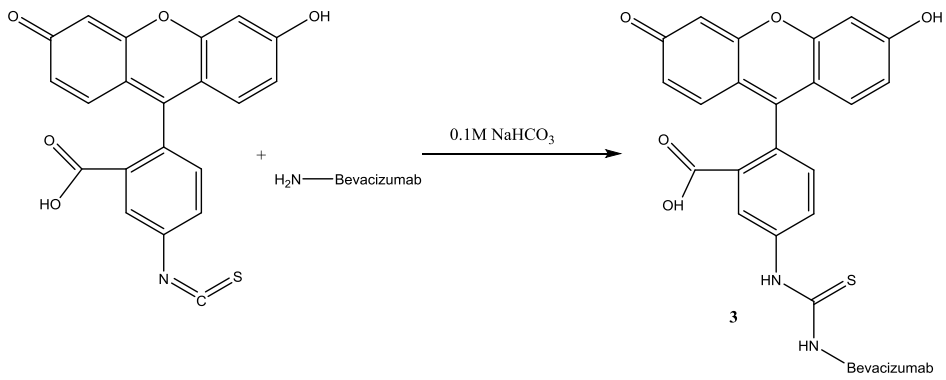

Scheme 2.1 - Fluorescein isothiocyanate (FITC) attachment to Bevacizumab (Avastin).

The higher the concentration of PLLA within the microspheres, the less Bevacizumab was encapsulated. However greater than 80% encapsulation was noted for all blends using a single dose of Bevacizumab (Table 2.9). Bevacizumab 1.25 µg, 0.05 mL (25mg/mL solution) was initially encapsulated as this is the standard intravitreal dose for treatment of AMD. Currently around 40 mg of microspheres gives high encapsulation of 1.25 µg Bevacizumab (single dose) but increasing the number of microspheres would increase the injection volume (microspheres in solution) beyond the limit which could be successfully injected intavitreally (100 µL of solution). The encapsulation efficiency is lower for larger doses of Bevacizumab when encapsulated with the same mass of microspheres because the microspheres become saturated. In an attempt to improve encapsulation efficiency, the Bevacizumab was lyophilized to investigate the effect this has on encapsulation and activity of the released Bevacizumab.

The concentration of Bevacizumab encapsulated was determined as described previously for the dye experiments. Briefly, the washings from the preparation of the microspheres were collected and the absorbance was measured using a UV spectrophotometer at 280 nm. The concentration determined from the washings was then deducted from the total concentration of Bevacizumab added to the microspheres during preparation and the percentage of Bevacizumab not encapsulated within the microspheres was calculated. Additionally, in order to corroborate the results, 10mg of Bevacizumab encapsulated microspheres were dissolved in DCM and the Bevacizumab was extracted into water (3 x 2 mL). The concentration of Bevacizumab was then determined using a UV spectrophotometer measuring at a wavelength of 280 nm against a calibration curve.

Table 2.9 - Comparing microsphere polymer blend ratio with encapsulation efficiency, Bevacizumab dose and mean diameter.

Blend ratio	Encapsulation efficiency (%)	Dose Bevacizumab (µg)	Mean microsphere diameter (µm)[a]
100 PLLA	90 ± 10	1.25	22 ± 4
80:20 PLLA:PLGA	84 ± 6	1.25	18 ± 5
70:30 PLLA:PLGA	85 ± 7	1.25	17 ± 5
65:35 PLLA:PLGA	85 ± 6	1.25	18 ± 4
58:42 PLLA:PLGA	72 ± 7	2.5	12 ± 5
58:42 PLLA:PLGA	88 ± 4	1.25	12 ± 5
50:50 PLLA:PLGA	90 ± 2	1.25	9 ± 3
50:50 PLLA:PLGA	62 ± 4	2.5	10 ± 6
42:58 PLLA:PLGA	89 ± 6	1.25	10 ± 4
35:65 PLLA:PLGA	90 ± 7	1.25	10 ± 7
30:70 PLLA:PLGA	92 ± 7	1.25	11 ± 5
20:80 PLLA:PLGA	92 ± 6	1.25	11 ± 3
100 PLGA	93 ± 7	1.25	10 ± 5

[a]Data expressed as mean ± S.D. (n = 2; three sets of data corresponds to three separately synthesised batches of microspheres

The lyophilised Bevacizumab in 50:50 PLLA:PLGA microsphere blend had a slightly lower level of encapsulation (85.3 ± 6.8) relative to a un-lyophilized Bevacizumab (90.4 ± 2.1). The release rate and shape was similar to that of non-lyophilised Bevacizumab which also remained active (Figure 2.17). This was a very interesting result as it is comparable to the non-lyophilised Bevacizumab, however it does involve an extra step in preparation which increases the chances of contamination and decreases yield.

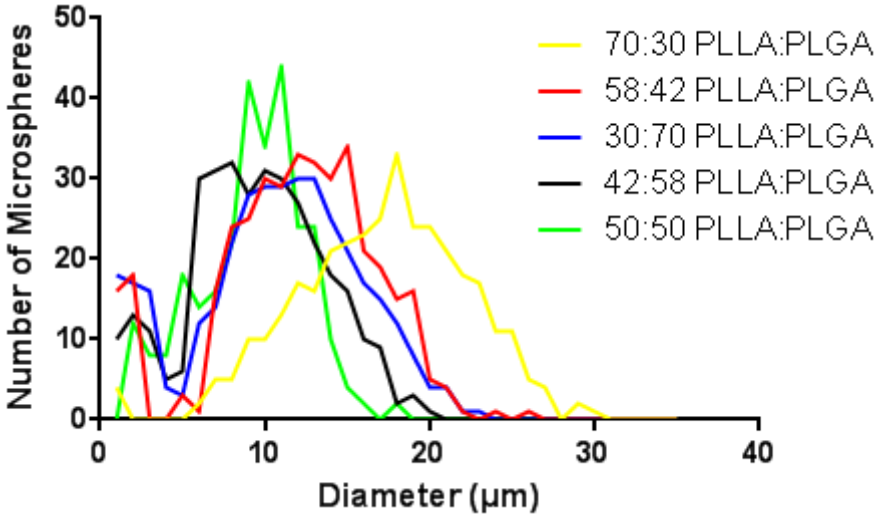

Figure 2.13 - The microsphere diameter and distribution for selected PLLA:PLGA blends.

The morphology of the non-lyophilised Bevacizumab encapsulated microspheres was probed by a scanning electron microscope and images showed that the microspheres were highly spherical with a reasonably smooth surface texture (Figure 2.14A). There were a few protrusions on the surface of the spheres, slightly more than would be observed on the spheres without Bevacizumab encapsulation, however these do not appear to affect the spherical shape of the microspheres dramatically. Degradation of PLLA:PLGA polymers has been previously studied for different systems[144,156], however not for treatment of AMD. In conjunction with measuring release for the degradation on the microsphere, they were also investigated by SEM (Figure 2.14). From SEM analysis (Figure 2.14) the degradation of the Bevacizumab-encapsulated microspheres can be clearly observed, as the smooth surface and spherical nature of the microspheres begins to degrade. Pores within the microspheres begin to form and develop over time. Finally, the structure of the microspheres becomes unrecognisable due to the break-down of the microspheres.

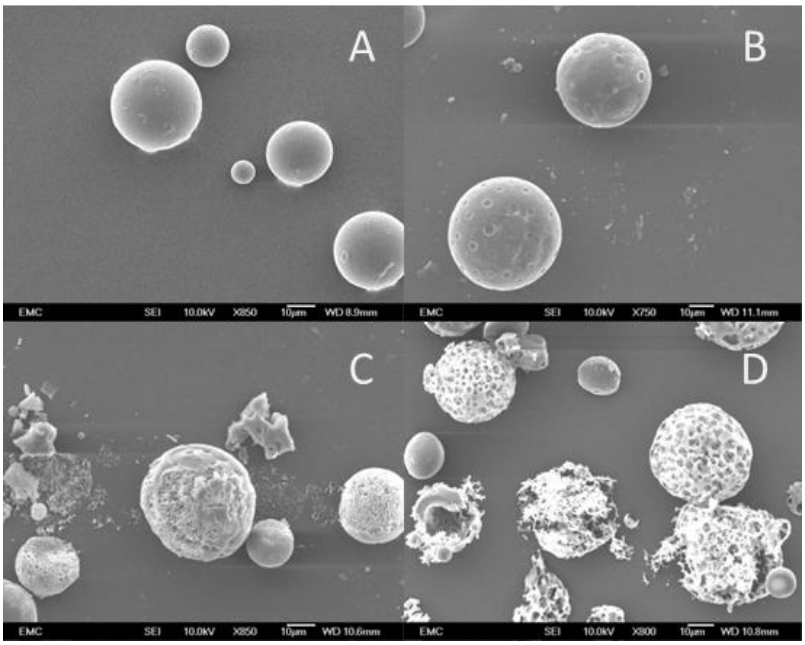

Figure 2.14 - Scanning electron micrographs of the non-lyophilised Bevacizumab-encapsulated 50:50 PLLA:PLGA microsphere blend prepared using the solvent evaporation technique over time: (A) 1 day post preparation, original magnification x 850; (B) After 10 days, original magnification x 750; (C) After 55 days, original magnification x 850; (D) After 90 days, original magnification x 800.

The release of Bevacizumab was monitored over several weeks by measuring the concentration of Bevacizumab released into the supernatant from the microspheres using UV spectrometry against a calibration curve. The blend which provided the longest release profile with a high encapsulation efficiency was the 58:42 PLLA:PLGA microsphere blends (Figure 2.15). Using this blend, Bevacizumab can be released steadily for around 68 days. There is an initial burst release of the Bevacizumab from the microspheres over 3 days before the remaining Bevacizumab is gradually released over the remaining weeks. This "burst effect" can be seen where a high percentage of the total encapsulated material is released before a slower steadier release is observed. The remaining microspheres were collected after 68 days and broken down with DCM (10 mL) and any remaining Bevacizumab was extracted into water (3 x 2 mL). The concentration of remaining Bevacizumab was measured using UV spectrometry; however no Bevacizumab was detected in any of the samples, showing complete release of the encapsulated Bevacizumab.

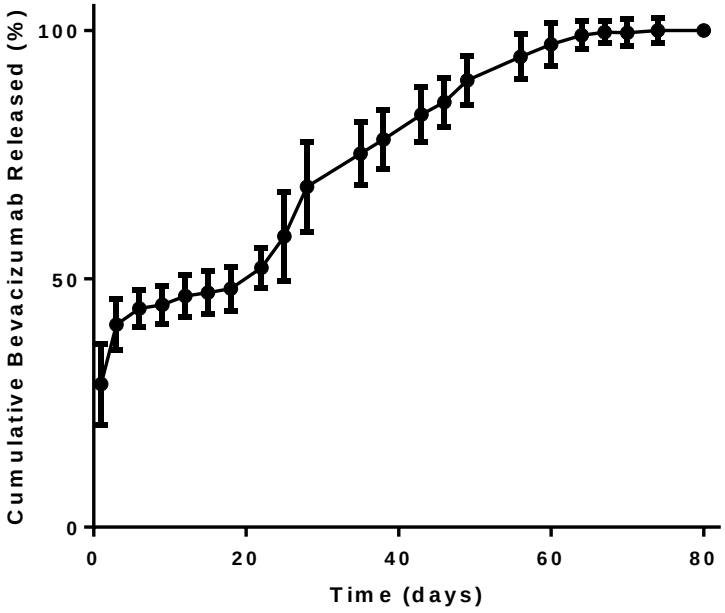

Figure 2.15 - Drug Release Data from 40 mg of 58:42 PLLA:PLGA microspheres loaded with Bevacizumab 1.25 µg. Data expressed as mean ± S.D. (n = 3; three sets of data correspond to three separately synthesised batches of microspheres)

2.4 Measuring the activity of Bevacizumab released from PLLA:PLGA microspheres.

An important area within this study was to investigate if the Bevacizumab was still active post-release. During the encapsulation process, reasonably harsh chemicals and conditions were utilised which could denature the Bevacizumab antibody. As the PLLA:PLGA polymers degrade, an acidic microenvironment is produced which could also inhibit the incorporated Bevacizumab[157]. The long storage and release of the Bevacizumab within the microspheres may also have caused the Bevacizumab to become inactive. The supernatant containing the released Bevacizumab was collected from all the sample points during the release studies and combined. Gel-electrophoresis was used to compare the original Bevacizumab to Bevacizumab which has been encapsulated and released from the microspheres. The original Bevacizumab was also compared to the lyophilised Bevacizumab which has been encapsulated and released from the microspheres. Both samples and the positive control, anti-VEGF mIgG1, showed the same breakdown components with the same mobilities (Figure 2.16).

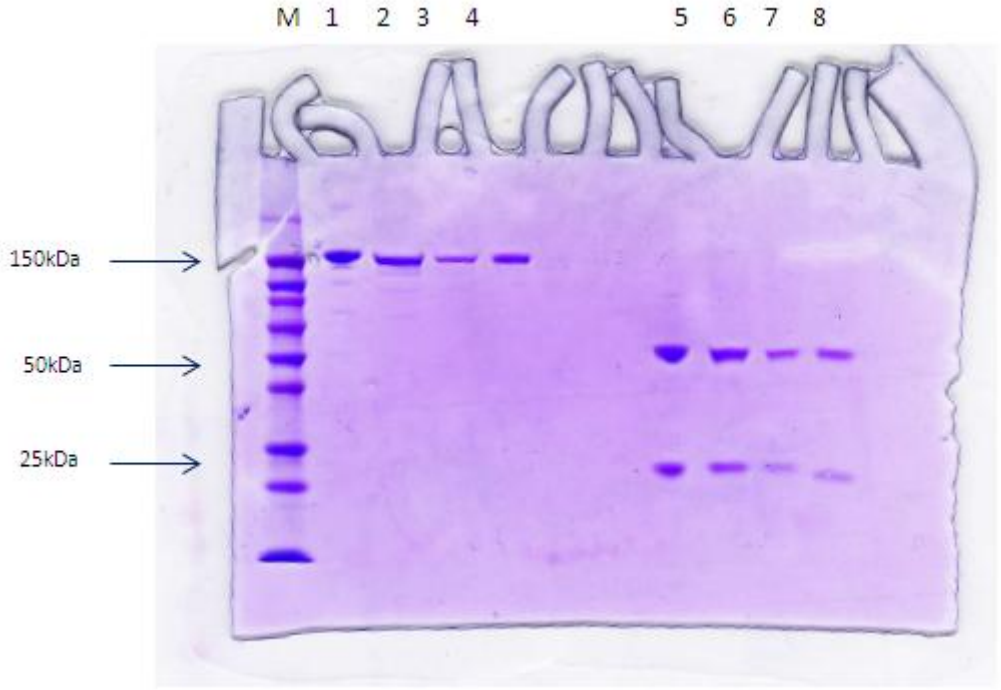

M = Marker (Novex Sharp Pre-stained Protein Standard, Invitrogen)
1 = Original Bevacizumab -
2 = Bevacizumab post encapsulation and release sample -
3 = Bevacizumab lyophilised before encapsulation -
4 = Positive Control (anti-VEGF, mIgG1) -
5 = Original Bevacizumab +
6 = Bevacizumab post encapsulation and release sample +
7 = Bevacizumab lyophilised +
8 = Positive Control (anti-VEGF, mIgG1) +
+/- = with or without mercaptoethanol

Figure 2.16 - Gel-electrophoresis was used to compare the original Bevacizumab to Bevacizumab which has been encapsulated and released from the microspheres. It can be seen that the original Bevacizumab, lyophilised Bevacizumab and Bevacizumab which has been encapsulated and released showed the same breakdown components with the same mobilities as the positive control anti-VEGF mIgG1. (Gel prepared by Chris Hughes, University of Southampton General Hospital)

To further investigate if the Bevacizumab was still active post-release from the microspheres, an enzyme-linked immunosorbent assay (ELISA) was undertaken (Figure 2.17). This showed that Bevacizumab was still active once released from the microspheres, with only a slight reduction in optical density (OD) compared to

unencapsulated Bevacizumab. Surprisingly the lyophilised Bevacizumab was also active once released from the microspheres, although a greater error was observed.

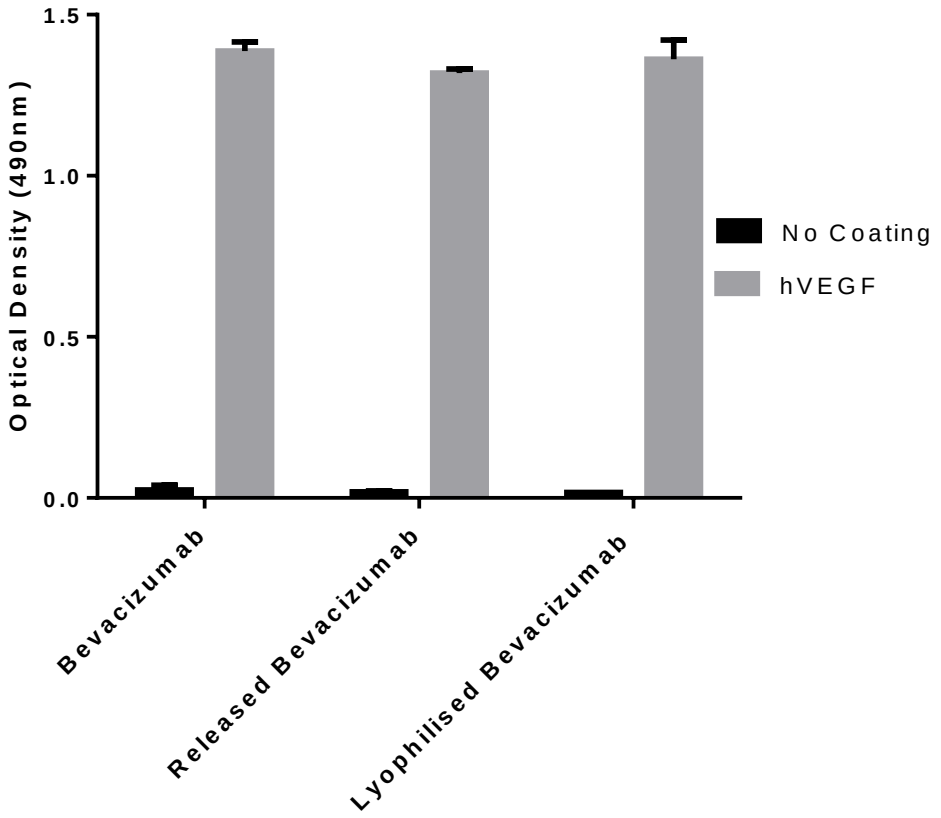

Figure 2.17 - ELISA comparing the activity of pure unencapsulated Bevacizumab to lyophilised Bevacizumab and to Bevacizumab which has been encapsulated and released from the microspheres over 80 days. Error bars refer to the standard deviation of samples performed in duplicate.

Another technique used to investigate activity was circular dichroism which can be used to examine the secondary structure and folding properties of proteins in solution[158]. Using circular dichroism, we could compare the α-helix, β-sheets and random coils present within the Bevacizumab antibody pre- and post-release. Viewing the circular dichroism spectrum of Bevacizumab released from the microspheres, we can see α-helix present below 220 nm and random coil present at higher wavelengths (Figure 2.18). Unfortunately the circular dichroism spectrometer at the University of Southampton required repair (a new lamp) between running samples and therefore the original Bevacizumab pre-release sample was sent to be

sampled at the University of Warwick. It appeared the sample had degraded during the time it was sampled, resulting in a poor spectrum being obtained which could not be used to compare to the post microsphere release sample obtained at Southampton (Appendix C). This would be an interesting area of further investigation so see if the secondary structure changes between the two Bevacizumab samples.

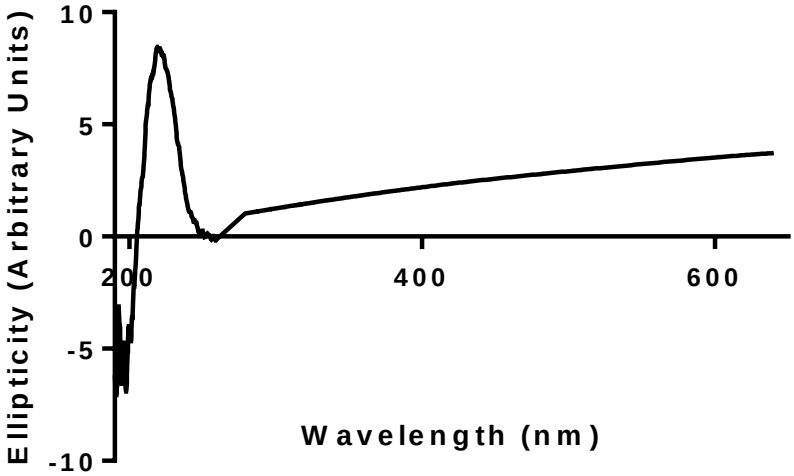

Figure 2.18 - Circular dichroism spectrum of Bevacizumab which has been encapsulated and released from the microspheres over 80 days.

Bevacizumab was shown to have a steady release after an initial burst stage and release could be sustained for around 70 days. This could allow for patients to be treated less frequently and with Bevacizumab which importantly is still active. A potential drawback with this method is that, as the dose of Bevacizumab is increased, encapsulation efficiency decreases. It appears that the microspheres become saturated and this could potentially limit increasing the 70 day release period of the Bevacizumab. Bevacizumab encapsulated and released is only a single dose, it will delay the time Bevacizumab is released into the eye and increase the time in which active Bevacizumab is present within the eye. This may be an effective treatment as it stands and this will need to be investigated further *in vivo*. Other drugs such as Lucentis® or VEGF trap-eye drugs would be of interest to investigate using this method, as better encapsulation or longer release may be obtained. In order to address the limit of the 70 day release period, surface-modified microspheres were investigated.

2.5 Investigating surface activation of PLLA:PLGA microspheres.

2.5.1 Activating the surface of PLLA:PLGA microspheres.

It was theorised that by modifying the surface of the microspheres, the initial burst release could be delayed or stabilised. The modified surface could extend the release or a secondary shell could be added to possibly increase the release of drugs and dyes. The first stage was to modify the surface to see what affect this had on the microspheres and to provide a method to attach other polymers, biologicals/proteins or small molecules. Two methods were utilised to activate the surface of the microspheres, one made use of sodium hydroxide to break the polymer structure of the microspheres to form an acid group which could be reacted further (Scheme 2.2A). The second route made use of a diamino linker, which would activate the surface to give a free amine which could be reacted further (Scheme 2.2B).

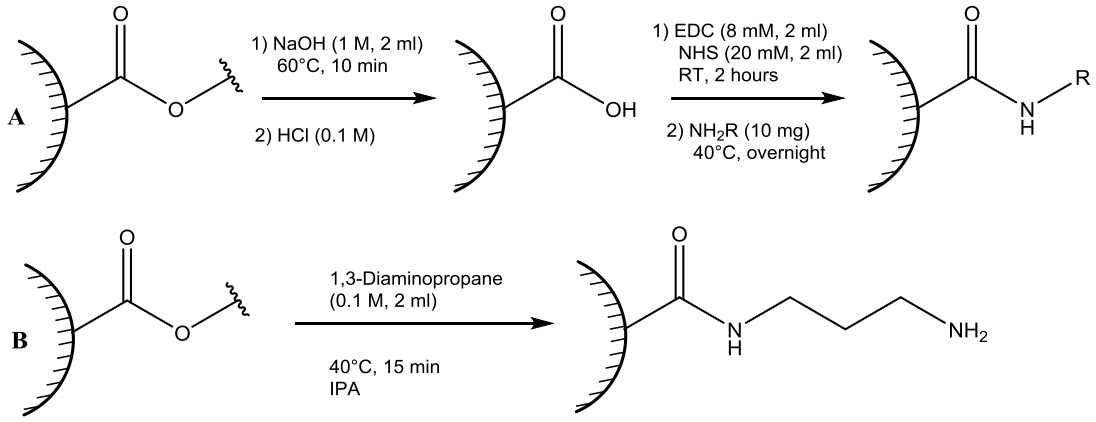

Scheme 2.2 - Two routes exploited to activate the surface of the microspheres.

It was observed that when sodium hydroxide was used the microspheres appeared to lose their shape under SEM (Fig. 2.19). This is likely due to the basic conditions breaking down the PLGA/PLLA polymers into the corresponding acids (Method A, Basic conditions, Scheme 2.2). The conditions however, appear to be too harsh and the microsphere morphology is lost (Fig. 2.19A). Method B using a diamino linker approach (aminolysis) to activate the surface appeared to retain the microsphere morphology by SEM (Fig. 2.19B).

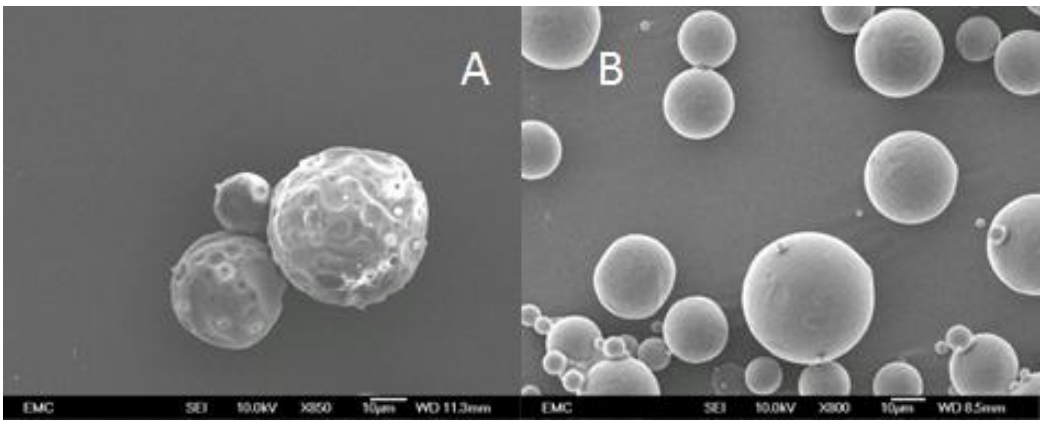

Figure 2.19 - Scanning electron micrographs of the surface activated microspheres. (A) Sodium hydroxide base method, original magnification x 850; (B) Diamino surface activation method (aminolysis), original magnification x 800.

Once the surface of the microspheres was activated, the number of amine groups on the surface was investigated. Using the Orange II dye the number of free amines on the surface could be calculated (Scheme 2.3). This was achieved by adding the Orange II dye in an acidic solution to the amine-coated microspheres and forming an ion pair with the free amines. The spheres were then vigorously washed with water several times in order to remove any dye which was not paired with an amine. To the microsphere/dye solution, sodium hydroxide was added to neutralise the solution and break down the ion-pair. To calculate the concentration of the unpaired Orange II dye UV-Vis spectrometry was used, measuring at 484 nm against a calibration curve. Assuming that there was a 1:1 ion pairing, the concentration of the amines on the surface could be calculated. Using this method, a calculated 37.1 μmol g^{-1} amine molecules are present on the surface of the microspheres. The same batch of microspheres could then be reacted further with FITC before being reacted with Orange II dye again (Scheme 2.3B). As the FITC is covalently bonded to the amines on the surface these amines will not be able to ion pair with the dye, only any remaining free amines will react. After washing away any unpaired dye and releasing the Orange II dye using sodium hydroxide, the percentage of amines which did not react with the FITC could be calculated. Using this approach it was calculated that 97.4% of the amines reacted with the FITC, showing excellent surface attachment was achieved. When the same reaction was undertaken with

Orange II on microspheres which did not undergo activation with diaminopropane no attachment of the dye was observed.

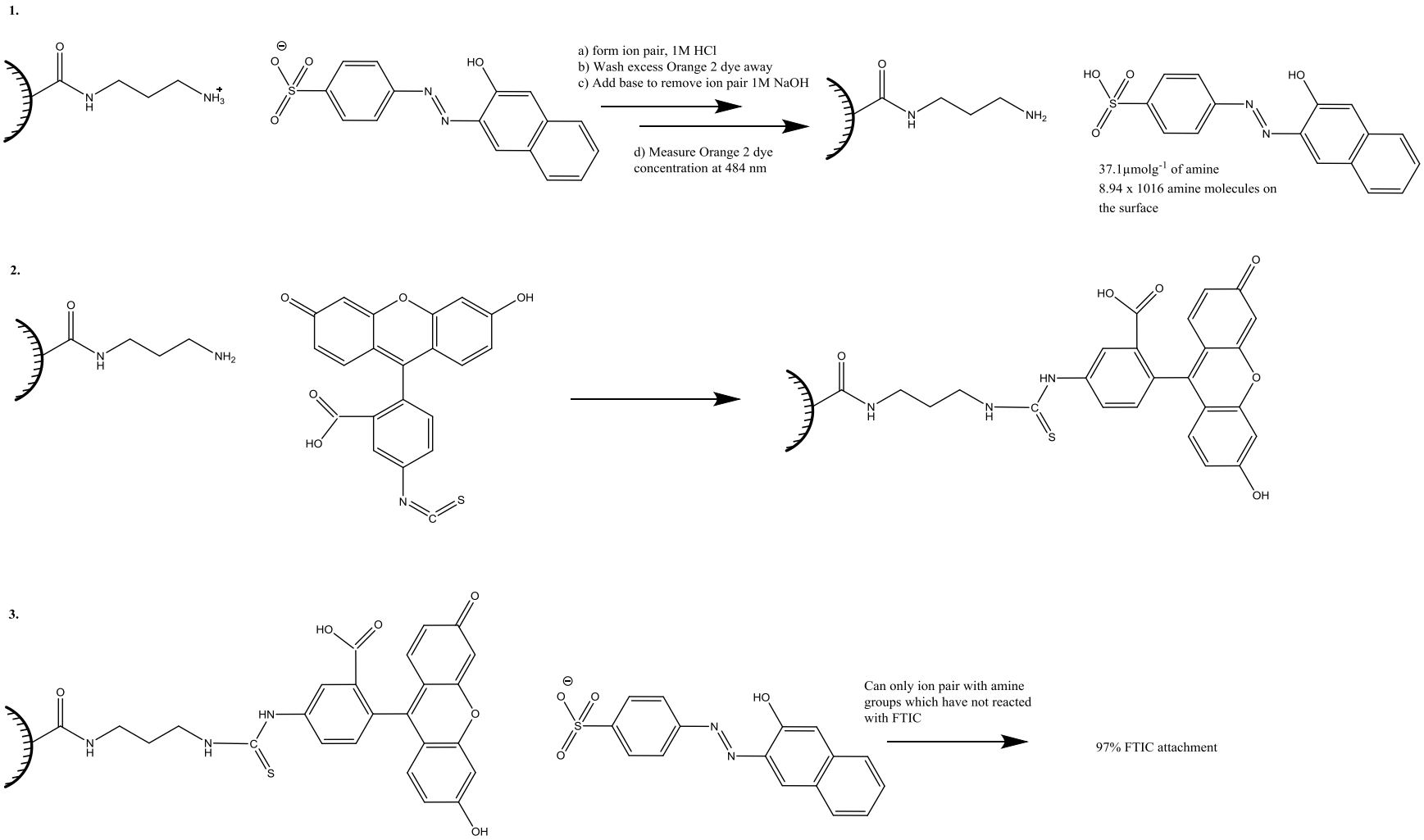

Scheme 2.3 - Use of Orange II dye to investigate surface activation

NMR was used to further probe attachment of both the sodium hydroxide and diamino-activated microspheres attached to Fluorescein. Method A (Basic conditions) using the sodium hydroxide approach was reacted using peptide coupling conditions with Fluoroeseinamine to attach Fluorescein to the surface. The diamino activated microspheres (aminolysis method) were reacted with Fluorescein isothiocyanate to attach Fluorescein to the surface. The microspheres were then dissolved in chloroform and an NMR spectrum was obtained, however as might be expected the PLGA/PLLA polymer peak intensities overshadowed the Fluorescein peaks even with optimised parameters. The same problem was observed with IR and UV-Vis spectrometry with no Fluorescein being observed. Using a fluorescence spectrophotometer (Cary Eclipse) an excitation wavelength (494 nm) could be pulsed onto the microspheres and if Fluorescein was attached to the surface the emission could be recorded. Using the fluorescence spectrophotometer both the sodium hydroxide and diamino surface activated microspheres with a Fluorescein marker attached were analysed, however only the diamino activated-Fluorescein attached microspheres produced a result (Figure 2.20). The emission spectrum of Fluorescein which is attached to the surface of the microspheres can be seen from the input excitation wavelength of 494 nm, which was not observed with the sodium hydroxide-activated (Method A) microspheres.

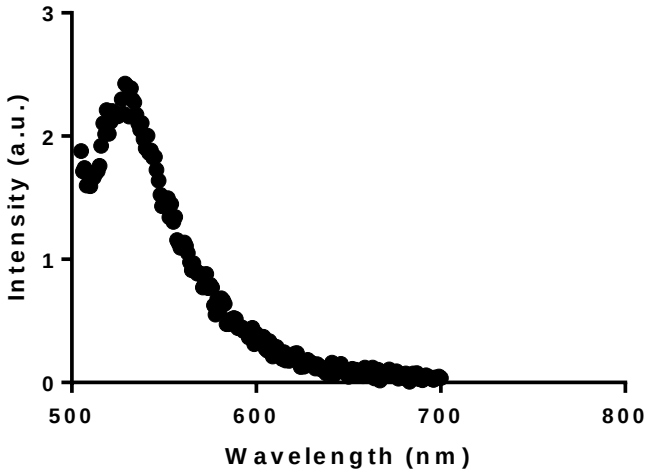

Figure 2.20 - Fluorescence spectrophotometry spectrum from aminolysis activated activated-Fluorescein attached microspheres. The spectrum shows the emission spectrum of Fluorescein attached surface of the microsphere after excitation at 494 nm.

Another approach involved the use of confocal microscopy to image the microspheres, enabling us to see if any Fluorescein had attached to the surface (Figure 2.21). The fluorescence of the Fluorescein can be observed in the images and at the edges of the microspheres a more intense colour is observed. This argues that the Fluorescein is attached at the surface and not encapsulated within the microspheres, as at the edges of the microspheres they are observed from their side and layers on top of each other are observed, increasing the intensity of the colour. If the Fluorescein was encapsulated the middle of the microspheres this should show the highest intensity of colour as this would be the thickest point on the microspheres. This fluorescence at the edge of the microspheres was not observed with the sodium hydroxide-activated microspheres. Although they appeared slightly yellow by eye, only poor images were obtained.

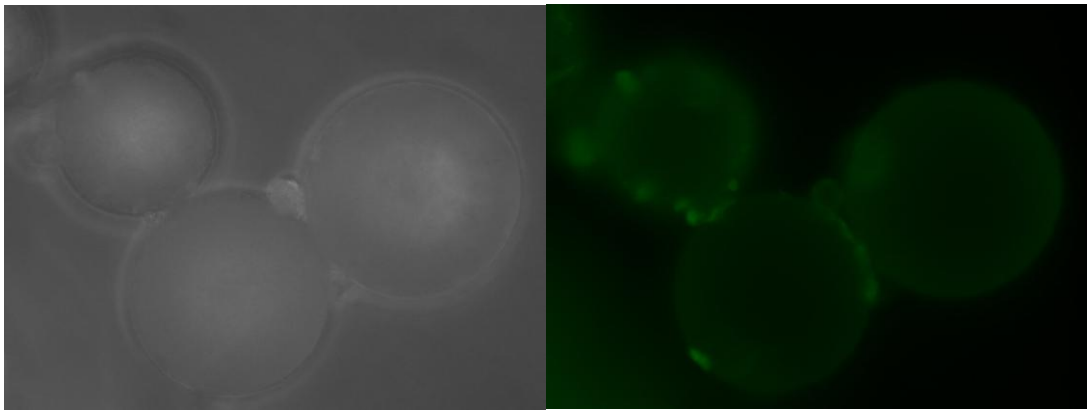

Figure 2.21 - Confocal microscopy image from method B, diamino activated-Fluorescein attached microspheres, showing a more intense florescence at the edges of the microspheres.

An attempt to probe into what was happening on the surface of the microspheres was investigated by NMR spectroscopy (Figure 2.22). An NMR spectrum was obtained at 1, 2 and 20 minutes after addition of 1,3-diaminopropane and it can be seen that the peak present assigned to the PLGA is gradually becoming reduced. This is because the PLGA polymer is being broken down to its corresponding acid and diaminopropane amide. It can be seen that the ratio of the PLLA peak to the PLGA peak decreases from 1:0.25 to 1:0.18 after 1 minute and after 20 minutes the PLGA peak has disappeared. To investigate whether only PLGA reacted with the diaminopropane or if this process was just faster than that for PLLA the Orange II test was utilised. Using 50:50 PLLA:PLGA, 100% PLLA and 100% PLGA microspheres, the Orange II dye was added to see how many amine groups were present after reacting the microspheres under the same aminolysis conditions (1,3-diaminopropane, Methanol, 37 ^{O}C, 15 min). This confirmed that it was only PLGA reacting as after 15 minutes the 100% PLLA microspheres showed no amine groups present, which suggests no breakdown of the PLLA polymer into the corresponding acid had occurred. On the other hand PLGA had 48.6 µmol g^{-1} amines present which was an increase on the 30.9 µmol g^{-1} present on the 50:50 microspheres.

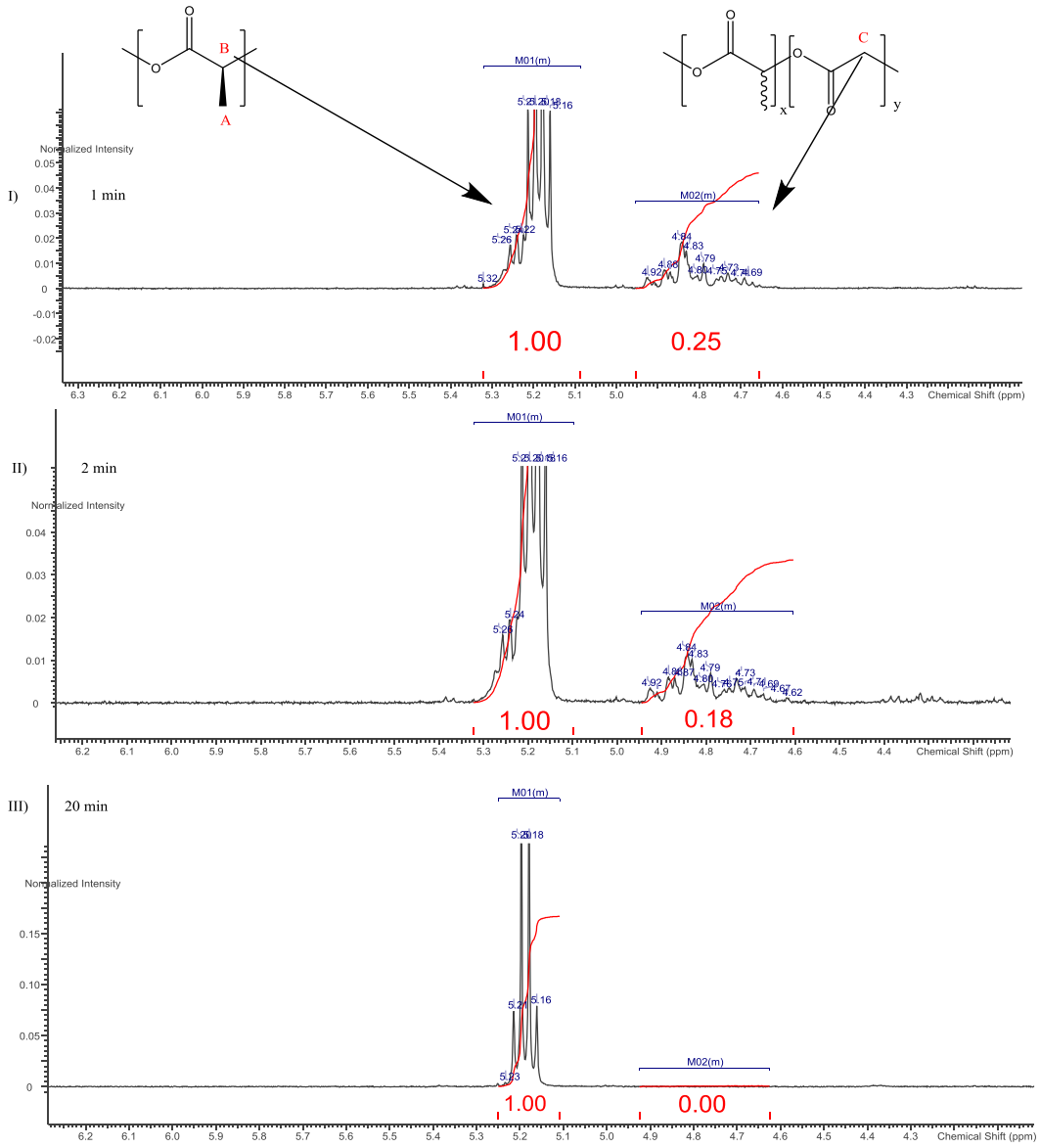

Figure 2.22 - NMR spectra of 50:50 PLLA:PLGA microspheres reacting with 1,3-diaminopropane in methanol over: I) 1 minute; II) 2 minutes and; III) 20 minutes.

This lack of breakdown with the PLLA microspheres could be due to the increased crystallinity of the L-Lactide polymer. SEM was used to confirm these studies and it can be clearly seen that the PLLA microspheres remain fully intact compared to the 100% PLGA microspheres which had broken down (Figure 2.23).

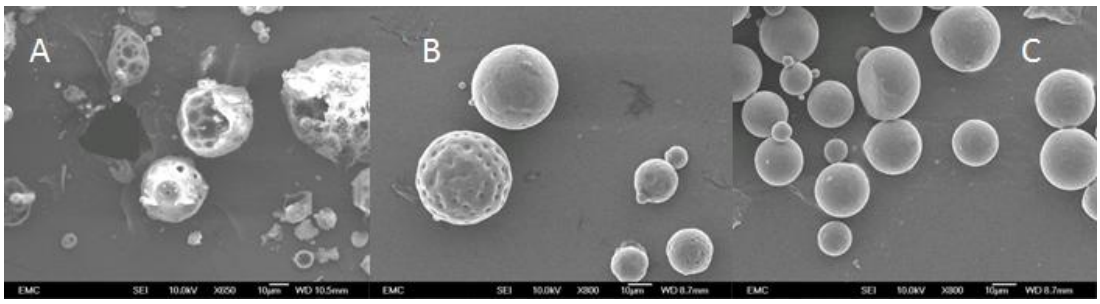

Figure 2.23 - Scanning electron micrographs of the microspheres under aminolysis conditions (1,3-diaminopropane, methanol, 37 ^{O}C, 15 min): (A) 100% PLGA, original magnification x 650; (B) 50:50 PLLA:PLGA, original magnification x 850; (C) 100% PLLA, original magnification x 850.

The conditions for amine surface attachment were optimised to allow the greatest surface coverage of the amines without significantly breaking down the microsphere structure. The relative number of amine groups on the surface were investigated using three different solvents: methanol, ethanol and isopropyl alcohol (IPA)[159]. Using these three solvents, a study was undertaken to determine the rate at which aminolysis occurred (Figure 2.24). Rhodamine B was encapsulated within the microspheres and this was used to measure microsphere degradation over time and indirectly how much surface coverage was obtained. Experimental details are described in Chapter 6; briefly, the Rhodamine-encapsulated microspheres were added to the aminolysis conditions with either methanol, ethanol or isopropyl alcohol and removed at set time points and washed with water to stop any further reaction. The microspheres were centrifuged and the supernatant was measured using UV-Vis spectrometry to determine the percentage of Rhodamine released. Methanol gave the greatest Rhodamine release (Figure 2.24) and therefore indirectly suggested the most amines were on the surface (this was confirmed by the Orange II test against ethanol and IPA after the same time periods); however the SEM shows that the microspheres had been destroyed (Figure 2.25).

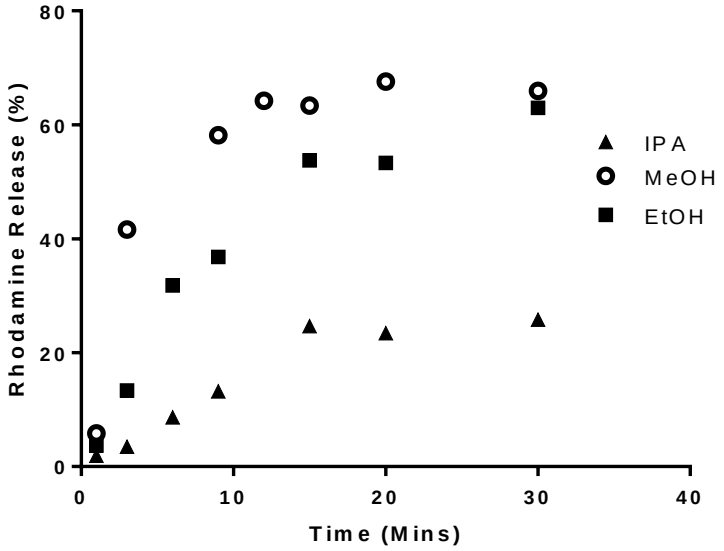

Figure 2.24 - Graph showing Rhodamine release from Rhodamine-encapsulated microspheres added to the aminolysis conditions in the presence of either methanol, ethanol or isopropyl alcohol as solvent.

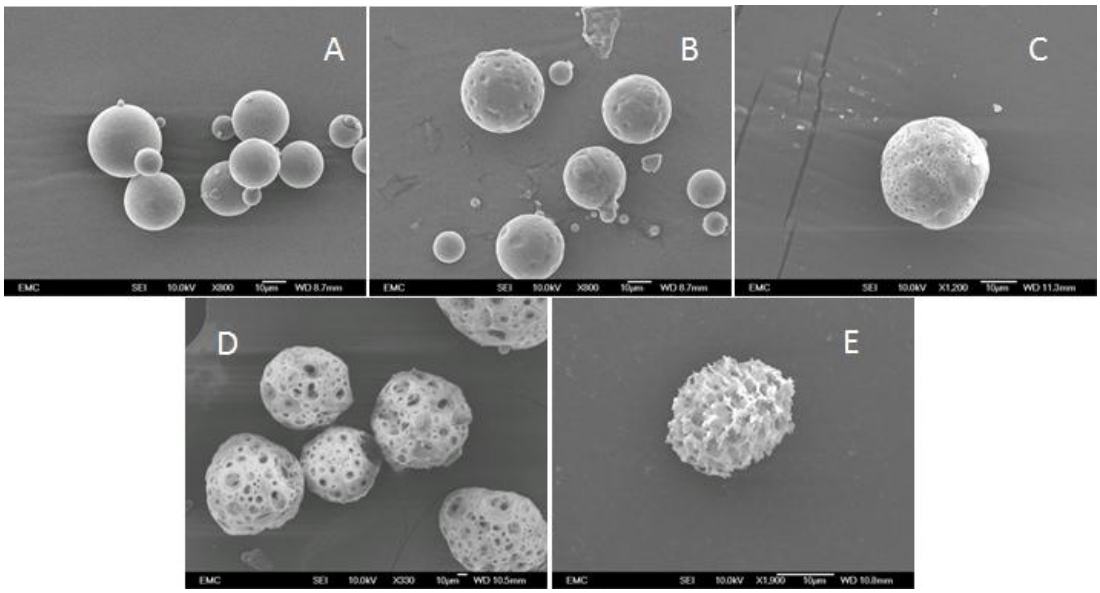

Figure 2.25 Scanning electron micrographs of the 50:50 PLLA:PLGA microspheres under aminolysis conditions over time (1,3-diaminopropane, Methanol, 37 ^{O}C): (A) 1 minute, original magnification x 800; (B) 9 minutes, original magnification x 800; (C) 12 minutes, original magnification x 1, 200; (D) 20 minutes, original magnification x 330; (E) 30 minutes, original magnification x 1, 900

From the SEM pictures the extent of the degradation to the microspheres can be seen. The linker also plays an important role in the rate of polymer breakdown and rate of amine attachment, as described in previous studies[159]. 1,2-Diaminoethane was used as a comparison to 1,3-diaminopropane but after 2 minutes in methanol as the solvent the microspheres were highly degraded. Longer diamino linkers attach slowler and further work of interest would be to investigate these longer linkers and see what affect this change has on amine attachment and polymer degradation rate.

2.5.2 Attachment of proteins and polymers onto the surface of PLLA:PLGA microspheres.

It was decided that the aminolysis conditions using IPA for 15 minutes would be optimal for good surface activation without excessively degrading the microspheres and this was used for further reactions. Further modification of the surface is of interest to establish whether release rates could be extended for delivery of drugs and dyes. After surface activation using a 15 minute IPA aminolysis reaction, the natural proteins laminin, collagen and fibronectin were attached to the surface. This was acheived by mixing the protein with the diaminopropane-attached microspheres before 1-ethyl-3-(3-dimethylaminopropyl)carbodiimide (EDCI) was added and then the mixture was left overnight. ^{1}H and ^{13}C NMR spectra were obtained for all three peptide-functionalised microspheres, however no peptide was observed, possibly due to the strength of the PLLA/PLGA polymer signals.

The proteins laminin, collagen and fibronectin were selected for use as a secondary layer on the microspheres because they are naturally found within the body and should not cause any immune or biological responses. In view of the difficulty of definitively saying that surface attachment had occurred, Rhodamine-encapsulated microspheres were treated under aminolysis conditions before either laminin, collagen or fibronectin was attached. The Rhodamine release rates were then investigated, firstly to see if a change in rate had occurred from previously unaltered Rhodamine microspheres, therefore giving indirect evidence that attachment had occurred and secondly to see if the initial burst effect was delayed or longer release rates could be obtained before trying to use this approach with other molecules or drugs such as Bevacizumab. The protein-attached microspheres show a longer release profile in comparison with that for the 50:50 PLLA:PLGA microspheres,

giving increased evidence that they have attached to the surface. The release profiles themselves are very interesting as all three peptides provide a longer release period for Rhodamine than the 50:50 microspheres, with the best protein, fibronectin, giving a release time of around 155 days (Figure 2.26). It is difficult to say if fibronectin provides longer release times than collagen and laminin as the surface coverage and attachment may have been larger for these microspheres. The same batch of microspheres was used for all three protein attachments, therefore the number of amines present on the surface after aminolysis should have been similar for all three protein-coated microspheres. To confirm how much protein had attached proved difficult, as the Orange II dye would react with the proteins therefore could not be used to investigate surface coverage. All three protein coated microspheres did have longer release profiles but not all of the Rhodamine which was encapsulated was released. To check Rhodamine was still not leaching out, the samples were checked over a period of 220 days and no Rhodamine was observed. For comparison the microspheres which had been reacted under aminolysis conditions but not reacted further with proteins were kept under the same conditions. A rapid release of Rhodamine was observed, probably as a result of the breakdown of the microspheres under these aminolysis conditions.

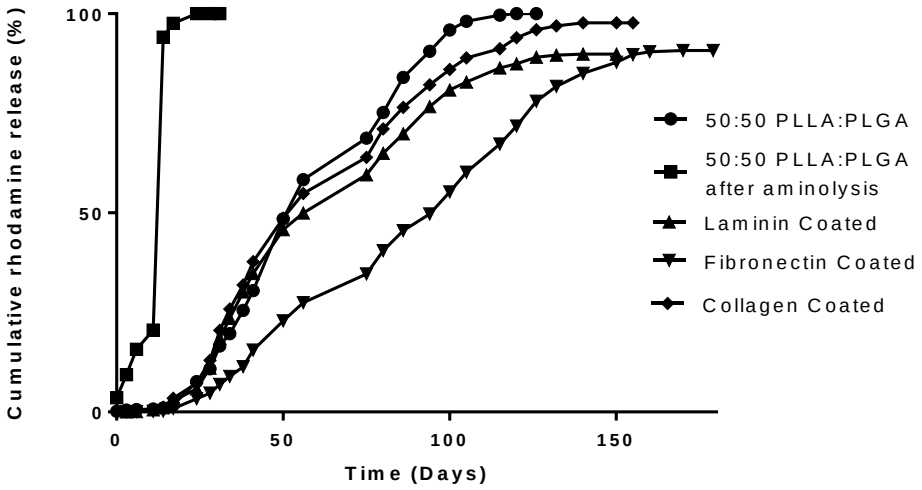

Figure 2.26 - Graph showing Rhodamine release from protein-coated Rhodamine-encapsulated microspheres.

Under SEM, the morphology of the protein-coated microspheres were seen to have changed and although it cannot be said this is due to attachment, it is an interesting

observation (Figure 2.27). The microspheres appear to differ from both the 50:50 PLLA:PLGA microspheres and the microspheres which had been reacted under aminolysis conditions (Figure 2.25). These protein-coated microspheres were also investigated for RPE cell growth and this is discussed in detail later (Surface active agents, Chapter 5).

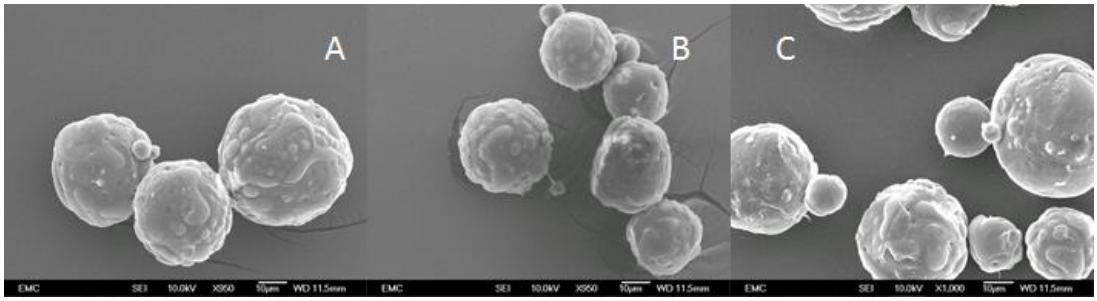

Figure 2.27 - Scanning electron micrographs of the protein-coated microspheres: (A) Fibronectin-coated microspheres, original magnification x 950; (B) Laminin coated-microspheres, original magnification x 950; (C) Collagen-coated microspheres, original magnification x 1, 000.

2.5.3 Use of polyoxazolines as a secondary shell on the microspheres for delayed release.

In order to investigate the surface attachment and the secondary layer concept, the use of synthetic polymers was then examined. Polyoxazolines were the initial choice as ethyl polyoxazoline is FDA approved[160] and the side chain of the polymer can be easily changed, allowing the polymers to be made hydrophilic or hydrophobic as required. They are also of interest because of the thermoresponsive properties that they exhibit which could be utilised in further work. The ring opening method used to prepare these polymers allows the chain length to be selected with low polydispersity and the termination step should allow for ideal attachment to the amine surface on the microspheres (Scheme 2.4).

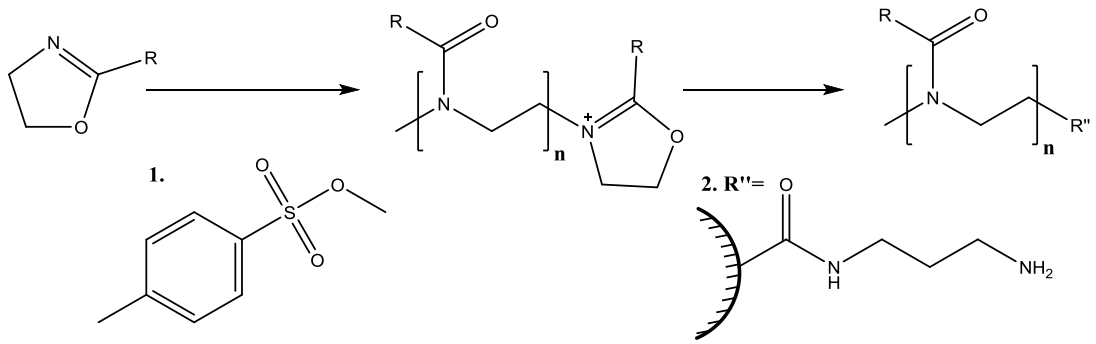

Scheme 2.4 - Initial unsuccessful route for attachment polyoxazoline polymers to the surface of the microspheres.

The reaction proved to be problematic because of the final termination step. In the termination step, the polymer can be capped by alcohols, amines, acids or water so this reaction is carried out in a minimum amount of acetonitrile and is then capped immediately by one of these functional groups. Because the final polymer solution is highly concentrated, it acts like an organic solvent when the microspheres are added, dissolving the microspheres. Using solvents in which the microspheres are insoluble (eg. water, alcohols), the polymer solution is simply terminated resulting in formation of the standard polymer with little or no attachment to the microspheres.

An alternative approach utilising guest-host complex chemistry was investigated in collaboration with Adam Fisher who had been doing similar work with polyoxazolines on glass surfaces. Cyclodextrin was attached to the surface of the microspheres by reaction with the amines on the surface using coupling conditions (10 mg EDCI, carboxymethyl-β-cyclodextrin sodium salt 10 mg, in H_2O mixed for 1h before addition to aminolysed microspheres). Excess cyclodextrin and EDCI was then removed by several washes. The complementary polyoxazoline polymers were produced as before but with an adamantane group used as the initiator and Rhodamine B used as the termination step (see Figure 2.28).

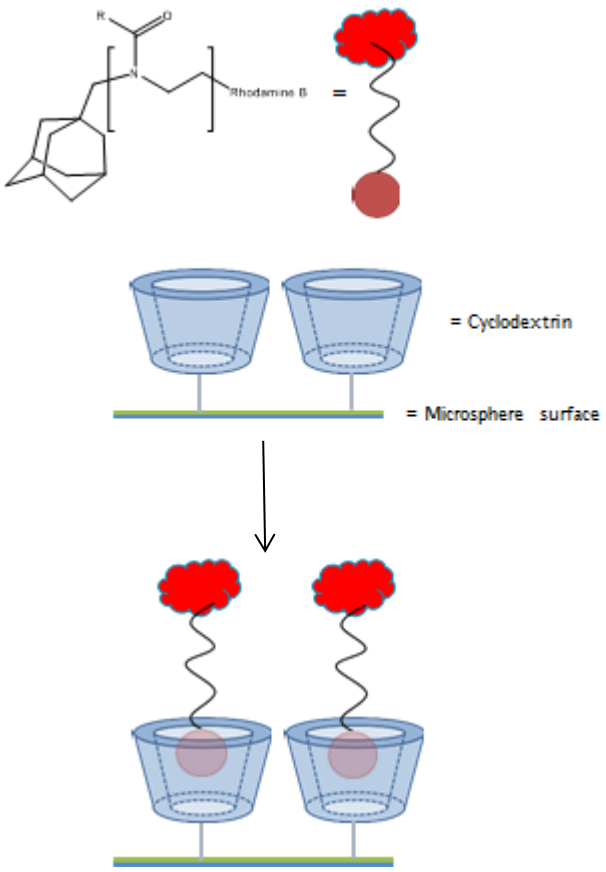

Figure 2.28 - Pictorial representation of host-guest microspheres. Adamantane/polyoxazoline/Rhodamine polymer complexes with cyclodextrin surface-coated microspheres in aqueous solutions.

When these were added in water, the adamantane terminus should complex within the cyclodextrin cavity creating a secondary layer around the microspheres. To confirm that guest-host complex formation was occurring, one batch of microspheres was reacted under aminolysis conditions before being split into two batches. The first batch was left as the amine surface (Figure 2.29 batch A). The second batch was reacted with cyclodextrin (Figure 2.29 batch B). The two batches were kept separately but treated identically. The adamantane/polyoxazoline/Rhodamine polymer was added to the microspheres and the mixture was stirred for 30 minutes. The two lots were then centrifuged and washed 5 times to remove any unreacted polymer within the supernatant. It can clearly be seen that the microspheres with the cyclodextrin-functionalised surface (Figure 2.29 batch B) have reacted with the adamantane/polyoxazoline/Rhodamine polymer while the unreacted non-cyclodextrin functionalised surface coated microspheres (Figure 2.29 batch A) have

just been retained (Figure 2.29). The reaction was repeated with adamantane attached to the surface and cyclodextrin attached to the polyoxazoline backbone but no complex formation was observed.

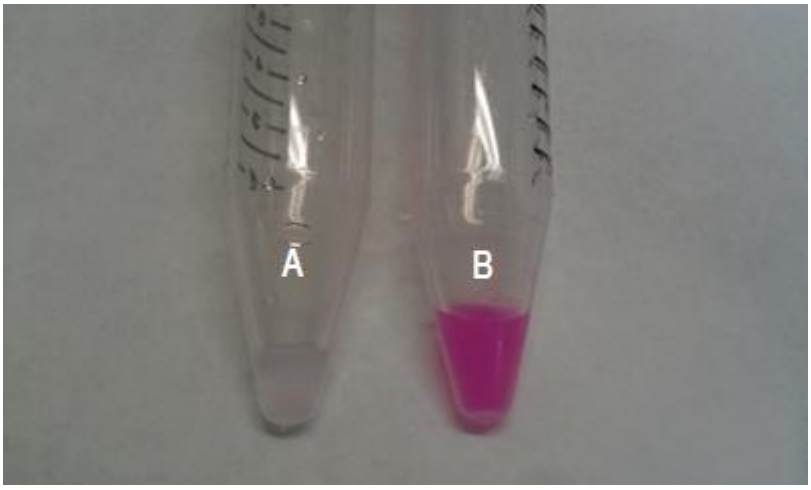

Figure 2.29 - Reaction of activated microspheres with adamantane/polyoxazoline/Rhodamine polymer: (Left, A) Non-cyclodextrin functionalised microspheres after addition of adamantane/polyoxazoline/Rhodamine polymer and washing; (Right, B) Cyclodextrin-functionalised microspheres after addition of adamantane/polyoxazoline/Rhodamine polymer and washing. It can clearly be seen that the adamantane/polyoxazoline/Rhodamine polymer is still present on the Cyclodextrin-functionalised microspheres. Note: when the tubes are centrifuged down the pink microspheres appear at the bottom of the tubes with the supernatant remaining clear, showing the polymer/dye is attached to the microsphere and not in solution.

This approach was investigated by NMR analysis but with no dye attached to the polyoxazoline polymers. After adamantane initiation and chain growth steps, the polymers were simply capped with water. No cyclodextrin resonances were observed on the surface of the microspheres by NMR, as might be expected, the spectrum being dominated by PLLA:PLGA polymer peaks. When the adamantane-polyoxazoline polymers were complexed with the microspheres, only the isopropyl polymer was detected by NMR (Figure 2.30). However this does not necessarily mean the other polymers failed to complex, but could be due to the intense PLLA:PLGA polymer peaks hiding the data. It was also observed that the methyloxazoline polymer-coated microspheres were very difficult to dissolve in

$CDCl_3$ which also suggests that attachment has occurred as the PLLA:PLGA microspheres readily dissolve in chloroform whereas the methyloxazoline polymer does not. Therefore the insolubility of the complex is consistent with the presence of a methyloxazoline polymer surface coating on the microspheres. By SEM, the surface of the microspheres appear different and a rougher surface appearance is evident (Figure 2.31).

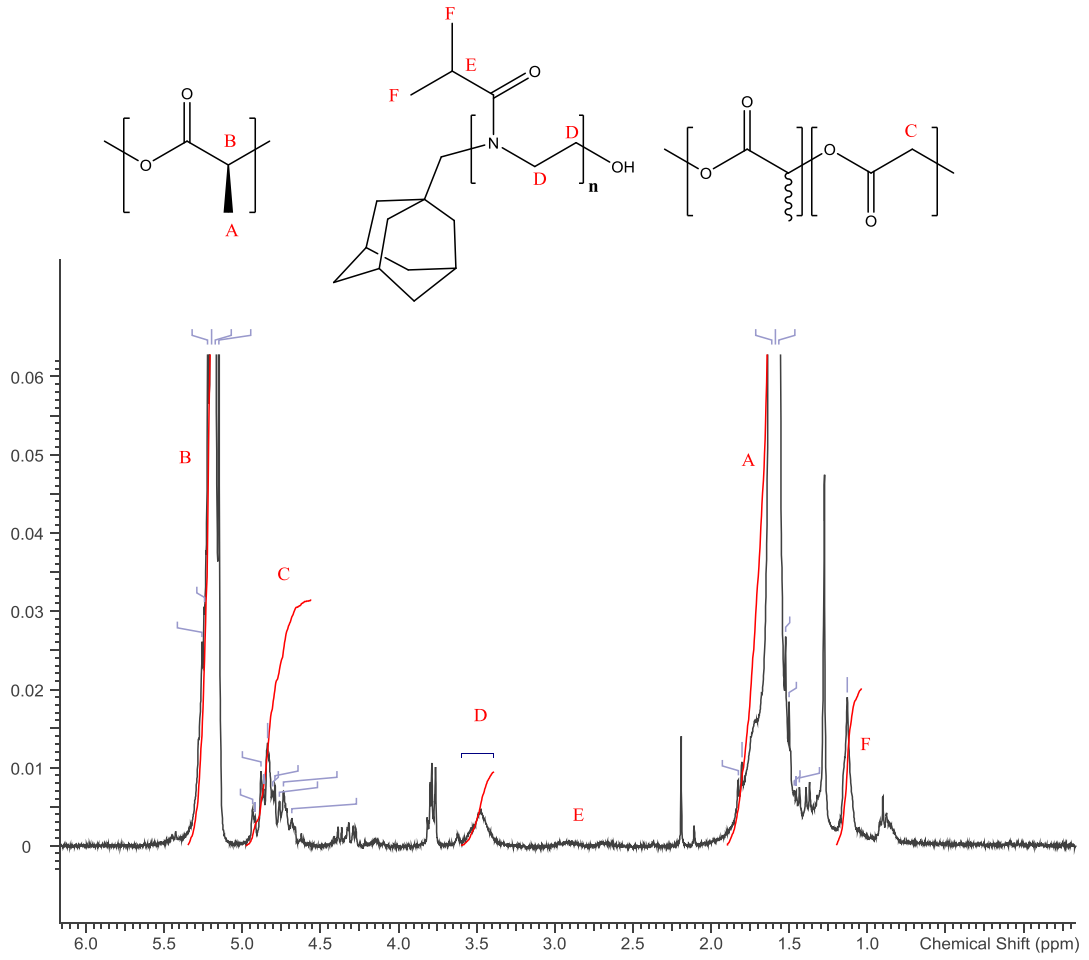

Figure 2.30 - NMR spectrum of isopropyloxazoline polymer surface attached microspheres. There are a few impurities present but the distinctive peaks on the back bone of the oxazoline polymer (D) can be observed at around 3.5 ppm. The large PLLA:PLGA peaks can be observed and there is some PLGA present as the aminolysis was not taken to completion in order to maintain the microsphere shape.

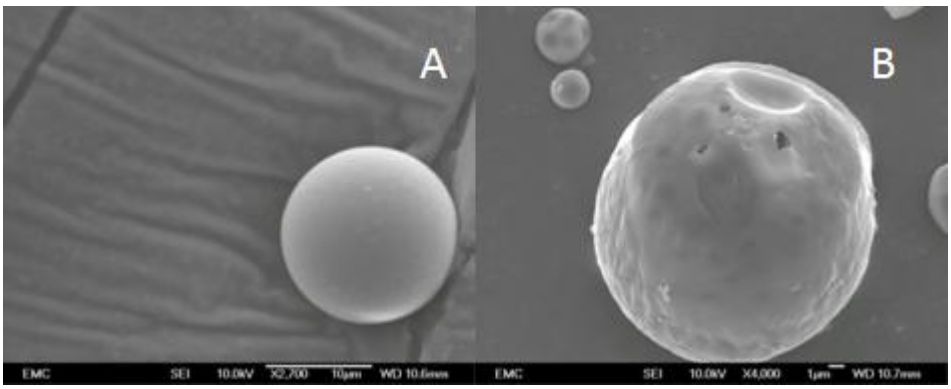

Figure 2.31 - Scanning electron micrographs of the ethyloxazoline-surface attached microspheres: (A) 50:50 PLLA:PLGA microspheres before ethyloxazoline attachment, original magnification x 2, 700; (B) Ethyloxazoline-surface attached microspheres, original magnification x 4, 000.

2.5.4 Investigating the release properties of surface coated PLLA:PLGA microspheres.

The final investigation involved the use of Rhodamine-encapsulated 50:50 PLLA:PLGA microspheres and an assessment of how the secondary polyoxazoline coating would affect release (Figure 2.32).

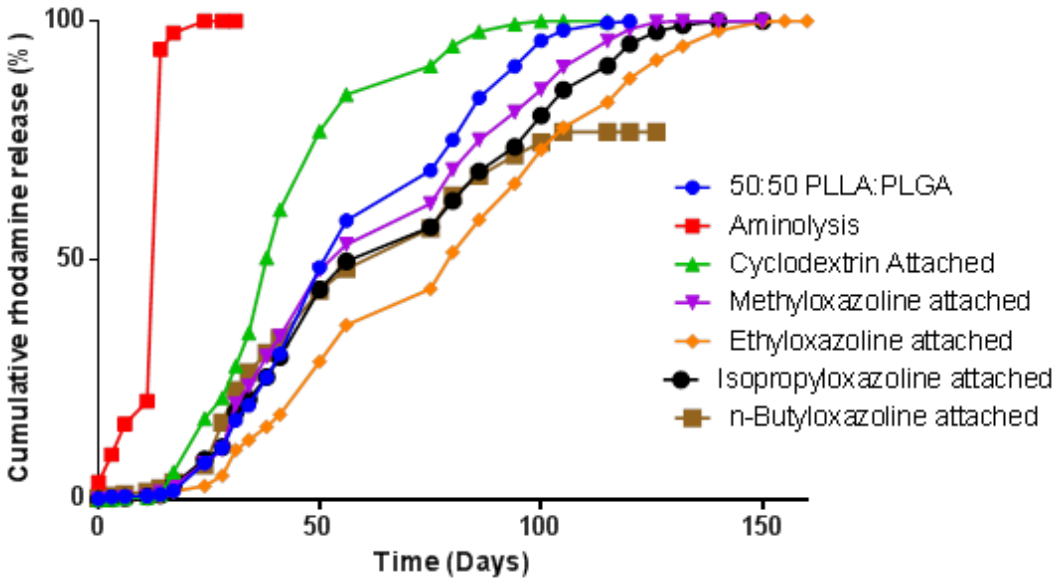

Figure 2.32 - Rhodamine release rates from polyoxazoline-coated Rhodamine encapsulated microspheres.

All coated microspheres give a slightly longer release period than the 50:50 PLLA:PLGA microspheres, with the ethyl oxazoline-coated microspheres giving release up to 145 days. This provides additional evidence that the surface has been modified, with the release being constant and with no large release initially ("burst") as was observed in other cases. The microspheres which have the cyclodextrin covered surface with no polymer attached give a sudden release around 14 days for a short period of around 35 days. This could be useful for other applications which may require a large release after a set time point, or they could be used in conjunction with other microsphere types. The butyloxazoline microspheres were difficult to get into solution and floated, probable reflecting to the hydrophobic nature of the polymer. They did not give a full release, however this hydrophobic behaviour agrees with the butyl polymer being attached to the microspheres as the cyclodextrin-coated microspheres did not exhibit this behaviour.

Zeta potentials were obtained in order to understand how the microspheres may interact within the back of the eye. The Zeta potential can be used to understand colloid stability as it is a measure of electric potential difference across the ionic layers surrounding a charged particle[70]. The higher the potential in mV (either positive or negative), the more stable the colloid solution will be. If the Zeta potential equals zero the colloid will precipitate out of solution[70]. Using a Zetasizer Nano ZS (Malvern Instruments, UK), the Zeta potential can be used to see if any changes have occurred due to the activation and subsequent reaction on the surface of the microspheres. The information is also useful to see how the microspheres might act within the eye, as a stable colloid would be preferred, preventing the microspheres from aggregating together within the eye.

Table 2.10 - The Zeta Potentials and electric mobilities of 50:50 PLLA:PLGA microspheres with different surface coatings and encapsulations.

Microsphere	Zeta Potential (mV)	Standard Deviation[a]	Electrophoretic Mobility (µmcm/Vs)	Standard Deviation[a]
50:50 PLLA:PLGA	0.64	1.02	0.05	0.08
Bevacizumab encapsulated 50:50 PLLA:PLGA	-0.25	0.08	-0.02	0.01
Laminin coated 50:50 PLLA:PLGA	-37.40	2.90[b]	-2.93	0.23[b]
Methyloxazoline coated 50:50 PLLA:PLGA	-35.80	2.46	-2.80	0.19
50:50 PLLA:PLGA Nanospheres	-27.40	10.50	-2.15	0.82

[a]Data expressed as mean ± S.D. (number of samples run = 5). [b]Data expressed as mean ± S.D. (number of samples run = 3).

A zeta potential above the value of 25 mV (either positive of negative) generally results in stability for colloids (Table 2.10). The 50:50 PLLA:PLGA microspheres have a very low zeta potential and they do not form colloids in solution, agitation being required to keep them from sinking in solution. The encapsulation of Bevacizumab does not affect the Zeta potential greatly and this may be problematic within the eye. The coated microspheres have a far larger Zeta potential and gives further evidence attachment has occurred. The hydrophilic nature of the methyloxazoline polymer and the laminin may result in the larger potential. Using a surface coating could allow the Bevacizumab-encapsulated microspheres to have a different zeta potential and possibly act more like a colloid, which would be interesting for future investigations. The size of the particle appears to play a role as the nanospheres also have a larger zeta potential than the chemically similar 50:50 PLLA:PLGA microspheres.

To assess the feasibly of an injection of microspheres into the eye, Fluorescein encapsulated 50:50 PLLA:PLGA microspheres were injected into the cavity of a rabbit's eye (this was undertaken by Dr. Philip Alexander at the University of

Southampton General Hospital) and the results are shown in Figure 2.33. In the bottom right of the picture Figure 2.33A shows the optic disc during subretinal injection. The optic disc is in focus which is why the microspheres are out of focus. Figure 2.33B shows the microspheres in focus. Importantly the microspheres shown have moved from the subretinal space into the vitreous cavity. To aid viewing of the microspheres within the eye for future studies, Fluorescein had been encapsulated (Figure 2.33C). The microspheres are biocompatible as shown in previous studies[99] however, inflammation and immune response could still occur. The rabbits were viewed every 2 weeks to check on the eye health and no inflammation was observed. The injection gave positive and effective results for delivering the microspheres with no issue arising because of needle blockage or adverse effects occurring with the eye due to the size of needle or technique. Studies to investigate the degradation and movement of the microspheres are on-going. Planned future work involves use of the Bevacizumab-encapsulated microspheres and how release rates are affected *in vivo.* Arg-Gly-Asp-Ser (RGDS)- laminin- and fibronectin-coated microspheres are to be investigated to see if any immune response is observed within the rabbits. The laminin, fibronectin and collagen surface attached microspheres were investigated for cell growth within the surface active agents chapter within this thesis. The laminin, fibronectin and collagen surface attached microspheres were compared to RGDS coated microspheres and a control to see if the microspheres biocompatibility is improved with the surface coating.

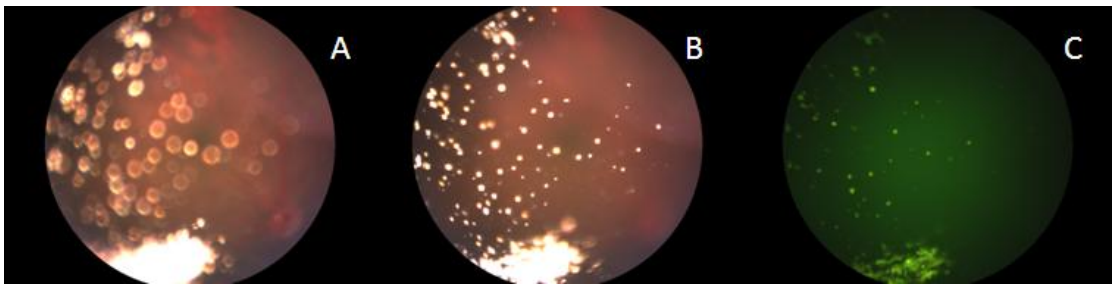

Figure 2.33 - Images of Fluorescein-encapsulated 50:50 PLLA:PLGA microspheres which have been injected into the cavity of a rabbits eye: A) Image of the optic disc in the bottom right of the picture; B) Image of the cavity of the eye; C) Image of the cavity of the eye under UV light. Microspheres are clearly separated and have moved away from the injection site.

Importantly the microspheres show no immune response, with Bevacizumab being successfully encapsulated and released without any loss in Bevacizumab activity. Activation and coating of the microspheres has shown to improve the colloidal properties of the microspheres and extend the release period of encapsulated dyes. This work can now be used to see if extended Bevacizumab release can be obtained and if the zeta potentials of the Bevacizumab-encapsulated surface coated microspheres differ from the standard Bevacizumab-encapsulated microspheres.

3. Fibres

3.1 Introduction

Various methods have been utilised for RPE cell growth on to surfaces and these approaches can be applied and adapted for treatment of AMD[101]. Using electrospun fibres of poly-MMA:PEGM, RPE cells can grow and proliferate. However when these fibres are capped with an *N*-succinimidyl group on the PEG polymer side chain, RPE cell attachment and growth is greatly enhanced[115]. The *N*-succinimidyl-activated MMA:PEGM co-polymers have been investigated for replacement of the Bruchs membrane within the eye as a possible treatment for AMD. With the dry form of AMD, the Bruchs membrane becomes distorted and damaged due to the build-up of waste products called Drusen, which in turn results in photoreceptor cell death. It is proposed that the Bruchs membrane could be replaced by the MMA:PEGM co-polymer based fibrous mats with RPE cells grown on the surface as a treatment or cure for AMD.

It has been shown that RPE cells can be cultivated successfully on a *N*-succinimidyl-activated MMA:PEGM co-polymer electrospun fibres *in vitro*[115] (Figure 3.1). The next stage for treatment of AMD would be to successfully transplant these electrospun fibres into the eye and for RPE cells to be grown on these *in vivo.* The physical and mechanical properties of the fibres are crucial factors in the mimicking of the natural Bruchs membrane. The physical properties are also highly important to allow a surgeon to transplant the fibres successfully into a patient without the fibres tearing or splitting. The surgery time and incision size are also important factors to control in order to minimise patient discomfort. Currently the MMA:PEGM co-polymer electrospun fibres which have the best physical properties allowing manual manoeuvring by hand without tearing or ripping are around 50 µm in thickness (matt depth). The natural human Bruchs membrane is less than 10 µm thick and this is an important parameter which would need to be mimicked for successful treatment of AMD.

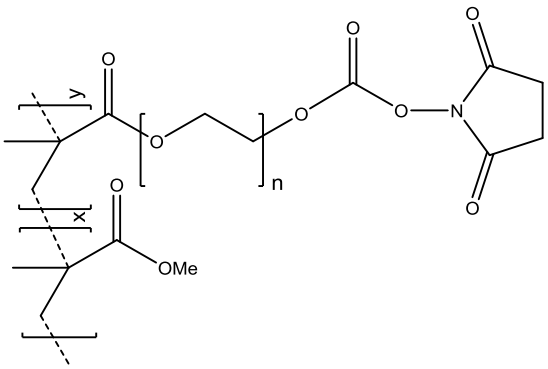

Figure 3.1 - *N*-succinimidyl-activated MMA:PEGM co-polymer which has been shown to improve RPE cell attachment[115].

In order to replace damaged Bruchs membrane convincingly with the electrospun polymers, the fibrous mat would need to be around 10 µm in depth, yet still be tough enough to survive physical transplantation. From previous work, use of an individual fibre of around 1.9 µm in width resulted in a fibrous mat cross-section depth of around 50 µm, which would be too bulky for transplantation[115, 150]. Accordingly, initial investigation was focussed on getting the individual fibres thinner which should reduce the overall depth of the electrospun mats. The first area examined was the electrospinning process itself in order to see whether different parameters could reduce the MMA:PEGM polymer fibrous mat depth. As well as attempting to reduce the individual fibre width, further optimisation of the conditions in an attempt to spin a tighter mesh with individual fibres closer together is required. It was envisaged that this would reduce the electrospun mat depth by reducing the void volume while maintaining the physical strength of the electrospun mat.

3.2 Optimisation of fibrous electrospun mats.

3.2.1 Optimisation of the electrospinning process.

The first area for investigation was optimisation of the electrospinning technique. Previously reported[150] electrospinning methods using these polymer mats utilised a solution of polymer at a concentration of 0.55 g mL^{-1} in methyl ethyl ketone (MEK). A stainless steel collector was placed 15 cm from the needle tip and connected to a high-voltage supply (Gamma High Voltage, Ormond Beach, FL) set at 16 kV. The syringe pump was set to run at 9.5 mL h^{-1} to form the fibrous mat[115].

The first area in the electrospinning process which was investigated was the effect of increasing the voltage across the needle and collector plate within the electrospinning arrangement. An increased voltage might increase the repulsive forces between the fibrous jets formed resulting in an altered fibre width. Conversely reducing the voltage from the standard 16 kV would have the same effect. It was observed as the voltage increased, the fibres remained of a similar width (Table 3.1). At 17 kV and 19 kV the fibres were slightly thinner but not statistically different. At 21.5 kV, the solution was electrosprayed instead of being electrospun, with the voltage causing the electrostatic forces within the Taylor Cone to be too large, resulting in no fibres forming. Above 19 kV, arcing occurred between the needle and collector plate intermittently, because of the high voltage. Not only was this a safety concern, it also interrupted the electrospinning process, forming poorer quality and irreproducible fibrous mats. When the voltage was reduced, the fibre width increased and a problem of needle blockage was observed. At 13.8 kV, the electrospinning needed to be stopped on three occasions to clear the needle; this was likely due to the Taylor cone only just being above the electrostatic threshold for fibre formation and the flow rate being too high, not allowing enough time for the fibres to form. When the voltage was 10 kV, no fibres formed and only drops were observed because the voltage was below the threshold for fibre formation and was insufficient to create enough electrostatic repulsion within the Taylor cone.

Table 3.1 - The effect of electrospinning voltage on fibre width.

Voltage	Mean fibre width (µm)[a]	Electrospun mat width (µm)[b]
21.5	N/A	N/A
19	4	67
17	4	63
16	4	60
15	5	66
13.8	5	75
10	N/A	N/A

[a]Mean calculated using 10 randomly selected fibres from 4 different areas on polymer mat, viewed by SEM, total number of fibres measured = 40.

[b]Measured using SEM with the mat placed on its edge.

Only a small affect was observed on the depth of the electrospun polymer mats using different voltages. 1 mL of polymer solution was used at each voltage, however not all of the polymer was spun onto the collector plate as fibres were observed around the outside of the plate and on the frame supporting the syringe pump. This loss of material may also account for some of the variations observed with electrospun mat depth.

Whilst keeping the voltage constant at 16 kV, the distance between the needle tip and collector was altered. At larger distances between the collector and needle tip, the fibres began to bead or break mid collection (Figure 3.2). This beading occurs as a result of instabilities within the polymer jet. At smaller distances, the fibre mat size increased up to around 10 µm in depth, with 15 cm between the needle and receiver plate being optimal for the MMA:PEGM polymer system. As might be expected, arcing was also observed at shorter distances which affected polymer mat quality.

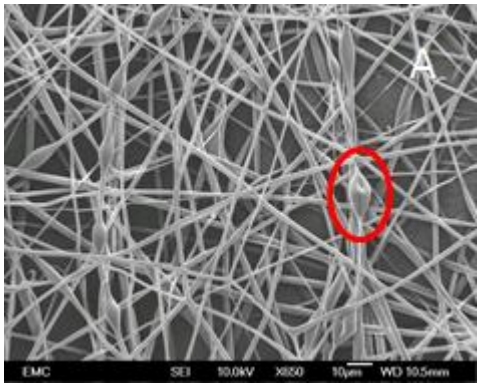

Figure 3.2 - Scanning electron micrographs of 60:40 MMA:PEGM polymer formed using a 25 cm distance between the charged needle tip and collector plate. An example of beading is highlighted. Original magnification x 650.

Previous equipment utilised a bevelled needle (i.e a non-perpendicular point) of 21 gauge. A flat pointed needle which had a perpendicular point was used to see how this would affect the electrospinning process. A 31 gauge needle which has an internal diameter of 0.13 mm was also used which is far thinner than the 0.51 mm of the 21 gauge. Using a bevelled needle, the drop which forms the microspheres was slightly misshapen and it was thought this may affect fibre formation. Using a flat point needle however, had little effect on the fibre size and structure. Using a smaller bore needle resulted in very poor mat formation. The mat was fluffy with a cotton-

wool like consistency on the macroscale and from the SEM it appears that the fibres sit on top of each other rather than intertwine (Figure 3.3).

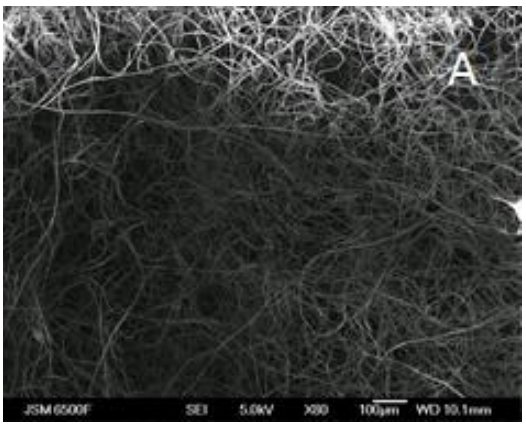

Figure 3.3 - Scanning electron micrographs 60:40 MMA:PEGM polymer using a 31G needle. Original magnification x 80.

Another parameter which affects the electrospinning process is the flow rate of the polymer solution and so this was investigated further. The syringe pump was set to run at 9.5 mL h^{-1} using conditions reported previously[115]. Flow rate is an important factor as a slow flow rate may cause a blockage or not provide enough solution for droplet formation and therefore prevent fibre formation. A high flow rate would not give enough time for polarisation to occur within the Taylor cone. An improvement over previously optimised conditions was observed with 15 mL h^{-1} producing thinner fibres than at 9.5 mL h^{-1}. Fibre width remained reasonably constant with an increase in fibre width at high and low flow rates, which is contrary to the literature reports[161] (Table 3.2).

Table 3.2 - The effect of flow rate on fibre width.

Flow rate (mL h^{-1})	Mean Fibre width (µm)[a]
20	7
18	5
15	5
12.5	5
10	6
9.5	6
7	No fibre formation due to blockages

[a]Mean calculated using 5 randomly selected fibres from 4 different areas on polymer mat, viewed by SEM, total number of fibres measured = 20.

The viscosity of the electrospun polymer solution is a critical parameter in fibre width. Viscosity not only depends on the viscosity of the solvent but also on the polymer concentration and the polymer molecular weight. The molecular weight of the MMA:PEGM co-polymer system can vary because of the radical polymerisation method and they can have a high polydispersities as a result (M_n 7940, M_w 15934, PD 2.01) (Scheme 3.1). The polymer concentration in the electrospinning solution, however, could be investigated (Table 3.3). As viscosity decreased, so does individual fibre width, until the polymer concentration was too dilute and electrospraying occurred. When the solution was too viscous, blockages occurred and only a few fibres were formed before the blockage had to be cleared. A polymer concentration of 0.55 g mL^{-1} provided the best results as previously observed, however, this was not significantly different to the concentrations of 0.5 g mL^{-1} and 0.4 g mL^{-1}.

Table 3.3 - The effect of polymer concentration on fibre width.

Polymer concentration (g mL^{-1})	Mean fibre width (µm)[a]
2	Blockage
1.5	Some fibres formed but blockage kept occurring, unable to create mat which could be handled without splitting.
1	11
0.75	6
0.55	5
0.5	6
0.4	5
0.25	electrosprayed

[a]Mean calculated using 5 randomly selected fibres from 4 different areas on polymer mat, viewed by SEM, total number of fibres measured = 20.

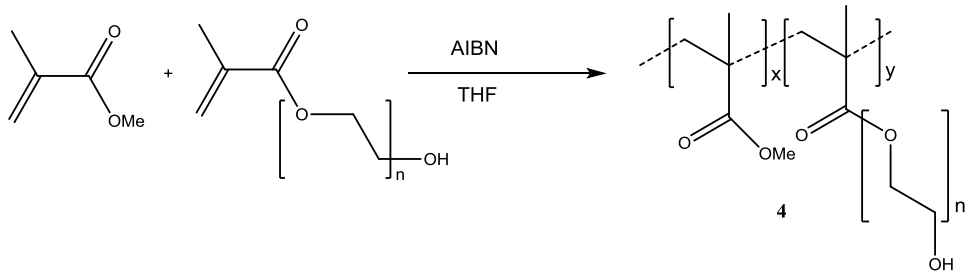

Scheme 3.1 - Synthesis of poly(methyl methacrylate-co-poly(ethylene glycol) methacrylate) (MMA-PEGM).

Varying the solvent was investigated as different volatilities would affect the fibre width. Varying solvents would also affect the viscosity of the solution and the solution conductivity. Different solvents would also change the charge distribution within the polymer solvent system as a result of the different polarities of the solvents. Various solvents compatible with the MMA:PEGM polymer were investigated (Table 3.4). The higher boiling point solvents chloroform and 2-butanone provided thinner fibres than DCM. This was likely to be because of the solvents being less volatile allowing more time for the fibres to elongate and become thinner before the solvent evaporated. Using a polar solvent mix to alter the solution conductivity resulted in thicker electrospun fibres, which were difficult to remove from the collector plate. It appeared that residual solvent was still present caused the

fibres to stick to the collector plate, which often resulted in tearing of the electrospun mat during removal from the collector plate.

Table 3.4 - The effect of solvent on fibre width.

Solvent	Mean fibre width (µm) [a]
Chloroform	5
DCM	6
THF	Electrosprayed
2-Butanone	5
50:50 Methanol: DCM	8

[a]Mean calculated using 5 randomly selected fibres from 4 different areas on polymer mat, viewed by SEM, total number of fibres measured = 20. Concentration held at 0.55 g mL^{-1} in solution.

The electrospinning process was difficult to fully understand and patterns of behaviour were not clear. Many polymer solutions simply electrosprayed or did not appear to charge and simply dripped out of the syringe. Some of the conditions produced excellent electrospun mats with good images and were easy to handle with excellent physical strength. When these conditions were repeated, however, very poor quality mats were obtained which would tear when handled very gently or could not be peeled from the collector plate. Looking at these using SEM, it appeared that beading or ribboning had occurred (Figure 3.4). Ribboning occurs when a skin forms on the polymer jet rather than all of the polymer fibre drying uniformly at the same time. When the solvent inside the jet evaporates the outer polymer skin collapses forming a flat ribbon with raised edges as shown in Figure 3.4, and results in a larger fibre width. Electrospraying of the polymer solutions occurred on numerous occasions rather than the desired electrospinning process.

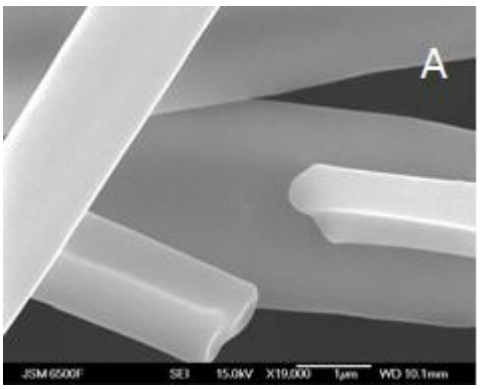

Figure 3.4 - Scanning electron micrographs 60:40 MMA:PEGM polymer where ribboning has occurred. Original magnification x 19 000.

Different ratios of MMA to PEGM have previously been examined for optimised RPE cell growth[115, 150], but to see if the electrospun fibres could be optimised to create smaller mats, the effect of the ratio was investigated (Table 3.5). NMR was used to confirm the desired ratios had formed by comparison of the methyl group on the MMA with the PEG backbone, however due to peak overlap the ratio had to be estimated.

Table 3.5 - The effect of the polymer ratio on fibre width.

Polymer Ratio (MMA:PEGM)	Mean fibre width (μm)[a]	Estimated ratio MMA:PEGM	Contact angle of polymer films (°) (n = 3)
60:40 PEGM, M_n 300	5	56:44	77 ± 5
50:50 PEGM, M_n 300	4	50:50	76 ± 6
40:60 PEGM, M_n 300	5	41:59	54 ± 3
50:50 PEGM, M_n 500	5	55:45	46 ± 4
60:40 PEGM, M_n 500	4	67:33	51 ± 8
40:60 PEGM, M_n 500	5	30:70	43 ± 5

[a]Mean calculated using 5 randomly selected fibres from 4 different areas on polymer mat, viewed by SEM, total number of fibres measured = 20.

All blends resulted in similar fibre widths and no obvious pattern was observed between the composition ratio of the co-polymer and the fibre width. Possibly a slight trend in the higher the percentage of MMA present the thinner fibres formed, however nothing was statistically demonstrated. Comparison between the 50:50

MMA:PEGM co-polymer using PEGM M_n 300 compared to the larger PEGM M_n 500 showed an increase in fibre width when moving to the larger PEG chain, however the opposite is true for the 60:40 co-polymer. Contact angles were measured for these mats which showed that fibres prepared using the large molecular weight PEGM were significantly more hydrophilic (Figure 3.5). This could have affected the electrospinning of the fibres by altering the surface charge density in solution. The polymers with a larger contact angle, hence the most hydrophobic have a slightly smaller fibre width, however, this general trend is not significant. The PEG group with a M_n 300 gave a co-polymer (M_n 7940 and M_w 15934) almost half the width of the MMA:PEGM co-polymer containing PEG with a M_n 500 (M_n 16031 and M_w 33620), however fibre width does not drastically change.

Figure 3.5 - Contact angle images showing difference between PEGM side chains: A) PEGM, M_n 500; B) PEGM, M_n 300. Distilled water with a drop size of 1 µl used.

Although it has been shown in the literature that the MMA:PEGM co-polymer produces good cell adhesion, the inconsistency in the nature of the electrospun mats formed is an issue. The mats obtained would need to be highly reproducible and therefore other polymer systems were examined in an attempt to reduce fibre widthand increase the strength of the electrospun mat.

3.3 Measuring the mechanical strength of the fibrous mats formed.

An adult humans Bruchs membrane was first gold coated and then imaged by SEM to gain further insight into the structure of the membrane itself (Figure 3.6). From image A (Figure 3.6), the fibrous nature of the membrane is observed. The electrospinning technique should allow us to mimic this structure and allow porosity for biological transport. The natural Bruchs membrane does not appear as porous as our electrospun polymer mats but this is due to the natural biological process being

far more effective at transporting material across membranes. The width of the membrane can also be seen in image B (Figure 3.6), and a similar depth is what we would hope to mimic with our electrospun mats.

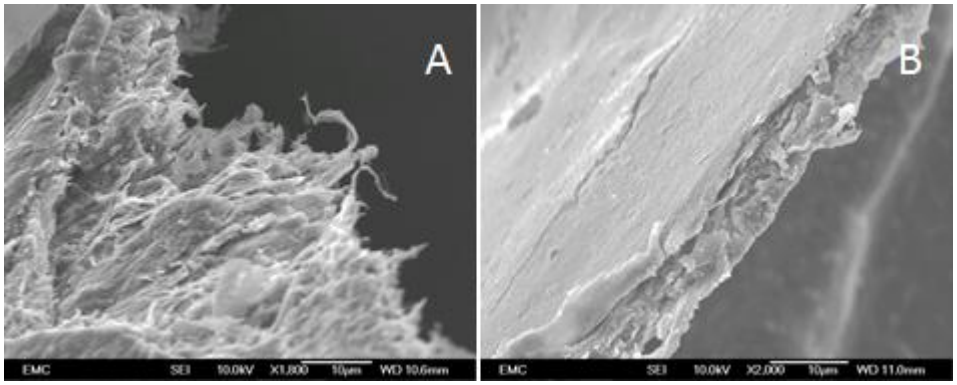

Figure 3.6 - Scanning electron micrographs of a human Bruchs membrane: A) Showing the fibrous nature of the Bruchs membrane, original magnification x 18 000; B) Showing the depth of the Bruchs membrane, original magnification x 20 000.

The mechanical strength of the electrospun fibres was investigated with the help of Dr. Atul Bhaskar of the University of Southampton Engineering Department. Using two 60:40 MMA:PEGM electrospun mats each having a depth of 75µm (total depth 150 µm), placed on top of one another and clamped at each end the Young's modulus, elongation, stress-to-fail and toughness were determined (Appendix B). The Young's modulus of elasticity for the electrospun mat was calculated at 17.2 MPa, which is greater than that of a human Bruchs membrane which has a Youngs modulus of around 2 MPa[82]. The much larger value than that for the natural Bruchs membrane reflects in part the use of two electrospun mats, however the use of a single mat resulted in unreliable results. The fibres have a far larger Youngs modulus than that of the natural Bruchs membrane, however they require a large amount of handling when being transplanted into the eye which must also be taken into account. The elongation, stress-to-fail and toughness parameters were also determined (Table 3.6).

Table 3.6 - Various physical properties of 60:40 MMA:PEGM polymers.

Young Modulus	17.2 MPa
Elongation	15%
Stress to Fail	0.25 MPa
Toughness	14.2 kJ m^{-3}

Unfortunately, there is little mechanical data for natural Bruchs membrane regarding the elongation and toughness of this material. Obtaining mechanical strength data on electrospun fibres is notoriously difficult[75]. The elongation and toughness values have been included as they provide some insight into the properties of the fibres and eventually it would be interesting to compare the properties of electrospun fibres with those of a natural Bruchs membrane. The stress-to-fail electrospun fibre data has no direct comparison with the natural Bruchs membrane, however, it is of interest as it indicates the manner in which these fibres break. They do not split in a quick and brittle fashion but they slowly stretch as individual fibres before they individually break and finally split into two discreet portions. Further work on the mechanical and physical strengths of both the fibres and the natural Bruchs membrane would be of interest, however quite specialist equipment would be required. The problem encountered during this work was that the fibres were of a delicate nature and the equipment being used was designed to measure the mechanical strength for far sturdier materials.

3.4 Alternative polymer systems investigated to reduce individual fibre width.

3.4.1 Investigating lower molecular weight polymers.

In order to try to reduce the fibre width further and therefore to reduce the depth of the electrospun mat other polymer systems were investigated. Atom transfer radical polymerization (ATRP) is a living type polymerisation which allows more controlled and uniformed polymer growth. This will result in a reduction in the polydispersities of the polymers which should directly affect the electrospinning process through the formation of thinner fibres (Scheme 3.2). This could be important for obtaining more manageable and reproducible electrospun polymer mats.

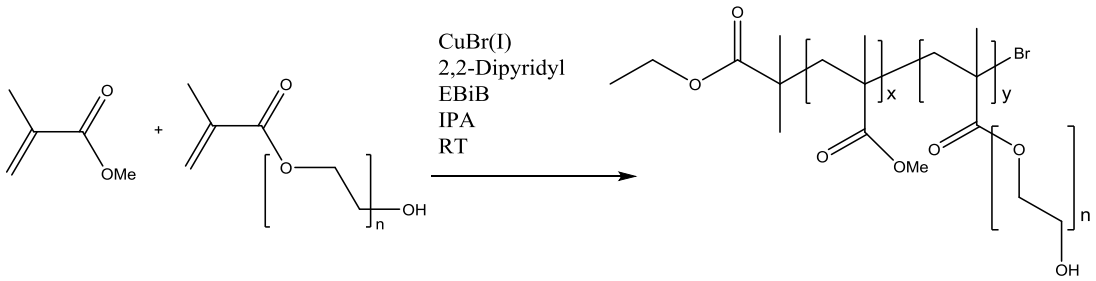

Scheme 3.2 - Synthesis of poly(methyl methacrylate-co-poly(ethylene glycol) methacrylate) under ATRP reaction conditions.

This approach successfully led to the more controlled formation of the MMA:PEGM co-polymer with a similar molecular weight to the polymer formed by radical polymerisation but with a lower polydispersity (M_n 11474, M_w 20323, PD 1.76). However the use of copper would not be viable for materials for transplantation within the body. Although this MMA:PEGM co-polymer produced by an ATRP reaction could not be used for biological application, it would be of interest to see what effect the lower polydispersitys has on the electrospinning process. The use of this polymer resulted in electrospraying rather than electrospinning resulting in no useable fibre mats. This could be because of the reduced entanglement between chains using this polymer and further investigation was required.

In order to get low polydispersity polymers with a higher molecular weight, different polymer systems were also explored. Polyoxazoline were investigated as these polymers are formed by a cationic ring-opening polymerisation (CROP) process (Scheme 3.3). This is a living polymerisation which allows the chemist to have optimum control over chain length and therefore the molecular weight can be tightly controlled. Samples of polymers were prepared and electrospun in order to investigate the effect of molecular weight on the width of the electrospun fibres (Scheme 3.4).

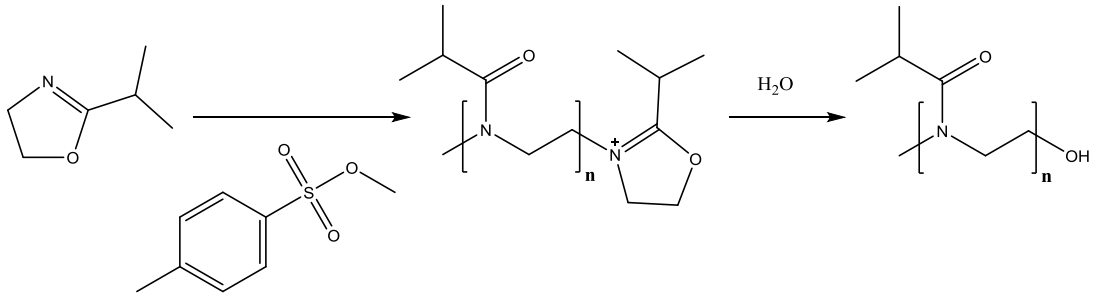

Scheme 3.3 - Cationic ring-opening polymerisation (CROP) forming isopropyl polyoxazoline polymers.

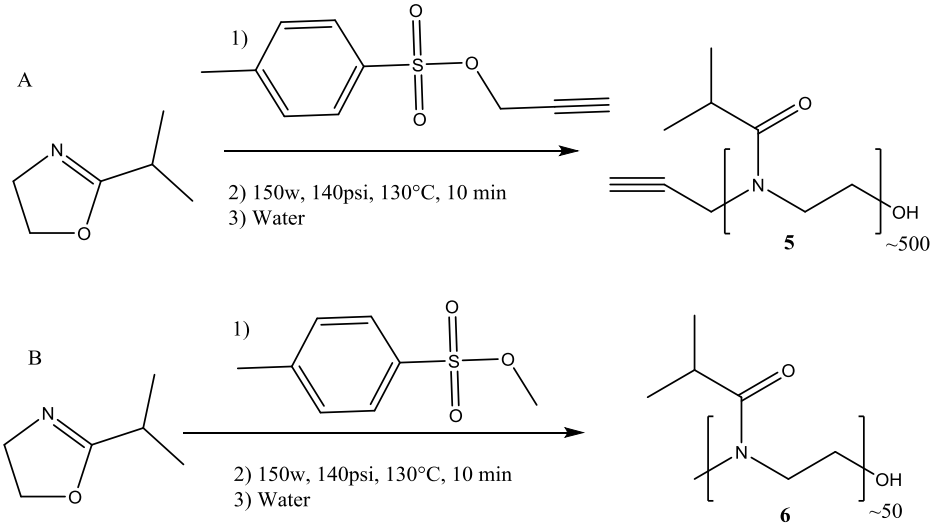

Figure 3.4 - Formation of isopropyl polyoxazoline polymers investigated for electrospinning.

The polymerisation was successful with the NMR spectra confirming formation of the desired product. The size of the polymers was also investigated using UV-Vis spectroscopy by viewing the lower critical solution temperature (LCST) of the polymer. It has been shown that the chain length and molecular weight of the polymers affect the LCST of the polymer[162-164,197]. The LCST of the polymers can give an indication of chain length, with longer polymers having a lower LCST. For both of the polyoxazolines prepared, the LCST values corresponded with the expected chain lengths confirming that the expected 500- (LCST 35.1 ^{o}C) and 50-repeat (LCST 43.0 ^{o}C) unit chain length polymers had formed.

Electrospraying was observed for both of these polyoxazoline polymers under numerous conditions. It was thought the polymers might be too small for successful

entanglement between strands to occur. However, the higher molecular weight polymer which had a chain length of around 500 repeat had comparable molecular weight (GPC results, M_n 16180, M_w 33816, PD 2.10) to the MMA:PEGM co-polymers. Surprisingly, this high molecular weight polymer still electrosprayed and higher chain lengths of polyoxazoline polymers are difficult to obtain because of the very small amount of initiator required. The polydispersity was unexpectedly higher than the ARTP reaction, but was comparable to the co-polymers formed by radical polymerisation. It has been shown that some polymers with a high hydrophilicity are difficult to spin into fibres[104], which is likely to be the case for the polyoxazoline polymers which are hydrophilic. Consequently other approaches involving the use of co-polymer methacrylate systems were explored.

3.4.2 Investigating MMA co-polymers to reduce fibre width.

It has been shown that the poly-MMA:PEGM electrospun mats provide an excellent surface for RPE cell growth. However the electrospun mats are too thick for transplantation. Smaller mats do not have the strength for the manipulation required for them to be inserted into the eye. The use of co-polymer methacrylate systems may overcome this problem of fibrous mat depth and strength, however they still need to be receptive to RPE cell growth. Co-polymer methacrylate systems were investigated to see their effect on electrospun mat formation and whether any improvements could be achieved with respects to cell growth.

To mimic the MMA:PEGM co-polymers, oxazoline-based co-polymers with MMA were prepared with varying success (Scheme 3.5). The FDA-approved[160] polyethyl oxazoline has been used as a PEG mimic by other groups[165,166] and ethyl oxazoline was reacted with MMA which could then be reacted further via a CROP process to form the PEG mimic.

The oxazoline ring was incorporated into the MMA using AIBN radical polymerisation as in previous reactions, successfully preparing the oxazoline:MMA co-polymer (Scheme 3.5). Presence of peaks at 3.68 ppm and 4.12 ppm confirmed the presence of the oxazoline ring within the polymer, however a very large polydispersity was observed (M_n 18389, M_w 166933, PD 9.07).

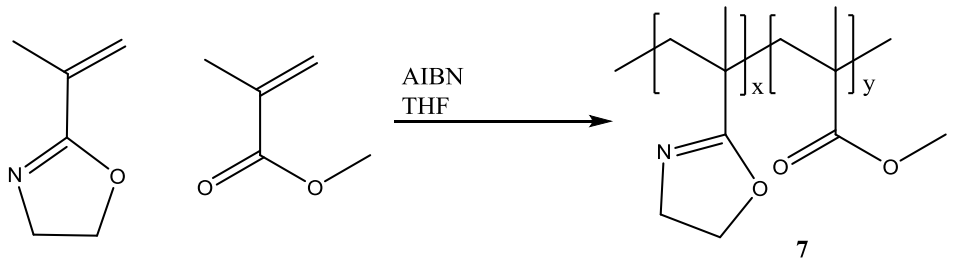

Scheme 3.5 – Preparation of MMA:ethyl oxazoline co-polymer.

The oxazoline ring on the MMA:oxazoline co-polymer was reacted with ethyl oxazoline under microwave conditions to form a PEG mimic side chain. The reaction however, was unsuccessful. To investigate whether the oxazoline ring on the MMA:oxazoline co-polymer backbone was hindered sterically, an extended oxazoline was prepared. Preparation of the extended oxazoline was successful, however, formation of the co-polymer failed and only polymethyl methacrylate was obtained. This could be due to the decrease in stability during the polymerisation using the acrylate over a methyl acrylate (Scheme 3.6).

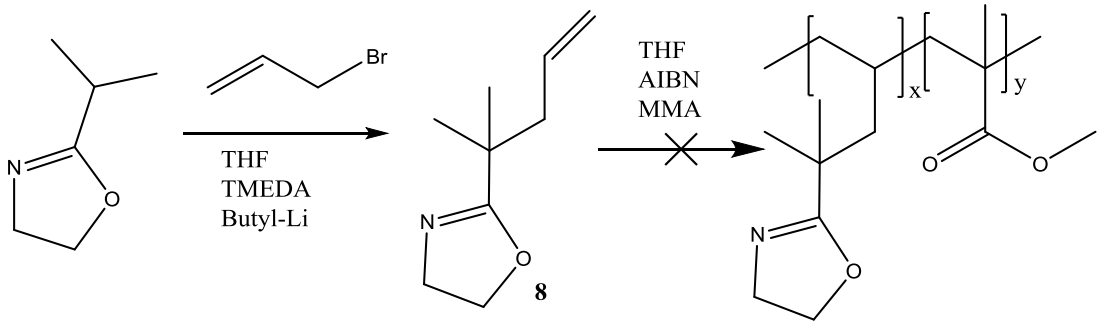

Scheme 3.6 - Preparation of extended oxazoline and subsequent failed polymerisation.

Application of this work has constantly been the driving factor and only options which could realistically be used within the body were investigated. Only materials with the ideal properties which would allow for feasible transplantation and a genuine chance of gaining FDA approval have been investigated. To improve the fibrous mats developed, co-polymers based on materials used for soft contact lenses were investigated. *N*-Vinyl-2-Pyrrolidone (NVP) has been used in co-polymers for contact lens formation[71], and therefore would not be an unrealistic choice for use in the back of the eye as a permanent replacement for the Bruchs membrane. Soft contact lenses have excellent strength and flexibility which are highly desirable properties for a Bruchs membrane replacement. NVP was successfully polymerised

with MMA using radical polymerisation with the appearance of NMR peaks for the CH_2 groups of the pyrrolidinone at around 1.80 ppm, 2.20 ppm and 3.00 ppm. Several conditions for the formation of an electrospun mat were then investigated (Scheme 3.7).

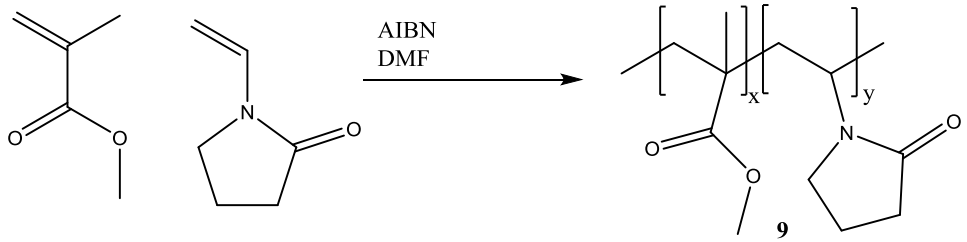

Scheme 3.7 - Formation of MMA:NVP co-polymer.

2-(Dimethylamino)ethyl methacrylate (DEM) is another monomer which has been used in hydrogel formation for use in contact lenses[168] and could be reacted with MMA using the same radical polymerisation methodology (Scheme 3.8). The reaction of MMA with DEM was successful with peaks at around 2.30 ppm from the methyl groups on the DEM moiety in the NMR spectrum confirming formation.

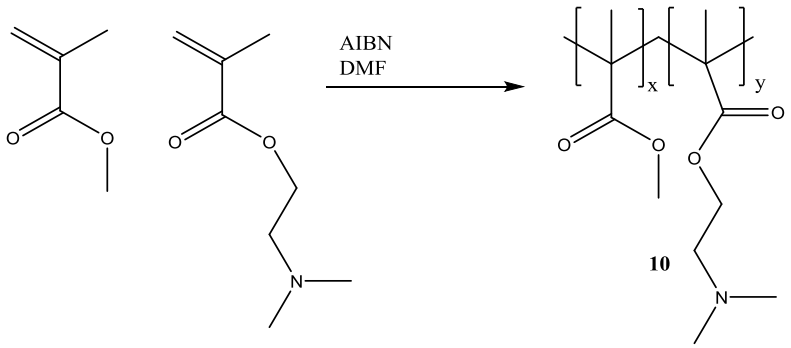

Scheme 3.8 - Formation of MMA:DEM co-polymer.

The reaction of DEM and NVP with PEGM was also investigated in an attempt to form the corresponding co-polymers, however both these reactions were unsuccessful. The PEGM chain may have sterically hindered the polymer formation, however it appeared from NMR spectra that the PEGM had preferentially reacted with itself leaving the NVP and DEM monomer starting materials as residue. Some DEM and NVP may have been incorporated, however the resulting product was difficult to handle and acted more like a gel, because of the high hydrophilicity of the PEGM, resulting in good entanglement between the side chains.

The co-polymers MMA:DEM and MMA:NVP polymers were electrospun using the optimised parameters previously employed for the MMA:PEGM co-polymers. Little or no electrospinning occurred however, and adjustment of the conditions was therefore required. Various electrospinning parameters were explored using the MMA:DEM and MMA:NVP co-polymers to form electrospun mats (Table 3.7), however, unfortunately only poor quality electrospun mats were obtained (Figure 3.7). Electrospinning of the MMA:DEM co-polymer resulted in a large amount of beading with large beads forming within the fibres (Figure 3.7A). Beading occurs because of instabilities within the electrospun jet. These instabilities can occur due to uneven distribution of charge across the jet, resulting in areas with more polymer present. When the solvent dries during the electrospinning process these areas with a larger amount of polymer present shrink and the beads form (Figure 3.7A). The MMA:NVP co-polymer produced in a highly fibrous electrospun polymer. On a macroscale the electrospun material looked like cotton-wool and would be highly unsuitable for use as a polymer mat. Viewing the fibres by SEM, beading can again be observed with a large variation in fibre length and width. It appears that a combination of varying repulsion, droplet and jet instabilities and entanglement result in these irregular fibres.

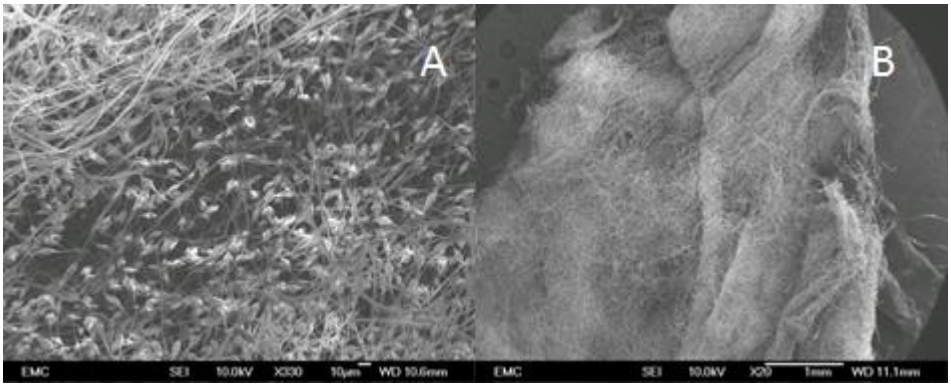

Figure 3.7 - Scanning electron micrograph of electrospun fibres: A) MMA:DEM co-polymer. Original magnification x 330; B) MMA:NVP co-polymer. Original magnification x 20.

Table 3.7 - Various electrospinning parameters attempted for MMA:NVP and MMA:DEM co-polymers.

Parameter	Conditions									
Voltage (kV)	16[b]	14	20	16	16	16	16	16	16	16[a]
Flow Rate (mL h^{-1})	9.5[b]	9.5	9.5	9.5	9.5	9.5	8	12	9.5	9.5[a]
Solvent	MEK[b*]	MEK	MEK	MEK	MEK	MEK	MEK	MEK	DCM	MEK[a]
Concentration (g mL^{-1})	0.55[b]	0.55	0.55	0.45	0.5	0.6	0.55	0.55	0.55	0.70[a]

*Methyl ethyl ketone (MEK)

[a]Conditions attempted with MMA:NVP co-polymer only

[b]Optimised conditions from MMA:PEGM co-polymer formation

3.5 Optimisation and investigation of succinimidyl functionalised MMA:PEGM co-polymers.

3.5.1 Activating MMA:PEGM co-polymers with succinimidyl functionality.

The MMA:PEGM co-polymer was reacted further to improve cell attachment as previously reported within the group[169], by further, attachment of succinimidyl groups onto the PEG chain terminus of the MMA:PEGM co-polymer (Scheme 3.9). Succinimidyl groups are widely used in the literature to facilitate protein and peptide coupling to polymer substrates[135].

Using various blend ratios, either a succinimidyl carbonate (Polymers iv, v and vi) or a succinimidyl ester (Polymer viii) group was introduced into the co-polymer (Table 3.8, Scheme 3.9). A new second carbonyl peak in the IR spectrum due to the cyclic imide was observed. The attachment of the succinimidyl group to the end of the PEG chain was confirmed by NMR spectroscopy. Peaks around 2.8 ppm on the spectrum are due to the protons on the succinimidyl group and peaks around 4.25 ppm due to protons next to the ester or carbonate linkage.

Table 3.8 - Ratios of the monomers used and succinimidyl functionalisation route of MMA:PEGM co-polymers.

Polymer	% MMA	% PEGM	PEGM Av MW	End group
i	60	40	360	OH
ii	40	60	360	OH
iii	50	50	500	OH
iv	60	40	360	Succinimidyl carbonate (Route 2)
v	40	60	360	Succinimidyl carbonate (Route 2)
vi	50	50	500	Succinimidyl carbonate (Route 2)
vii	60	40	360	Succinimidyl ester (Route 1)

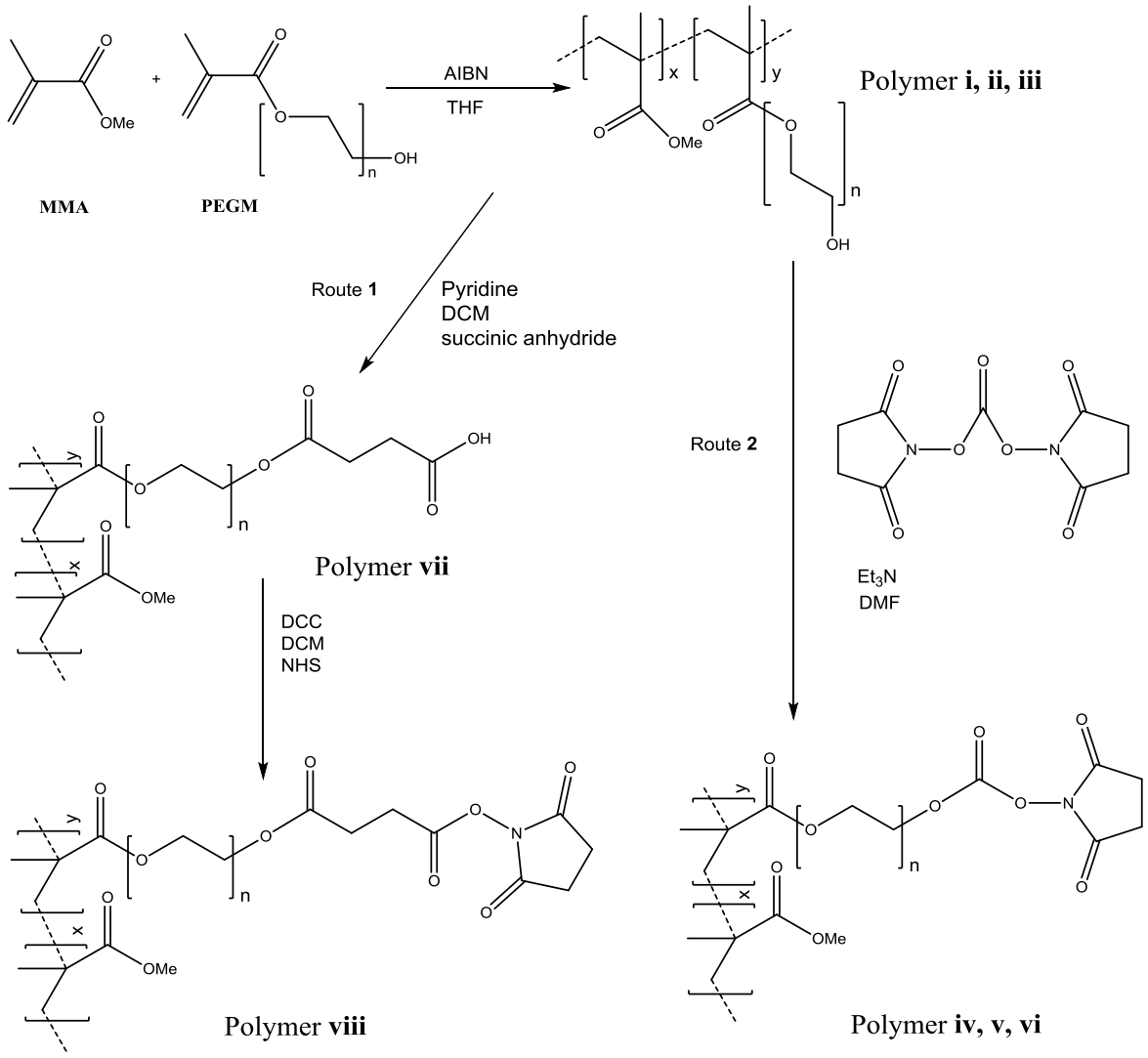

Scheme 3.9 - Formation of succinimidyl activated MMA:PEGM co-polymers.

The succinimidyl-activated MMA:PEGM co-polymers were electrospun into fibres and the width and morphology of the fibres was investigated using SEM (Figure 3.8). The unmodified polymers generally had a slightly larger average fibre width than their succinimidyl modified counterparts. The electrospun fibres of the 40:60 MMA:PEGM blend formed the largest fibres (Figure 3.8A). Ribboning was observed using this blend and this ribboning effect as a result of the collapse of the electrospinning jet resulted in this increase in width.

Contact angle experiments were used to determine the relative hydrophilicity of the various co-polymers (Table 3.9). Addition of either a succinimidyl carbonate or an ester resulted in an increase in hydrophobicity of the co-polymer. When the polymer

was simply spin-coated onto a glass slide all four succinimidyl activated co-polymers were more hydrophobic, with larger contact angles being observed. The fibres with larger numbers of PEG groups present (polymers v and vi) resulted in the largest difference between the non-succinimidyl counterparts.

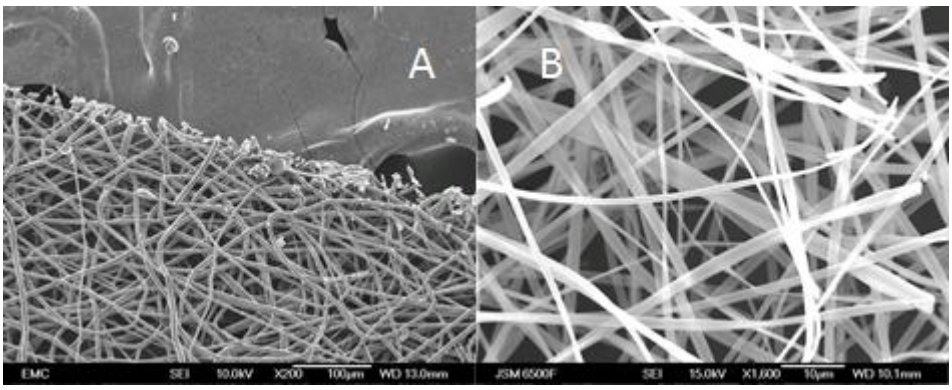

Figure 3.8 - Scanning electron micrograph of electrospun fibres: A) 40:60 MMA:PEGM co-polymer with ribboning occurring (polymer ii). Original magnification x 200; B) MMA:PEGM co-polymer iii. Original magnification x 1, 600.

It was noted however, that when the contact angle measurement was obtained for polymers v and vi using the electrospun fibres, full absorption of the water droplet into the mat occurred after 10 seconds (Appendix E). Although the contact angles for these polymers were greater (more hydrophobic) when simply spun onto a glass surface, when these samples were tested as fibres they were far more hydrophilic and effectively had a contact angle of zero. This might be expected as these polymers have a greater number of poly(ethylene glycol) (PEG) groups present and the addition of a terminated succinimidyl group does not make the fibres significantly more hydrophobic. This highlights the effect topography has on the contact angles and the differences in the contact angles between planar films and electrospun fibres prepared from the same polymers.

Table 3.9 - The average width, contact angle and swelling ratios for the succinimidyl-activated MMA:PEGM co-polymers.

Polymer	Fibre width (µm) (n = 15)[a]	Contact angle of polymer films (°) (n = 3) [a]	Contact angle of fibres (°) (n = 3) [a]	Swelling ratio (n = 3) [a]
i	2 ± 0.3	69 ± 4	60 ± 3	n/a
ii	3 ± 0.3	43 ± 3	0	n/a
iii	2 ± 0	44 ± 1	59 ± 1	n/a
iv	2 ± 0	92 ± 2	81 ± 0	1.96 ± 0.04
v	1 ± 0	843	0	2.16 ± 0.06
vi	1 ± 0	80 ± 3	0	2.11 ± 0.11
viii	1 ± 0	86 ± 1	79 ± 1	1.94 ± 0.18

[a]Values expressed as mean ± sem.

3.5.2 Examining gelation of succinimidyl activated MMA:PEGM co-polymer fibres.

When the succinimidyl-activated polymers were left in solution in transwells for cell seeding, the mats became gel-like. To investigate this further the polymers were added into solution and left before being electrospun. These polymers left in solution produced insoluble hydrogels (Figure 3.9). Co-polymers with a higher percentage of PEG groups present produced a hydrogel faster than polymers with a greater percentage of MMA. This effect has not previously been observed in the literature for these polymers and so was investigated further.

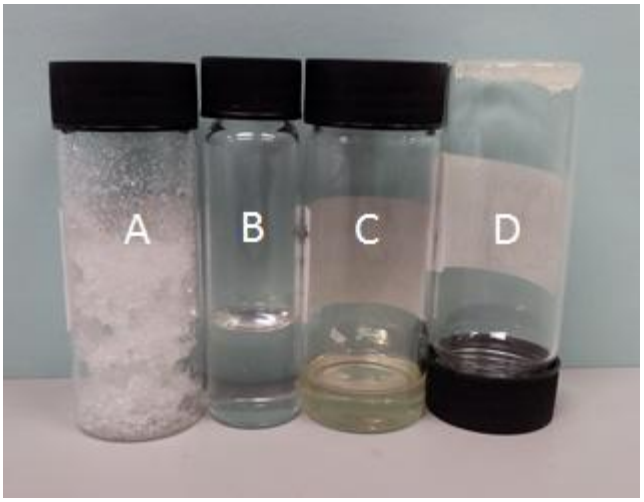

Figure 3.9 - Image of MMA:PEGM succinimidyl hydrogels: A) Dried polymer before electrospinning; B) Polymer dissolved in solution; C) Hydrogel formed from concentrated polymer solution; D) Hydrogel formed from electrospun fibres.

A brief investigation into the ambient conditions was undertaken to identify if the source of the gelation was due to a possible annealing process occurring. The polymer was dissolved in either DCM or methanol and treated with heat or light to see if gelation would occur (Table 3.10). In tubes 6 and 7, an acid and base were added respectively to see what effect this would have on the process, as an excess base (triethylamine, TEA) could be present if it was not completely removed during the purification process. After four weeks possible gelation had occurred in tubes 6 (DCM, TEA) and tube 8 when methanol was used as the solvent. Only small clumps of material were observed in the reaction tubes and no full gelation had occurred as observed with previous samples. This may have been because the samples were too dilute preventing full gelation. From these results it appeared that light and heat have no effect on gelation. These classic routes which cause crosslinking and therefore gel formation are not the underlying cause for gelation within the succinimidyl activated co-polymers.

Table 3.10 - The succinimidyl-activated MMA:PEGM co-polymers were examined under various conditions to see if an annealing effect was the root cause of the gelation observed.

Tube	Solvent	Light exposure	Heat	Addition Base/Acid
1	DCM	Covered	None	None
2	DCM	Light	40^{O}C	None
3	DCM	Covered	40^{O}C	None
4	DCM	Light	None	None
5	DCM	Covered	None	None
6	DCM	Covered	None	TEA
7	DCM	Covered	None	Acetic Acid
8	Methanol	Covered	None	None

To investigate this gelation process a model study was undertaken using *N*-hydroxysuccinimide derivatives. The *N*-(Benzyloxycarbonyloxy)succinimide was purchased as the carbonate derivative but the non-carbonate hydroxysuccinimide comparison required preparation (Scheme 3.10).

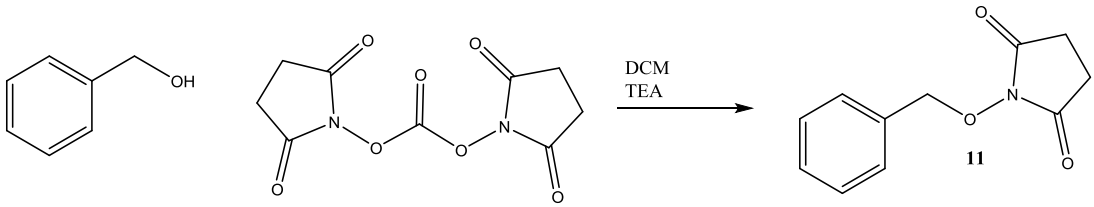

Scheme 3.10 - Formation of *N*-(benzyloxy)succinimide as a succinimidyl end group mimic.

The model study suggests that the succinimidyl group could react with unreacted PEG groups which still have the OH end group present (Scheme 3.11). The succinimidyl carbonate can react and be displaced with methanol as shown by formation of benzyl methyl carbonate. Any unreacted PEG end groups could react with the succinimidyl group forming a crosslink. The addition of a base also results in the succinimidyl ring opening and reacting with methanol. This could also occur to form a crosslink with any unreacted PEG chains.

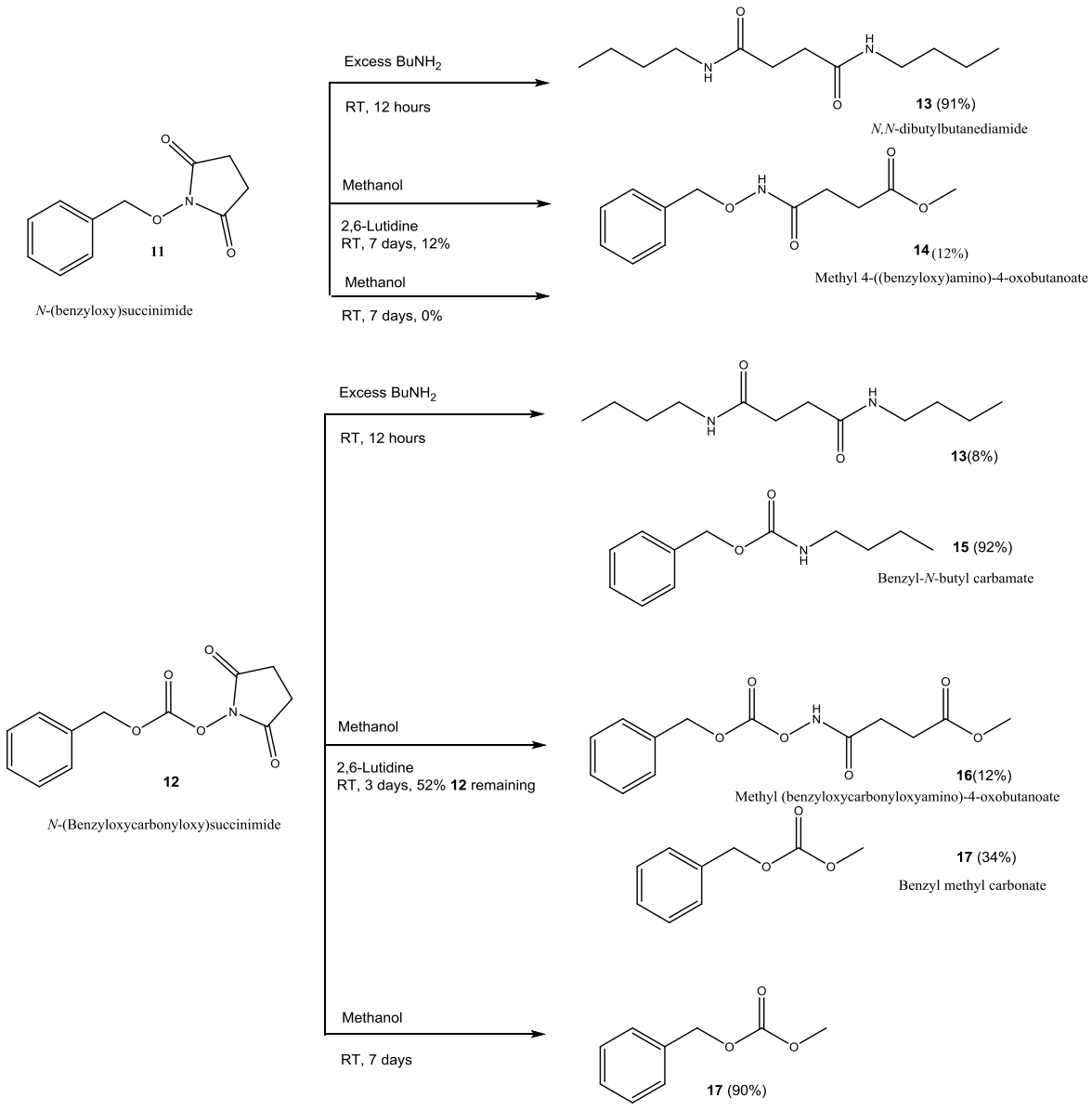

Scheme 3.11 – Investigating gelation of succinimidyl-functionalised MMA:PEGM co-polymers using succinimidyl mimics.

This route explains why co-polymers with a higher percentage of PEG groups present result in faster hydrogel formation than polymers with a greater percentage MMA. This also explains the results observed during the annealing study, why a gel only formed when excess base was present. When the carbonyl group is not present a displacement of the succinimidyl group did not occur, however the succinimidyl could undergo ring opening. The succinimidyl ester-activated co-polymers did not gelate in solution unless excess base was present and the ring opening route for crosslinking appears to require the presence of additional base.

From this study, it was shown that any unreacted PEG chains could react with the succinimidyl group and crosslink via a ring opening or displacement of the succinimidyl group (Scheme 3.12).

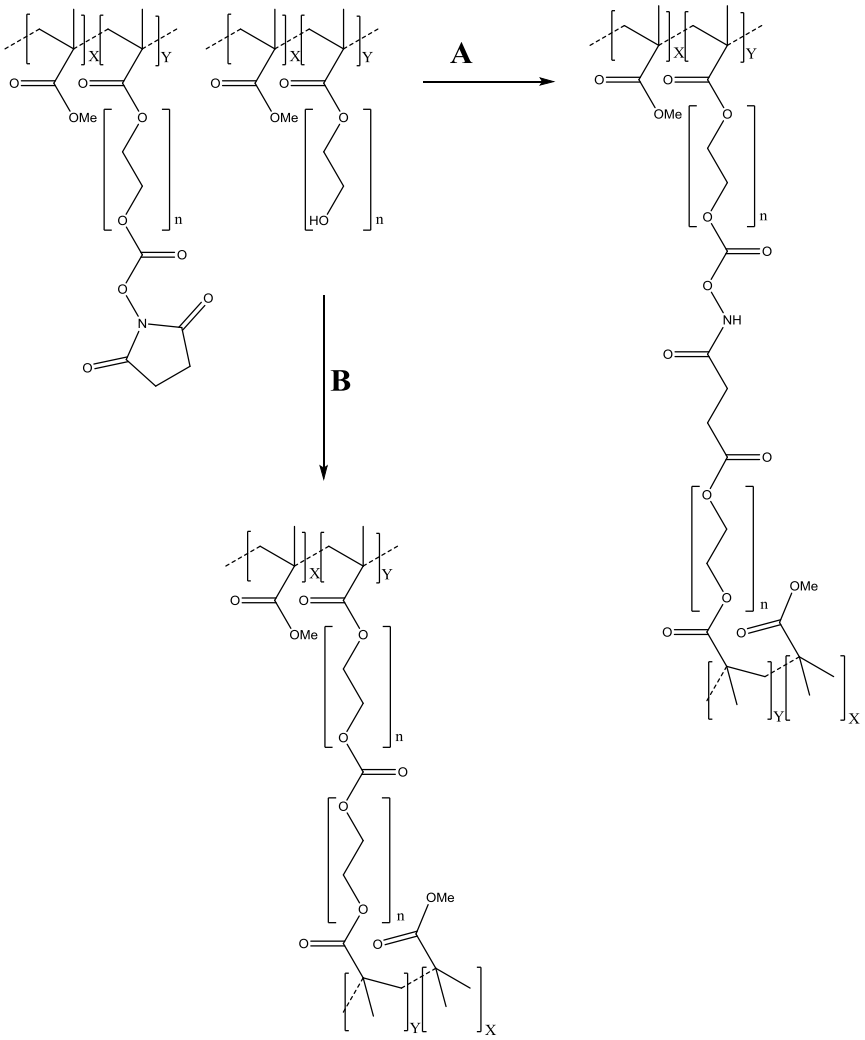

Scheme 3.12 - The two routes which result in cross-linked succinimidyl-functionalised MMA:PEGM gels.

To investigate the properties of the hydrogels formed, the swelling ratio was measured for hydrogels **iv-viii** (Table 3.9) (See experimental). Polymer **v** absorbed the most water due to the increased hydrophilic nature of the polymer because of the higher percentage of PEGM present. The increased percentage of PEGM present could also result in a greater number of unreacted hydroxyl groups being available to react with the succinimidyl moiety and thereby create more crosslinks. It is however,

difficult to quantify the number of the hydroxyl groups present using NMR spectroscopy because of signal overlap.

3.6 Investigating the RPE cell adhesion properties of succinimidyl activated MMA:PEGM co-polymer fibres.

The cell-adhesion properties of the optimised MMA:PEGM succinimidyl-activated co-polymers were then investigated. The 40:60 MMA:PEGM co-polymer was used as this is the fastest gelating co-polymer. The gelation observation may have an effect on cell growth using these succinimidyl activated co-polymers. The succinimidyl activated 40:60 MMA:PEGM co-polymer showed successful cell growth and although the fibres may gelate within the transwells it did not appear to affect the results of cell seeding (Figure 3.10, 3.11). Cell seeding onto the fibres was successful and a lactate dehydrogenase (LDH) assay was used to quantify the difference in cell growth between the functionalised and unfunctionalised polymers.

The LDH assay showed a significant difference in performance between the succinimidyl-activated co-polymers and the unsuccinimidyl functionalised MMA:PEGM co-polymers, with the probability of the result having occurred by chance less than 0.001% (Figure 3.10). Laminin is coated to improve biocompatibility and cell adhesion in a number of medical devices[170] and was used as a reference when the non-functionalised fibres were coated. The succinimidyl activated co-polymer gave an improved result over the laminin-coated fibres resulting with less cell death occurring.

An MTT assay (3-(4,5-Dimethylthiazol-2-yl)-2,5-diphenyltetrazolium bromide) was used to check that both the succinimidyl-activated and unsuccinimidyl functionalised fibres were non cytotoxic (Figure 3.11). Unfortunately the results are unreliable due to the positive and negative controls being within a narrow range. From previous work[150] and later studies (Figure 4.3, Chapter 4) the fibres showed little or no cytotoxic effects.

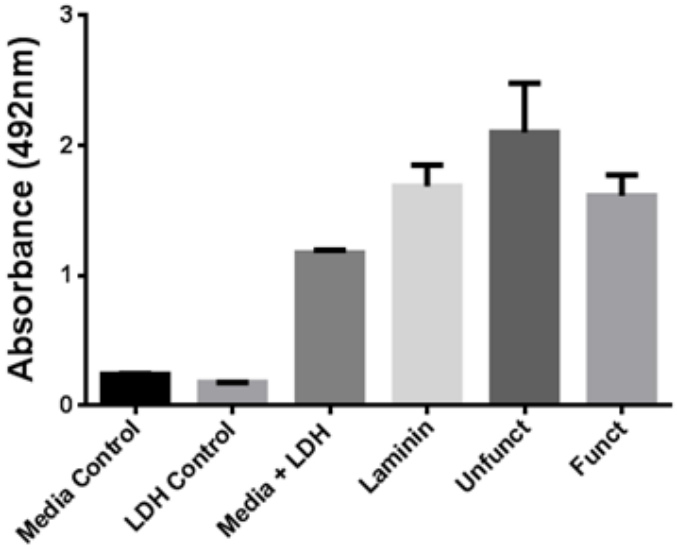

Figure 3.10 - LDH assay showing the difference in viable cell growth between the Laminin-coated, succinimidyl-activated co-polymers and the unsuccinimidyl-functionalised MMA:PEGM co-polymers. Greater absorbance is the results of increased cell apoptosis. Unfunctionalised fibres significantly different to functionalised fibres/Transwell controls P<0.001. Statistical analysis by analysis of variance (ANOVA) followed by Tukey-Kramer multiple comparison test (Statistical analysis by Heather Thomson at the University of Southampton General hospital).

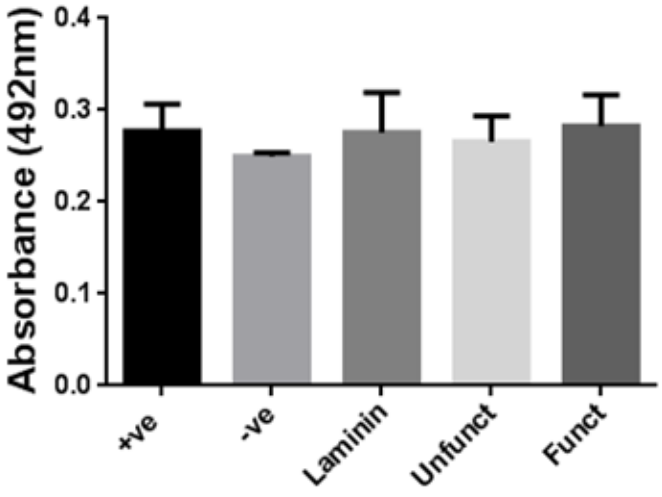

Figure 3.11 - MTT assay showing the cytotoxicity difference between the succinimidyl-activated co-polymers and the unsuccinimidyl functionalised MMA:PEGM co-polymers. (Positive and negative controls show error resulting in a null result. Further MMT assay in Chapter 4, shows cells are non-cytotoxic)

3.7 Investigating hydrogels for electrospinning.

3.7.1 Use of hydrogels to improve fibre formation and cell adhesion.

In view of the success of the MMA:PEGM hydrogels, other hydrogels were investigated to see if they could be utilised in a potential Bruchs membrane replacement. Silicone hydrogels are commonplace in contact lens manufacture and therefore these hydrogels were investigated since this chemistry is ocular compatible[172].

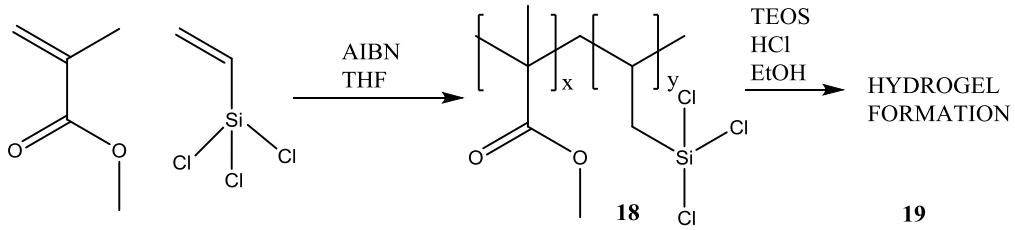

Scheme 3.13 - Formation of MMA:Silane hydrogels

Formation of the MMA:silane was successful although product analysis proved difficult because of the broad peaks in the NMR spectra (Scheme 3.13). The MMA:silane was taken on further and reacted with Tetraethyl orthosilicate (TEOS) which is used as a crosslinking agent in silicone polymers to form a hydrogel. A gel was formed and by NMR the peaks significantly broadened indicating additional crosslinking.

Attempts were then made to incorporate siloxane cross-linking into polyoxazolines. 3-Aminopropyl triethoxysilane was used to quench poly(2-isopropyl-2-oxazoline) and then further cross-linked under acid conditions (Scheme 3.14). It was hoped this additional crosslinking would aid electrospinning and fibre formation. Whilst NMR characterisation proved difficult because of the broad peaks, the LCST's of the polymer altered between the poly(2-isopropyl-2-oxazoline) polymer before and after cross-linking. Before cross-linking the poly(2-isopropyl-2-oxazoline) LCST was 39-42^{o}C (Scheme 3.14 A). The LCST of the longer branched polymers was 45-46^{o}C suggesting crosslinking had occurred (Scheme 3.14 B).

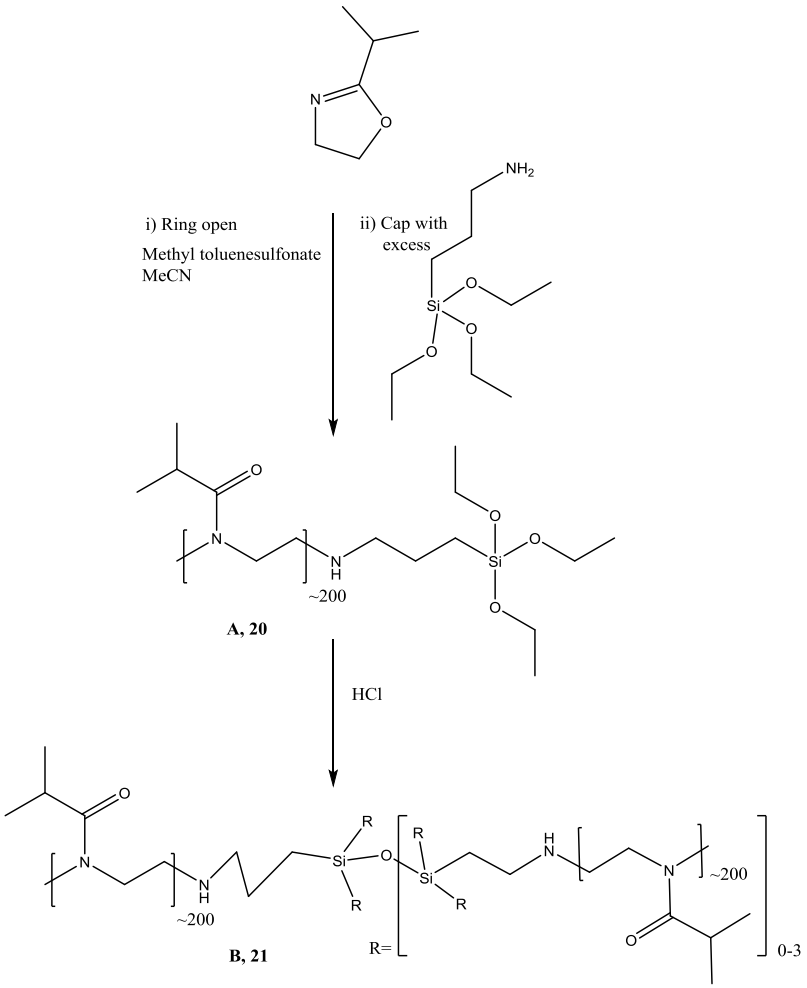

Scheme 3.14 - Formation of cross-linked polyoxazoline polymer.

However both the MMA:Silane and cross-linked oxazoline hydrogels could not be electrospun into fibres, because insolubility in suitable solvents. Although some hydrogel could be dissolved, only electrospraying occurred reflecting the low solution concentration. Further investigation into electrospinning of these hydrogels could be undertaken in future work by using melts to get the polymers into a liquid state and this approach may overcome some of the issues arising from low concentration during the electrospinning process[104].

3.7.2 Use of maleimide functionality to improve cell adhesion onto MMA:PEGM co-polymers.

One other approach for improving cell adhesion of the MMA:PEGM co-polymers involved introduction of a maleimide group. The maleimide group reacts specifically

with thiols, and can react with cysteine (Cys) found in cell proteins forming a carbon-sulfur linkage[174].

By forming an acid chloride from β-alanine the maleimide could be incorporated into the MMA:PEGM co-polymer[173] (Scheme 3.15).

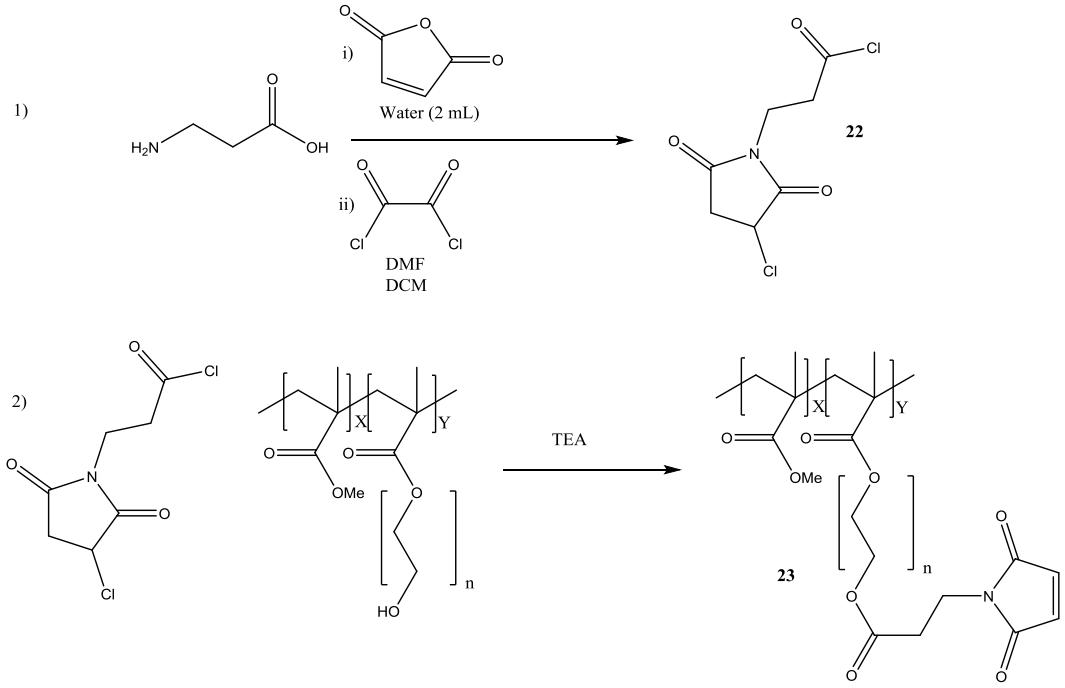

Scheme 3.15 - Formation of a maleimide-activated MMA:PEGM co-polymer from β-alanine.

The reaction was successful with maleimide peaks appearing at around 6.8 ppm in the NMR spectrum. Before investigating the biocompatibility of the maleimide polymer system and whether improved cell attachment could be obtained, it first had to be electrospun into fibres in order to mimic the Bruchs membrane. Numerous attempts to form electrospun fibres using the maleimide-activated MMA:PEGM co-polymer were undertaken with little effect. The maleimide-activated polymer was more difficult to get into solution in comparison with its succinimidyl counterpart. However it would still readily dissolve in DCM. Each factor affecting electrospinning was probed, but no useful electrospun fibres were formed. Electrospraying occurred in many of the attempts and, when a highly concentrated solution of the maleimide polymer was used, only a very fragile polymer film was formed on the collector plate (Figure 3.12).

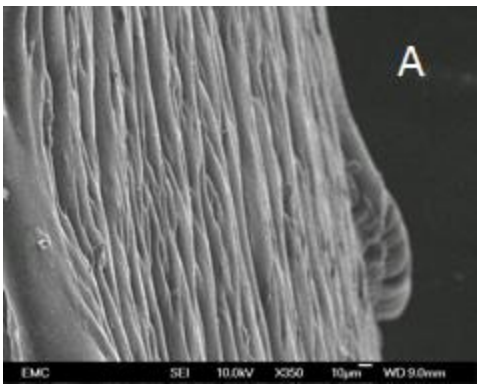

Figure 3.12 - Scanning electron micrograph of maleimide activated MMA:PEGM co-polymer which formed a polymer film. Original magnification x 350.

Changes to the polymer system resulted in limited success, with the major limitation being the electrospinning method using these different polymer systems. The succinimidyl-activated MMA:PEGM co-polymer showed promising results for cell attachment and proliferation, with the simple addition of a succinimidyl group increasing cell adhesion compared to the unfunctionalised MMA:PEGM co-polymer fibres (Figure 3.10). The results were comparable to laminin-coated fibres, a method which is used to coat numerous materials for biomedical applications. The succinimidyl-activated MMA:PEGM co-polymers formed thinner fibres than the unfunctionalised MMA:PEGM co-polymers, with fibres around 1.3 μm being formed using the faster flow rate of 15 mL h^{-1}, however the fibrous mats were still too large for transplantation. The gelation of the fibres has not been observed before and further work would be of interest to see what effect the topography of the gelated fibres has on cell growth. This gelation may give improved handling for transplantation and thinner mats could be produced with the intension they will then gelate before transplantation. To increase cell attachment and decrease cell death an investigation into the attachment cell adhesive peptides was undertaken.

4. Surface-Active Agents

4.1 Introduction

Work to improve cell adhesion was undertaken with the hope of improving cell growth and proliferation on the MMA:PEGM electrospun polymer fibres. The succinimidyl-activated MMA:PEGM co-polymers showed good cell adhesion and reduced cell apoptosis compared to the unfunctionalised MMA:PEGM co-polymers. Further improvement in cell growth and proliferation however would still be desirable and this was investigated with the possibility of applying any positive results to the electrospun fibrous mats or biodegradable microspheres.

The biodegradable PLGA:PLLA microspheres have been investigated for use as a delivery vehicle for cells[100]. Cell types which are anchorage dependant such as the RPE cells require a platform on which to seed and proliferate[175]. As the PLGA:PLLA microspheres degrade slowly over time, the cells have time to establish and mature on the surface before they are released. Using the biodegradable microspheres to deliver cells may provide advantages over a simple suspension of cells injected into the eye and has been shown to prevent backflow from injection sites[176]. An interesting observation from previous work was that microspheres with increased roughness resulted in better cell attachment, however these blends were of a larger diameter than required for injection. In order to reduce the diameter of the microspheres and have optimum cell attachment, cell recognition sequences could be utilised.

A number of approaches are exploited to improve cell adhesion, most commonly scaffolds of various compositions are coated in ECM proteins such as laminin or fibronectin to increase cell attachment[177]. Using these whole proteins however can lead to problems due to the high cost in obtaining pure proteins and possible immune response *in vivo*. Additional problems are encountered if the proteins bind in the wrong conformations as this will reduce cell adhesion[120].

Another method commonly used to improve cell attachment is by coating the scaffold with a peptide containing the peptide sequence RGD which was discovered

to be a crucial sequence for cell recognition and adhesion[125]. This key sequence is responsible for cell recognition and therefore allows the use of smaller peptides rather than a whole protein such as laminin. These small peptides work in the same way as the full proteins with the extracellular matrix (ECM) of the cell identifying and attaching to the peptide. Cell adhesion is a result of the recognition of this RGD sequence by integrin receptors in the ECM of cell surfaces. Integrins have been recognised as the superfamily of transmembrane glycoproteins that function in cell adhesion. There are at least 23 different integrins known in the literature and the integrin $\alpha_v\beta_3$ is expressed in the RPE cell type[137]. Excess RGD peptides can be problematic, however, as they can bind to receptors before they bind to the surface of the scaffold and inhibit cell adhesion.

Synthetic mimics of RGD peptides have also been utilised to increase cell adhesion. These mimics can show a greater activity by being optimised for ideal interactions with specific functional groups within the active site of an integrin. They can be cheaper than the natural RGD mimics and are less likely to invoke an immune response than natural products[181]. The attachment route onto a scaffold can also be planned unlike natural peptides which normally have more than one possible site of attachment.

Important features such as how the RGD peptide mimic is displayed from the surface of a biomaterial must be considered during design. The distance between the arginine and aspartic acid group on the peptide mimics is ideally between 8-12 bonds to give the greatest activity[133]. A linker between the biomaterial and the peptide has been shown to improve activity, due to the linker increasing the exposure of the peptide and a calculated minimum length of 3.5 nm has been shown to increase binding[134]. Surface distribution is another important factor to consider and this can be tailored in the biomaterial or surface design. Taking these features into consideration, small molecule RGD mimics can be prepared.

4.2 Preparation of synthetic RGD mimics to improve cell adhesion.

4.2.1 Preparation of an RGD mimic.

An RGD mimic known to be highly active against both integrins $\alpha_V\beta_3$ and $\alpha_{IIb}\beta_3$ was prepared with the intention of attaching it to the surface of the MMA:PEGM electrospun fibres to enhance cell growth[182] (Scheme 4.1, RGD B).

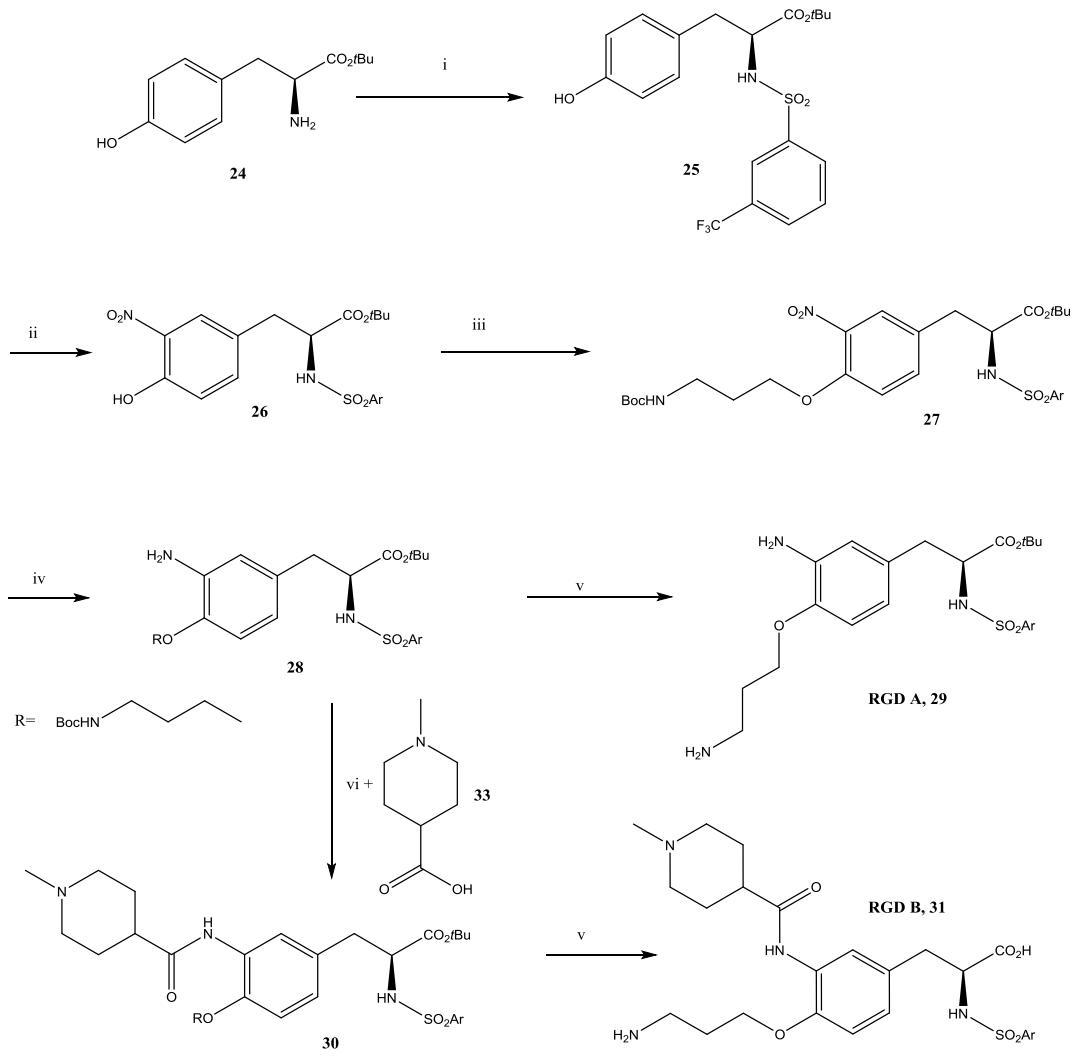

(i) $ArSO_2Cl$, Pyridine, DCM (ii) HNO_3, HOAc (iii) RBr, K_2CO_3, 18-crown-6, MeCN (iv) (5%)PtO_2, H_2, (v) TFA, DCM (vi) PyBOP, DIEA, DMF

Scheme 4.1 - Preparation of a RGD mimic active against both integrins $\alpha_V\beta_3$ and $\alpha_{IIb}\beta_3$.

In practice using this scheme two mimics could be prepared for testing, arbitrarily labelled for convenience RGD A and RGD B. The *tert*-butyl L-tyrosinate **24** was

reacted with a trifluoromethyl-containing sulfonyl chloride to protect the amine from further reaction in later steps but this group can also be used as a fluorine tag for X-ray photoelectron spectroscopy (XPS) (Scheme 4.1 step i) which would be a useful technique to confirm the presence of the RGD mimic on the surface of the MMA:PEGM co-polymer once reacted with the surface.

Pure product was obtained in a low yield after chromatography and therefore the product was taken on without additional purification. Using 70% nitric acid in acetic acid, the nitration step was attempted and during the reaction work up a precipitate formed, which was separated by filtration. After further analysis, it was shown that this was the undesired *N,N*-disulfonylated byproduct, which left the pure desired mono-sulfonylated product in the organic layer. Nitration of the product however, had not occurred. Nitric acid was distilled with sulfuric acid and using this the reaction yielded the nitrated product **26** under the more acidic conditions. A mediocre overall yield (56%) was obtained from the first two steps of the RGD mimic preparation.

The linker group to be attached onto the core tyrosine template was prepared (Scheme 4.2) in 78% yield and was then reacted with the phenol substituent on tyrosine template to give the protected linker attached tyrosinate product **27** (Scheme 4.1 step iii)**.**

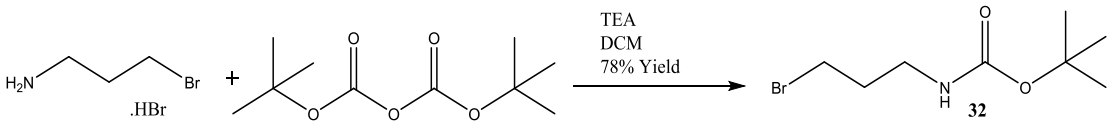

Scheme 4.2 - Preparation of linker group 32.

After linker attachment to the template, the nitro group was reduced successfully before the product **28** was split into two lots. One portion of this material was deprotected using trifluoroacetic acid to afford RGD A (Scheme 4.1). The product was successfully characterised by proton NMR, mass spectrum and infra-red analysis and, although only a small amount of material was acquired, it was sufficient for cell culture experiments.

The remaining protected material was reacted further to form the peptide mimic RGD B. A tertiary amine product was selected as this would prevent the amine from being able to react to the surface and avoid selectivity issues with the primary amine linker. To prepare the desired compound **30**, a coupling reaction with the desired acid **33** was required. The desired acid required for coupling to the tyrosine core was not commercially available and was therefore prepared via an Eschweiler-Clarke[198,199] reaction with 4-piperidinecarboxylic acid (Scheme 4.3).

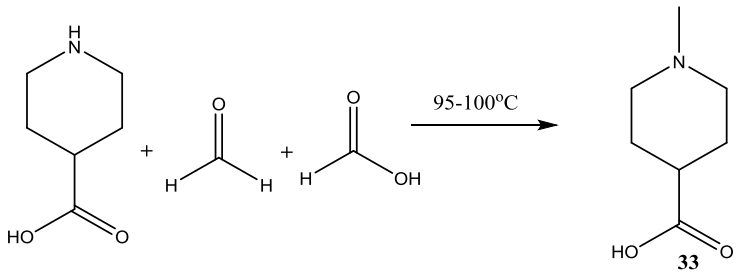

Scheme 4.3 - Methylation of 4-piperidinecarboxylic acid 33.

A 90% yield of **33** was obtained and this was successfully coupled to the tyrosine core. Trifluoroacetic acid was again used to produce the final deprotected peptide mimic RGD B.

4.2.2 Attachment of RGD peptide mimics onto MMA:PEGM co-polymers.

The prepared RGD mimics were then attached to the surface of the succinimidyl carbonate activated 60:40 MMA:PEGM polymer (Scheme 4.4).

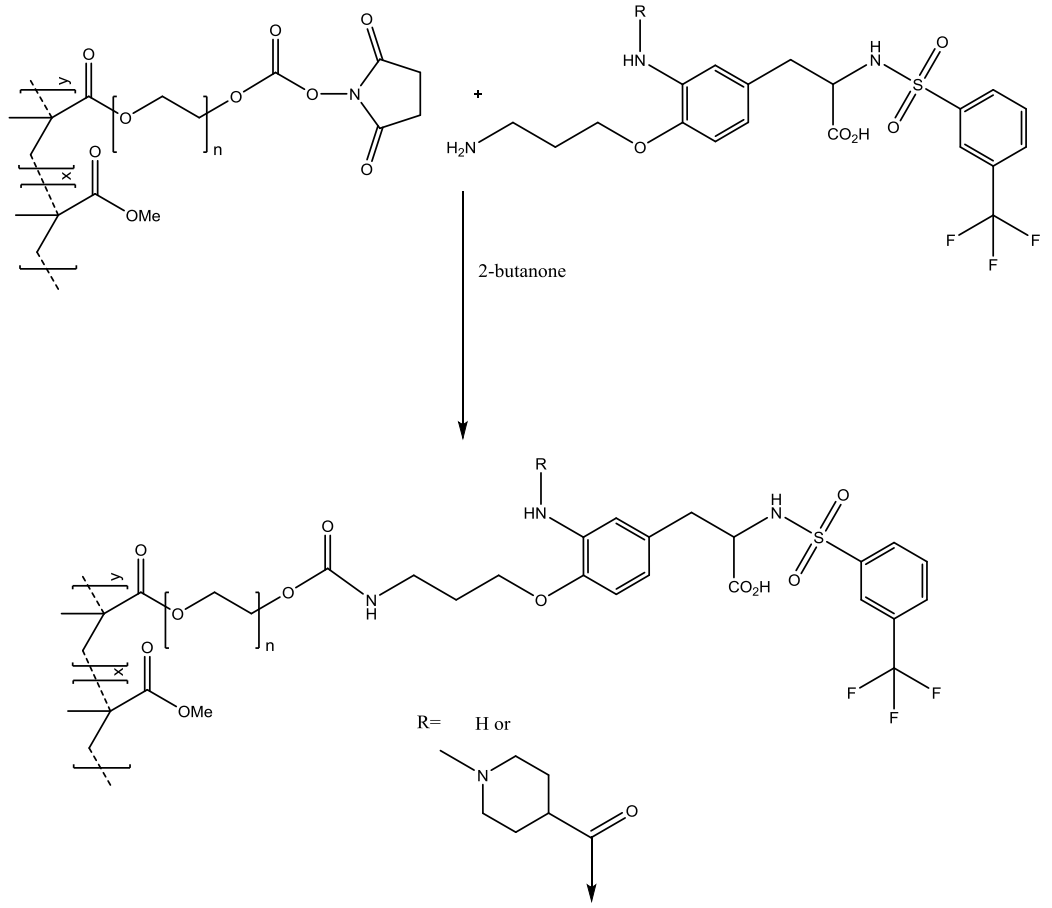

Scheme 4.4 - Attachment of RGD peptide mimics to MMA:PEGM co-polymer.

The NMR spectra of the RGD-surface functionalised MMA:PEGM co-polymers were inconclusive because of the broad peaks associated with the polymer which overwhelmed the peaks of the low concentration RGD peptide mimic. An XPS spectrum was obtained which showed peaks resulting from the 2p state of sulphur being present at around 165 eV[183] (Appendix F/G). The XPS results however are inconclusive as the fluoride 1s state was not observed (expected around 688 eV)[184]. Contact angles for the RGD mimic attached MMA:PEGM polymers were compared with those from MMA:PEGM succinimidyl-activated co-polymer. The contact angle for the 60:40 MMA:PEGM succinimidyl attached co-polymer was $88.6^{o} \pm 2.6^{o}$ (averaged over 5 drops of water) which was more hydrophobic than the MMA:PEGM polymer with RGD peptide B attached to the surface, which had a contact angle of $74.7^{o} \pm 3.3^{o}$. The smallest contact angle and most hydrophilic surface was the MMA:PEGM polymer functionalised with RGD peptide A attached

to the polymer ($71.3^{o}\pm 2.1^{o}$). This would be expected as the peptide mimics are more hydrophilic as a result of the acid and amine groups present and therefore show a decreased contact angle.

The RGD mimic-functionalised polymers were electrospun into fibres and analysed by SEM (Figure 4.1). The fibres are of a similar width to the succinimidyl-activated fibres although they have a larger distribution range (Table 4.1). By SEM, the RGD mimic-functionalised fibres appear to be more irregular than the succinimidyl-activated fibres and some beading is observed (Figure 4.1A and B).

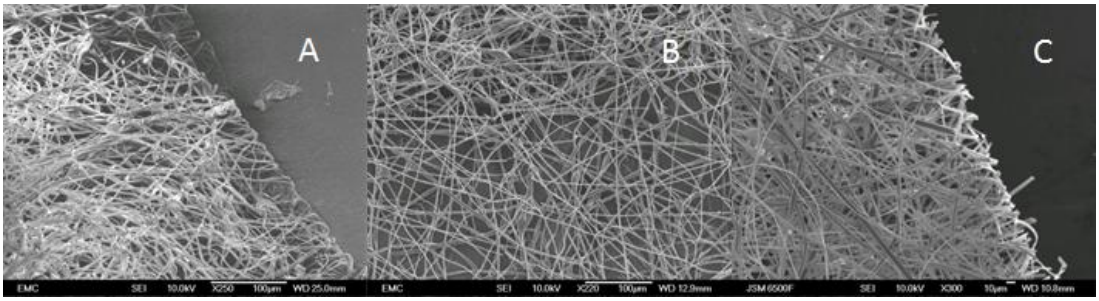

Figure 4.1 - Scanning electron micrographs of RGD surface-functionalised 60:40 MMA:PEGM co-polymer electrospun fibres: A) RGD A-functionalised polymer fibres, original magnification x 250; B) RGD B-functionalised polymer fibres, original magnification x 220; C) Succinimidyl-attached polymer fibres, original magnification x 300.

Table 4.1 - The average width and contact angle for the succinimidyl activated MMA:PEGM and RGD peptide mimic-functionalised co-polymers.

Polymer	Fibrewidth (µm) (n = 15)[a]	Contact angle of polymer films (^{o}) (n = 5) [a]
60:40 MMA:PEGM RGD peptide mimic A attached	4 ± 4	71 ± 2
60:40 MMA:PEGM RGD peptide mimic D attached	2 ± 4	75 ± 3
60:40 MMA:PEGM succinimidyl attached co-polymer	2 ± 0	89 ± 3

[a]Values expressed as mean ± standard error of the mean

The fibres are less homogeneous than the electrospun fibres of the succinimidyl activated polymers, probably due to the change in surface charge on the polymer and therefore the distribution of charge across the Taylor cone during the electrospinning process. This increases the evidence that the mimics have been incorporated onto the polymer and possible effects of the RGD mimics on the surface of the fibres can be investigated using an RPE cell line.

4.2.3 Investigation of RGD peptide mimics in RPE cell adhesion.

Following electrospinning, an immortalised RPE cell line (APRE-19) was seeded onto the surface of the scaffolds and cultured for a two week period. Samples of culture media were taken to assess cell viability utilising a LDH assay (see Experimental section). An increased absorbance in the LDH assay indicates an increase in cell death as LDH is released into the culture media during cell apoptosis (Figure 4.2).

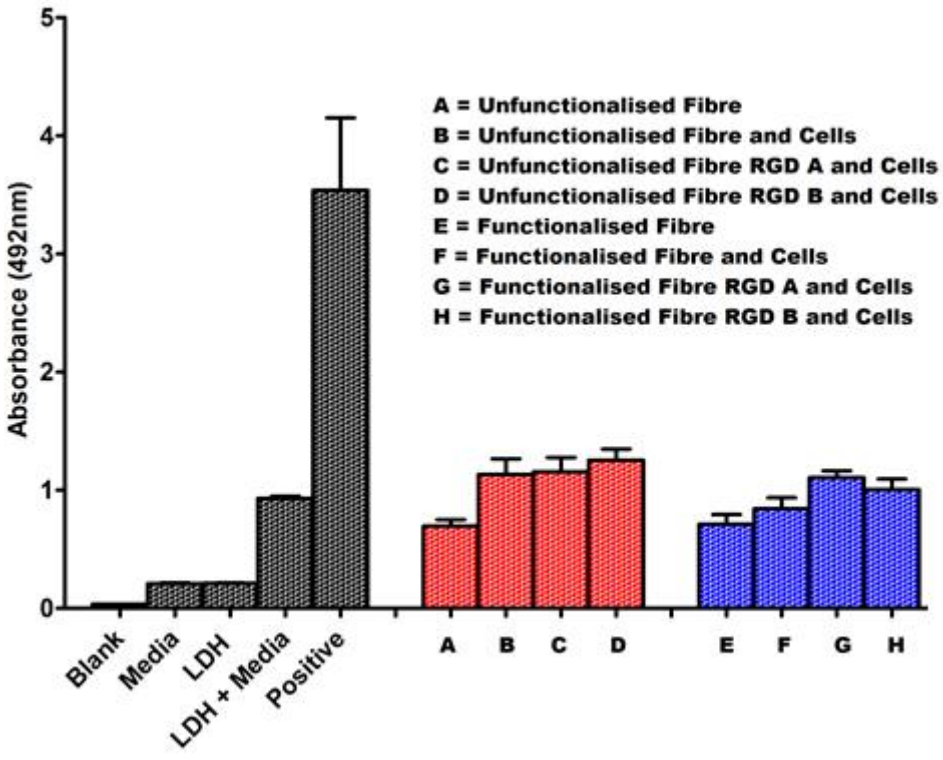

Figure 4.2 - LDH assay comparing cell death between the RGD A, RGD B and succinimidyl-functionalised 60:40 MMA:PEGM co-polymers.

The graph shows three groups of tests, firstly the control tests (black). Secondly, the non-functionalised MMA:PEGM co-polymer with no succinimidyl group. The RGD mimics were simply coated onto the polymer fibres (red). Thirdly, the succinimidyl activated MMA:PEGM electrospun fibres with the RGD mimics attached onto the fibres (blue).

The LDH assay demonstrates that the succinimidyl functionalised fibres result in significantly less cell death than the unfunctionalised fibres (columns B and F, Figure 4.2) (statistical analysis by student's t-test, conducted by Heather Thomson, University of Southampton General Hospital). When these unfunctionalised fibres (with an OH terminus at the end of the PEG chain in the MMA:PEGM co-polymer) were simply coated with the RGD mimics, cell death increased. The RPE cells are anchorage dependant and need a surface to establish themselves upon. If they bind to the RGD mimics without being attached to the surface, increased cell apoptosis is observed[86]. For the functionalised fibres cell death also increased when the RGD mimics were attached but a lower total cell death was observed in comparison with the unfunctionalised fibres with the RGD mimic incorporated.

RGD mimic A bound to the surface resulted in similar cell death levels to those seen for the unsuccinimidyl-functionalised co-polymers. RGD mimic B shows reduced cell death levels compared to the unsuccinimidyl-functionalised co-polymer but there is a slight increase in comparison with the succinimidyl-functionalised fibres alone.

Interestingly, the MMA:PEGM RGD mimic-functionalised polymers produced greater irregularity in the fibres and such surface composition may also play an important role in cell growth (Figure 4.1).

An MTT assay (3-(4,5-Dimethylthiazol-2-yl)-2,5-diphenyltetrazolium bromide) was used to confirm that the fibres and RGD mimics were non-cytotoxic (Figure 4.3). An MTT assay is used to assess cell viability as a function of redox potential. Actively respiring cells convert the water-soluble MTT (yellow) to an insoluble formazan (purple) which is viewed by absorbance spectroscopy. All the fibres with or without RGD mimic incorporated into the polymer showed no cytotoxic effects.

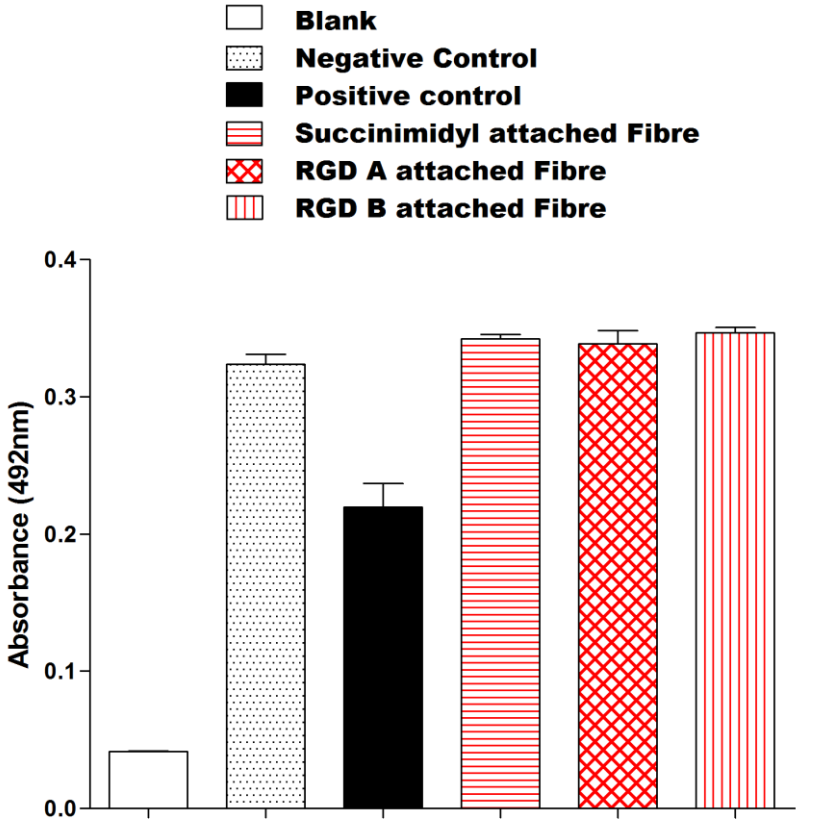

Figure 4.3 - MTT assay investigating the cytotoxicity of RGD A, RGD B and succinimidyl attached 60:40 MMA:PEGM co-polymer.

4.2.4 Investigation of aminoguanidine chalcone derivatives as surface active agents.

Different peptidomimetics could also be exploited to examine whether further improvement could be made on the RGD A and RGD B mimics previously prepared. Chalcone aminoguanidine derivatives have shown high bioactivity and by utilising the chalcone aminoguanidine as a core template, novel RGD peptide mimics can be developed[185,186]. Chalcones are of interest because of their ease in creation and attachment of a range of substituents to the molecule could provide an effective way to prepare several novel derivatives for testing (Scheme 4.5). It has been shown that the distance between the arginine and aspartic acid groups should ideally be between 8-12 bonds to give greatest activity[133]. By attaching groups to the aromatic rings, the acid moiety could be placed at the desired length away from the basic group.

Chalcone derivatives with bromine groups attached onto the aromatic rings were first explored (Scheme 4.5). This was to see if both rings could have functionality introduced without affecting chalcone formation and bromine was utilised because of its usefulness in coupling reactions. The final active chalcone aminoguanidines could then be formed with reaction with aminoguanidine hydrochloride. Evidence that the desired product had formed was obtained by NMR and MS, however small broad peaks at 6.35 ppm and 7.1 ppm were present in the proton NMR spectrum. The product was recrystallised with 2-nitrobenzoic acid forming white crystals and a crystal structure was obtained (Figure 4.4). The crystal structure showed that the desired product had formed and the additional peaks are likely due to the proton on the aminoguanidine group being scrambled between the different nitrogen centres. The crystal structure also shows a possible preferred conformation which is important when bound to the active site of the integrin. A crystal structure of the $\alpha_v\beta_3$ integrin has been obtained with an RGD ligand and this can be used to model future compounds developed[138].

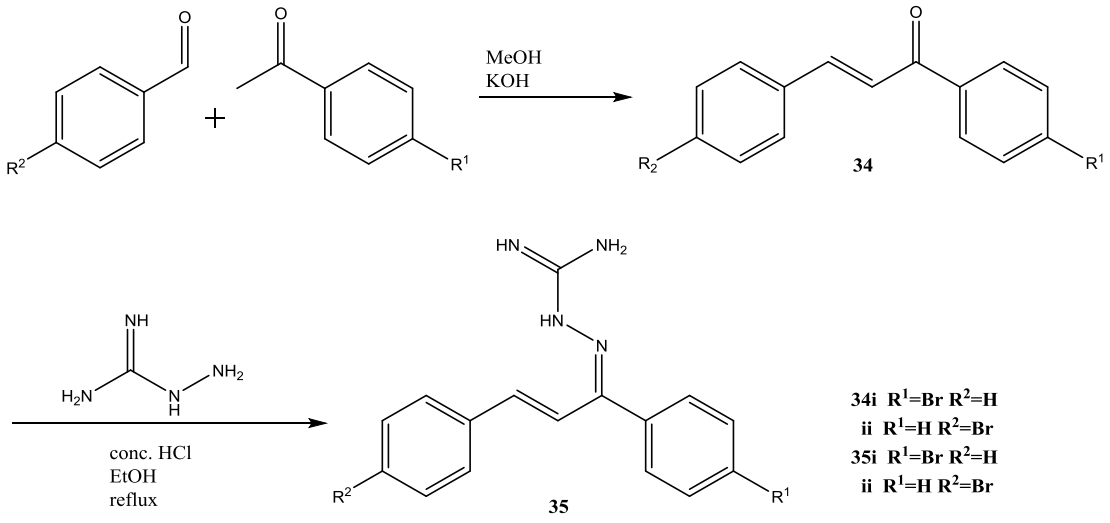

Scheme 4.5 - Formation of chalcone aminoguanidine derivatives

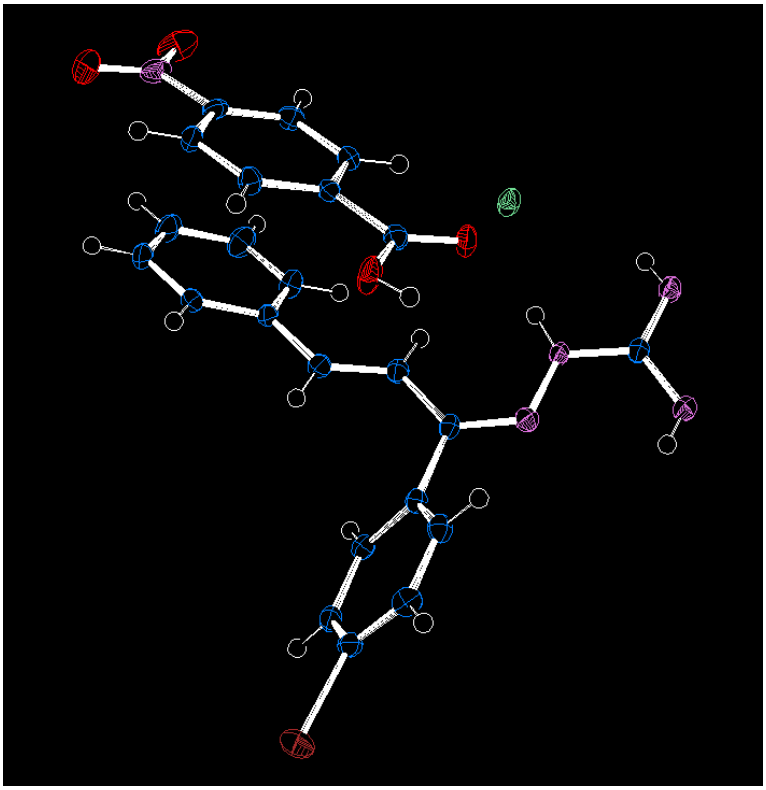

Figure 4.4 - Crystal structure of aminoguanidine chalcone.

Table 4.2 Crystallographic data for $C_{23}H_{16}N_5O_4Br.H_5C_7NO_4$

Empirical Formula	$C_{23}H_{16}N_5O_4Br$
Mass	510.34
Collection temperature/ K	150
Crystal System	Triclinic
Space Group	P-1
Unit Cell	a=7.333(5) b=12.425(5) c=13.512(5) α=89.431(5) β=75.587(5) γ=81.074(5)
Volume	1177.4
Z	2
R1	0.0362
wR2	0.1005

Attachment to the surface of the microspheres was then investigated. These microspheres can be used as another approach to deliver RPE cells and improve cell growth compared to an injection of a suspension of cells into the eye[100]. Any increased cell growth due to small molecule attachment can also be transferred onto the fibrous scaffolds at a later stage. Attachment to the microspheres was first investigated by formation of a chalcone with phenol functionality. This phenol could be reacted with a linker attached to the surface of the microspheres thereby incorporating the chalcone unit. Once the chalcone was attached onto the surface, the microspheres could be reacted with the aminoguanidine hydrochloride salt to form the potentially active aminoguanidine chalcone surface (Scheme 4.6).

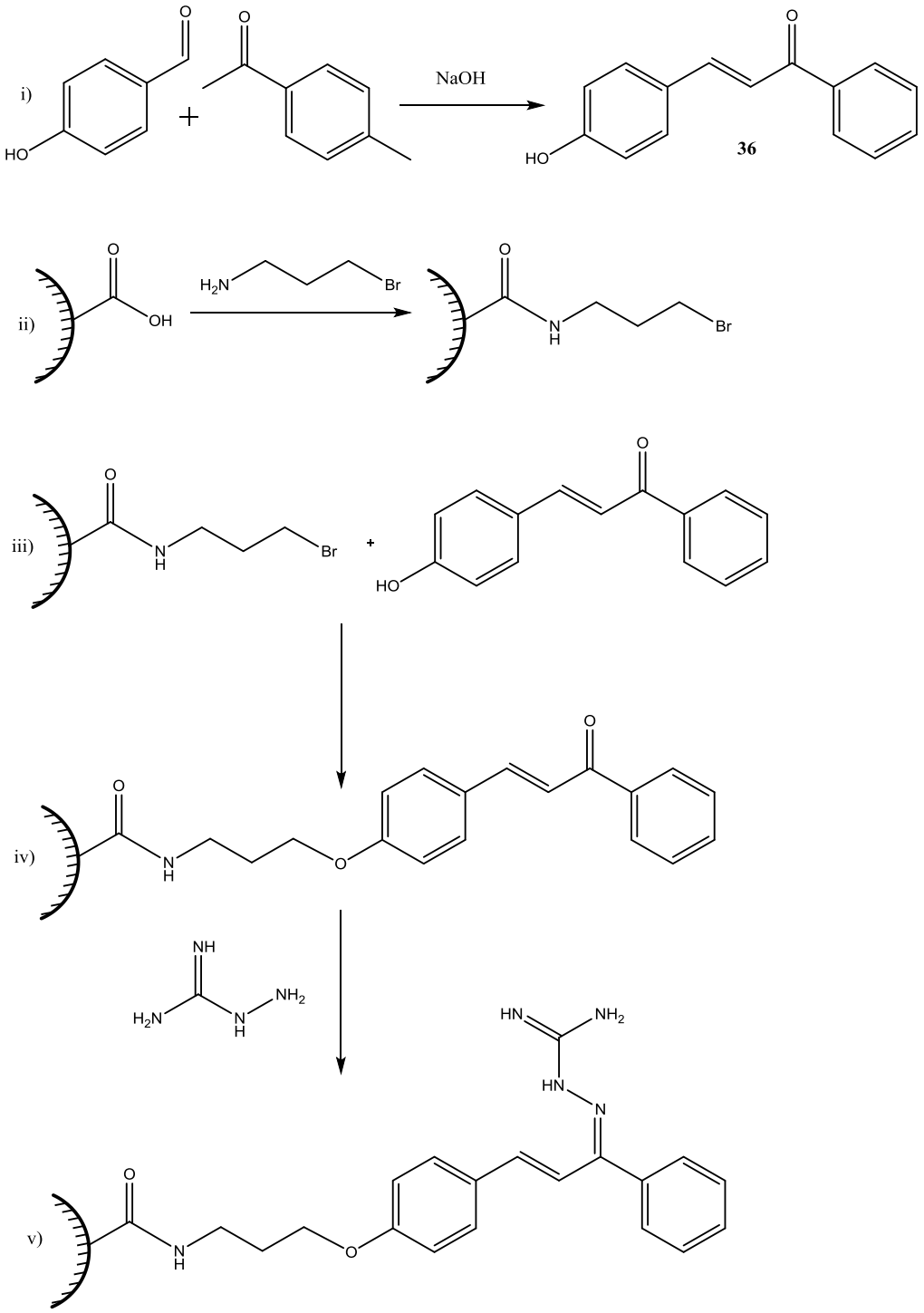

Scheme 4.6 - Formation of Chalcone coated microspheres.

By NMR it was difficult to determine if the linker had attached due to the large amount of polymer present in the microspheres overwhelming the spectrum. The chalcone was then reacted with the linker attached to the microspheres and again by NMR it was difficult to determine if the chalcone had attached onto the surface. UV-

Visible spectroscopy was attempted to see if the chalcone peak could be observed at around 350 nm, however nothing was observed. As no XPS marker groups were present on the chalcone to distinguish between the chalcone and the polymer it was reacted further with aminoguanidine hydrochloride in an attempt to form the aminoguanidine chalcone. By NMR and IR no alteration to the microsphere surface could be determined. The microspheres were dissolved and spun onto a glass surface to measure the contact angle, however no significant differences were observed between the activated microspheres, and the chalcone-functionalised microspheres. When probed under SEM it appeared the microspheres were of poor quality possibly because of the conditions utilised to attach the aminoguanidine moiety (Figure 4.5). Cell attachment and proliferation experiments would be a useful way to see if differences between the microspheres were obtained due to attachment of the aminoguanidine chalcone however, these were not attempted due to the limited resources and likely failure of the attachment onto the microspheres resulting in poor quality of the microspheres.

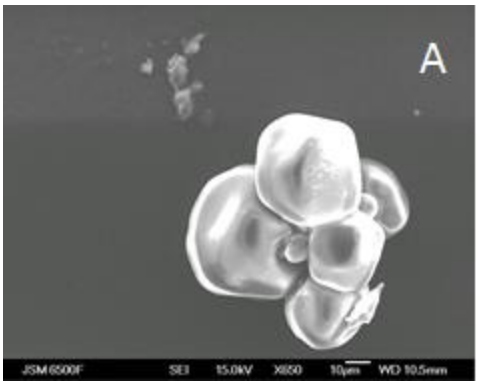

Figure 4.5 - Scanning electron micrograph of attempted aminoguanidine chalcone surface attached microsphere, original magnification x 650.

4.3 Investigation of natural surface active agents to improve cell adhesion.

4.3.1 Preparation of an RGDS tetrapeptide by solid phase synthesis.

In view of the unsuccessful attempts for attachment of an RGD mimic to the surface of the microspheres, a more traditional approach was undertaken. The natural peptide sequence RGDS was prepared using solid phase peptide coupling

methodology. The RGDS sequence (Arg-Gly-Asp-Ser) is found on fibronectin and interacts with $\alpha_v\beta_3$ integrin[188]. RGDS is not found on collagen unlike the RGD peptide sequence therefore resulting in greater specificity to desired cell types[189]. By synthesising the RGDS tetrapeptide, comparison can be made with the RGD mimics previously prepared. The behaviour of the tetrapeptide can also be compared with the laminin, collagen and fibronectin-functionalised microspheres.

The RGDS peptide was prepared using solid-phase peptide synthesis starting with protected serine attached to Wang resin (Scheme 4.7). After deprotection of the amine group by removal of the Fmoc moiety, the aspartic acid could then be attached. A deprotection could then be repeated before the pre-protected glycine moiety could be attached. The procedure could then be repeated to attach the final arginine group before a full deprotection of the peptide. Although 166 mg of peptide product was obtained after precipitation with diethyl ether, this was dramatically reduced after the peptide was purified using a solid phase extraction column (SPE, Sigma Aldrich) to obtain the pure RGDS peptide. Only 2.2 mg of pure RGDS peptide was obtained allowing for only a proton NMR and MS to confirm the structure of the desired product. Carbon NMR experiments were undertaken using extended scans with little success.

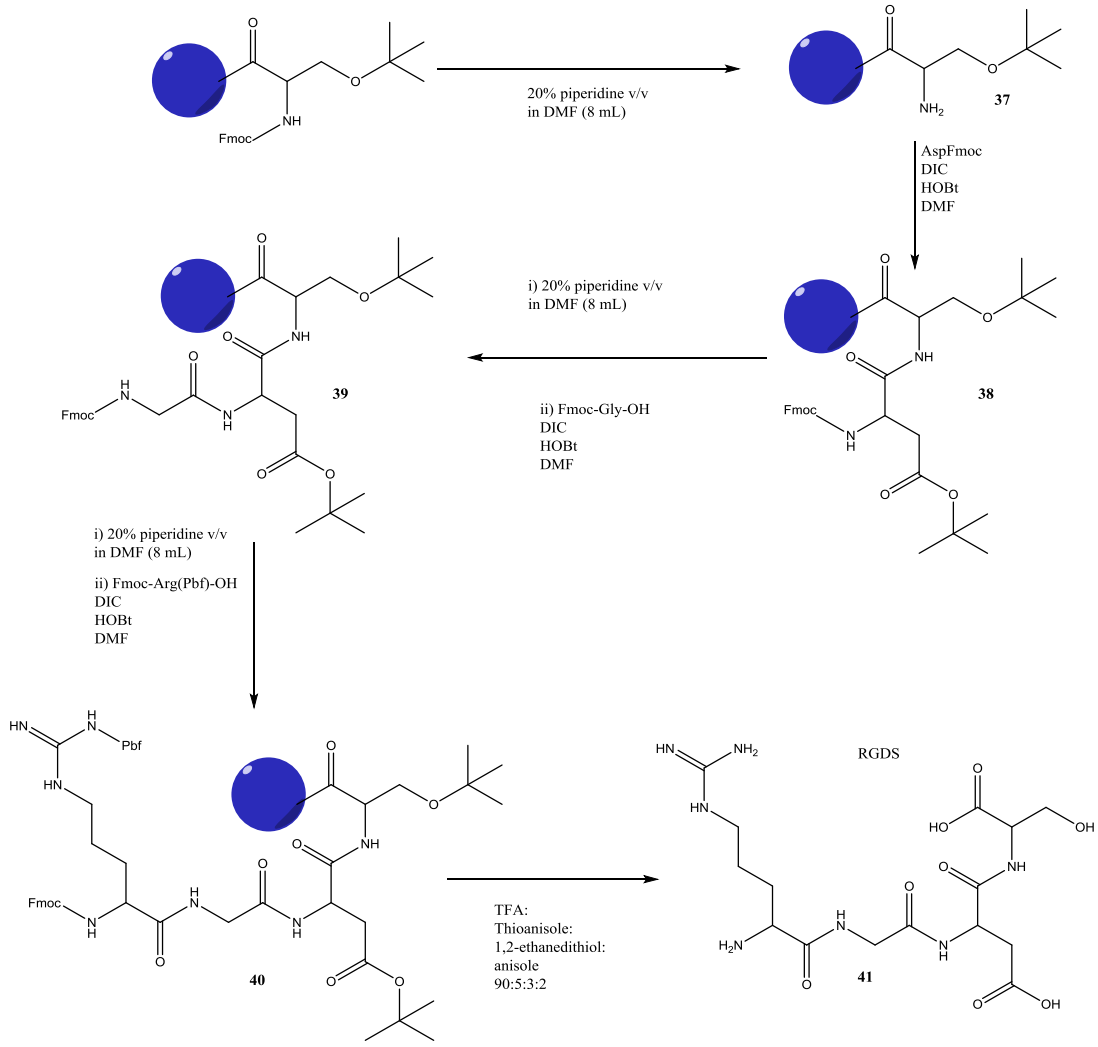

Scheme 4.7 - Formation of RGDS tetrapeptide by solid phase synthesis.

The RGDS peptide could then be attached to the microspheres which had undergone aminolysis using peptide cross coupling conditions previously performed. The microspheres were spun onto a glass surface and the contact angle measured showing an increased hydrophilicity with the amino- and RGDS- surface-activated microspheres (Table 4.3). It is difficult to detect the RGDS peptide on the surface of the microspheres, as there are no groups which could be used as an XPS tag. The PLLA:PLGA peaks within the NMR also result in overshadowing of the RGDS signal. Attachment of a florescent marker to the RGDS compound could be used but would offer no greater evidence of attachment that that previously determined within the microsphere chapter within this thesis. The microspheres were taken on with

caution to investigated cell growth to see if any further insight into attachment could be obtained.

Table 4.3 – Contact angles of PLLA:PLGA microspheres spin-coated onto a glass slide.

Microsphere	Contact angle of polymer films (°) (n = 3) [a]
50:50 PLLA:PLGA	108.2 ± 11.0
Surface-activated 50:50 PLLA:PLGA	71.2 ± 4.1
RGDS attached 50:50 PLLA:PLGA	80.9 ± 5.8

[a]Values expressed as mean ± standard error of the mean.

An immobilised RPE cell line (APRE-19) was then used to investigate the performance of the RGDS-coated microspheres to see if viable cells could be obtained. An LDH assay was first undertaken to investigate cell death (Figure 4.6). It can be observed that with the uncoated microspheres cell death increases. The RGDS coated microspheres unfortunately offer no improvement over the uncoated microspheres and no improvement over the control cells simply cultured in solution. This increase in cell death between the uncoated microspheres and the RGDS-coated microspheres is small and there are reasonably large errors associated with both sets of data, however there is no evidence for any improvement compared with the control group. This increase in cell apoptosis on the potentially RGD-coated microspheres may be the result of poor coating of the RGDS terapeptide because of the small quantity available. If attachment has occurred the attachment method may also hinder the RGDS peptide resulting in poor cell growth because of the conformation on the surface of the microspheres. Part of the active molecule may be attached to the surface and therefore unable to participate in cell recognition and attachment. This may also hinder the way the RGDS peptide is presented and is likely to be in the wrong conformation due to the restriction in rotation when bound onto the surface. Creating a linker would be interesting in further work as this may alleviate some of these issues associated with RGDS bound to the surface.

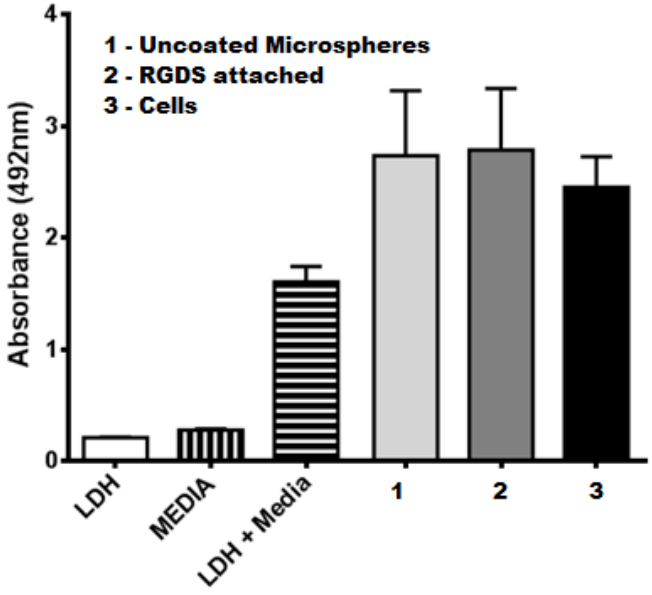

Figure 4.6 - Lactate Dehydrogenase assay comparing cell death between uncoated and RGDS coated microspheres.

An MTT assay was used to confirm that the microspheres were not cytotoxic and therefore not the underlining cause for the increased cell death observed (Figure 4.7). To investigate this further, the RGDS-attached microspheres cultured with RPE cells were imaged using the 4,6-diamidino-2-phenylindole (DAPI) stain, which allows the cell's nuclei to be visualised under UV light (Figure 4.8). From the DAPI stained fluorescent images, it is clear that cell growth is minimal. Only a few cells have attached onto the microspheres with many microspheres showing no cell attachment. The LDH assay can be misleading as only the amount of cell death is obtained from the assay and the number of cells which have grown is unknown. Although a greater number of cells have undergone apoptosis, a greater number of cells may have grown and the percentage of cell death may actually be smaller than comparable samples. However, using the DAPI stained images it is clear this was not the case for the RGDS-coated microspheres.

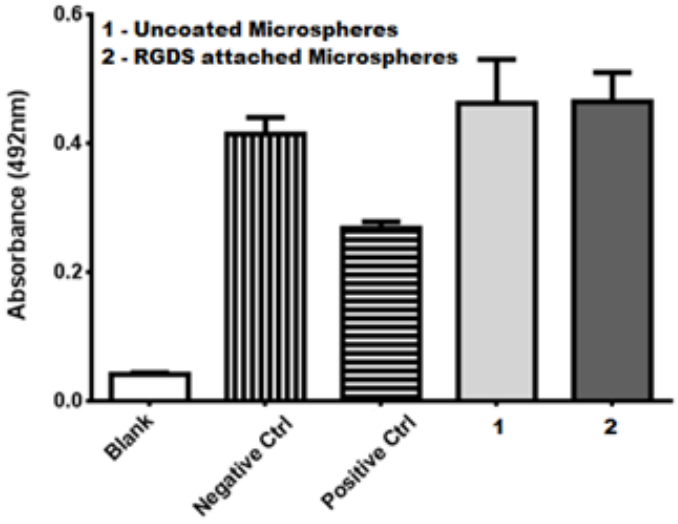

Figure 4.7 - MTT assay confirming the RGDS-coated microspheres were not cytotoxic to the RPE cells.

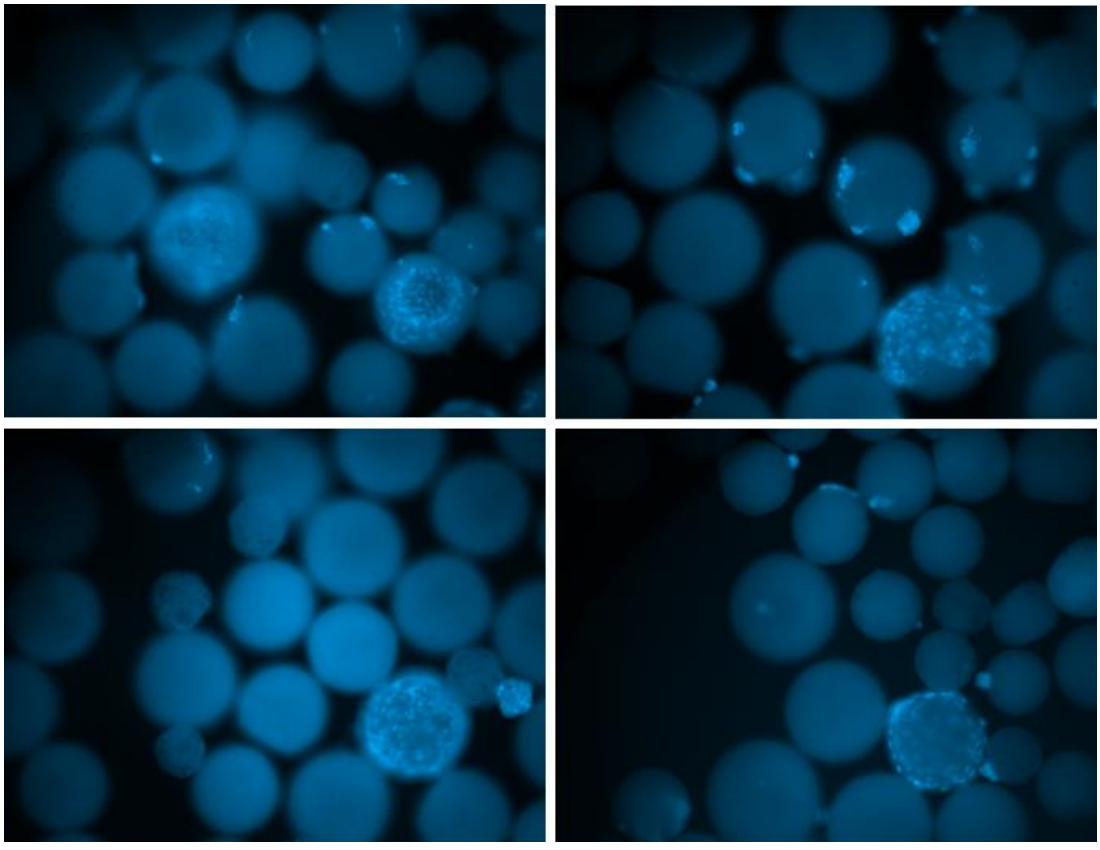

Figure 4.8 - DAPI stained fluorescence microscopy images of RGDS-coated microspheres showing cell growth. A more intense blue can be observed where cells have developed, however minimal cell growth can be observed on the microspheres.

4.3.2 Investigation of proteins to improve cell adhesion onto microspheres.

An RPE cell line was also undertaken to investigate the cell growth on the collagen, laminin and fibronectin-coated microspheres prepared in Chapter 2. An LDH assay was used to assess cell death on the attached collagen, laminin and fibronectin compared to cells grown in solution (Figure 4.9). The collagen-coated microspheres showed a large increase in cell apoptosis, however the cells in solution themselves also showed a high level of cell death. These results were atypical as the cells used as controls for the laminin and fibronectin experiments (3 and 5, Figure 4.9) did not exhibit this high cell death rate. Both the laminin and fibronectin showed very little cell death above that seen for the standard cells in solution when attached to the microspheres. This is likely to be due to the laminin and fibronectin being large glycoproteins (~200-500 kDa) and when attached to the surface of the microspheres the active cell recognition sites are likely to still be presented in a good orientation unlike the case for the surface linked peptides. Although there is no decrease in the level of cell death as might be hoped when laminin and fibronectin are attached, there is no evidence for an increase in cell death either. An increase in cell death would have negative implication for use of these natural proteins to prolong encapsulation of drugs as a secondary shell. The results give confidence that the ECM proteins could be used as a secondary coating and could be injected into the eye with little or no adverse effects. As no derogatory effects have been observed, the use of encapsulated secondary ECM coated microspheres could be an exciting prospect for as a drug delivery system treatment of AMD.

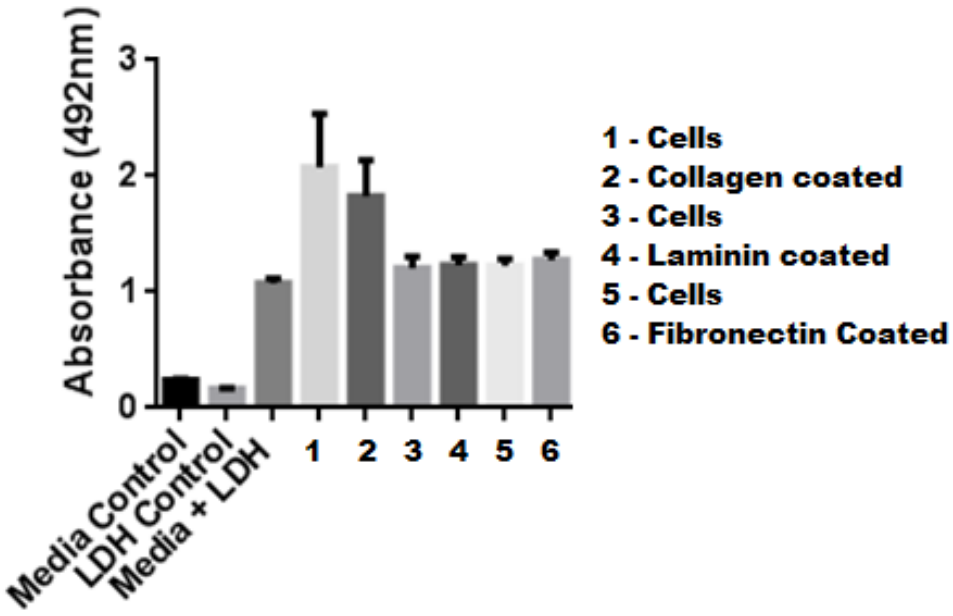

Figure 4.9 - Lactate Dehydrogenase assay comparing cell death between Collagen, Laminin and Fibronectin coated microspheres. (LDH assay prepared by Heather Thomson).

It has been shown that adhesion of RPE cells onto the MMA:PEGM electrospun fibres are slightly reduced using the active mimics. No improvement of cell adhesion was observed when the natural peptide RGDS was investigated. Further investigation into confirming the surface attachment of the RGDS peptide is required and this may be the root cause of why no improvement in cell adhesion was observed.

Using the same method of attachment on to the surfaces of the microspheres the natural proteins, laminin, collagen and fibronectin did however show good RPE cell growth and further investigation into RPE cell delivery into the eye would be of interest.

5. Summary and conclusions

5.1 Microspheres

5.1.1 Optimisation of PLLA:PLGA biodegradable microspheres.

In order to increase the therapeutic effect of current drugs used to treat AMD the use of biodegradable microspheres was investigated. The possibility of prolonging the intervals required between injections was designed to reduce the complications associated with clinical treatments such as low patient compliance and the use of a clean room (which is also required and therefore increases costs). Other retinal issues such as endophthalmitis, increased intraocular pressure and uveitis are all associated with repeat treatments.

PLLA:PLGA assemblies are commonly investigated as drug delivery systems due to their biodegradability and biocompatibility properties and these properties have been utilised for Bevacizumab delivery. PLLA and PLGA already have regulatory approval for human clinical use and further treatments for new target areas developed using these PLLA:PLGA systems are realistic and achievable. PLGA polymers have been investigated for Bevacizumab delivery by others, however using PLLA:PLGA blends an improvement in Bevacizumab delivery can be obtained over those previously reported with PLGA.

PLLA:PLGA microspheres are advantageous in that their degradation can be tuned based on the ratio of different monomer units present and has been investigated for various disease targets. In this project well-defined PLGA:PLLA microspheres have been obtained with modified prolonged release profiles and with a high encapsulation efficiency of Bevacizumab. It has also been shown that Bevacizumab retains its activity once encapsulated and released, therefore making this method a plausible candidate for sustained drug release within the eye.

A large percentage of the work was initial optimisation using various PLLA:PLGA microsphere blends and conditions in order to obtain the optimised diameter, blend

ratio with a high encapsulation level and a good release profile. Initially the work was aimed at obtaining microspheres which would be small enough that they could be injected via a 31 gauge needle. This very fine needle is what is currently used to inject into the subretinal space within the eye to achieve minimal harm. To decrease the diameter of the microspheres the polymer concentration used for their preparation was first probed. A 1% concentration gave the smallest microspheres, however the yield was severely reduced. A 2.5% concentration was optimal although the microspheres with a greater percentage of PLLA resulted in larger microspheres. It was also observed that the PLLA microspheres gave a rougher surface and a less uniform spherical shape when compared with the PLGA microsphere blends. The different PLLA:PLGA ratios used within the blends play a significant role in encapsulation and release, and initial work was aimed at producing all the microsphere blends within the desired diameter range so that encapsulation could be probed at a later stage.

Other parameters such as the stabilising solution were investigated, resulting in a low molecular weight PVA at 0.1% w:v concentration being the preferential choice. The solvent in which the polymer solution was prepared was also probed, and it was found that solvent viscosity has a greater role in microsphere diameter than the solvent volatility and speed of evaporation. The greatest improvement to microsphere diameter was by changing the Resomer® from the PLLA Resomer 207 to PLLA Resomer 206. PLLA Resomer 206 has a lower molecular weight, with a lower inherent viscosity compared to that of Resomer 207. This lower viscosity allows the shear force required to split the microsphere drops in solution to be smaller, creating smaller microspheres. All microsphere blends using the optimised parameters could be produced below 30 µm enabling them to be injected using the desired 31 gauge needle. Porous microspheres were investigated as a possibility to tune drug release further and highly porous microspheres were obtained by a gas evolution method, however the diameter of the microspheres was difficult to control and they were unsuitable for Bevacizumab delivery.

Encapsulation efficiency was investigated to evaluate how drugs could be encapsulated without high drug loss and what effect they would have on the microsphere diameter and structure. Rhodamine B and Fluorescein dyes were

initially used as drug mimics in order to optimise the encapsulation procedure. Various emulsion and microsphere preparation methods were investigated to see the effect of these on encapsulation and differing results were obtained depending on the dye used. Rhodamine resulted in better encapsulation with more hydrophobic blends of microspheres containing a greater percentage of PLLA, while Fluorescein had greater encapsulation efficiency with more hydrophilic PLGA blends. Both dyes however reached saturation around 5-10 mg per 50 mg of microspheres prepared. The stabiliser concentration did not affect the total encapsulation but when different Resomers were used encapsulation increased. The PLLA Resomer 209S which has a molecular weight ~200, 000 resulted in improved encapsulation, however the microsphere diameter increased beyond a useable point. Using Resomer 207S however did improve the level of microsphere encapsulation with all blends having good encapsulation above 80%.

Release of the dyes was investigated once the encapsulation was optimised. PLLA-based microspheres gave the lengthiest profile with release of the dye occurring over 100 days. The longer release time is probably the result of the more hydrophobic nature of PLLA and the greater crystallinity because of the L-Lactide being present, resulting in slower degradation of the microspheres. A “burst effect” can be seen where a high percentage of the total encapsulated material is released before a slower steadier release is observed. Work to prevent this quick release would be of interest in order to obtain a uniform and constant release profile. Nanospheres were also investigated and were prepared via a dialysis method. These nanospheres gave a much quicker release compared to the microspheres with all the encapsulated dye being released after 20 days. The nanosphere release profile would be ineffective for drug delivery into the eye, but may be useful in combination with other formulations to provide a quick initial release.

5.1.2 Investigating encapsulation and release of Bevacizumab encapsulated microspheres.

Exploiting the optimised methods developed from the previous microsphere experiments Bevacizumab encapsulating microspheres were investigated as a possible treatment for AMD. To investigate the encapsulation and release of Bevacizumab, FITC was attached in order to detect Bevacizumab which had been

released from the microspheres. Although attachment was successful difficulty in encapsulation was observed. However it was found that measuring the UV spectra at 280 nm Bevacizumab could be detected directly and a calibration graph could be produced for Bevacizumab without the need of an additional fluorescence attachment step. Bevacizumab was successfully encapsulated in PLLA:PLGA microspheres though only a single dose of 1.25 µg could be encapsulated per 40 mg of microspheres. Additional Bevacizumab would saturate the microspheres and was wasted. It was discovered that 40 mg of microspheres was the upper limit of microspheres which could be successfully injected into the eye. A maximum volume of 100 µL can be injected into the sub retinal space and any additional microspheres above 40 mg would result in loss of microspheres being pulled into the syringe when suspended in 100 µL of saline. In an attempt to improve encapsulation the Bevacizumab was lyophilised, however encapsulation did not increase. All of the final Bevacizumab-encapsulating microsphere blends were below 20 µm with a spherical and uniform diameter when analysed by SEM. Various microsphere blends were investigated with the 58:42 PLLA:PLGA blend giving the best overall results with the longest release.

The 58:42 PLLA:PLGA microsphere blend gave an average sphere diameter of 11.9 ± 4.8 µm which would allow for feasible injection into the eye. Encapsulation of Bevacizumab was above 85% and a steady release after an initial burst effect could be sustained for 68 days. This could allow patients to be treated less frequently with Bevacizumab, which importantly is still active. A potential draw back with the 58:42 PLLA:PLGA microspheres was the same as for the other blends, in that this method uses only a single dose of Bevacizumab. As the amount of Bevacizumab is increased the encapsulation efficiency decreases, and it appears that the microspheres become saturated, which could potentially limit increasing the 68 day release period of the Bevacizumab in further work.

Activity was tested using a combination of electrophoresis, ELISA and circular dichromism techniques. All three methods showed positive results for Bevacizumab activity showing that this would still be an effective treatment after enduring microsphere formulation. Currently Bevacizumab is administered every 4-6 weeks however the half-life of Bevacizumab after intravitreal injection is around 7 days in a

human eye[26]. Although the Bevacizumab encapsulated and released is only a single dose, it will delay the time Bevacizumab is released into the eye and increase the time in which active Bevacizumab is present within the eye. This may be an effective treatment as it stands and this will need to be investigated further.

Going forward the microspheres will need to be tested *in vivo* to investigate whether the release profile remains the same within the sub retinal space and how the Bevacizumab would accumulate within the eye. Other AMD treatment drugs such as Lucentis® would be interesting to investigate using this method, as a better encapsulation or longer release may be obtained. Improvements in encapsulation would be important to allow for encapsulation of larger doses, which would allow for longer periods between injections for the patients. However, a good release profile would still need to be maintained. Investigating the effect Bevacizumab has within the eye at a lower concentration but for a longer period would be very interesting as this is what we would expect the current microspheres to provide. Further *in vivo* tests are currently planned by our colleagues at Southampton General Hospital.

5.1.3 Functionalisation of the PLLA:PLGA microspheres to prolong release lifetime.

Further examination of the microspheres was undertaken investigating, the possibility of activating or coating the microsphere surface which could be used to avoid possible immune issues, improve encapsulation, release rates and cell attachment. Using the 50:50 PLLA:PLGA microspheres two routes for activating the microspheres were successfully achieved. Using caustic conditions an acid functional group surface could be obtained by ester hydrolysis. These sites could be reacted further and groups could be coupled onto the surface using coupling agents such as EDCI and DCC. Aminolysis was another successful approach used to activate the surface, which resulted in lower levels of degradation to the microspheres than the caustic conditions. To investigate how much surface activation could be obtained the Orange II dye was employed to ion pair with quaternary amines and then used to estimate the number of amine groups present on the surface. FITC was then reacted onto the surface showing that *ca.* 97% of the amines present could be reacted with.

It was discovered that using the aminolysis conditions only the PLGA polymer within the microsphere blend was degrading. Care had to be taken in order to maintain a good microsphere structure and to balance the number of amines present on the surface with degradation of the amine. A short study investigating the choice of solvent and diamino linker was used to determine the optimum conditions for microsphere activation. Treatment with IPA for 15 minutes appeared to give a good surface coverage without over degradation of the microspheres

Using the activated microspheres, surface attachment of various compounds could be obtained. The surface-activated microspheres could be used to attach proteins to delay the release of an encapsulated drug or to improve the biological profile of the microspheres by decreasing possible immune effects. The proteins laminin, collagen and fibronectin were attached to the surface using peptide coupling conditions. These protein-functionalised microspheres were investigated to see what effect this secondary coating of protein would have on release. Rhodamine-encapsulated microspheres were used to investigate what effect protein attached microspheres had on the degradation and release of the dye. When fibronectin, collagen and laminin were attached to the Rhodamine-encapsulated microspheres, dye release occurred over a longer period than for all blends of uncoated microspheres. Fibronectin-coated microspheres released Rhodamine over a period of 155 days, however more work is required to see if this was solely due to fibronectin or if other factors played a part, such as a better surface coating for fibronectin. By coating the microspheres, the burst effect seen with previously uncoated microspheres was not observed, which may contribute to the longer release times. A possible negative side to this method is that some dye is lost in the preparation of the surface-activated microspheres. Dye is lost during the aminolysis step and therefore, although a longer period of release is observed, a lower total quantity is released.

As part of the study of alternative surface coatings to improve release times from the microspheres, polyoxazoline polymers were investigated as an alternative to proteins. Polyoxazolines can be easily prepared with different chain lengths and hydrophobicities depending on the side chain present and as the methyl and ethyl polyoxazolines are FDA approved, they could be used for possible future treatments. This change in hydrophobicity would be interesting to see how degradation and

release rate are affected and whether this could be used to tune and optimise drug or dye release. Initial work to end-cap the polyoxazolines on to the microspheres was unsuccessful because the neat polyoxazoline product acted like a solvent and dissolved the microspheres. The polyoxazolines could not be diluted in any solvent which would not dissolve the microspheres (e.g. methanol, water) as this would terminate the polyoxazoline polymers and they would not then react with the microsphere amine surface. Any solvent which would not terminate the polyoxazolines chain (e.g. DCM, chloroform, ethyl acetate) would dissolve the microspheres. To overcome this problem β-cyclodextrin was coated onto the surface of the microspheres and adamantane was capped onto the surface of the polyoxazoline polymers. This would produce a secondary layer around the microspheres when the adamantane bound into the cyclodextrin under the aqueous conditions present within the eye.

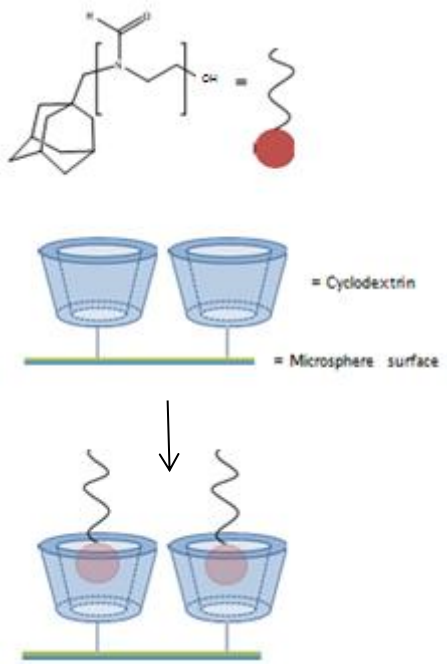

Figure 5.1 - Pictorial representation of host-guest microsphere formation. The adamantane capped polyoxazoline polymer complexes with cyclodextrin surface-coated microspheres in an aqueous medium.

Evidence for this attachment was obtained when Rhodamine-polyoxazoline-adamantane polymers were prepared and added to cyclodextrin surface-functionalised microspheres. The microspheres became pink and the colour could not be washed away. If the sample was placed in the centrifuge the pink

microspheres would sink to the bottom and an aqueous solution would remain clear showing that the dye was not simply in the solution and was fully attached onto the microspheres. The properties of the microspheres also changed depending on the polymer attached with the butyl polyoxazoline-coated microspheres clumping because of the hydrophobic nature of the polymer coating. When the butyl polyoxazoline-coated microspheres were studied for dye release, full release was not observed. The butyl polyoxazoline-coated microspheres did not appear to degrade fully probably because of they were not fully immersed in solution due to their high hydrophobicity. Using the other microspheres with polyoxazoline surface-coatings a longer release profile was obtained than for their non-coated counterparts, with the ethyl polyoxazoline polymer releasing dye over a period of 145 days. The polyoxazoline-surface coated microspheres appeared to have a delayed release until around 35 days when there was a sudden increase in the level of dye released (Figure 2.32, Microsphere chapter). If this delay is consistently observed then this could be used *in-situ* with quicker releasing microspheres or nanospheres providing a smooth overall release profile with possibly greater total encapsulation. Again however, as with the polyoxazoline-surface coated microspheres some encapsulated dye is lost during preparation of the surface-activated microspheres. During the aminoloysis reaction before the cyclodextrin is attached, dye is released, lowering the encapsulation efficiency.

One interesting result was the high mV obtained for the zeta potentials of surface-covered microspheres. The laminin-coated and the methyl polyoxazoline-coated microspheres showed potentials of -37.40 and -35.80 mV respectively. A result either positive or negative of 25 mV or greater results in colloid formation which is the case for the surface-coated microspheres. For the Bevacizumab-encapsulated microspheres a zeta potential of -0.25 mV was obtained suggesting that the microspheres are not likely to act as a colloid. This may be problematic within the back of the eye as microspheres may clump together or simply sink causing sight problems. Further work *in vivo* is required to see how the Bevacizumab-encapsulated microspheres will behave within the eye and if any clumping is observed. This could be problematic, however the surface-coating method for the microspheres could be applied to the Bevacizumab-encapsulated microspheres and may not only increase

drug delivery time, but the colloidal properties may overcome any possible clumping issues within the eye.

Initial work *in vivo* (undertaken by Heather Thomson and Phillip Alexander at The University of Southampton General Hospital) has shown that the microspheres can be effectively injected into rabbits and the desired cavity of the eye with no technical or mechanical issues (such as needle blockage or loss of material). The tests have also shown no initial negative effects in vision and no immune response has been observed. Further work *in vivo* is required to see how release rates are affected and if any build-up of the drug is observed. Investigations into how the microspheres interact within the eye and if surface activated microspheres are preferred because of their stable colloid properties are still required.

Further work into improving encapsulation of Bevacizumab would be of interest in order to encapsulate more than a single dose. Use of other AMD treatment drugs may allow for greater encapsulation and a longer release profile. Further work into the surface-activated microspheres is required to assess whether a joint approach would provide a better release profile. The combination of nanospheres suitable for a quick release of drug with the delayed releasing behaviour of surface-coated microspheres may result in a greater total level of encapsulation. Further investigation into the length of diamino linker which is used to activate the microspheres via aminolysis may also provide better surface coverage and attachment for the proteins.

5.2 Fibre formation

5.2.1 Optimisation of the electrospinning process.

The use of microspheres as a drug delivery system is aimed at preventing progression of the disease AMD. However, for a potential cure, further work into replacing the damaged retinal cells is required. The loss of photoreceptor cells within AMD is traced back to the Bruchs membrane becoming damaged due to waste build up (Drusen formation) or neovascularization (blood vessel growth and subsequent leakage). Treatments which have been investigated previously include Bruchs membrane replacements and the cultivation of RPE cells on succinimidyl fibrous mats[115,150]. Previous work resulted in electrospun mats of around 50 μm in depth

with individual fibres being within the region of 2 µm wide. However, natural unadulterated Bruchs membrane within a healthy individual is less than 10 µm in depth. These electrospun mats were therefore unsuitable for transplantation into the eye.

In order to decrease the width of the individual electrospun fibres and potentially the depth of the electrospun mat, yet still retain the physical strength of a larger mat, the electrospinning process was re-examined. In the present study each parameter affecting the electrospinning process has been investigated in an attempt to optimise the polymer mat produced. Unfortunately no improvements were observed when the solvent, polymer concentration, voltage or collector plate distance were varied. Ribboning and beading was observed in many cases, which resulted in increased fibre width. By increasing the flow rate to 15 mL h^{-1} from 9.5 mL h^{-1} the width of individual fibres decreased, however, fibrous mats with a depth of around 10 µm could not be obtained. Varying the ratio between MMA and PEGM in the polymer had little effect on fibre width, with all of the blends giving results within a comparable range (3.9-5.5 µm). A major contributor to the variation in fibre width observed was more than one fibrous strand was forming from the Taylor cone drop. It was also observed that the strand was dividing mid-fibre formation which also occurred in combination with more than one initial fibre strand forming (Figure 5.2).

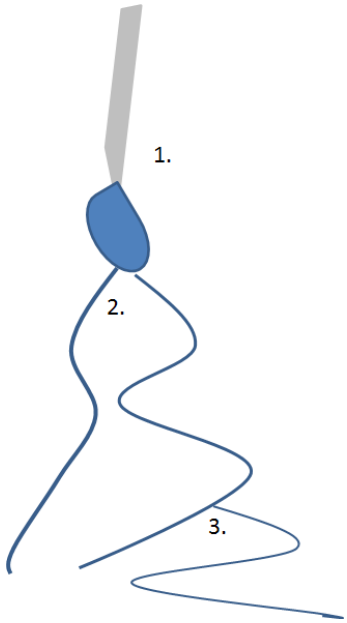

Figure 5.2 – Schematic representation of fibre formation from one or more points on the Taylor cone resulting in a wide range of fibre widths: 1) Needle tip and polymer Taylor cone; 2) More than one fibre forming from initial drop; 3) fibres splitting before reaching the collector plate, resulting in reduced and unevenly size fibres.

A comparison between the natural Bruchs membrane and the electrospun mats showed that the fibres developed had the required mechanical strength to mimic the Bruchs membrane. The Youngs modulus of the electrospun fibres was far larger than the natural Bruchs membrane however this was required to allow for feasible transfer into the eye by a surgeon. The "stress-to-fail" gave a good representation of how the fibres split and how this fraying may occur and possible issues which may arise because of this during surgery or once they are in the back of the eye. More data on the mechanical properties of natural Bruchs membrane would be of interest, however specialist equipment is required to handle the small and delicate Bruchs membrane in order to get reliable results.

In an attempt to improve the electrospinning process, MMA:PEGM co-polymers with a lower polydispersity was prepared under ATRP conditions. No improvement in electrospun fibre depth was observed, possibly due to low entanglement between chains and the use of copper catalyst in the synthesis could pose a problem if this material was used as a potential therapy within the eye. Polyoxazolines were used in an attempt to form lower polydispersity polymers in order to see how electrospinning of these would affect fibre width. Unfortunately only electrospraying

was observed likely to be because of the high hydrophilicity of the polymer, which can affect the charge distribution across the Taylor cone.

Co-polymers using MMA were studied to see how these would affect the electrospinning process and if thinner or stronger fibres could be obtained. In order to keep the possibility of treatment viable, contact lens-approved or FDA-approved polymers were investigated. MMA co-polymers with oxazolines, NVP and DEM were successfully produced, however no improvements in the fibrous mats obtained from electrospinning of these were observed.

5.2.2 Investigation of succinimidyl-activated MMA:PEGM co-polymers.

The MMA:PEGM co-polymers are the precursors to the cell-adhesive succinimidyl activated MMA:PEGM co-polymers. If the width of the MMA:PEGM co-polymer fibres could be reduced this would then be taken further onto the succinimidyl activated MMA:PEGM co-polymers. Slight success was achieved in reducing fibre width and this was taken into consideration when the succinimidyl-activated MMA:PEGM co-polymers were electrospun resulting in slightly thinner fibres. Fibres around 1.3 µm could be obtained using the increased electrospinning flow rate of 15 mL h^{-1}. The succinimidyl-activated MMA:PEGM co-polymers of all blends were slightly thinner than their non-activated counterparts. Contact angle experiments were used to investigate the difference between the succinimidyl activated and the non-activated MMA:PEGM co-polymers as well as the difference between the MMA and PEGM ratios within the MMA:PEGM co-polymers. The succinimidyl-activated co-polymers were more hydrophobic than their non-activated counterparts when the contact angles were obtained on the polymers simply spin coated onto a glass surface. When the contact-angle measurements were obtained for the electrospun mats however, the contact angles reduced to zero for the higher PEG containing polymers, which was not the case when contact angles were obtained on spin-coated surfaces. This highlights the effect topography has on the contact angles and these differences in perceived hydrophobicity and topography may also have an effect on cell proliferation.

It was observed that when the succinimidyl-activated polymers were left in the transwells with solution present for cell seeding, the mats became gel-like and produced insoluble hydrogels. The higher percentage of PEG groups present within

the gel resulted in more water absorption during swelling experiments within the gels obtained, due to the presence of the additional hydrophilic PEG groups. It was also observed that co-polymers with a higher percentage of PEG groups present produced a hydrogel faster than polymers with a greater percentage of MMA. This effect had not previously been observed in the literature and was investigated further. Initial tests showed that it was not an annealing process which was occurring, since treatment with heat and light resulted in no gel formation.

Using succinimidyl carbonate and *O*-succinimidyl model compounds a study was undertaken to determine how this crosslinking occurs within the succinimidyl-activated MMA:PEGM co-polymers. From this study two possible routes resulted in crosslinking between polymer chains if there were unreacted PEG groups present. The unreacted PEG group with an OH terminus can displace the succinimidyl group or it can react with the succinimidyl group and leading to ring opening. The presence of a base is required for the latter to occur, however some residual base may be present from the formation of the initial polymer which explains why crosslinking is also observed on the succinimidyl ester-activated MMA:PEGM co-polymers. Although cell studies have been undertaken using MMA:PEGM *N*-succinimidyl fibres the effect of the polymers gelling had been observed after cell studies had been conducted. The different structure of the gels may have an effect on the cell adhesion and proliferation properties and this was investigated. An MTT assay was used to confirm that the gels were non-toxic and the LDH assay showed decreased cell death compared to the unfunctionalised fibres and laminin-coated fibres. Coating of scaffolds with ECM proteins is common practice and lower cell apoptosis with succinimidyl-activated polymers is a very promising result. Further work on both the succinimidyl-fibrous scaffolds and succinimidyl MMA:PEGM gels is required *in vivo*, however thinner materials need to be designed for use as a feasible Bruchs membrane replacement. Although currently the fibres are too large for Bruchs membrane replacement these materials may also find other uses because of their interesting biocompatible and mechanical properties.

5.2.3 Investigation of gels for electrospinning.

When the MMA:PEGM fibres became gelatinous cell proliferation was not hindered and it was thought other hydrogels could be of interest so were investigated further.

Silane hydrogels are commonly prepared and co-polymerisation with MMA and polyoxazoline produced successful gel products. The approach to form the gels first before formation of the fibrous structure was problematic however as these gels were difficult to dissolve and electrospin into fibres. Polymer and hydrogel melts have been produced in the literature to form electrospun hydrogel fibres, however initial tests were unsuccessful and difficult to melt. Further work would be required for successful electrospinning of the hydrogels, possibly with the use of hydrogels which are more susceptible to melting before electrospinning is undertaken.

The addition of a succinimidyl group onto the MMA:PEGM co-polymers produced a particularly positive result in reducing cell apoptosis compared to ECM proteins. The maleimide group is not too dissimilar to succinimidyl and reacts specifically with thiols and therefore the amino acid cysteine, forming a carbon-sulfur linkage. By forming a maleimide activated MMA:PEGM co-polymer it was hoped cell adhesion could be improved further. By forming an acid chloride from β-alanine the maleimide was successfully incorporated into the MMA:PEGM co-polymer. The maleimide activated polymer was more difficult to get into solution in comparison with its succinimidyl counterpart and electrospinning proved difficult. Some poor quality fibre mats were obtained but they readily broke when handled and could not be placed into transwells. Use of maleimide groups incorporated with succinimidyl groups would be interesting further work. Use of both groups might result in the polymer retaining its desirable physical properties with the succinimidyl-activated co-polymer and increased cell adhesion might be obtained because of the maleimide groups present. It would be interesting to see if this cooperative effect would result in improved or hindered cell adhesion.

Further work *in vivo* is required for the succinimidyl activated MMA:PEGM copolymer to see if cell growth can be obtained within the eye. *In vivo* work would also be required to see if any immune response is observed and to test the feasibility of transplanting the fibrous mat into the eye. Thinner and stronger electrospun mats are still a target and further work with more advanced electrospinning apparatus may provide a solution. Currently we only electrospin from a single needle, however specialist techniques could use several injectors to provide an intertwined mat with improved characteristics. Further studies into the physical properties of natural

Bruchs membranes would be of interest providing more information on the structure and desirable properties which need to be designed into future polymers.

5.3 Surface active agents

5.3.1 Preparation of peptidomimetics to improve cell adhesion.

To improve cell adhesion for both the MMA:PEGM electrospun polymer fibres and PLLA:PLGA microspheres surface active agents were investigated. The succinimidyl activated MMA:PEGM co-polymers showed good cell adhesion and reduced cell apoptosis when compared with the unfunctionalised MMA:PEGM co-polymers. However, an improvement in this cell growth and proliferation, could still be obtainable and this was investigated with the possibility of applying any positive results to the electrospun fibrous mats or biodegradable microspheres.

Conventionally, to improve cell adhesion, biocompatible scaffolds of various compositions are coated in ECM proteins or protein fragments to increase cell attachment. Using these whole proteins however can lead to problems due to the high cost, possible immune response or loss of ECM protein due to lack of attachment. Initial work involved the development of a compound which could be covalently attached to the fibres or microspheres which would increase cell adhesion. As RPE cells would be the primary target an RGD mimic which showed high activity to $\alpha_V\beta_3$ was prepared. Two mimics were successfully prepared, one with a primary amine as the arginine mimic and another with a secondary amine present. The mimics were obtained in a mediocre yield, however they were successfully attached onto the MMA:PEGM electrospun fibres, with XPS showing the distinct 2pS shell present on the surface of the fibres.

The RGD mimic-functionalised fibres showed no improvement compared to the MMA:PEGM co-polymer after electrospinning. The RGD B mimic-functionalised fibres showed the least cell apoptosis, however this was more than the succinimidyl activated fibres. Cell adhesion could still be improved using cell recognition molecules and this approach could be useful in further work where succinimidyl derivatives offer little improvement, however these mimics appear ineffective for these desirable RPE cells. The RGD mimic-functionalised fibres had added irregularity when compared with the succinimidyl activated fibres and this change in

topography could also play a role in the cell adhesion observed. An MTT assay also confirmed that the RGD mimic-functionalised fibres were non-cytotoxic, however further work on the toxicity of the RGD mimics would need to be undertaken before *in vivo* work could begin.

Another linker-attached RGD mimic was investigated using a chalcone fragment as a core template. Chalcone aminoguanidines could be an effective way to prepare several novel derivatives for testing. The chalcone was added onto the surface of the microspheres before reaction with aminoguanidine hydrochloride to form the final product. This addition of the aminoguanidine was to introduced a basic group to mimic the arginine in RGD mimics, however it appeared that the reaction was unsuccessful and the microspheres structure was damaged. A more traditional approach was taken and the peptide RGDS which is known to play a role in cell recognition was prepared using solid phase peptide synthesis. It had previously been shown that peptide coupling could be achieved onto the microspheres using laminin, collagen and fibronectin and therefore the same method was chosen to couple the RGDS peptide to the microspheres. The RGDS peptide however did not improve cell adhesion onto the microspheres with the DAPI stain confirming that only a few cells had matured. The LDH assay demonstrated increased cell apoptosis had occurred when compared with cells cultivated in solution. RGDS peptides have been successfully coated onto surfaces previously within the literature and this result is likely to be due to poor coating of the RGDS tetrapeptide or to the attachment method which may hinder the RGDS peptide recognition properties resulting in poor cell growth.

5.3.2 Investigating ECM proteins for improved RPE cell adhesion.

Finally microspheres which had the ECM proteins laminin, collagen and fibronectin attached to the surface were investigated for cell attachment and proliferation. The proteins did not improve cell growth however there was no increase in cell death (collagen result disregarded due to the poor control result). An increase in cell death would have a negative implication for use of these natural proteins to prolong encapsulation of drugs as a secondary shell. Although cell attachment is not improved, the ECM proteins could be used to enhance the current properties of the microspheres to form a stable colloid in solution for better drug delivery. With little

or no adverse effects the ECM proteins could be used as a secondary coating to improve the properties of the current uncoated microspheres and possibly increase release times of encapsulated compounds.

The use of coated microspheres have shown to be successful and other applications are being investigated, such as enucleation of red blood cells. Further work into changing the linkers for the mimics, peptides and proteins which have been attached to both the microspheres and fibres would be of interest and to see what affect this would have on cell recognition. The topography appears to be another area which requires further investigation, as the RPE cells are anchorage dependant it appears that surface structure plays a key role in attachment and this effect may explain some of the results observed.

5.4 Final thoughts and future challenges

The work has provided some interesting initial data which can now be investigated further for the treatment of AMD. The PLLA:PLGA microspheres have shown to be a viable administration route to the back of the eye for the treatment of AMD. Bevacizumab can be successfully encapsulated and released with its activity remaining high. Initial work on activating the microspheres has proved successful and this can now be applied to the Bevacizumab loaded microspheres to prolong the release profile and improve its physical properties.

Gelation of the electrospun fibres has successfully shown no adverse effect on cell growth and plausible rationale has been established in to the gel formation. Continuation on reducing the electrospun fibre width is required, however further investigation into the physical properties of the gelated fibres is warranted. Thinner gels may have improved physical strength and better manual handling for transplantation.

Future challenges still remain with both the biodegradable microspheres and electrospun fibres/gels requiring further investigation in animal models. Initial work however has shown these polymer systems could potentially provide a treatment option for disease targets in the body, specifically AMD.

6. Experimental

6.1 General

All laboratory solvents were obtained from Fisher Scientific, Loughborough, UK and were used without further purification unless stated otherwise. All other chemicals were obtained from Sigma-Aldrich, Dorset, UK and were used without further purification unless stated otherwise. All NMR spectra were collected using a Bruker DPX400 or DPX300 NMR spectrometer (Bruker, Coventry, UK) (operating at 400 MHz or 300 MHz for ^{1}H and 100 or 75 MHz for ^{13}C spectra. IR spectra were collected with a Nicolet 380 FT-IR Spectrometer with a SmartOrbit Golden Gate Attenuated Total Reflection (ATR) attachment (Fisher Scientific, Loughborough, UK). Gel permeation chromatography (GPC) was performed using a Hewlett Packard 1090 liquid chromatograph with a Hewlett Packard 1037A refractive index detector. GPC was undertaken at the University of Sheffield; narrow standard calibration was used, on a PLgel, 5 μm Mixed C, 650 mm long column at 40^{o}C, eluting with chloroform:methanol 3:1 (2 mM LiBr) at a flow rate of 1 mL min^{-1}. Electrospray Mass spectra were recorded on a Micromass platform, recorded with a quadrupole mass analyser. Melting points were measured on an electrothermal melting point apparatus and are uncorrected. The single X-ray experiment was carried out on Nonius Kappa CCD diffractometer at 293(2) K with graphite-monochromated Mo-Kα 0.71073 Å radiation and corrected for Lorentz and polarization effects, and for absorption. The structure was solved by direct methods and refined on F^2 by full matrix least-squares methods anisotropically for non-hydrogen atoms. Data was solved by WinGX software. XPS analysis was performed using ThermoVG Thetaprobe (thermo scientific, Waltham, USA). The electron energy analyser was operated with a pass energy of 200 eV, dwell time of 50 ms, with a step size of 1 eV and with 5 scans being obtained.

6.2 SEM

Following fabrication, samples of each microsphere or fibre blend were mounted on carbon stubs (PELCO Tabs, Fisher Scientific) and sputter-coated with gold/palladium (Anatech Hummer 6.2 Sputter Coater) prior to imaging using a JEOL JSM-5910 scanning electron microscope (Jeol UK, Herts, UK). Micrographs at four random areas for each blend were taken and measured at 10 kV for fibres, 15 kV for microspheres.

6.3 Microspheres

6.3.1 General optimised microsphere synthesis procedure.

Poly(vinyl alcohol) (0.05 g, RMM 31,000–50,000, Sigma-Aldrich) was added to deionized water (50 mL) and the mixture was rapidly stirred (2500 rpm). W:w ratios of PLLA (Resomer L 206S, i.v. 0.8–1.2 dL g^{-1}, 0.1% in chloroform, 25°C, RMM ~100,000 obtained from Boehringer Ingelheim) and PLGA (Resomer RG 755 S, i.v. 0.5–0.7 dL g^{-1}, 0.1% in chloroform, 25°C, RMM ~20,000-80,000 obtained from Boehringer Ingelheim) having a total mass of 0.1 g were dissolved in dichloromethane (DCM) (4 mL). The PLLA:PLGA DCM solution was then added to the rapidly stirring PVA solution and the mixture was left to stir for 20 min to allow solvent evaporation. The solution was then transferred to a centrifuge tube and centrifuged for 4 min at 4000 rpm. The PVA solution was then decanted off and the microspheres were washed 3 times in deionised water. The microspheres were then isolated by filtration and dried in a vacuum desiccator.

100% PLLA

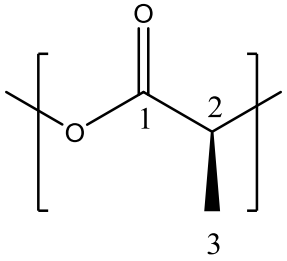

FTIR ν_{max}/cm^{-1} 2994, 1746, 1453, 1127, 1180; ^{1}H NMR:δ_H (400 MHz, $CDCl_3$) 1.60 (s, 3H, H_3), 5.18 (q, 1H, H_2); $^{13}C\{^{1}H\}$ NMR:δ_C (75 MHz, $CDCl_3$) 16.6 (C3), 69.0 (C2), 170.0 (C3).

100% PLGA 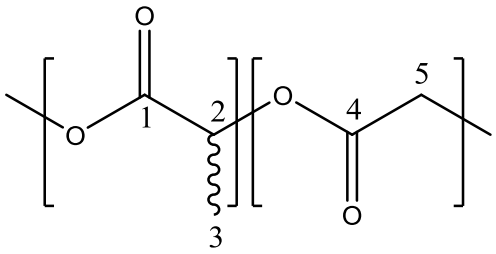

FTIR ν_{max}/cm^{-1} 2990, 2972, 1740, 1455, 1127, 1180; ^{1}H NMR:δ_H (400 MHz, $CDCl_3$) 1.60 (s, 3H, H_3), 4.80 (m, 1H, H_8), 5.19 (m, 1H, H_2); $^{13}C\{^{1}H\}$ NMR:δ_C (75 MHz, $CDCl_3$) 16.6 (C3), 69.0 (C2), 67.0 (C5), 166.1 (C4), 170.0 (C1).

6.3.2 Stabiliser change.

As step 6.3.1, with either PVA, RMM 85 000–124 000 or PVP RMM ~40 000 for Poly(vinyl alcohol) (0.05 g, RMM 31,000–50,000. Concentration of 1%, 0.5% and 0.1% were utilised by dissolving 0.5 g, 0.25 g and 0.05 g of stabiliser in 50 mL of deionised water.

6.3.3 Resomer change.

As step 6.3.1, with resomer types replaced. Used in various ratios w:w.

PLLA resomers used:

Resomer L 207S, i.v. 1.5–2.0 dL g^{-1}, 0.1% in chloroform, 25°C, RMM ~150,000,

Resomer L 206S i.v. 0.8–1.2 dL g^{-1}, 0.1% in chloroform, 25°C, RMM ~100,000,

Resomer L 209 i.v. 2.6–3.2 dL g^{-1}, 0.1% in chloroform, 25°C.

PLGA resomers used:

Resomer RG 755 S, i.v. 0.5–0.7 dL g^{-1}, 0.1% in chloroform, 25°C, RMM ~20,000-80,000,

RG 756 S i.v. 0.71–1.0 dL g^{-1}, 0.1% in chloroform, 25°C, RMM ~76,000-150,000.

6.3.4 Porous microspheres.

Gas forming approach.

PVA (0.05 g, RMM 31,000–50,000, Sigma-Aldrich) was added to deionized water (50 mL) and the mixture was rapidly stirred (2500 rpm). W:w ratios of PLLA (Resomer L 206S) and PLGA (Resomer RG 755 S) having a total mass of 0.1 g were dissolved in dichloromethane (4 mL). Using either a 3%, 10%, 20%, or 40% w/v of ammonium hydrogen carbonate was added to the DCM/polymer solution (4 mL) and was emulsified with water (0.5 mL). The PLLA:PLGA/DCM/ammonium hydrogen carbonate solution was then added to the rapidly stirring PVA solution and the mixture was left to stir for 20 min to allow solvent evaporation. The solution was then transferred to a centrifuge tube and centrifuged for 4 min at 4000 rpm. The PVA solution was then decanted off and the microspheres were washed 3 times in deionised water. The microspheres were then isolated by filtration and dried in a vacuum desiccator

Salt leaching approach.

PVA (0.05 g, RMM 31,000–50,000, Sigma-Aldrich) was added to deionized water (50 mL) and the mixture was rapidly stirred (2500 rpm). W:w ratios of PLLA (Resomer L 206S) and PLGA (Resomer RG 755 S) having a total mass of 0.1 g were dissolved in dichloromethane (4 mL). Using one of either 10% calcium carbonate (0.4 g); or with either 10% or 20% sodium oleate (0.4 g or 0.8 g); or with 10% sucrose (0.4 g) was added to the DCM/polymer solution. The PLLA:PLGA/DCM/salt solution was then added to the rapidly stirring PVA solution and the mixture was left to stir for 20 min to allow solvent evaporation. The solution was then transferred to a centrifuge tube and centrifuged for 4 min at 4000 rpm. The PVA solution was then decanted off and the microspheres were washed 3 times in deionised water. The microspheres were then isolated by filtration and dried in a vacuum desiccator

6.3.5 Swelling measurements.

The fibrous mats or porous microspheres were immersed in deionized water for 48 hours at room temperature. After absorption the hydrogel or microspheres were filtered in a stainless steel mesh and the swelling/absorption values were calculated as follows:

$$Swelling = \frac{W_s - W_d}{W_d}$$

where, W_s is the weight of the swollen hydrogel/microspheres after 48 hours in water and W_d is the weight of the hydrogel/microspheres when dry.

6.3.6 Dye-encapsulated microspheres.

Optimised dye encapsulated microspheres (w/o/w) method.

Poly(vinyl alcohol) (0.05 g, RMM 31,000–50,000, Sigma-Aldrich) was added to deionized water (50 mL) and the mixture was rapidly stirred (2500 rpm). W:w ratios of PLLA (Resomer L 206S) and PLGA (Resomer RG 755), total mass 0.1 g were dissolved in dichloromethane (4 mL).

Rhodamine B or Fluorescein (See Table 6.1) was added to the PLLA:PLGA in DCM solution and the mixture was then emulsified for 1 min with water (0.5 mL). The PLLA:PLGA/dye in DCM solution was then added to the rapidly stirring PVA solution (2500 rpm) and the mixture was left to stir for 20 min to allow solvent evaporation. The solution was then transferred to a centrifuge tube and centrifuged for 4 min at 4000 rpm. The PVA solution was then decanted off and the microspheres were washed 4 times in deionised water. The microspheres were then isolated by filtration and dried in a vacuum desiccator.

Table 6.1- Dye added during microsphere formulation

Dye	Mass of dye added during preparation (mg)
Rhodamine B	5
Rhodamine B	10
Rhodamine B	20
Fluorescein sodium salt	5
Fluorescein sodium salt	10
Fluorescein sodium salt	20

6.3.7 Measuring encapsulation of dye within microspheres.

The concentration of residual dye (Rhodamine B or Fluorescein) was determined by collecting the washings from the preparation of the microspheres and measuring the absorbance using a UV spectrophotometer (Shimadzu UV-1601 spectrophotometer). The concentration determined from the washings was then taken from the total concentration of the dye added to the microspheres during preparation and the percentage of dye not encapsulated within the microspheres could be calculated.

Additionally, 0.01 g of dye encapsulated microspheres were dissolved in DCM and the dye was extracted into water (3 x 2 mL). The concentration of the dye was then determined using a UV spectrophotometer (Shimadzu UV-1601 spectrophotometer) measuring against a calibration curve measuring at 553 nm for Rhodamine and 495 nm for Fluorescein.

6.3.8 General conditions for measuring dye release from microspheres.

Dye encapsulated microspheres (of varying blends) (0.02 g) were added into centrifuge tubes (Fisher Scientific) with phosphate buffered saline (PBS 0.01 M, 1 mL, pH 7.4, Sigma-Aldrich). The sealed tubes were kept at 37^{o}C and at set intervals the microspheres were centrifuged and the supernatant was collected for sampling after filtration through a 0.45 µm syringe filter (Fisher Scientific). The concentration of dye was then determined measuring absorbance on a UV spectrometer (Shimadzu UV-1601 spectrophotometer) against a calibration curve. Fresh PBS (1 mL) was added to the centrifuge tubes and placed back at 37^{o}C.

6.3.9 Nanosphere formation[62].

PLGA (RG 756 S, 0.025 g), PLLA (Resomer L 206S, 0.025 g) and Rhodamine B (0.001 g) were added to DMF (5 mL) within dialysis tubing (either 8 kDa or 12 kDa) and this was then placed in 5 L of water. The water was changed daily for a two further days (three days in total) before the dialysis tubing was removed and the polymer nanospheres were lyophilised to yield the final nanospheres.

6.4 Bevacizumab Microspheres

6.4.1 Bevacizumab encapsulated microspheres.

PVA (0.05 g, RMM 31,000–50,000, Sigma-Aldrich) was added to deionized water (50 mL) and the mixture was rapidly stirred (2500 rpm). W:w ratios of PLLA (Resomer L 206S) and PLGA (Resomer RG 755), total mass 0.1 g were dissolved in DCM, (4 mL). Bevacizumab (1.25 µg, 0.05 mL as a 0.025 g mL^{-1} solution, Avastin®, Genentech) was then added in to the PLLA:PLGA in DCM solution and emulsified for 1 min. The PLLA:PLGA/Bevacizumab/DCM solution was then added to the rapidly stirring PVA solution and the mixture was left to stir for 20 min to allow solvent evaporation. The solution was then transferred to a centrifuge tube and centrifuged for 4 min at 4000 rpm. The PVA solution was then decanted off and the microspheres were washed 4 times in deionised water. The microspheres were then isolated by filtration and dried in a vacuum desiccator.

6.4.2 FITC attachment onto Bevacizumab[190].

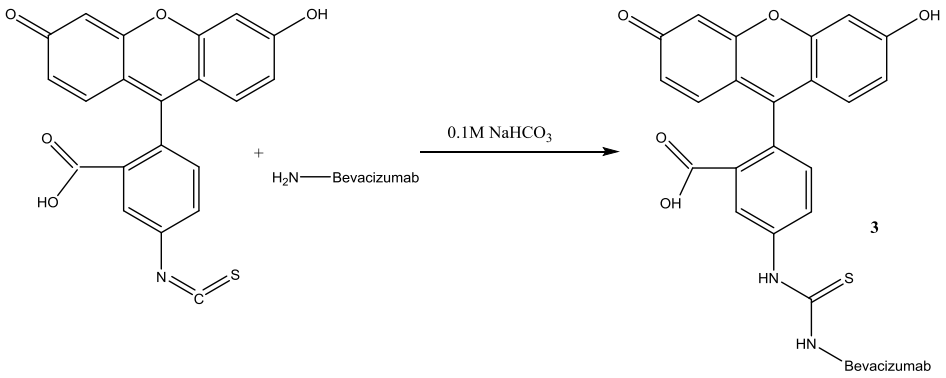

FITC (0.002 g) was dissolved with 0.1 M Sodium bicarbonate solution (2 mL). Bevacizumab (Avastin, 0.001 g) in 0.04 mL phosphate buffered saline **(**PBS) solution was added to the FITC solution at 37^{o}C. The mixture was stirred for 2 hours before being purified by dialysis and lyophilised to give the final product.

6.4.3 Measuring Bevacizumab encapsulated microspheres.

The concentration of Bevacizumab was determined by collecting the washings from the preparation of the microspheres and measuring the absorbance using a UV spectrophotometer (Shimadzu UV-1601 spectrophotometer) at 280 nm. The concentration determined from the washings was then taken from the total concentration of Bevacizumab added to the microspheres during preparation and the percentage of Bevacizumab not encapsulated within the microspheres could be calculated.

Additionally, 0.01 g of Bevacizumab-encapsulated microspheres were dissolved in DCM and the Bevacizumab was extracted into water (3 x 2 mL). The concentration of Bevacizumab was then determined using a UV spectrophotometer (Shimadzu UV-1601 spectrophotometer) measuring at a wavelength of 280 nm against a calibration curve.

6.4.4 Measuring activity of Bevacizumab released from microspheres.

1. Electrophoresis

Samples of the original Bevacizumab (5 μg, Genentech, San Francisco), the Bevacizumab released from the microspheres (5 μg) and positive control anti-VEGF mIgG1 (prepared in-house by Chris Hughes) (2 μg) were loaded onto a 10% Bis-Tris ready-made gel (Invitrogen, Thermofisher, UK), in loading buffer with (2 μg) or without β-mercaptoethanol (Sigma-Aldrich). This compound reduces di-sulphide bonds in the antibody (150 kDa for the dimer), resulting in breakdown into the constituent heavy (2 x 50 kDa) and light chains (2 x 25 kDa). The gel was run using an XCell *SureLock*® Mini-Cell (Invitrogen) at 200 V for 1 hour in MOPS buffer (Sigma-Aldrich), before staining in Coomassie Blue (Sigma-Aldrich) to visualise the bands.

2. ELISA

A 96-well ELISA plate (NUNC) was coated by incubating at 4°C overnight with 1 μg mL^{-1} human VEGF (Abcam) in PBS. The plate was then blocked by incubating at 37°C for 1.5 hours in blocking buffer (3% BSA/PBS). 100 μg mL^{-1} of the microsphere supernatant samples (or 50 μg mL^{-1} for the original Bevacizumab) in blocking buffer (3% BSA/PBS) were placed into wells in duplicate.

Bevacizumab (Avastin) was detected using a 1:1000 dilution (in blocking buffer) of goat-anti-human kappa, horseradish peroxidase HRP (Sigma-Aldrich), and incubating at room temperature for 1 hour. The HRP substrate was made by dissolving an *o*-Phenylenediamine tablet (20 mg, Sigma-Aldrich) in citrate (24.7 mL, 19.2 g L^{-1} citric acid, Sigma-Aldrich) before adding sodium phosphate (25.3 mL, 28.4 g L^{-1} Na_2HPO_4, Sigma-Aldrich), 50 mL distilled water, and 30% H_2O_2 (40 μL, Sigma-Aldrich). After incubating in the dark for 3 minutes, the reaction was stopped with 2.5 M H_2SO_4 and read on the plate reader (Dynatech MR4000) at 490 nm. After each step, the plate was washed 3 times with PBS/0.05% Tween 20 (Sigma-Aldrich).

6.4.5 Circular dichroism (CD) spectroscopy.

Bevacizumab (Avastin) released from the microspheres was added to a 1 cm cuvette and the spectrum was recorded on Jasco J-720 CD Spectrophotometer at 22^{o}C.

Bevacizumab (14 µl) was diluted in water (2 mL) to give a UV absorbance 0.36. In a 1 cm cuvette the spectrum was recorded on Jasco J-815 CD Spectrophotometer at 20^{o}C at the University of Warwick.

6.5 Activated Microspheres.

6.5.1 Surface activation of microspheres by caustic solution.

Microspheres (0.25 g) were suspended in 1 M NaOH (2 mL) and stirred at 60°C for 10 minutes. The spheres were washed with 0.1 M HCl (10 mL) and deionized water (3 x 50 mL). The microspheres were centrifuged (4000 rpm) and dried under vacuum.

6.5.2 Surface activation by aminolysis[159].

Microspheres (0.15 g) were added to a premade solution (26 mL) of 1,3-diaminopropane (268 µL) in IPA (32 mL). The solution was heated at 40^{o}C in a sand bath for 15 min before being washed with water (6 x 40 mL) and dried under vacuum.

6.5.3 Orange II test[191].

A premade solution (1 mL) of Orange II (1.5 mL, 0.014 g mL^{-1}) in 1 M HCl (2 mL) solution was added to the microspheres (0.04 g) and left for 30 min at 40^{o}C. The microspheres were then washed with water (3 x 40 mL) and once with 1 M HCl solution (1 mL). The microspheres were added to 1 M NaOH (7 mL) and left for 10 min at 40^{o}C before the washings collected. The washings were acidified to pH 3 (using universal pH paper) by addition of HCl (110 µL) and the absorbance was measured at 484 nm).

6.5.4 Peptide/polymer attachment to surface activated microspheres.

The microspheres were then coupled to an amine by addition of 1-ethyl-3-(3-dimethylaminopropyl) carbodiimide (EDCI) solution (0.008 M, 2 mL) before addition of *N*-hydroxysuccinimide (0.02 M, NHS, 2 mL). After 2 hours the desired peptide or protein was added (0.02 M) and allowed to stir overnight before washing with water (4 x 40 mL) and drying under vacuum.

6.5.5 Confocal microscopy.

Confocal microscopy was performed using a laser scanning confocal microscope (Zeiss LSM 510 Meta) and a 60× objective. The FITC was visualized by exciting with UV light at 495 nm.

6.5.6 Fluorescence spectrometry.

Fluorescence spectrometry was performed on Cary Eclipse (Agilent, USA) exciting at a wavelength of 494 nm and recording an emission spectrum between 500-700 nm.

6.5.7 Adamantane initiated Rhodamine capped polyoxazoline polymer formation.

2-Isopropyl-2-oxazoline, 2-methyl-2-oxazoline, 2-ethyl-2-oxazoline or 2-butyl-2-oxazoline (1 mL, 8.6×10^{-3} mol) was added to a solution of dry acetonitrile (2 mL) and adamantyl p-toluenesulfonate (146 µL, 9.6×10^{-5} M, prepared in house by A. Fisher via reaction of 1-adamantanemethanol with tosyl chloride). The solution was purged with nitrogen within a microwave vial and reacted under microwave radiation (150 W, 140 psi, 130°C, 10 min). Once the sample had cooled Rhodamine B (0.02 g) was added and the solution was transferred to a dialysis bag (2 kDa molecular weight cut-off) and dialysed for 3 days. The resulting solution was lyophilised to remove water.

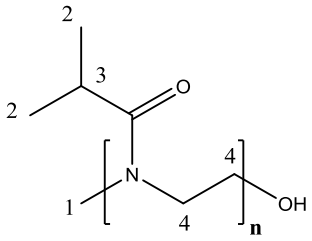

Poly(2-isopropyl-2-oxazoline).

FTIR ν_{max}/cm^{-1} 2990, 2900 (CH), 1650 (amide), 1450 (CH_2). ^1H NMR:δ_H (300 MHz, $CDCl_3$) 1.15 (6 H, br s, H2), 2.75 (1 H, m, H3), 3.50 (4 H, br s, H4), NMR comparable with literature[164]. H1 was not detected due to the intensity of the other peaks in the spectrum.

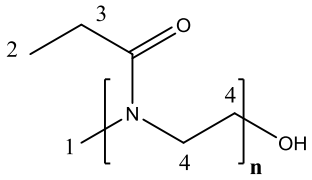

Poly(2-ethyl-2-oxazoline).

FTIR ν_{max}/cm^{-1} 2990, 2900 (CH), 1650 (amide), 1450 (CH_2). ^1H NMR:δ_H (300 MHz, $CDCl_3$) 0.98 (3 H, br s, H2), 2.30 (2 H, m H3), 3.40 (4 H, br s, H4).

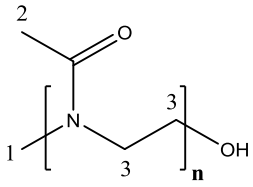

Poly(2-methyl-2-oxazoline).

FTIR ν_{max}/cm^{-1} 2990, 2900 (CH), 1650 (amide), 1450 (CH_2). ^1H NMR:δ_H (300 MHz, $CDCl_3$) 1.88 (3 H, br s, H2), 3.50 (4 H, br s, H3).

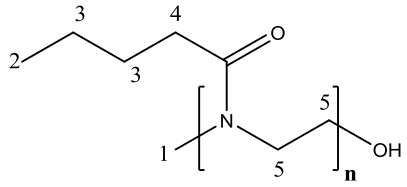

Poly(2-butyl-2-oxazoline).

FTIR ν_{max}/cm^{-1} 2990, 2900 (CH), 1650 (amide), 1450 (CH_2). ^1H NMR:δ_H (300 MHz, $CDCl_3$) 0.86 (3 H, br s, H2), 1.45 (4 H, m, H3), 2.25 (2H, m, H4), 3.50 (4 H, br s, H5).

6.5.8 Cyclodextrin coated microsphere formation.

Microspheres (0.15 g) were added to a premade solution (26 mL) of 1,3-diaminopropane (268 µL) in IPA (32 mL). The solution was heated at 40^{o}C in a sand bath for 15 min before being washed with water (6 x 40 mL) and dried under vacuum. EDCI (0.01 g, 0.05 mmol), carboxymethyl-β-cyclodextrin sodium salt (0.01 g, 0.80 mmol) was added in H_2O (1 mL) and mixed for 1 hour before addition to the aminolysed microspheres. The excess cyclodextrin and EDCI was washed with water (5 x 40 mL) before microspheres were dried under vacuum.

6.5.9 Zeta potentials.

Microsphere samples (0.002 g) were added to MilliQ water (600 µL). 100 µL of this was diluted into 1200 µL of MilliQ water. The sample added to a 0.01 cm cuvette and the zeta potential was measured using a Malvern Zetasizer (Worcestershire, UK)

6.6 Fibres

6.6.1 General Preparation of (w:w) MMA:PEGM co-polymers[192].

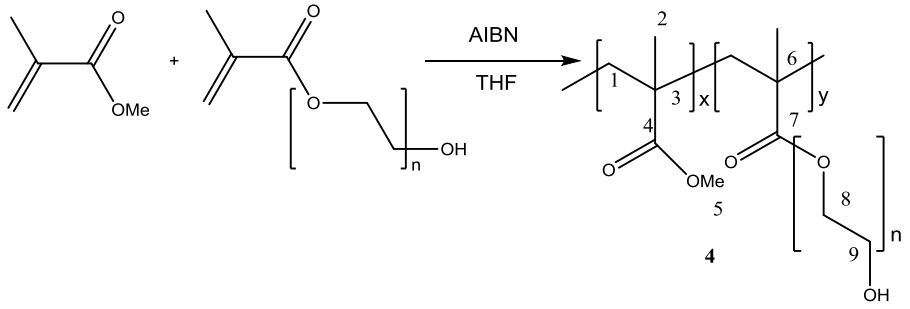

Example for 60:40 w:w MMA:PEGM polymer:

To THF (15 mL) was added to MMA (0.60 g, 0.72 mL, 5.9 mmol), PEGM (1.2 g, estimated 3.9 mmol) and azobisisobutyronitrile (AIBN) (0.0096 g, 0.06 mmol). The solution was degassed by bubbling nitrogen for 20 minutes before being refluxed for around 20 hours under nitrogen. The resulting polymer solution was purified by twice precipitating in diethyl ether (50 mL) yielding a transparent solid which was then dried under vacuum (1.18 g, 95%) FT-IR ν_{max}/cm^{-1} 2949 (CH), 1710 (CO). ^{1}H NMR:δ_H (300 MHz, $CDCl_3$) 0.90 (3H, br d, H2), 1.61 (2H, br s, H1), 1.86 (2H, br s, H1), 3.59 (3H, br s, H5), 3.66 (2H, br s, H9), 4.11 (2H, br s, H8). $^{13}C\{^{1}H\}$ NMR:δ_C (75 MHz, $CDCl_3$) 16.5 (C2) 18.7 (C2), 44.5 (C3), 44.8 (C6), 51.7 (C5), 54.3 (C1), 61.6 (PEG chain), 64.0 (PEG chain), 70.2 (PEG chain), 70.5 (PEG chain), 72.6 (PEG chain) 129.7 (PEG chain), 177.0 (C7), 177.7 (C4). GPC: 50:50 MMA:PEGM (PEGM M_n300) M_n 7940, M_w 15934, PD 2.01. GPC: 50:50 MMA:PEGM (PEGM M_n500) M_n 16031, M_w 33620, PD 2.10 NMR corresponds to literature data[115].

It was difficult to confirm ratio of MMA to PEGM because of peak overlap however an estimate could be calculated.

Mass of MMA used (g)	Mass of PEGM (g)	M_n PEGM	Estimated ratio of MMA:PEGM
0.6	1.8	300	56:44
0.5	1.5	300	50:50
0.4	1.2	300	41:59
0.5	2.5	500	55:45
0.6	2.0	500	67:33
0.4	3.0	500	30:70

6.6.2 General Preparation of NHS carbonate activated MMA:PEGM co-polymers[169].

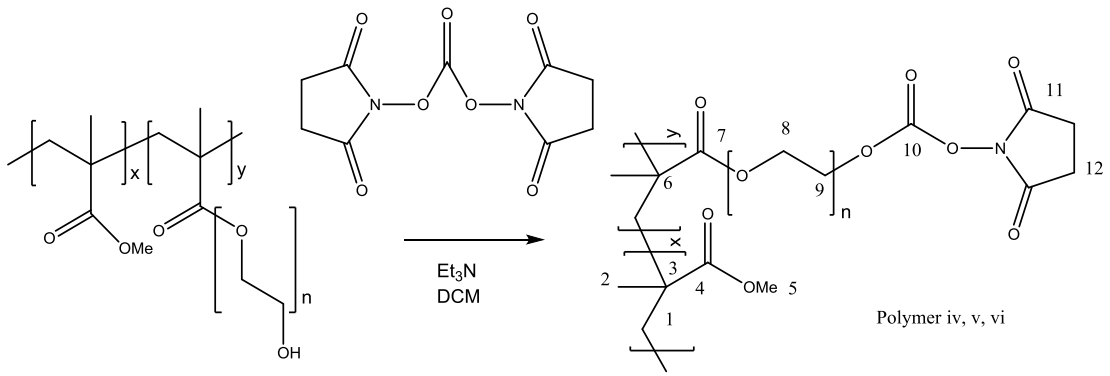

To DCM (40 mL) was added MMA:PEGM co-polymer (0.7 g), disuccinimidyl carbonate (DSC) (0.2 g) and triethylamine (0.2 mL). The reaction was left to stir overnight before being precipitated in diethyl ether twice (2 x 40 mL) yielding a white solid (0.89 g, 98 %). FTIR ν_{max}/cm^{-1} 2949 (CH), 1724 (CO) 1784 (CO-N cyclic imide). ^1H NMR:δ_H (300 MHz, $CDCl_3$) 0.90 (3H, br d, H2), 1.85 (2H, br s, H1), 2.84 (2H, br s, H12), 3.55 (3H, br s, H5), 3.70 (2H, br s, H9 in PEG chain), 4.10 (2H, br s, H8), 4.50 (2H, br t, H9 adjacent to carbonate). $^{13}C\{^1H\}$ NMR:δ_C: 100 MHz, $CDCl_3$ 16.5, 18.7, 25.6, 44.6, 44.9, 80 51.8, 54.4, 68.0, 68.3, 70.6, 177.8, 178.1. GPC: 50:50 MMA:PEGM (PEGM M_n500) M_n 17194, M_w 49716, PD 2.89. NMR corresponds to literature data[115].

6.6.3 General Preparation of MMA:PEGM acid capped co-polymers[169].

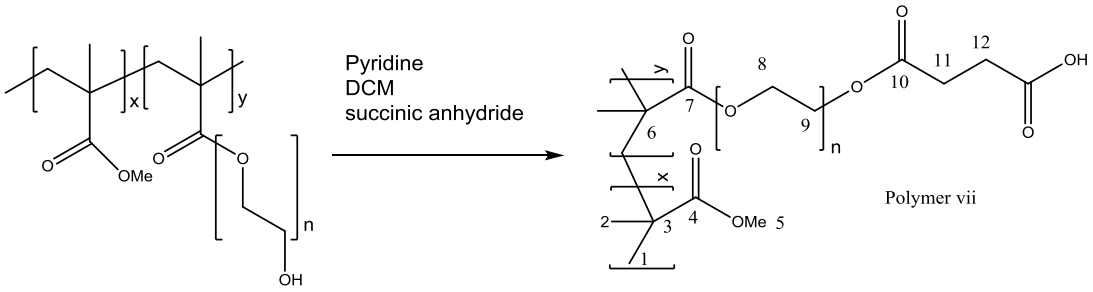

To DCM (40 mL) was added MMA:PEGM co-polymer (1 g), succinic anhydride (0.38 g, 3.8 mmol). Pyridine (0.5 mL) was added and the mixture was refluxed for 2 hours under nitrogen. The polymer was precipitated in diethyl ether (2 x 40 mL), yielding a white solid, which was then dried under vacuum. FTIR ν_{max}/cm^{-1} 3350 (OH), 1720 (CO). ^{1}H NMR:δ_H (300 MHz, $CDCl_3$) 1.00 (3H, br d, H2), 1.85 (2H. br s, H1), 2.70 (4H, br s, H11, H12), 3.55 (3H, br s, H5), 3.70 (2H, br s, H9), 4.10 (2H, br s, H8), 4.30 (2H, br s, H9 next to ester). $^{13}C\{^{1}H\}$ NMR:δ_C: 75 MHz, $CDCl_3$ 16.5, 18.7, 44.5, 44.9, 45.5, 51.8, 52.3, 54.4, 61.7, 63.8, 68.5, 69.0, 70.5, 72.6, 177.0, 177.8. NMR corresponds to literature data[115].

6.6.4 General Preparation of succinimidyl ester activated MMA:PEGM co-polymers[169].

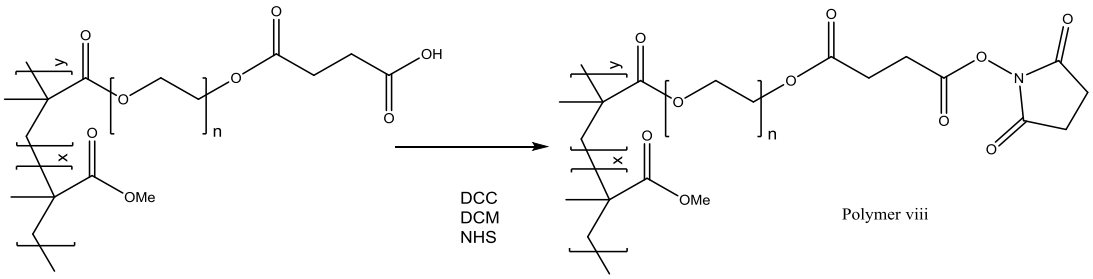

Acid capped MMA:PEGM co-polymer (polymer vii, 1 g) was dissolved in DCM (40 mL) and *N*-hydroysuccinimide (NHS) (0.6 g, 0.005 mol) was added. In an additional beaker *N*,*N*-dicyclohexyl carbodiimide (DCC) (0.003 mol, 0.6 g) was dissolved in DCM (25 mL). The DCC solution was added dropwise to the polymer/NHS solution. The reaction mixture was stirred overnight at room temperature and the resulting suspension was filtered to remove dicyclohexyl urea (DCU) before being precipitated in diethyl ether (2 x 40 mL), before being dried under vacuum. FTIR ν_{max}/cm^{-1} 2949 and 2993 (CH), 1784 (CO-N cyclic imide), 1722s (CO). ^{1}H

NMR:δppm (400 MHz, $CDCl_3$) 0.85 (br s), 1.02 (br s), 1.81 (br s), 2.84 (m), 2.96 (m), 3.59 (br s), 3.64 (br s), 4.11 (br s), 4.28 (br s) $^{13}C\{^1H\}$ NMR:δppm (100 MHz, $CDCl_3$) 16.5, 18.7, 25.4, 25.6, 26.2, 28.7, 44.5, 44.9, 51.8, 54.3, 61.7, 64.2, 68.5, 68.9, 70.6, 72.6, 72.1, 169.0, 171.0, 177.0, 177.8, 178.1. GPC: M_n 18389, M_w 127136, PD 6.91, NMR corresponds to literature data[115].

6.6.5 Optimised electrospinning parameters.

Into a 1 mL syringe a 0.55 g mL^{-1} solution of polymer in methyl ethyl ketone was added. A grounded stainless steel collector was placed 15 cm from the needle tip. The needle was then connected to a high voltage supply (Gamma High Voltage, Ormond Beach, Florida) set at 16 kV. The syringe pump was set to run at 15 mL h^{-1}. The resulting electrospun fibrous material was dried by vacuum desiccation to remove any residual solvent.

6.6.6 ATRP Polymerisation.

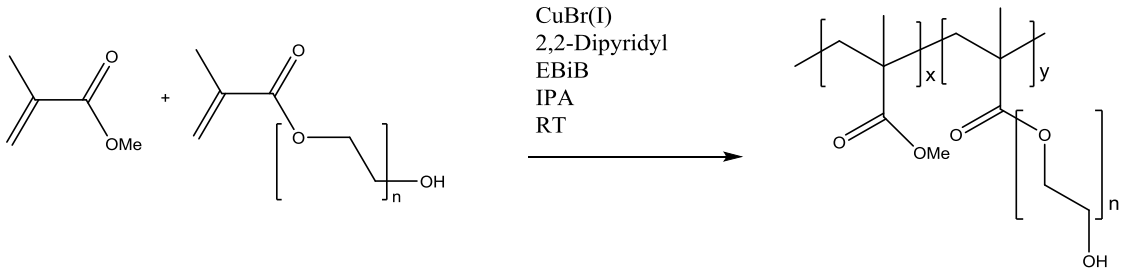

MMA (0.5g, 5 mmol), PEGM (1.5g, ~5 mmol), CuBr (0.3 g, 2 mmol) and 2,2-Bipyridine (0.33 g, 0.2 mmol) were added in to IPA (5 mL). The solution was degassed by bubbling nitrogen for 30 minutes before ethyl α-bromoisobutyrate (EBiB, 0.37 mL, 0.28 g, 1.4 mmol) was added and the reaction was then stirred at room temperature for 16 hours. The reaction mixture was filtered through an active aluminium oxide plug and precipitated from chloroform and hexane. FT-IR ν_{max}/cm^{-1} 2949 (CH), 1710 (CO). ^1H NMR:δ_H (300 MHz, $CDCl_3$) 0.90 (3H, br d), 1.61 (2H, br s), 1.86 (2H, br s), 3.59 (3H, br s), 3.66 (2H, br s), 4.11 (2H, br s). $^{13}C\{^1H\}$ NMR:δ_C (75 MHz, $CDCl_3$) 16.5 and 18.7 (C2), 44.5 (C3), 44.8 (C6), 51.7 (C5), 54.3 (C1), 61.6 (PEG chain), 64.0 (PEG chain), 70.2 (PEG chain), 70.5 (PEG chain), 72.6 (PEG chain) 129.7 (PEG chain), 177.0 (C7), 177.7 (C4). GPC: M_n 11474, M_w 20323, PD 1.76. NMR corresponds to literature data[115].

6.6.7 Polyoxazoline polymer formation.

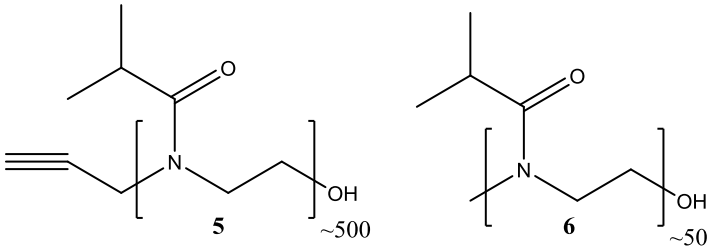

2-Isopropyl-2-oxazoline, (1 mL, 8.6×10^{-3} M) was added to a solution of dry acetonitrile (2 mL) and methyl p-toluenesulfonate (0.027 mL, 0.021 mg, 0.01 µmol) or propargyl p-toluenesulfonate (2.85 µL, 2.3 µg, 0.001 µmol). The solution was purged with nitrogen within a microwave vial and reacted under microwave radiation (150 W, 140 psi, 130°C, 10 min). Once the sample had cooled the solution was transferred to a dialysis bag and dialysed for 3 days. The resulting solution was lyophilised to remove water. FTIR ν_{max}/cm^{-1} 2990, 2900 (CH), 1650 (amide), 1450 (CH_2). ^1H NMR:δ_H (300 MHz, $CDCl_3$) 1.15 (6 H, br, s, methyl), 2.75 (1 H, m, $CH_3CH_3C\underline{H}CO$), 3.50 (4 H, br, s, CH_2 backbone). LCST 50 repeat unit polymer = 43.0°C. LCST 500 repeat unit polymer = 35.1°C. GPC 500 repeat unit M_n 16180, M_w 33816, PD 2.10.

6.6.8 Spin coating and contact angle experiments.

The chosen polymer solution in DCM (0.5 mL, 0.5 g mL^{-1}) was applied to a glass surface and spun at 5000 rpm for 30 seconds and the resulting film was used for contact angle measurements. Contact angles were also measured directly on the electrospun fibres of the activated polymers. Contact angles were calculated using a drop size of 1 µl of distilled H_2O, run on a Kruss DSA100 using a Drop Shape Analyser (DSA) running SMARTDROP contact angle software for windows v1.90.0.14.

6.6.9 *N*-(Benzyloxy)succinimide formation.

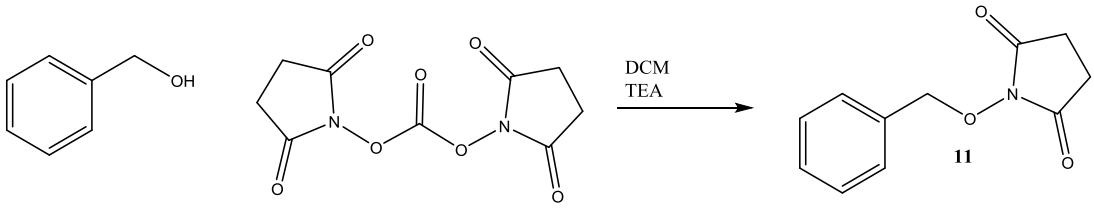

To benzyl alcohol (1 g, 9.24 mmol) in DCM (10 mL), disuccinimidyl carbonate (2.84 g, 11.09 mmol) and triethylamine (2.28 g, 32.5 mmol, 4.5 mL) were added. The reaction was stirred at room temperature overnight then washed with water (3 x 50 mL). The organic layer was dried (anhydrous $MgSO_4$) and concentrated *in vacuo* to give a solid which was crystallised (Methanol) to provide the desired product as white crystals (1.82 g, 7.3 mmol, 79%). m.p. 133-136 °C[193] (lit. 139-141 °C). IR (DCM) 1780, 1704 (CO), 1390 (NO); ^{1}H NMR:δ_H (300 MHz, $CDCl_3$) 2.50 (s, 4H, CH_2 Succinimidyl), 5.01 (s, 2H, CH_2), 7.20-7.35 (m, 5H); ^{13}C NMR (75 MHz, $CDCl_3$) δ/ppm: 25.4, 78.6, 128.5, 129.4, 129.9, 133.0, and 171.0. Crystal structure obtained and details reported in the appendix.

6.6.10 Reactions of succinimidyl derivatives.

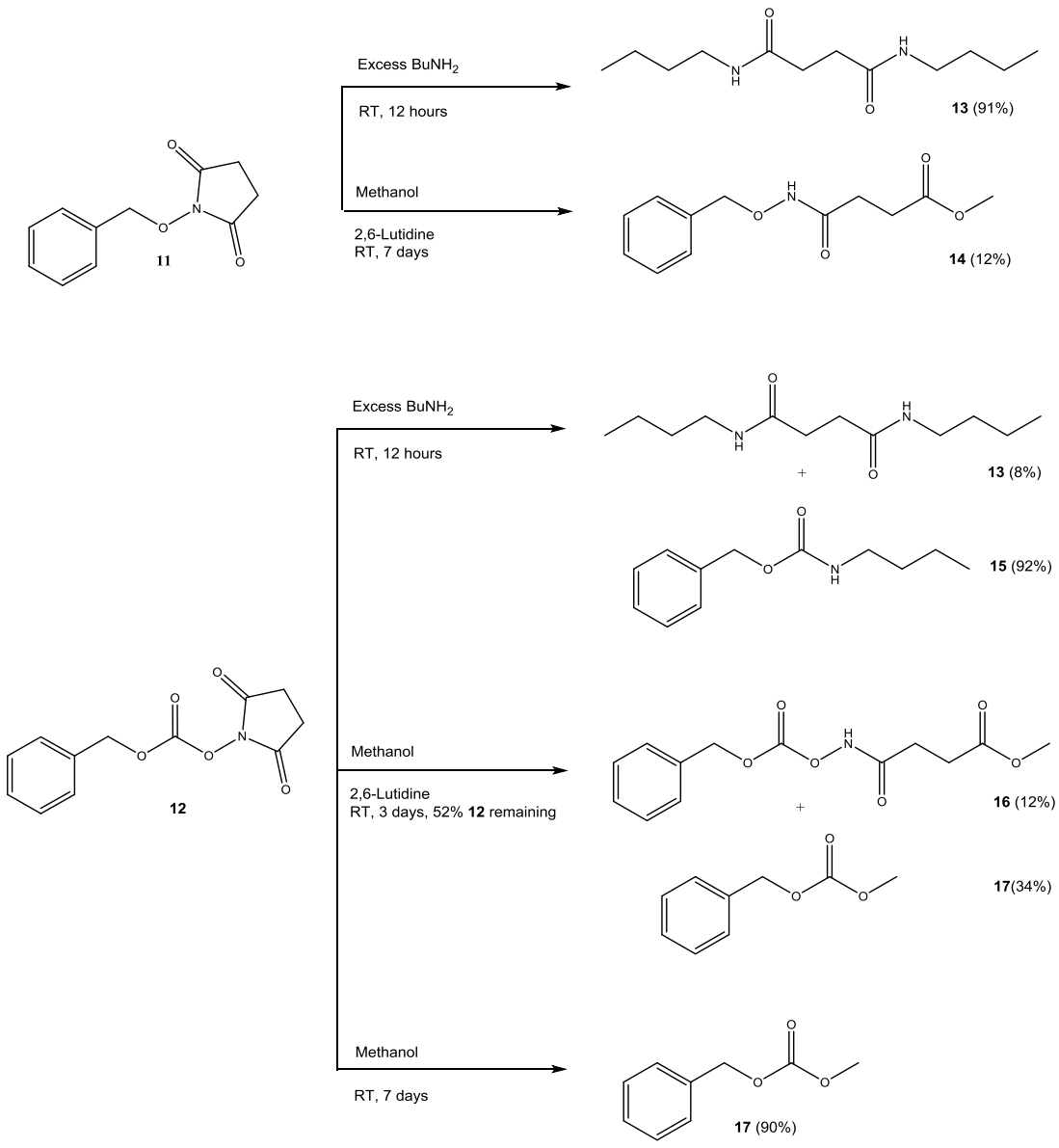

Preparation of *N*,*N*-dibutylbutanediamide (13).

N-(Benzyloxy)succinimide **11** (0.25 g, 1.1 mmol) was added portion-wise to 1-butylamine (20 mL) and the mixture was stirred at room temperature overnight. The reaction mixture was concentrated *in vacuo* and the resulting solid was recrystallised from toluene to provide **13** as a white solid (0.23 g, 1.0 mmol, 91%), R_f 0.71 (20% MeOH: 80% CH_2Cl_2), m.p. 189°C (lit.[15] 188-190°C). ^{1}H NMR (300 MHz, $CDCl_3$) δ/ppm: 3.19 (dt, 4H, *J* = 8.4, 7.0 Hz, NHC$\underline{H}_2$), 2.51 (s, 4H, COC$\underline{H}_2$), 1.51 - 1.25 (m,

8H, *n*-C*H*$_2$), 0.90, (t, 6H, *J* = 7.1 Hz, *n*-C<u>H</u>$_3$). ^{13}C NMR (75 MHz, $CDCl_3$) δ/ppm: 172.3 (<u>C</u>ONH), 39.3, 32.0, 31.6, 20.0, 19.8, (<u>C</u>H$_2$), 13.7 (*n*-<u>C</u>H$_3$). IR (neat) ν_{max}/cm^{-1}: 3297 (m, CONH), 2956 (m), 2930 (m), 2873 (m), 1632 (s, CONH), 1547 (s), 1464 (m), 1423 (m), 1338 (m), 1213 (m), 1157 (w), 725 (m). LMRS (ES$^+$): *m/z* 251.3 ([M+Na]$^+$, 100%).

Preparation of methyl 4-((benzyloxy)amino)-4-oxobutanoate (14).

N-(Benzyloxy)succinimide **11** (0.50 g, 1.9 mmol) was stirred in methanol and 2,6-lutidine for 7 days. The reaction mixture was then concentrated *in vacuo*. Purification by column chromatography (99% CH_2Cl_2/1% ethyl acetate, Silica 60) then recrystallisation (toluene/pet. ether 80-100 °C) provided a white solid **14** (0.24 g, 0.8 mmol, 12%), m.p. 93 °C. Starting material was also obtained (86%). ^{1}H NMR (300 MHz, $CDCl_3$) δ/ppm: 7. 7.35 (5H, m, Ar<u>H</u>), 4.72 (s, 2H, ArC<u>H</u>$_2$), 3.72 (s, 3H, OC<u>H</u>$_3$), 2.51 (t, 2H, *J* = 7.1 Hz, C<u>H</u>$_2$), 2.26 (t, 2H, *J* = 7.1 Hz, C<u>H</u>$_2$). ^{13}C NMR (75 MHz, $CDCl_3$) δ/ppm: 171.7, 129.1, 128.5, 78,1, 77.7, 77.3, 39.4, 31.5, 28.8, 20.0, 13.7. IR (DCM) ν_{max}/cm^{-1}: 2988, 2923 (w), 1780 (w), 1731 (s), 1681 (s), 1658 (w), 1518 (w). LRMS (ES) (M+Na$^+$), found 272.

Preparation of Benzyl-*N*-butyl carbamate (15)[194].

N-(Benzyloxycarbonyloxy)succinimide **12** (0.5 g, 2.0 mmol) was added portion wise to 1-butylamine (20 mL) and the mixture was stirred at room temperature overnight. The reaction mixture was concentrated *in vacuo* and purified by column chromatography (100% CH_2Cl_2, Silica 60) to provide a colourless oil **15** (0.38 g, 1.8 mmol, 92%), and **13** also obtained (12%). R_f 0.65 (CH_2Cl_2),. ^{1}H NMR (400MHz, $CDCl_3$) δ/ppm: 7.35 (5H, m, Ar<u>H</u>), 5.00 (s, 2H, C<u>H</u>$_2$), 3.10 (q, 2H, *J* = 6.6 Hz, NHC<u>H</u>$_2$), 1.42 (m, 2H, C<u>H</u>$_2$), 1.20 (m. 2H, C<u>H</u>$_2$), 0.79 (t, 3H, *J* = 7.1 Hz, C<u>H</u>$_3$). ^{13}C NMR (100 MHz, CDCl3) δ/ppm 156.5 (O$_2$<u>C</u>N), 136.8 (<u>Ar</u>), 128.8 (2C, <u>Ar</u>H), 128.2 (<u>Ar</u>H), 128.0 (2C, <u>Ar</u>H), 66.4 (O<u>C</u>H$_2$), 40.8 (N<u>C</u>H$_2$), 32.0 (NCH$_2$<u>C</u>H$_2$CH$_2$CH$_2$), 19.9 (NCH$_2$CH$_2$<u>C</u>H$_2$CH$_2$). 13.7 (<u>C</u>H$_3$). IR (neat) ν_{max}/cm^{-1} 3334 (m), 2957 (m), 1694 (s), 1244 (s). HRMS (ESI+) calcd for $C_{12}H_{17}NNaO_2$ [M+Na]+ 230.11515, found 230.11517. NMR corresponds to literature data[194].

Preparation methyl (benzyloxycarbonyloxyamino)-4-oxobutanoate (16).

N-(Benzyloxycarbonyloxy)succinimide **12** (0.50 g, 2.0 mmol) was stirred in methanol and 2,6-lutidine at room temperature for 3 days. The reaction mixture was then concentrated *in vacuo*. Purification by column chromatography (95% CH_2Cl_2/5% ethyl acetate, Silica 60) provided a colourless oil **16** (0.067 g, 0.24 mmol, 12%), with **17** (34%) and **12** (52%) also being recovered. R_f 0.52 (95% CH_2Cl_2/5% ethyl acetate), ^{1}H NMR (400 MHz, $CDCl_3$) δ/ppm: 2.56 (t, 2H, *J* = 6.1 Hz, C$\underline{H}_2$CH$_2$) 2.72 (t, 2H, *J* = 6.6 Hz, CH$_2$C$\underline{H}_2$) 3.71 (s, 3H, C$\underline{H}_3$) 5.27 (s, 2H, ArC$\underline{H}_2$) 7.32 - 7.44 (m, 5H, $\underline{Ar}$). ^{13}C NMR (100 MHz, $CDCl_3$) δ/ppm: 27.7 ($\underline{C}$H$_2$CH$_2$), 28.7 ($\underline{C}$H$_2$CH$_2$) 52.1 ($\underline{C}$H$_3$), 71.5 (Ar$\underline{C}$H$_2$), 128.5 (2C, $\underline{Ar}$H), 128.7 (2C, $\underline{Ar}$H), 128.9 ($\underline{Ar}$H), 135.3 ($\underline{Ar}$), 155.8 (O$\underline{C}$O$_2$), 170.5 (N$\underline{C}$=O), 173.3 (O$\underline{C}$=O). IR (neat) ν_{max}/cm^{-1}: 3216 (m), 2954 (m), 1789 (s), 1730 (s), 1438 (m), 1213 (s). HRMS (ES$^+$): Calcd. for $C_{13}H_{16}NO_6$ 282.09721 (M+H$^+$), found 282.09756.

Preparation of Benzyl methyl carbonate (17)[195].

N-(Benzyloxycarbonyloxy)succinimide **12** (0.50 g, 2.0 mmol) was stirred in methanol for 7 days. The reaction mixture was then concentrated *in vacuo*. Purification by column chromatography (100% CH_2Cl_2, Silica 60) to provide a colourless oil **17** (0.30 g, 1.8 mmol, 90%), and **12** (9%) being recovered. R_f 0.72 (DCM), ^{1}H NMR (400 MHz, $CDCl_3$) δ 3.70 (s, 3H, OC$\underline{H}_3$), 5.16 (s, 2H, C$\underline{H}_2$), 7.26–7.42 (m, 5H, Ar$\underline{H}$). ^{13}C NMR (100 MHz, $CDCl_3$) δ/ppm 54.8 ($\underline{C}$H$_3$), 69.6 ($\underline{C}$H$_2$), 128.3 (2C, $\underline{Ar}$H), 128.5 ($\underline{Ar}$H), 128.6 (2C, $\underline{Ar}$H), 135.3 ($\underline{Ar}$), 155.8 (O$\underline{C}$O$_2$). IR (neat) ν_{max}/cm^{-1} 2932 (m), 1743 (s), 1454 (m), 1261(s), 945 (m). HRMS (ESI-) 165. NMR corresponds to literature data[195].

6.6.11 MMA:Oxazoline co-polymer.

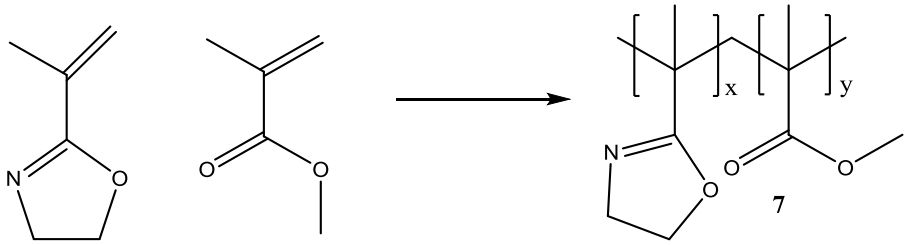

To THF (12 mL) were added MMA (1 g, 1.06 mL, 0.01 mol), 2-Isopropenyl-2-oxazoline (1 g, 0.94 mL, 0.009 mol) and azobisisobutyronitrile (0.011 g, 0.07 mmol). The solution was degassed by bubbling nitrogen for 20 minutes before being refluxed for 20 hours under nitrogen. The resulting polymer solution was purified by twice precipitating diethyl ether before being dried *in vacuo*. FT-IR ν_{max}/cm^{-1} 2948, 2841, 1725, 1635. ^1H NMR:δ_H (300 MHz, $CDCl_3$) 0.95 (br, CH_3, CMe), 1.75 (br, CH_2), 3.55 (br s, CH_3, OMe), 3.68 (br s, CH_2, Ox ring), 4.12 (br s, CH_2, Ox ring).

6.6.12 MMA:NVP co-polymer.

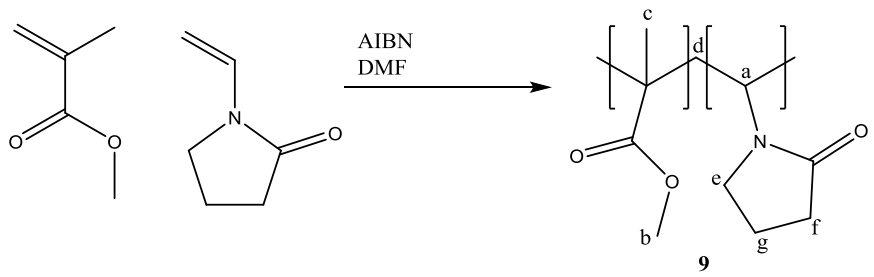

To tetrahydrofuran (THF) (12 mL) was added MMA (1 g, 1.06 mL, 0.01 mol), 1-vinyl-2-pyrrolidinone (NVP, 1 g, 1.04 mL, 0.009 mol) and azobisisobutyronitrile (0.011 g, 0.07 mmol). The solution was degassed by bubbling nitrogen for 20 minutes before being refluxed for 20 hours under nitrogen. The resulting polymer solution was purified by twice precipitating diethyl ether before being dried *in vacuo*. FT-IR ν_{max}/cm^{-1}2949, 1723, 1677, 1428, 1191, 1144. ^1H NMR:δ_H (300 MHz, $CDCl_3$) 0.95 (br d, CH_2, d), 1.70 (s, CH_3, c) 1.80 (m, CH_2, g), 2.25 (m, 2H, CH_2, f), 3.10 (m, CH_2, e), 3.35 (m, CH_3, b), 4.40 (m, CH_2, a). GPC: M_n 15786, M_w 328683, PD 20.82.

6.6.13 MMA:DEM co-polymer.

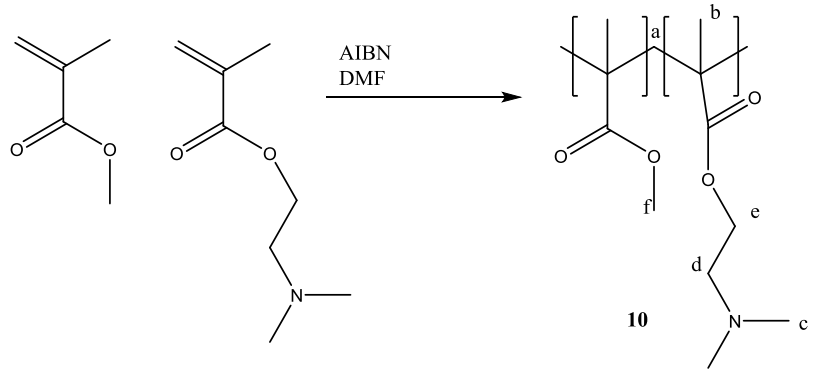

To tetrahydrofuran (THF) (12 mL) were added MMA (1 g, 1.06 mL, 0.01 mol), 2-(dimethylamino)ethyl methacrylate (DEM, 1 g, 1.07 mL, 0.006 mol) and azobisisobutyronitrile (AIBN) (0.011 g, 0.07 mmol). The solution was degassed by bubbling nitrogen for 20 minutes before being refluxed for 20 hours under nitrogen. The resulting polymer solution was purified by twice precipitating diethyl ether before being dried *in vacuo*. FT-IR ν_{max}/cm^{-1} 2947, 2769, 1238, 1450, 1722. ^1H NMR:δ_H (300 MHz, $CDCl_3$) 0.85 (m, CH_3, b), 1.90 (m, CH_2, a) 2.30 (s, CH_3, c), 2.60 (m, CH_2, d), 3.55 (m, CH_3, f), 4.05 (s, CH_2, e). GPC: M_n 23408, M_w 142896, PD 6.10.

6.6.14 Formation of 2-2-methylpent-4-en-2-yl)-2-oxazoline.

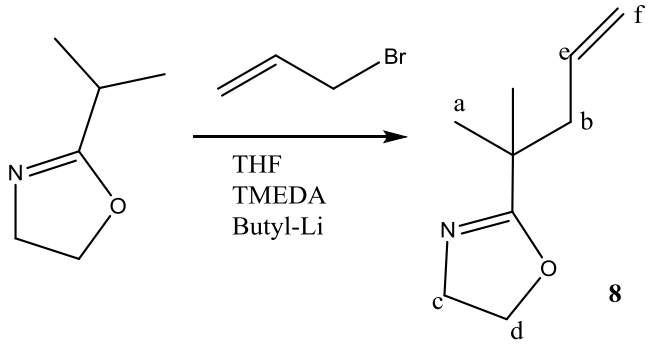

To a 3-necked round bottom flask of tetramethylethylenediamine (TMEDA, 2.64 mL, 17.3 mmol) and dry THF (100 mL) were added and cooled to -78^{o}C for 20 min. The solution was maintained at -78^{o}C and butyl lithium in hexanes (6.92, 17 mmol) was added slowly and the mixture was left for 2 hours before 2-isoproyl-2-oxazoline (2.1, 17.3 mmol) was added still maintaining the temperature at -78^{o}C. After a further 2 hours allyl bromide (1.47 mL, 2.06 g, 16.9 mol) was added dropwise and the reaction was allowed to warm to room temperature slowly. The reaction was

quenched with methanol (100 mL) and reduced under vacuum. The reaction was quenched with water and DCM before being purified by column chromatography (100% DCM, Silica 60). FT-IR ν_{max}/cm^{-1} 3020, 2975, 1615, 1150. ^{1}H NMR:δ_H (300 MHz, $CDCl_3$) 1.22 (s, 6H, a), 2.40 (d, 2H, *J* = 6.4 Hz, b), 3.75 (t, 2H, *J* = 7.2 Hz, d), 4.15 (t, 2H, *J* = 7.2 Hz, c), 5.01 (m, 2H, f), 5.69 (m, 1H, e). $^{13}C\{^{1}H\}$ NMR:δ_C (75 MHz, $CDCl_3$) 25.3, 36.5, 42.1 (F), 54.2, 67.1, 117.8, 134.3, 177.8. ESI+MS: 154 $(M+H)^+$.

6.6.15 MMA:silane Hydrogel formation.

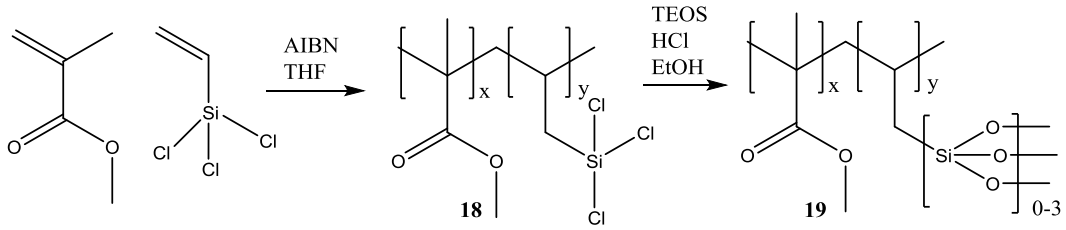

To dry THF (15 mL), MMA (0.5 g, 4.4 mmol) and allyltrichlorosilane (0.87 g, 4.4 mmol) were added and the solution was degassed with nitrogen for 20 min. AIBN (0.0096 g) was added and the solution was then heated at 70°C for 20 hours. Solvent was removed under vacuum yielding a yellow solid. The polymer **18** (0.5 g) was added to ethanol (0.05 mL) and TEOS (0.1 mL) and stirred for 5 min before a solution of water (0.01 mL) and HCl (80 µL) were added. The reaction was heated at 80°C for 30 min to give a pale yellow gel. FT-IR ν_{max}/cm^{-1} 2947, 2840, 1725, 1447, 1187, 1145, 1076. ^{1}H NMR:δ_H (300 MHz, $CDCl_3$) 0.70 (s, CH_3), 1.50 (m, CH_2, CH_2Si), 3.68 (m, CH_2), 5.00 (m, CH_3), 5.65 (m, CH_2). The peaks in the NMR remain at the same chemical shift however the peaks broaden between co-polymer and gel product (with Si crosslinking) due to reduced rotation. GPC polymer: M_n 66239, M_w 181893, PD 2.74

6.6.16 Triethoxysilane capped poly(2-isopropyl-2-oxazoline).

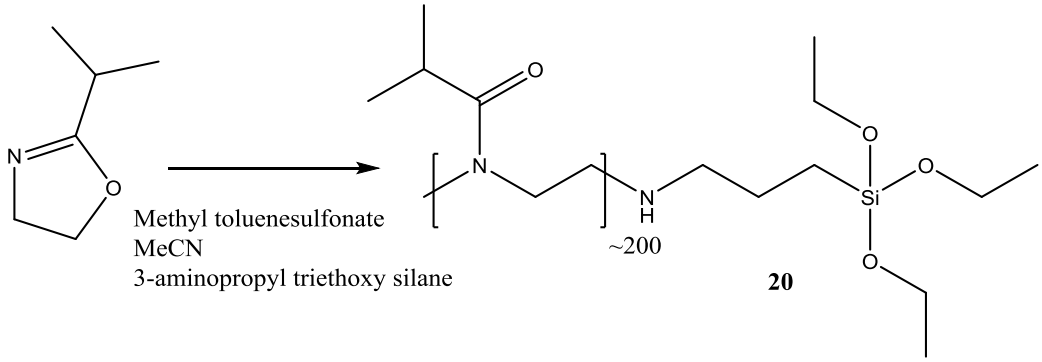

2-Isopropyl-2-oxazoline, (1 mL, 8.6×10^{-3} mol) was added to a solution of dry acetonitrile (2 mL) and methyl p-toluenesulfonate (0.026 mL, 0.032 g, 0.017 mmol). The solution was purged with nitrogen within a microwave vial and reacted under microwave radiation (150 W, 140 psi, 130°C, 10 min). Once the sample had cooled 3-aminopropyl triethoxysilane (0.02 mL, 0.019 g, 0.086 mmol) was added and the reaction was kept at 80^{o}C overnight. The solvent was removed under vacuum forming a pale orange solid. FTIR ν_{max}/cm^{-1} 2990, 2900, 2300 (w), 1629, 1450. ^{1}H NMR:δ_H (300 MHz, $CDCl_3$) 1.15 (6 H, br, s, methyl), 2.85 (1 H, m, $CH_3CH_3C\underline{H}CO$), 3.55 (4 H, br, s, CH_2 Backbone) 1.40 (CH_2, CH_2Si, weak), 3.70 (CH_2, CH_2Si, weak), 3.80 (CH_2, CH_2Si, weak). LCST 39-42^{o}C.

6.6.17 Poly(2-isopropyl-2-oxazoline) hydrogel.

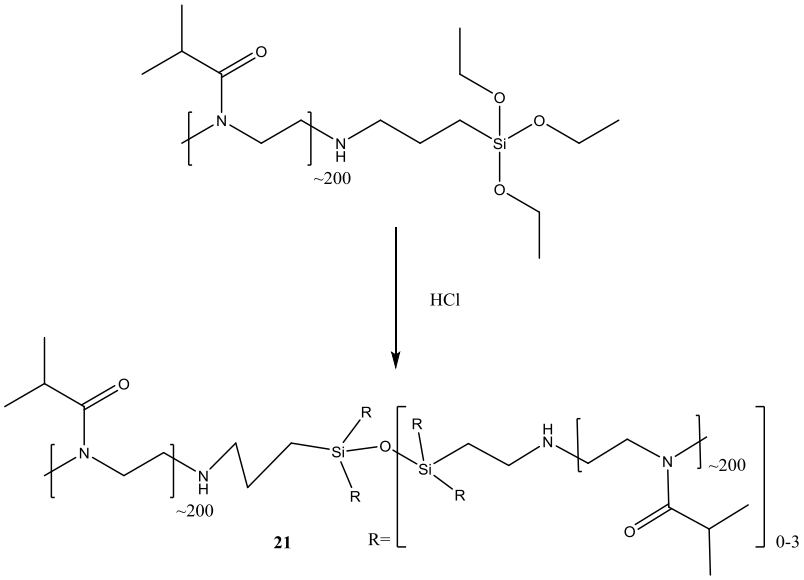

The polymer **20** prepared in section 6.6.16 (0.13 g) was added to ethanol (1 mL) before HCl (0.01 mL) was added. The reaction was heated at 80^{o}C for 1 hour. The solvent was removed under vacuum forming a light yellow solid. FTIR ν_{max}/cm^{-1} 3000, 2900, 2300, 1650, 1450. ^{1}H NMR:δ_H (300 MHz, $CDCl_3$) 1.15 (6 H, br, s, methyl), 2.60-3.05 (1 H, m, $CH_3CH_3C\underline{H}CO$), 3.40-3.70 (4 H, br, s, CH_2 backbone). LCST 45-46^{o}C.

6.6.18 3-Chloro-2,5-dioxo-1-pyrrolidinepropanoyl Chloride[173].

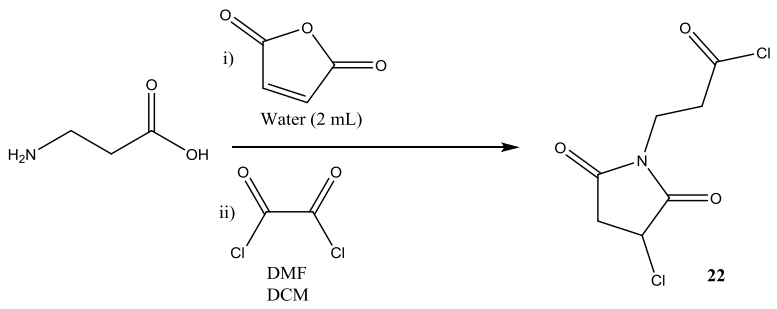

Following the procedure described in reference 173, β-Alanine (1 g, 11.2 mmol) was dissolved in water (2 mL) before maleic anhydride (1.10 g, 11.1 mmol) was added and the mixture was stirred for 3 hours. The product was filtered and washed with water (3 x 50 mL) to give the intermediate acid (0.79 g, 4.3 mmol). The acid was then dried under vacuum before oxalyl chloride (1.63 g, 1.1 mL, 12.9 mmol) was

added with DMF (1 drop) in DCM (10 mL) and the mixture was stirred overnight. Excess solvent and oxalyl chloride were removed under vacuum to give the final product as a yellow oil. FTIR ν_{max}/cm^{-1} 2930, 1730, 1669, 760. ^{1}H NMR:δ_H (300 MHz, $CDCl_3$) 4.66 (dd, 1H,), 3.90 (t, 2H), 3.35 (dd, 1H), 3.28 (t, 2H), and 2.94 (dd, 1H). $^{13}C\{^{1}H\}$ NMR:δ_C: 100 MHz, $CDCl_3$ 172.5, 172.4, 171.3, 48.5, 43.6, 39.2, 34.5. NMR corresponds to literature data[173].

6.6.19 Maleimide Terminated MMA:PEGM co-polymer[173].

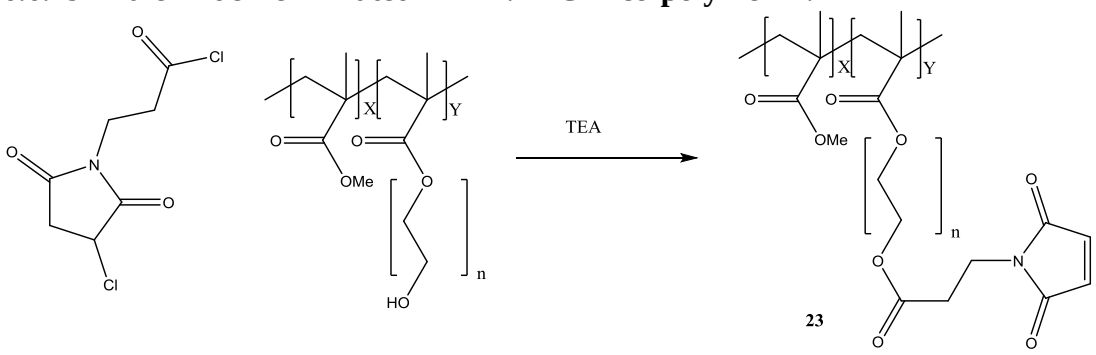

MMA:PEGM polymer (0.49 g) was dissolved in DCM (10 mL) before dry pyridine (1 drop) and DMAP (0.005 g) were added. The acid chloride **22** prepared in step 6.6.18 (1 mL) was added. The reaction mixture was stirred for 72 hours at room temperature before DCM was removed *in vacuo*. The solid was washed with methanol and stirred for 1 hour before being filtered off. The precipitate was dissolved in DCM (10 mL) and TEA (1 mL) was then added. The mixture was stirred for 4 hours after which the DCM was removed *in vacuo*. Dialysis in methanol for 24 hours gave the final polymer dark yellow/brown solid. FTIR ν_{max}/cm^{-1} 1720, 1650, 1640. ^{1}H NMR:δ_H (300 MHz, $CDCl_3$) 0.70 and 9.5 (br s, CH_3), 1.70 (br s, CH_2), 3.60 (br s, CH_3), 3.70 (br s, CH_2, PEG), 4.00 (br s, CH_2, PEG), 6.72 (br s, CH Maleimide).

6.7 Surface active agents.

6.7.1 Preparation of RGD mimic A and B[182].

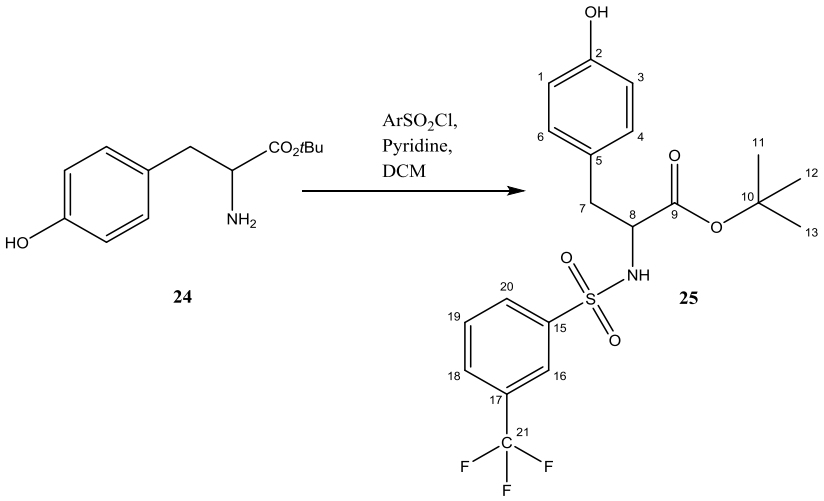

To *t*-Bu-tyrosine (1 g, 4.21 mmol) in DCM (50 mL), pyridine (0.35 mL, 4.21 mmol) and sulfonyl chloride (0.68 mL, 4.21 mmol) was added slowly. The reaction mixture was allowed to stir at room temperature for 5 hours. The reaction was washed with brine and extracted before being concentrated under vacuum. The crude reaction mixture was added to glacial acetic acid and allowed to stir for 3 hours. Water (30 mL) was added to the reaction mixture and a precipitate formed which was filtered off. The organic layer was then extracted with DCM (3 x 20 mL), combined, dried over $MgSO_4$ and concentrated *in vacuo* to yield a yellow solid (0.75 g, 40 %). m.p. 94-96^{o}C (lit 95-95.2 ^{o}C)[159] FTIR ν_{max}/cm^{-1} 3350 (OH), 1728 (C=O), 1324 and 1140 (S=O), 1131 and 1103 (CF_3). ^{1}H NMR:δ_H (300 MHz, $CDCl_3$) 1.25 (s, 9H, 3H, H11-13), 3.01 (m, 2H, H7), 4.12 (m, 1H, H8), 5.15 (br s, OH), 6.70 (d, 2H, H1,3), 7.10 (d, 2H, H4,6), 7.71 (m, 2H, H18,19), 7.85 (d, 1H, H20), 8.10 (s, 1H, H16) ^{13}C{^{1}H} NMR:δ_C (75 MHz, $CDCl_3$) 170.0 (C9), 155.0 (C2), 141.2 (C15), 131.3 (C17), 130.7 (C4/6), 130.4 (C18), 129.8 (C20), 129.2 (C18), 126.7 (C5), 124.2 (C16), 115.4 (C1/3), 83.1 (C10), 57.3 (C8), 38.6 (C7), 27.6 (C11/12/13) ESI-MS: 444 (M-H)$^{-}$.

6.7.2 Nitration of RGD mimic A and B[182].

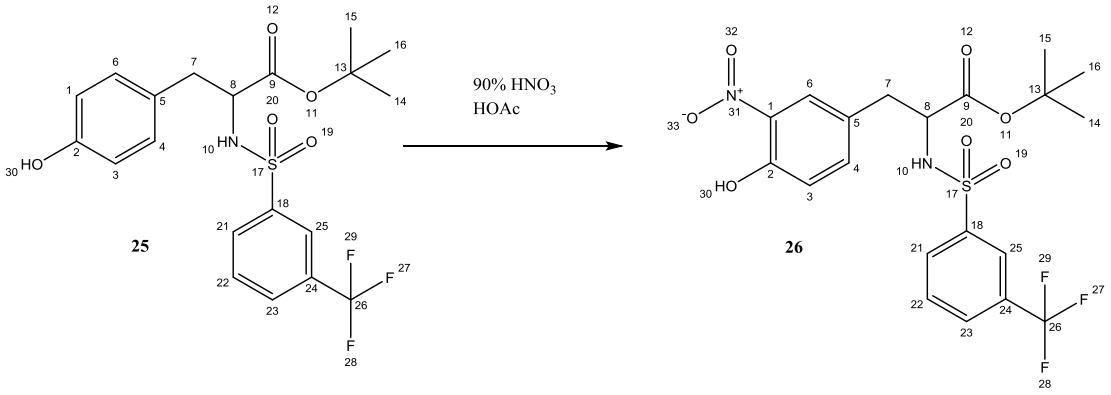

To **25** (0.75 g, 1.68 mmol) in acetic acid (66 mL), 90% nitric acid (0.12 mL, 1.68 mmol) in acetic acid (10 mL) was added dropwise keeping the reaction temperature between 16-20 ^{o}C. The reaction mixture was allowed to stir at room temperature for 3 hours. The reaction mixture was poured on ice and extracted with DCM (3 x 10 mL), combined, dried over $MgSO_4$ and concentrated. The crude product was purified by column chromatography (silica, eluting 33 % EtOAc:Petrolum ether 40-60), affording pure **26** as a yellow gum (0.39 g, 44 %). FTIR ν_{max}/cm^{-1} 3271 (OH), 1730 (C=O), 1538 (NO), 1150 and 1128 (S=O), 1070 and 1180 (CO). ^{1}H NMR:δ_H (300 MHz, $CDCl_3$) 1.26 (s, 9H, H14-16), 2.94 (dd, *J* = 14.3, 6.6, 2H, H7), 4.02 (m, 1H, H8), 5.50 (br s, OH), 7.00 (d, *J* = 8.8, 1H$_3$), 7.36 (dd, *J* = 8.8, 2.2, 1H, H4), 7.49 (t, 1H, H6), 7.71 (m, 2H, H22,23), 7.85 (d, *J* = 8.1, 1H, H21), 8.10 (s, 1H, H25). ^{13}C{^{1}H} NMR:δ_C (75 MHz, $CDCl_3$) 169.1, 154.3, 140.8, 139.1, 132.4, 131.0, 130.4, 129.9, 129.4, 127.5, 125.9, 124.2, 120.2, 83.1, 57.3, 38.6, 27.6. ESI-MS: 489 $(M-H)^-$

6.7.3 Preparation of *tert*-butyl (3-bromopropyl)carbamate 32 [196].

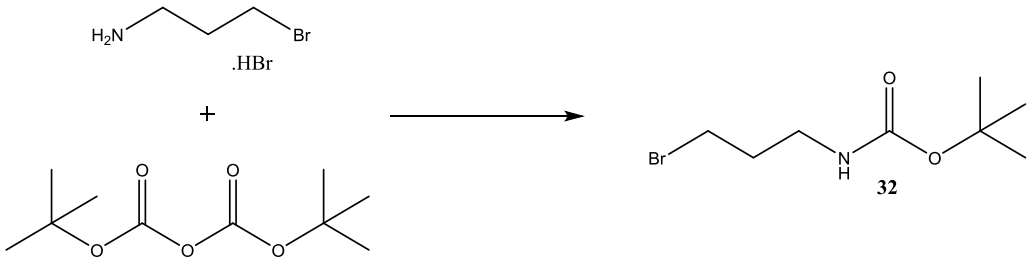

To a solution of 3-bromopropylamine hydrobromide (1 g, 4.75 mmol) in DCM (30 mL), were added di-*tert*-butyl dicarbonate (2 g, 10 mmol), in DCM (20 mL), and triethylamine (0.8 mL). The mixture was stirred at room temperature for 1 hour, then

diluted with DCM (20 mL), and washed twice with saturated bicarbonate solution, then once with brine. The organic layers were dried over Na_2SO_4, filtered and evaporated to dryness. The crude product was purified by column chromatography (silica, 7 % EtOAc:Petrolum ether 40-60), affording the desired as a colourless oil (78 %). FTIR ν_{max}/cm^{-1} 2974 (NH), 1684 (C=O), 643, 562 (CBr). ^1H NMR:δ_H (300 MHz, $CDCl_3$) 4.70 (1H, s, l, NHBoc), 3.46 (2H, t, CH_2Br, J = 6.5 Hz), 3.31 (2H, q, CH_2NHBoc, J = 6.5 Hz), 2.07 (2H, m, –CH_2–, J = 6.5 Hz), 1.46 (9H, s, CH_3-Boc). ^{13}C NMR: ($CDCl_3$, 75 MHz) δ 155.9 (OC(O)NH), 79.4 ($C(CH_3)_3$), 39.0 (CH_2NHBoc), 32.7 (CH_2), 30.8 (CH_2Br), 28.3 (CH_3-Boc). ESI-MS no ion detected.

6.7.4 Attachment of linker to RGD mimic A and B[182].

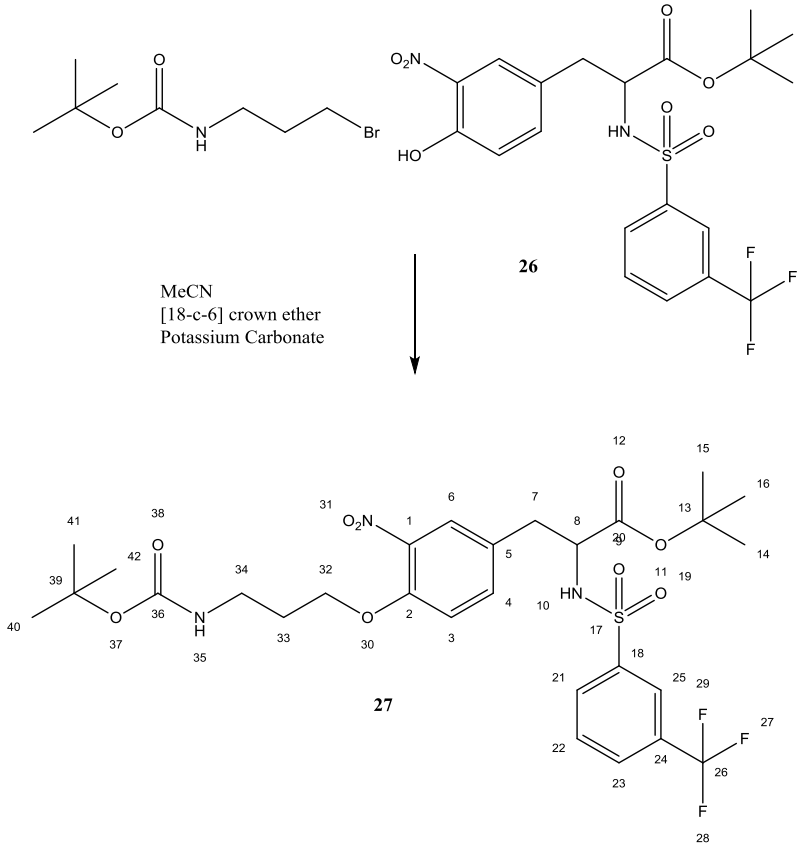

To a solution of **26** (0.25 g, 0.51 mmol) in acetonitrile (20 mL) under nitrogen were added *tert*-butyl (3-bromopropyl)carbamate **32** (0.12 g, 0.51 mmol), potassium carbonate (0.071 g) and [18-c-6] crown-ether (0.13 g). The reaction mixture was heated under reflux for 22 hours. The solvent was removed under vacuum and the residue was dissolved in DCM and washed with 0.1 N HCl in water. The organic

layer was dried with $MgSO_4$ and the product was purified by column chromatography (silica, DCM/EA 8:1) affording the desired product as a yellow oil (0.15 g, 46 %). FTIR ν_{max}/cm^{-1} 1687 (C=O), 1530 (NO), 1153 (S=O). ^1H NMR:δ_H (300 MHz, $CDCl_3$) 1.17 (s, 9H, H14-16) 1.35 (s, 9H, H40-42) 1.91 - 2.00 (m, 2 H, h33) 2.91 (dd, *J* = 7.0, 5.85 Hz, 1 H, H34) 2.98 (dd, *J* = 8.7, 5.4 Hz, 1 H, H34) 3.28 (d, *J* = 6.2 Hz, 2 H, H7) 3.96 - 4.15 (m, 3 H, H32+NH) 5.07 - 5.13 (m, 1 H, H8) 5.88 (d, *J* = 9.1 Hz, 1 H, NH) 6.90 (d, *J* = 8.7 Hz, 1 H, H3) 7.31 (dd, *J* = 8.7, 2.2 Hz, 1 H, H4) 7.50 - 7.57 (m, 2 H, H6,22) 7.71 (d, *J* = 8.0 Hz, 1 H, H23) 7.89 (d, *J* = 7.6 Hz, 1 H, H21) 7.95 (s, 1 H, H25). $^{13}C\{^1H\}$ NMR:δ_C (75 MHz, $CDCl_3$) 169.3, 155.6, 151.4, 141.1, 138.9, 135.6, 131.7, 130.4, 129.9, 129.3, 127.8, 126.5, 124.0, 114.4, 83.5, 79.0, 67.9, 57.07, 38.0, 37.8, 29.0, 28.3, 27.6. ESI-MS: 646 $(M-H)^-$.

6.7.5 Reduction of RGD mimic A and B [32]

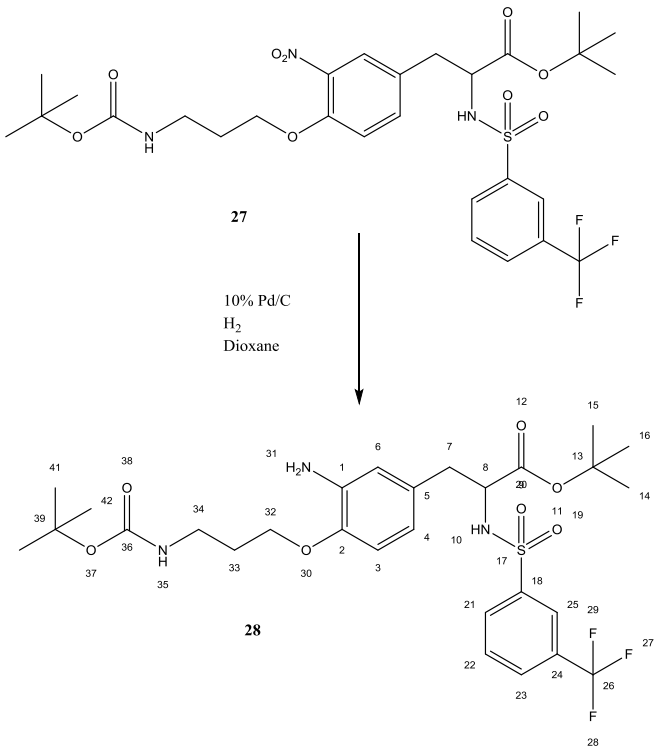

Product **27** (0.16 g, 0.25 mmol) and 10 % Pd/C (0.0045 g) in dioxane (1 mL) were stirred under hydrogen for 24 hours. The catalyst was removed by filtration through celite and the filtrate was concentrated *in vacuo.* The product was purified by column chromatography (silica, eluting 6:1 DCM:Ethyl Acetate), affording **28** as a brown solid (0.77 g, 50 %). m.p. 60-61 ^oC[32] (lit 61-61.2 ^oC) FTIR ν_{max}/cm^{-1} 3440 (1^o NH), 1253 (C-O-C), 1657 (C=O), 1158 (S=O). ^1H NMR:δ_H (300 MHz, $CDCl_3$) 1.12 (m,

9H, H14-16) 1.37 (s, 9 H, H40-42) 1.90 (t, *J* = 6.4 Hz, 2 H, H33) 2.80 (dd, *J* = 6.0, 3.1 Hz, 2 H, H7) 3.25 (d, *J* = 6.2 Hz, 2 H, H34) 3.91 (t, *J* = 5.8 Hz, 2 H, H32) 4.71 - 4.78 (m, 1 H, H8) 5.43 (d, *J* = 9.1 Hz, 1 H, NH) 6.34 (dd, *J* = 8.2, 2.0 Hz, 1 H, H4) 6.38 (d, *J* = 2.2 Hz, 1 H, H6) 6.53 (d, *J* = 8.0 Hz, 1 H, H3) 7.51 (t, *J* = 8.0 Hz, 1 H, H22) 7.69 (d, *J* = 7.6 Hz, 1 H, H23) 7.85 (d, *J* = 8.0 Hz, 1 H, H21) 7.97 (s, 1 H, H25). Shift in the 3/4/6 protons easily detected from NO_2 SM. $^{13}C\{^1H\}$ NMR:δ_C (75 MHz, $CDCl_3$) 169.7, 156.0, 145.5, 141.3, 136.2, 132.0, 131.6, 131.2, 130.7, 130.4, 129.7, 129.1, 129.0, 128.6, 127.7, 125.0, 124.1, 124.1, 121.3, 119.2, 116.1, 111.4, 82.7, 79.2, 65.9, 60.3, 38.8, 37.9, 29.6, 28.3, 27.6 ESI-MS: 616$(M-H)^-$.

6.7.6 Preparation of 1-methylpiperidine-4-carboxylic acid 33[187].

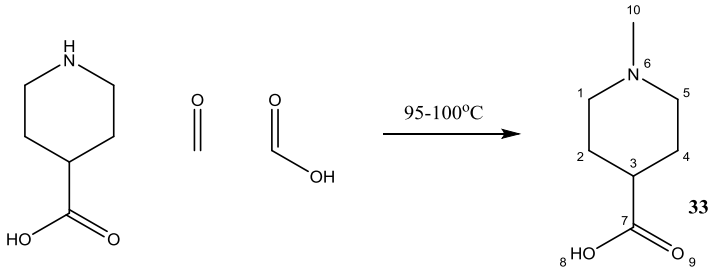

33

Formaldehyde solution (37 %, 0.43 mL, 15.58 mmol) was slowly added to a stirred solution of isonipecotic acid (1 g, 7.74 mmol) in 97 % formic acid (1.46 mL, 38.7 mmol). The mixture was heated to 90-100 ^oC. A vigorous evolution of carbon dioxide began after 2-3 min. Heat was removed until gas evolution subsided and then the mixture was heated at 95-100 ^oC for 8 hours. The product was recrystallized from IPA to give a white solid (1.01 g, 90 %). m.p. 222 ^oC (lit[187] 220-240 ^oC) FTIR ν_{max}/cm^{-1} 1394 (C=O), 1046, 1163, 961 (C-N). ^1H NMR:δ_H (300 MHz, MeOD) – 1. 86 (2H,m, H4), 2.07 (2H, m, H2), 2.31 (1H, m, H3), 2.78 (3H, s, H10), 2.90 (2H, m, H5), 3.38 (2H, m, H1).$^{13}C\{^1H\}$ NMR:δ_C (75 MHz, MeOD) 180.1, 54.7, 44.5, 43.7, 41.1, 27.7, 27.0. LMESI-MS: 142 $(M+H)^+$.

6.7.7 Attachment of 1-methylpiperidine to RGD mimic A and B[182].

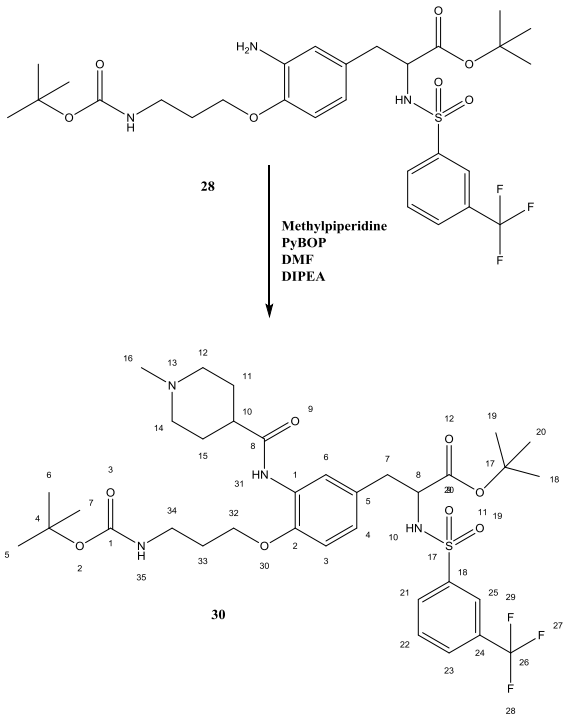

1-Methylpiperidine-4-carboxylic acid **33** (0.03 g, 0.21 mmol) and benzotriazol-1-yl-oxytripyrrolidinophosphonium hexafluorophosphate (PyBOP, 0.11 g, 0.21 mmol) were suspended in DMF (2 mL) under nitrogen. *N*,*N*-Diisopropylethylamine (DIPEA, 0.072 mL, 2 eq.) was added and the reaction mixture was allowed to stir until the precipitate dissolved. Product **28** (0.13 g, 0.21 mmol) in DMF (1 mL) was added in one portion. The mixture was stirred for 2 days at room temperature. The reaction was taken up with ethyl acetate and washed with brine and concentrated. The product was columned on silica gel using 5% MeOH in DCM to give a colourless oil (0.018 g, 7 % yield). FTIR ν_{max}/cm^{-1} 1220 (C-N), 3000 (CH), 1710 (C=O), 1359 (S=O). ^{1}H NMR:δ_H (300 MHz, $CDCl_3$) 1.13 (m, 9H, H18-20) 1.31 (s, 9H, H5-7) 1.85 (m, 2 H, H33) 2.11 (br. s, 4 H, H11,15) 2.69 (m, 5 H, H16,12) 2.92 (m, 2 H, H7) 3.24 (br. s, 3 H, H34,10) 3.51 (br. s, 2 H, H14) 3.94 (br. s, 3 H, H32,8) 6.70 (dd, *J* = 17.5, 7.6 Hz, 2 H, H3,4) 7.50 (t, *J* = 7.6 Hz, 1 H, H22) 7.68 (d, *J* = 8.0 Hz, 1 H, H23) 7.95 (m, 2H, H21,6) 7.90 (m, 1 H_{25}). ^{13}C{^{1}H} NMR:δ_C (75 MHz, $CDCl_3$). More material required for clear spectrum (even with extended scans) ESI-MS: 741 $(M-H)^-$.

6.7.8 Deprotection to form RGD mimic B[182].

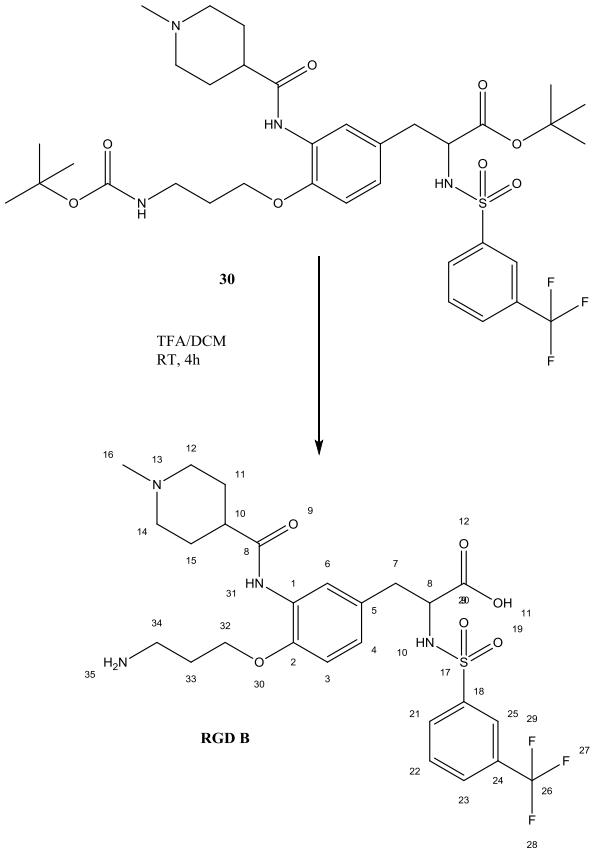

Trifluoroacetic acid (TFA, 0.5 mL) and DCM (0.5 mL) were combined and added to a round bottom flask of product **30** (0.018 g) in an ice bath. The mixture was stirred at RT for 4 hours before the reaction was concentrated under vacuum. The final product was obtained as a light brown solid (TFA salt) (0.015 g, 100 %). FTIR ν_{max}/cm^{-1} 2968 (CH) 1326 (C-N), 3400 (NH) 1220 (C-O-C), 1636 (C=O), 1158, 1326 (S=O). ^{1}H NMR:δ_H (300 MHz, MeOD) 2.05 (m, 2 H, H33) 2.22 (m, 4 H, H11,15) 2.81 (m, 5 H, H16,7) 3.11 (m, 5 H, H12,14,10) 3.64 (m, 2 H, H32) 4.15 (br. s, 3 H, H8,34) 6.91 (dd, *J* = 18.3, 8.0 Hz, 2 H, H3,4) 7.64 (s, 2 H, H25,21) 7.88 (dd, *J* = 13.2, 7.70 Hz, 2 H, H22,23) 7.98 (s, 1 H, H6). $^{13}C\{^{1}H\}$ NMR:δ_C (75 MHz, MeOD) 174.0, 150.1, 143.8, 131.5, 131.1, 130.4, 129.8, 127.9, 125.7, 124.7, 112.9, 66.9, 66.6, 59.1, 54.8, 44.0, 41.0, 39.1, 38.4, 28.2, 27.8. HRMS – 587.2146.

6.7.9 Deprotection to form RGD mimic A[182].

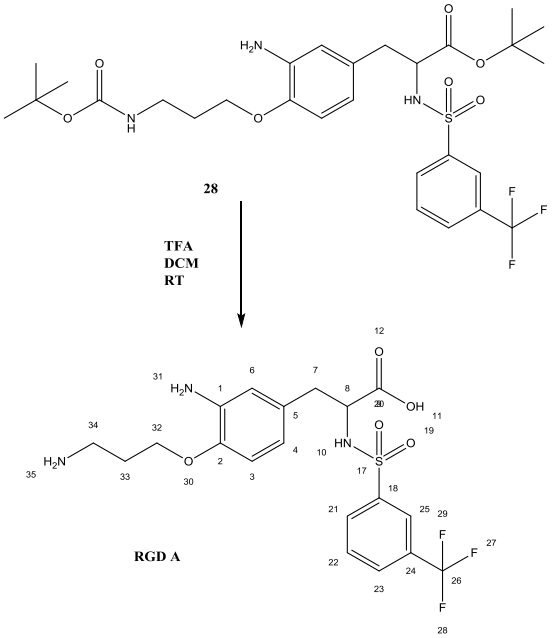

TFA (0.2 mL) and DCM (0.2 mL) were combined and added to a round bottom flask of product **28** (0.01 g) in an ice bath. The mixture was stirred at RT for 4 hours before the reaction was concentrated under vacuum. The final product was obtained as a yellow solid (TFA salt) (0.002 g, 30%). FTIR ν_{max}/cm^{-1} 1068 (C-N), 3077 (NH), 1678 (C=O), 1127, 1326 (S=O). 1H NMR:δH (300 MHz, MeOD) 2.01 (m, 4H, H33/NH) 2.99 (m, 5H, H33/7) 4.16 (m, 3 H, H32/8) 7.00 (m, 3 H, H3/4/6) 7.84 (m, 4 H, H21/22/23/25). $^{13}C\{^{1}H\}$ NMR:δ_C no peaks observed due to low yield. ESI-MS: $460(M-H)^-$

6.7.10 Preparation of 4-bromo chalcone[39].

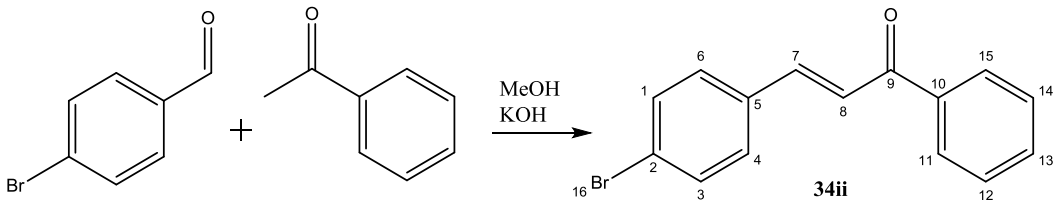

To a stirred solution of 4-bromobenzaldehyde (0.5 g, 2.7 mmol) and acetophenone (0.31 mL, 2.7mmol) in methanol (30 mL), 6M KOH (10.5 mL) was added and the reaction mixture was stirred for 48 hours. The product was filtered off and washed with cold water and methanol. The resulting product was re-crystallised from MeOH

to give a while solid (0.64 g, 84 %). m.p. 121 °C (lit 121 °C)[180] FTIR ν_{max}/cm^{-1} 3000 (ArH), 1654 (C=O), 1440 (C=C), 534 (CBr). ^{1}H NMR:δ_H (300 MHz, $CDCl_3$) 7.56 (m, 8H), 7.66 (d, *J* = 15.7 Hz, 1H), 7.94 (dd, *J* = 6.9, 1.4 Hz 2H). $^{13}C\{^{1}H\}$ NMR:δ_C (75 MHz, $CDCl_3$) 190.2 (C9), 143.3 (C7), 138.0 (C10), 133.8 (C5), 132.9 (C13), 132.2 (C1, C3), 129.8 (C12, C14), 128.6 (C6, C4), 128.5 (C11, C15), 124.8 (C2), 122.5 (C8). MS – no peak detected in by ESI, CI or on GC.

6.7.11 Preparation of aminoguanidine chalcone[39].

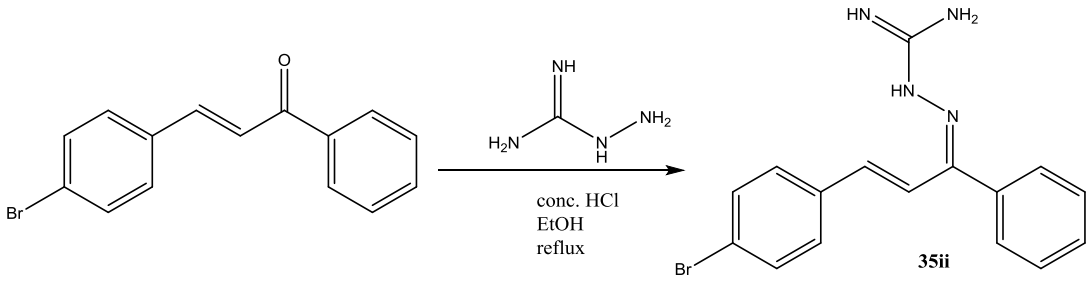

(*E*)-3-(4-Bromophenyl)-1-phenylprop-2-en-1-one (0.2 g, 0.7 mmol), aminoguanidine hydrochloride (0.77 g, 0.7 mmol) and concentrated HCl (0.14 mL) were added to ethanol (4.2 mL) and the mixture was heated under reflux for 24 hours under nitrogen. The solvent was then removed under vacuum and the residue was washed with water and extracted with ether. The white solid was re-crystallized from DCM ether to yield an off white solid (0.22 g, 92 %). Producing crystals as the HCl salt or purification by alumni and silica proved unsuccessful. The product (0.08 g) was dissolved in MeOH (1 mL) and added to 2-nitrobenzoic acid (0.039 g) in MeOH (1 mL). The solvent was removed under vacuum and the residue was dissolved in the minimum of hot acetone. The solution was left in the fridge for 72 hours to allow white crystals to form. (m.p. 86 °C decomp.) FTIR ν_{max}/cm^{-1} 3150 (NH stretch), 1680 (C=C), 1619 (C=N), 1541 (NH bend), 1136 (CN), 508 (CBr). ^{1}H NMR:δ_H (300 MHz, DMSO-d_6) 6.84 (d, *J* = 16.1 Hz, 1 H) 7.48 (m, 3 H) 7.63 (m, 4 H) 7.77 (m, 3 H). $^{13}C\{^{1}H\}$ NMR:δ_C (75 MHz, DMSO-d_6) 119.1, 122.9, 128.3, 129.1, 129.5, 130.0, 131.6, 134.6, 135.8, 139.5, 152.3, 156.0. ESI-MS: 343 $(M+H)^+$.

6.7.12 Preparation of para-bromo chalcone[39].

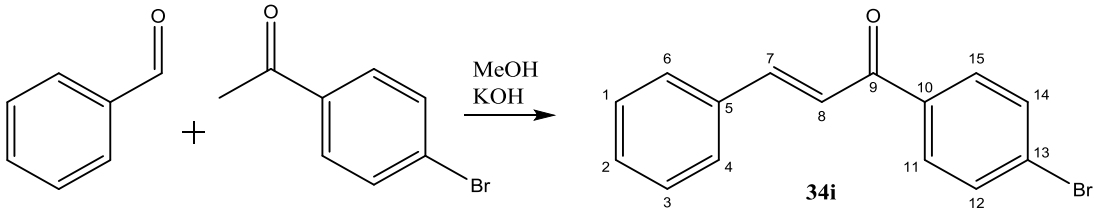

To a stirred solution of 4-bromoacetophenone (0.93 g, 4.7 mmol) and distilled benzaldehyde (0.48 mL, 4.7 mmol) in methanol (30 mL), 6M KOH (19 mL) was added and the reaction mixture was stirred until a solid formed. The product was filtered off and washed with cold water and methanol. The resulting product was re-crystallised from MeOH to give a white solid (0.78 g, 58 %). m.p. 102 ^{o}C (lit[39] 101-103 ^{o}C). FTIR ν_{max}/cm^{-1} 3020 (ArH), 1680 (C=O), 1400 (C=C). ^{1}H NMR:δ_H (300 MHz, $CDCl_3$) 7.91 (dt, *J*= 8.60 Hz, *J* = 2.01 Hz, 2H6,4), 7.84 (d, *J* = 8.8 Hz, 1H7) 7.66 (m, 4H, ArH), 7.48 (m, 4H, 3ArH, H8). ^{13}C{^{1}H} NMR:δ_C (75 MHz, $CDCl_3$) 189.4 (C9), 145.4 (C7), 136.9 (C10), 134.6 (C5), 131.9 (C12/14), 130.7 (C11/15), 129.6 (C1/3), 129.0 (C6/4), 128.5 (C2), 127.9 (C13), 121.5 (C8). MS – no peak detected in by ESI, CI or on GC.

6.7.13 Preparation of aminoguanidine chalcone[39].

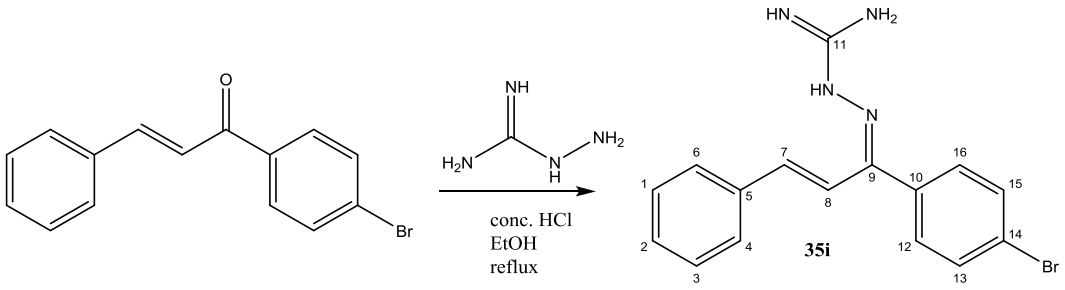

1-(4-Bromophenyl)-3-phenylprop-2-en-1-one (0.2 g, 0.7 mmol), aminoguanidine hydrochloride (0.77 g, 0.7 mmol) and concentrated HCl (0.14 mL) were added to ethanol (4.2 mL) and the mixture was heated under reflux for 24 hours. The solvent was then removed under vacuum and the residue was washed with water and extracted with ether. The resulting white solid was crystallised from MeOH to yield the desired product (1.56 g, 65 %). A sample of the product (0.045 g) was dissolved

in MeOH (1 mL) and added to 2-nitrobenzoic acid (0.022 g) in MeOH (1 mL). The product was left in the fridge for 72 hours yielding yellow crystals. (m.p. 80 ^{o}C decomp.). FTIR ν_{max}/cm^{-1} 3100, 3300 (NH stretch), 1650 (C=C), 1600 (C=N), 1580 (NH bend), 1120 (CN), 500 (CBr).^{1}H NMR:δ_H (300 MHz, $CDCl_3$) 6.77 (d, *J* = 15.7 Hz, 1H), 7.30 (m, 3H), 7.39 (d, 2H), 7.60 (m, 5H), $^{13}C\{^{1}H\}$ NMR:δ_C (75 MHz, $CDCl_3$) 153.6 (C9), 156.4 (C11), 143.2 (C7), 135.1 (C10), 135.0

6.7.14 Preparation of 4-hydroxy chalcone[179].

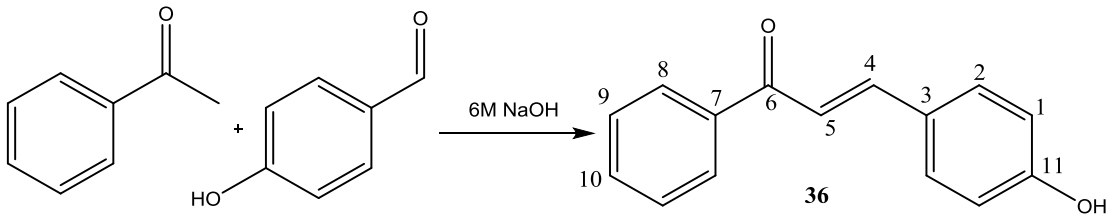

Acetophenone (1 g, 8.3 mmol) was dissolved in methanol (8 mL). 4-Hydroxybenzaldehyde (1.01 g, 8 mmol) and 6 M NaOH (4 mL) were added before the reaction solution was stirred at RT for 40 minutes. The reaction was transferred to the fridge to allow for crystallisation. Product was recrystallised from hot ethanol before being dried under vacuum to yield yellow crystals. (m.p. 171 ^{o}C (lit[178] 174-175 ^{o}C). FTIR ν_{max}/cm^{-1} 3350 (br, OH), 3100 (br, ArH), 1695 (C=C), 1420 (C=C).^{1}H NMR:δ_H (300 MHz, $CDCl_3$) 4.77 (s, 2H, H1), 6.75 (d, 1H, *J* = 8.4 Hz, H5) 7.45 (m, 6H, H2, H10, H8), 7.64 (d, 1H, *J* = 5.6 Hz, H8) 7.93 (d, 1H, *J* = 8.4 Hz, H4); $^{13}C\{^{1}H\}$ NMR:δ_C (75 MHz, $CDCl_3$) 117.0 (C2), 119.7 (C5), 127.7 (C3), 129.5 (C1), 129.7 (C8), 131.9 (C9), 133.9 (C10), 139.7 (C7), 147.0 (C4), 161.0 (C11), 192.7 (C6). ESI-MS: 223.2 $(M-H)^{-}$

6.7.15 Linker attachment to surface.

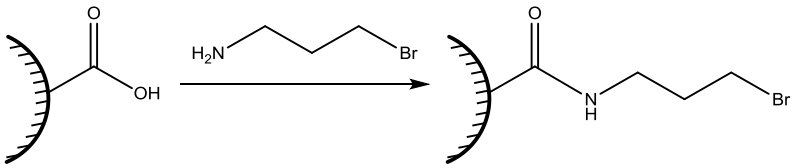

Caustic activated microspheres as prepared previously (0.35 g) were coupled to the bromoamine linker by addition of 1-ethyl-3-(3-dimethylaminopropyl)carbodiimide

(EDCI) solution (0.008 M, 2 mL) before the addition of *N*-hydroxysuccinimide (0.02 M, NHS, 2 mL). After 2 hours 3-bromopropylamine (0.67 g, 0.03 M) was added and allowed to stir overnight before washing with water (4 x 40 mL) and drying under vacuum.

6.7.16 Attachment of chalcone to microspheres.

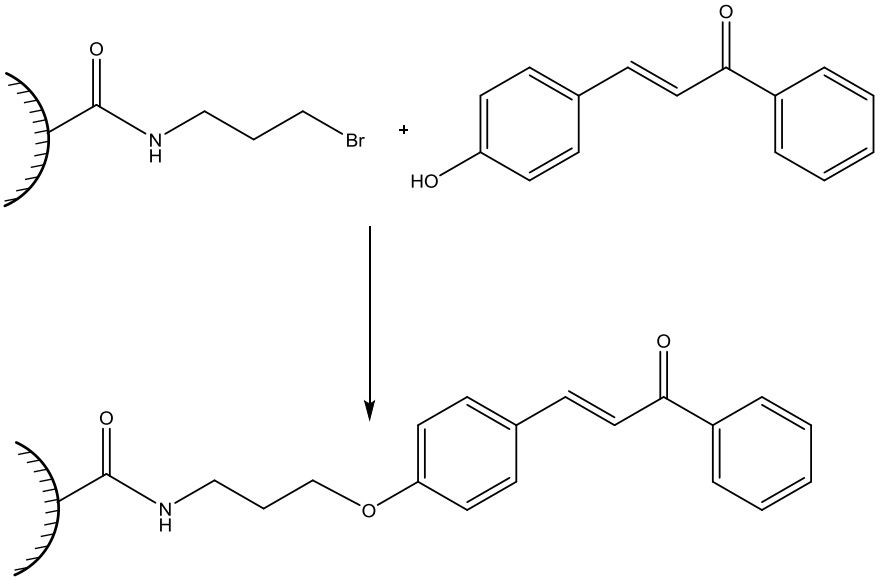

3-Bromopropylamine attached microspheres (0.1 g) were added to water (1 mL) followed by 4-hydroxy chalcone (0.05 g) and potassium carbonate. The mixture was left at 40°C overnight before being centrifuged and washed with DI water (4 x 40 mL) before being dried under vacuum.

6.7.17 Preparation RGDS tetrapeptide.

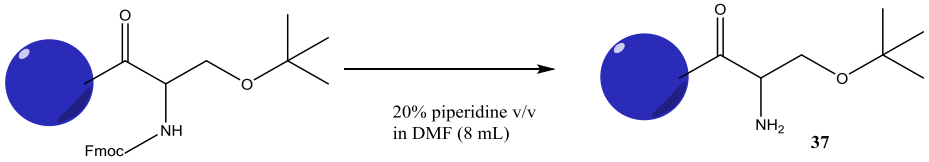

37

Fmoc-Ser-(OtBu)-Wang resin (0.4-0.8 mmol g^{-1}, 100-200 mesh, 1 g) was placed in a sintered glass column. 20% piperdine in DMF (10 mL) was added and nitrogen used to agitate the sample. After 30 min the resin was washed with DMF (3 x 10 mL).

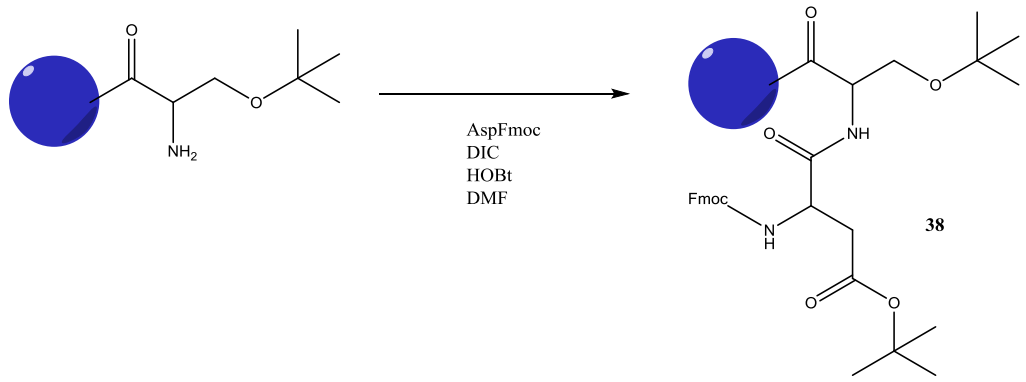

Fmoc-Asp (1.65 g, 4 mmol), HOBt (0.60 g, 4.4 mmol) and DIC (0.68 mL, 4.4 mmol) were combined in DMF (8 mL) and added to product resin (in DMF 2mL). Nitrogen gas was used to agitate sample at room temperature for 2 hours, the Kaiser test being used to confirm reaction progress) before the resin was washed with DMF (3 x 10 mL).

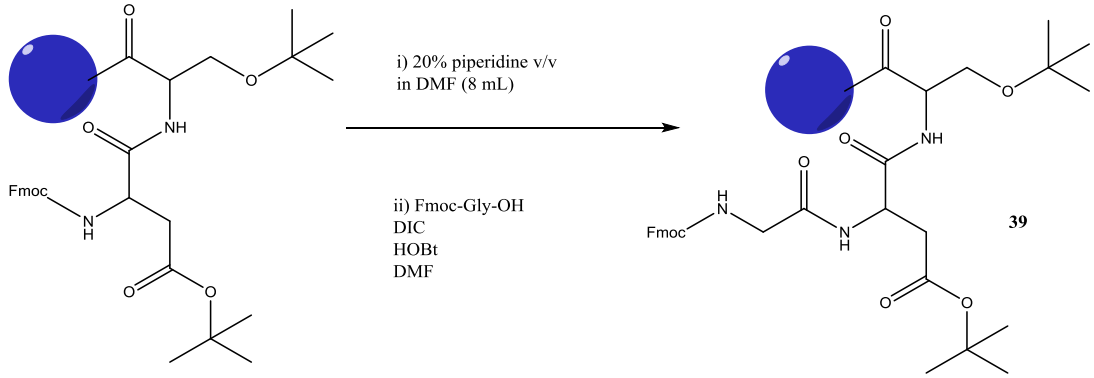

The product resin which was added to 20% piperdine in DMF (8 mL), with nitrogen used to agitate sample and after 30 mins the resin was washed with DMF (3 x 10 mL).

Fmoc-Gly-OH (1.190 g, 4 mmol), HOBt (0.60 g, 4.4 mmol) and DIC (0.68 mL, 4.4 mmol) were combined in DMF (8 mL) and added to product resin (in DMF 2 mL). Nitrogen used to agitate sample at room temperature for 2 hours before being washed with DMF (3 x 10 mL).

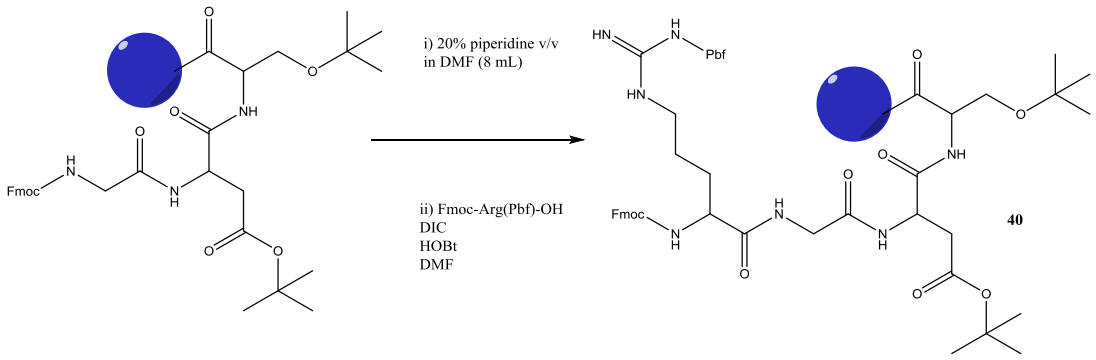

The product resin which was added to 20% piperdine in DMF (8 mL), with nitrogen used to agitate sample and after 30 min the resin was washed with DMF (3 x 10 mL).

Fmoc-Arg(Pbf)-OH (1.63 g, 2.5 mmol), HOBt (0.60 g, 4.4 mmol) and DIC (0.68 mL, 4.4 mmol) were combined in DMF (8 mL) and added to product resin (in DMF 2 mL). Nitrogen gas was used to agitate sample at room temperature for 2 hours after which the resin was washed with DMF (3 x 10 mL).

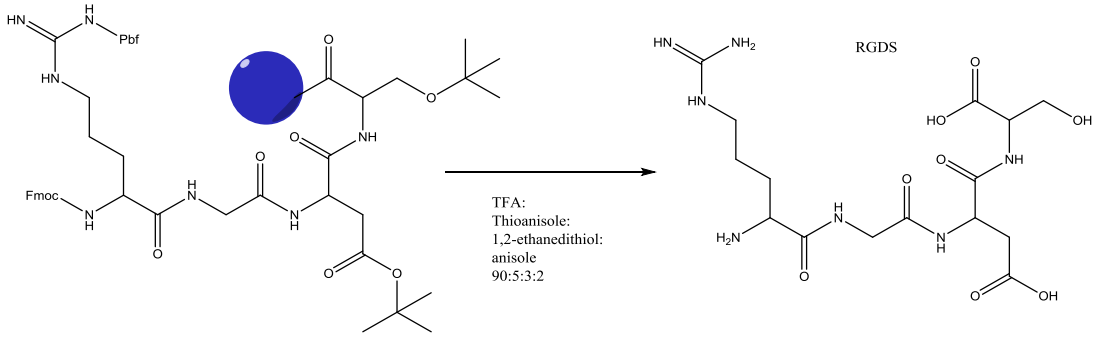

Wang product resin was suspended in TFA:thioanisole:1,2-ethanedithiol:anisole 90:5:3:2 (4 mL) for 2 hours. The product was filtered off and washed with DCM/Methanol (3 x 5 mL) and the product was precipitated in diethyl ether (0.166 g). An SPE column (1 g) was loaded with product in diethyl ether (0.154 g in 0.5 mL) and eluted with 10% Methanol in DCM to obtain pure RGDS compound (0.0022 g). FTIR ν_{max}/cm^{-1} 3400 (br), 3100 (br), 2920, 1700, 1662, 1590. ^{1}H NMR:δ_H (300 MHz, $CDCl_3$) 1.62 (m, 2 H, Arg) 1.85 (dd, *J* = 10.8, 6.4 Hz, 2 H, Arg) 2.61 (td, *J* = 7.5, 5.0 Hz 2 H, Asp CH2-acid) 3.17 (t, *J* = 6.8 Hz, 1 H, Arg) 3.78 (d, *J* = 4.4 Hz, 2 H, SerCH_2-OH) 3.92 (m, 1 H, Gly) 4.06 (d, *J* = 10.82, H, Arg CH_2Aminoguardine) 4.19 (t, *J* = 4.6 Hz, 1 H, Ser) 4.58 (m, 1 H, Asp). $^{13}C\{^{1}H\}$ NMR:δ_C No peaks observed due to low yield. ESI-MS: 434 $(M+H)^+$, 456 $(M+Na)^+$.

6.7.18 RGDS peptide attachment to surface activated microspheres.

To surface-activated microspheres (post aminolysis, 0.04 g) was added 1-ethyl-3-(3-dimethylaminopropyl)carbodiimide (EDCI) solution (0.4 mL) followed by addition of *N*-hydroxysuccinimide (0.04 mL). After 2 hours the RGDS peptide was added (0.0022 g) and allowed to stir overnight before washing with water (4 x 10 mL) and drying under vacuum.

6.7.19 Statistics.

All values represent mean ± standard error of the mean. Data were analysed by either Student's t-test or one way analysis of variance (ANOVA) using GraphPad Prism Software (GraphPad Software Inc., San Diego, CA, USA).

6.8 Cell testing

6.8.1 LDH assay.

Fibres were sterilised by irradiation with UV overnight. Prepared polymer fibre mats were seeded with an immortalised human Retinal Pigment epithelium cell line (ARPE-19). A cell seeding density of 150,000 cells per well was used. A sample of culture media (400 µL) was taken from each culture well to be tested twice a week for two weeks post seeding. The supernatant was then aliquoted into a 96 well plate (100 µL per well) in triplicate. Dye solution (11.25 mL, iodonitrotetrazolium chloride (INT) and sodium lactate) was then mixed with catalyst solution (250 µL, Diaphorase/NAD^+ mixture) immediately prior to the experiment. This mixture was then added to each well (100 µL for each well) and incubated at room temperature for 30 minutes in the absence of light. Absorbance of the samples at 492 nm was then measured using a spectrophotometer.

6.8.2 MTT Assay.

Samples of culture medium from seeded and unseeded scaffolds were tested twice a week for two weeks post seeding *in vitro*. ARPE-19 cells were counted and seeded at 10,000 cells per well in a 96 well plate. Cells were allowed to attach overnight. Culture medium (0.1 mL) from the scaffolds was then added to each well. Cells were

incubated with test solution at 37^{o}C for 48 hours. At the end of the incubation period of MTT solution (0.01 mL) was added to each well. The solution was mixed by tapping gently on the side of the tray and then incubated for 4 hours at 37ºC for cleavage of MTT to occur. The formazan produced in the wells containing live cells appeared as black crystals at the bottom of the wells. Colour development solution (isopropanol with 0.04 N HCl) (0.1 mL) was added to each well and the contents were mixed thoroughly by repeated pipetting with a multichannel pipettor. Within an hour the absorbance was measured on a plate reader.

6.8.3 DAPI stained images.

Samples of seeded microspheres taken and seeded onto slides allowing 6-8 hours to attach. Slides washed with PBS (3 x 10 mL). All slides were then washed twice with PBS, 4,6-diamidino-2-phenylindole (DAPI) (0.005 g ml^{-1} solution in DI water) kept in the dark at room for 1-2 hours. Cells visualised under UV light (Leica Microsystems UK Ltd, Milton Keynes, UK).

7. Appendices

7.1 Appendix A – Journal publications.

D. W. Pitt, A. J. Treharne, H. A. Thomson, J. A. Scott, A. J. Lotery and M. C. Grossel, *J. Mater. Chem. B*, 2013, **1**, 6627-6633.

7.2 Appendix B – Raw calculation of Mechanical test data.

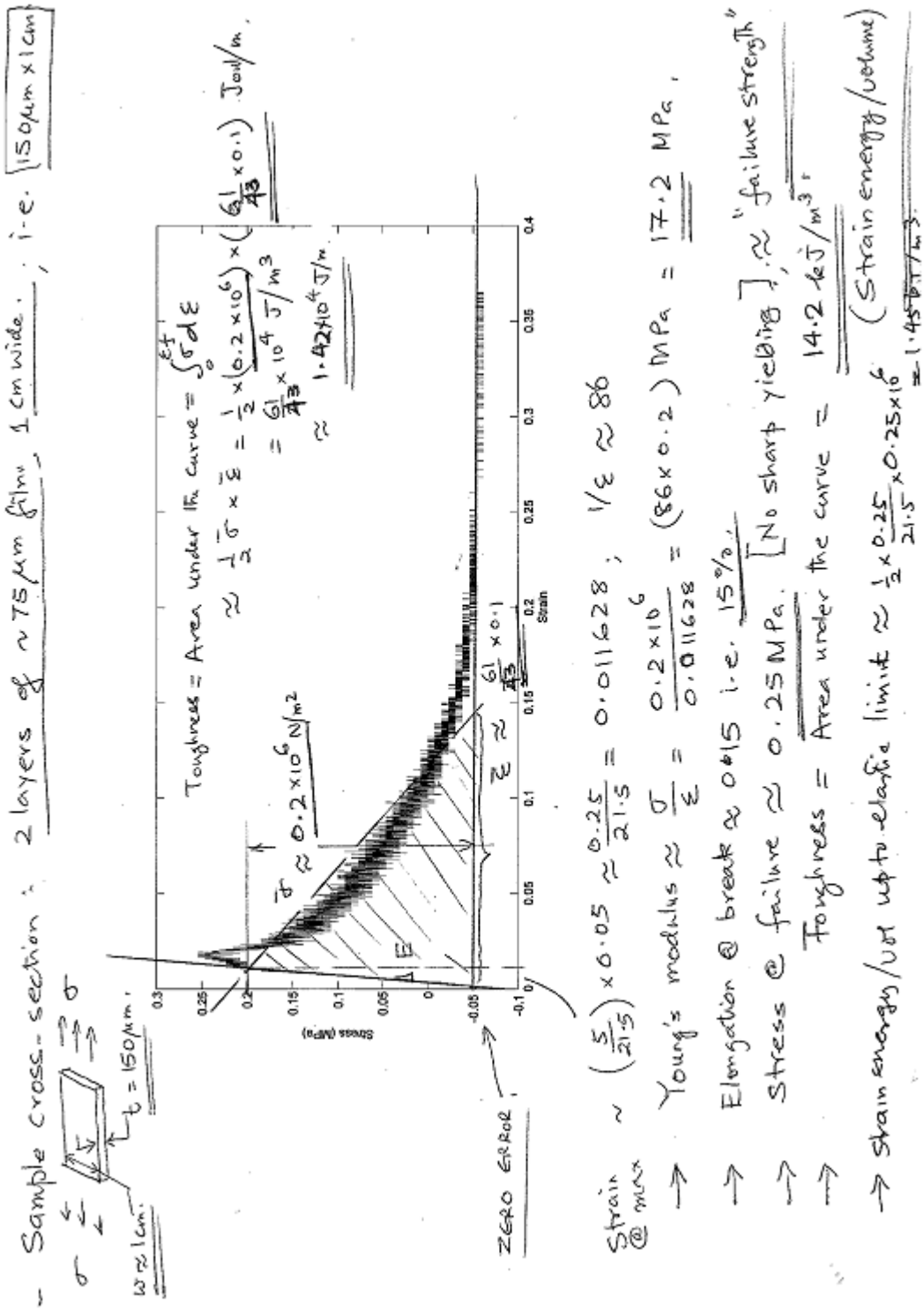

7.3 Appendix C – Failed circular dichroism spectrum of unencapsulated Bevacizumab.

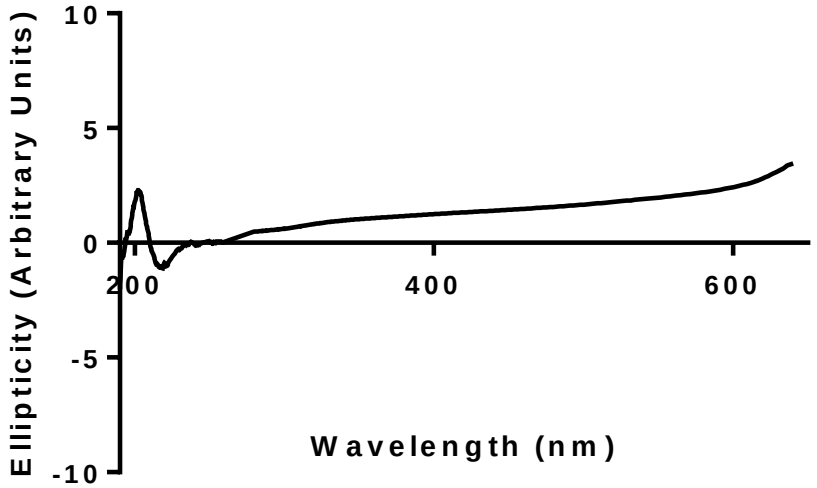

7.4 Appendix D – Calibration graph of FITC attached Bevacizumab.

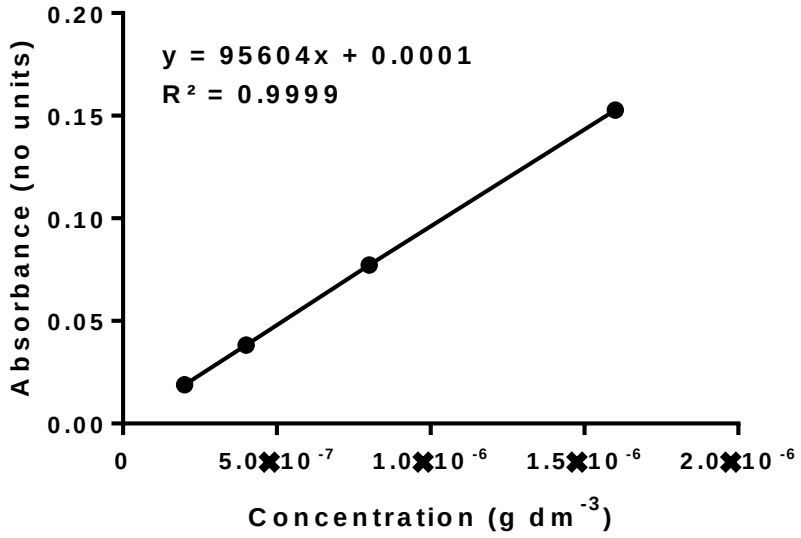

7.5 Appendix E – Frame grabs of absorption of contact angle drop over 10 seconds by 40:60 MMA:PEGM co-polymer.

7.6 Appendix F – An expanded XPS spectrum showing the 2p state of sulphur.

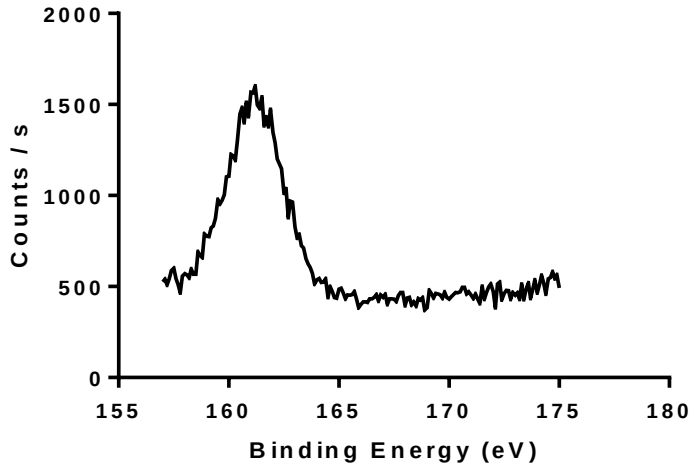

7.7 Appendix G – The full XPS spectrum obtained for the RGD mimic attached electrospun mats.

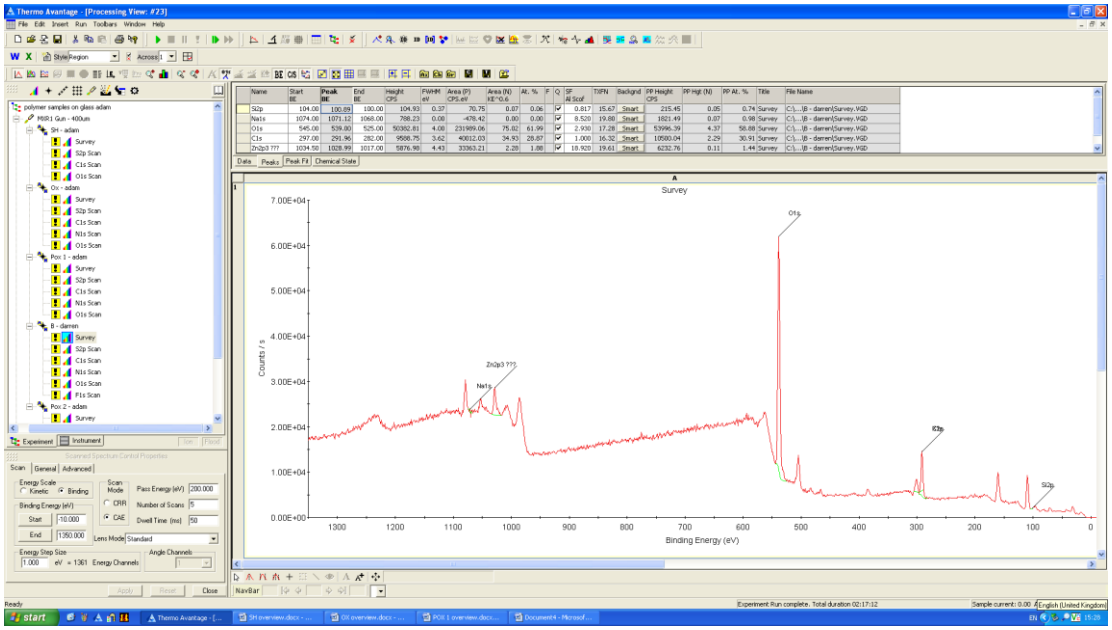

7.8 Appendix H – crystal structure of *N*-(benzyloxy)succinimide.

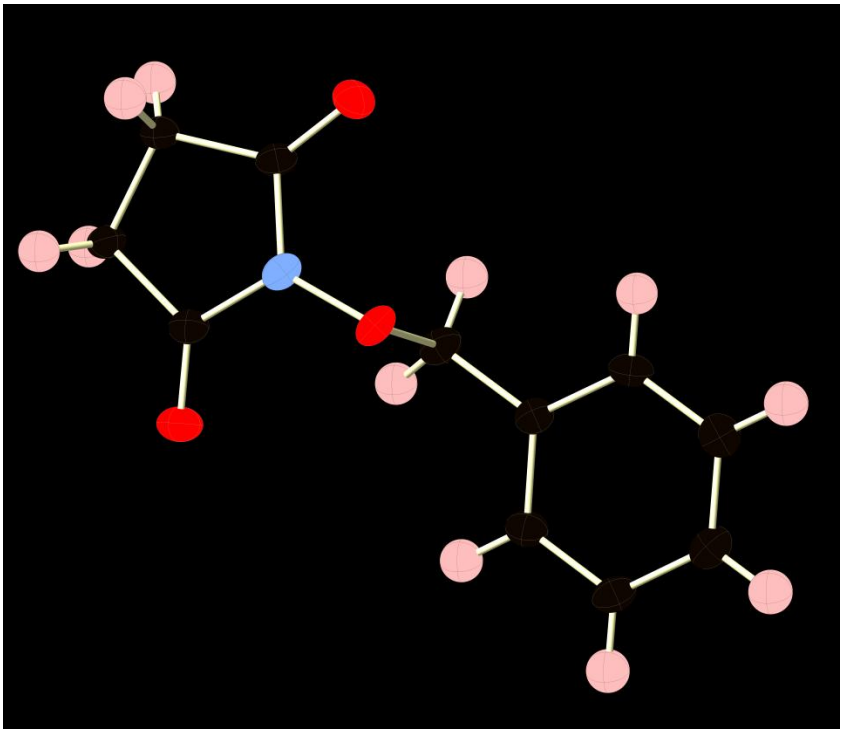

Empirical Formula	$C_{11}H_{11}N_1O_3$
Mass	205.1
Collection temperature/ K	100
Crystal System	Monoclinic
Space Group	P 2
Unit Cell	a=5.91(3) b=7.69(3) c=10.96(5) α=90 β=99.15(5) γ=90
Volume	491(3)
Z	1
R1	0.019

Structure solved by Dr. Peter Horton.

7.9 Appendix I – Structures of A, Fluorescein; B, Rhodamine B.

A

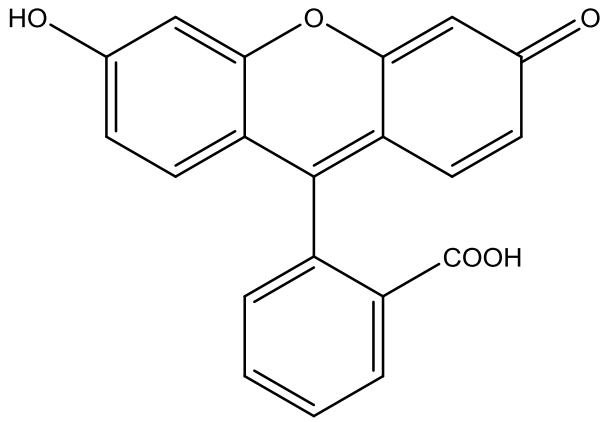

B

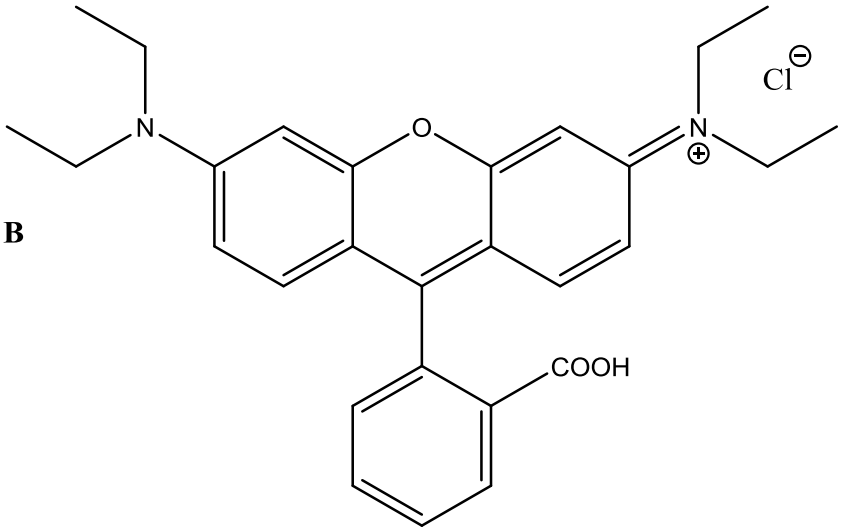

8. References

1. H. Scholl, M. Fleckenstein, P. Issa, C. Keilhauer, F. Holz and B. Weber, *Mol. Vis*., 2007, **13**, 196-205.
2. C. G. Owen, Z. Jarrar, R. Wormald, D. G. Cook, A. E. Fletcher and A. R. Rudnicka, *Br. J. Ophthalmol.*, 2012, **96**, 752–756.
3. W. Smith, J. Assink, R. Klein, P. Mitchell, C. C. Klaver, B. E. Klein, A. Hofman, S. Jensen, J. J. Wang and P. T. de Jong, *Ophthalmology*, 2001, **108**, 697-704.
4. K. Birke, E. Lipo, M. T. Birke and R. Kumar-Singh, *Plos One*, 2013, **8**, 1-7.
5. N. M. Bressler, *Arch. Ophthalmol.*, 2001, **119**, 198-207.
6. G. Virgili and A. Bini, *Cochrane Database Systematic Reviews*, 2007, **3**, CD004763.
7. K. J. Kim, B. Li, J. Winer, M. Armanini, N. Gillett, H. S. Phillips and N Ferrara, *Nature*, 1993, **362**, 841-844.
8. C. C. Wykoff, D. M. Brown, M. E. Maldonado and D. E. Croft, *Br. J. Ophthalmol.*, 2014, **98**, 951-955.
9. L. Hjelmqvist, C. Lindberg, P. Kanulf, H. Dahlgren, I. Johansson and A. Siewert, *J. Ophthalmol.*, 2011, DOI: 10.1155/2011/405724
10. D. Shukla, P. Namperumalsamy, M. Goldbaum and E. T. Cunningham Jr, *Indian J. Ophthalmol.*, 2007, **55**, 427-430.
11. C. Baudouin, F. Brignole and P. Gastaud, *Arch. Ophthalmol.*, 1991, **109**, 1220-1231.
12. R. Kim, *Indian J. Ophthalmol.*, 2007, **55**, 413–415.
13. M. L. Subramanian, G. Abedi, S. Ness, E. Ahmed, M. Fenberg, M. K. Daly, A. Houranieh and E. B. Feinberg, *Eye*, 2010, **24**, 1708-1715.
14. N. Ferrara, L. Damico, N. Shams, H. Lowman and R. Kim, *Retina*, 2006, **26**, 859-870.

15. D. F. Martin, M. G. Maguire, G. S. Ying, J. E. Grunwald, S. L. Fine and G. J. Jaffe, *N. Engl. J. Med*., 2011, **364**, 1897-1908.
16. D. Martin, M. Maguire, S. Fine, G. Ying, G. J. Jaffe, J. E. Grunwald, C. Toth, M. Redford and F. L. Ferris, *Ophthalmology*, 2012, **119**, 1388-1398.
17. G. J. Jaffe, D. F. Martin, C. A. Toth, E. Daniel, M. G. Maguire, G. S. Ying, J. E. Grunwald and J. Huang, *Ophthalmology*, 2013, **120**, 1860-1870.
18. R. D. Siepmann, W. F. Mieler and J. W. Miller, *N. Engl. J. Med.*, 2008, **358**, 2606-2617.
19. P. J. Rosenfeld, D. M. Brown and J. S. Heier, *N. Engl. J. Med.*, 2006, **355**, 1419-1431.
20. R. D. Jager, L. P. Aiello, S. C. Patel and E. T. Cunningham Jr., *Retina*, 2004, **24**, 676-698.
21. C.C. Muller-Goymann, *Eur. J. Pharmaceut. Biopharmaceut*., 2004, **58**, 343-356.
22. E. R. Gillies and J. M. Fréchet, *Drug Discovery Today*, 2005, **10**, 35-43.
23. R. Challa, A. Ahuja, J. Ali and R. K. Khar, *AAPS PharmSciTech*, 2005, **6**, 329–357.
24. J. Y. Lee, Y. M. Kang, E. S. Kim, M. L. Kang, B. Lee, J. H. Kim, B. H. Min, K. Park and M. S. Kim, *J. Mater. Chem.*, 2010, **20**, 3265-3271.
25. M. K. Nkanash, S. Y. Tzeng, A. M. Holdt and E. B. Lavik, *Biotechnol. Bioeng.*, 2008, **100**, 1010-1019.
26. M. W. Stewart, *Eye Reports*, 2011, **1**, 12-14.
27. S. D. Swanson, "*Selective MRI and MRS of PEGylated compounds," in Proceedings of the 14th Scientific Meeting International Society for Magnetic Resonance in Medicine*, A. Arbor, The University of Michigan, Mich., USA, 2006.
28. S. A. Molokhia, H. Sant, J. Simonis, C. J. Bishop, R. M. Burr, B. K. Gale and B. K. Ambati, *Vis. Res.*, 2010, **50**, 680–685.
29. D. Gulsen, C. Li, and A. Chauhan, *Curr. Eye Res.*, 2005, **30**, 1071-1080.
30. R. Herrero-Vanrell, C. A. Santiago and E. Barcia, *Invest. Ophthalmol. Vis. Sci.* 1999, **40**, 84-86.
31. R. Herrero-Vanrell, L. Ramirez, A. Fernandez-Carballido and M. Refojo. *Pharm. Res.*, 2000, **17**, 1323-1328.

32. P. Checa-Casalengua, C. Jiang, I. Bravo-Osuna, B. Tucker, I. Molina-Martinez, M. Young and R. Herrero-Vanrell, *J. Controlled Release*, 2011, **156**, 92-100.
33. N. Kunou, Y. Ogura and T. Yasukawa, *J. Controlled Release*, 1995, **37**, 143-150.
34. Alimera Sciences, 6120 Windward Parkway, Alpharetta, GA, U.S.A. GA 30005.
35. Auritec Pharmaceuticals Inc. 2285 E. Foothill Blvd., Pasadena, CA, U.S.A. 91107.
36. J. Lim, R. Wolitz, A. Dowling, H. Bloom, A. Irvine and D. Schwartz, *Am. J. Opthalmol*, 1999, **127**, 288-293.
37. T. Loftsson, *Int. J. Pharm*. 1994, **104**, 181-184.
38. L. Cheng, K. Y. Hostetler, M. F. Gardner, C. P. Avila Jr, G. Bergeron-Lynn, K. S. Keefe, C. A. Wiley and W. R. Freeman, *Invest. Ophthalmol. Vis. Sci.*, 1999, **40**, 1487-1495.
39. R. Zhang, R. He, J. Qian, J. Guo, K. Xue, and Y. F. Yuan, *Invest. Ophthalmol. Vis. Sci.*, 2010, **51**, 3575–3582.
40. N. Kuno and S. Fujii, *Polymers*, 2011, **3**, 193-221.
41. S. S. Banerjee, N. Aher, R. Patil and J. Khandare, *J. Drug Deliv*., 2012, DOI: 10.1155/2012/103973.
42. R. Gaudana, H. K. Ananthula, A. Parenky and A. K. Mitra, *AAPS Journal*, 2010, **12**, 348-360.
43. S. Sahoo, F. Dilnawaz and S. Krishnakumar, *Drug Discovery Today*, 2008, **13**, 144-151.
44. K. Janoria, S. Gunda, S. Boddu and A. Mitre, *Expert Opin. Drug Deliv.*, 2007, **4**, 371-388.
45. B. Short, *Toxicol. Pathol.*, 2008, **36**, 49-62.
46. S. G. Schwartz, I. U. Scott, H. W. Flynn Jr and M. W. Stewart, *Expert Opin. Drug Deliv.*, 2014, **11,** 61-68.
47. L. Yang, Y. Lan, H. Guo, L. Cheng, J. Fan, X. Cai, L. Zhang, R. Chen and H. Zhou, *Acta. Pharmacol. Sin.*, 2010, **31**, 1625-1634.
48. F. Li, B. Hurley, Y. Liu, B. Leonard and M. Griffith, *Open Ophthal. J.*, 2012, **6**, 54-58.

49. M. Abrishami, S. Zarei-Ghanavati, D. Soroush, M. Rouhbakhsh, M. R. Jaafari and B. Malaekeh-Nikouei, *Retina*, 2009, **29,** 699-703.
50. D. S. Boyer, *Retina Today*, 2013, **11**, 52-56.
51. G. Sandmann, F. Martetschläger, L. Mey, T. M. Kraus, A. Buchholz, P. Ahrens, U. Stöckle, T. Freude and S. Siebenlist, *Patient Safety in Surgery*, 2012, **6**, 25-31.
52. C. Wischke and S. P. Schwendeman, *Int. J. Pharm.*, 2008, **364**, 298–327.
53. C. S. Dias and A. K. Mitra, *J. Pharm. Sci.*, 2000, **89**, 572-578.
54. D. Ghate and H. F. Edelhauser, *Expert Opin. Drug Deliv.*, 2006, **3**, 275-287.
55. H. Makadia and S. Siegel, *Polymers*, 2011, **1**, 1377-1397.
56. X. S. Wu, D. Wise, D. J. Trantolo, D. E. Altobelli, M. J. Yaszems and M. Dekker, *Encyclopedic Handbook of Biomaterials and Bioengineering: Materials/Applications*, New York, 1995, 1015–1054.
57. D. Garlotta, *J. Polym. Environ.*, 2000, **9**, 63-84.
58. P. Menei, V. Daniel, C. Montero-Menei, M. Brouillard, A. Pouplard-Barthelaix and J. P. Benoit, *Biomaterials*, 1993, **14**, 470–478.
59. S. Kamei, Y. Inoue, H. Okada, M. Yamada, Y. Ogawa and H. Toguchi, *Biomaterials*, 1992, **13**, 953-958.
60. S. Siegel, J. Kahn, K. Metzger, K. Winey, K. Werner and N. Dan, *Eur. J. Pharm. Biopharm.*, 2006, **64**, 287-293.
61. J. M. Schakenraad, M. J. Hardonk, J. Feijen, I. Molenaar and P. Nieuwenhuis, *J. Biomed. Mater. Res.*, 1990, **24**, 529-545.
62. V. N. Nagavarma, K. S. Yadav Hemant, A. Ayaz, L. S. Vasudha and H. G. Shivakumar, *Asian J. Pharm. Clin. Res.*, 2012, **5**, 16-23.
63. Y. Yeo, N. Baek, and K. Park, *Biotechnol. Bioprocess Eng.*, 2001, **6**, 213-230.
64. P. O'Donnell and J. McGinity, *Adv. Drug Deliv. Rev.*, 1997, **28**, 25-42.
65. H. Tamber, P. Johansen, H. Merkle and B. Gander, *Adv. Drug Deliv. Rev.*, 2005, **57**, 357-376.
66. D. Maurice, *J. Ocul. Pharmacol. Ther.*, 2001, **17**, 393-401.
67. Y. Tabata and Y. Ikada, *Adv. Polym. Sci.*, 1990, **94**, 107-141.
68. G. Spenlehauer, M. Vert, J. Benoit and A. Boddaert, *Biomaterials*, 1989, **10**, 557-563.

69. M. Sam, D. Gayathri, V. Prasanth and B. Vinod, *Journal of Pharmacy Research*, 2010, **3**, 1172-1177.
70. R. J. Hunter, *Zeta Potential In Colloid Science: Principles And Applications*. Academic Press, UK, 1988.
71. A. William and S. Ebnesesajjad, *Handbook of Biopolymers and Biodegradable Plastics: Properties, Processing and Applications*, Oxford, 2013.
72. W. Yu and H. Xie, *J. Nano. Mater.*, 2012, DOI: 10.1155/2012/435873.
73. J. Sunness, N. Bressler, Y. Tian, J. Alexander and C. Applegate, *Invest. Ophthalmol. Vis. Sci.*, 1999, **40**, 1761-1769.
74. M. Fleckenstien, P. Charbel, H. Helb, S. Schmitz-Valckenberg, R. Finger, H. Scholl, K. Loeffler and F. Holz, *Invest. Ophthalmol. Vis. Sci.*, 2008, **49**, 4137-4144.
75. R. Simita, *J. Electronmicros.*, 1961, **10**, 111-118.
76. M. Ugarte, A. A. Hussain and J. Marshall, *Br. J. Ophthalmol*., 2006, **90**, 621–626.
77. C. A. Curcio, M. Johnson, S. J. Ryan, A. P. Schachat, C. P. Wilkinson, D. R. Hinton, S. Sadda, and P. Wiedemann, *Retina*, Elsevier, China, 5th edition, 2013, 465-481.
78. R. S. Ramrattan, T. L. van der Schaft, C. M. Mooy, W. C. de Bruijn, P. G. Mulder and P. T. de Jong, *Invest. Ophthalmol. Vis. Sci.*, 1994, **35**, 2857-2864.
79. Y. Yamada, K. Ishibashi, I. A. Bhutto, J. Tian, G. A. Lutty and J. T. Handa, *Exp. Eye Res.*, 2006, **82**, 840-848.
80. A. Bird and J. Marshall, *Trans. Ophthalmol. Soc.*, 1986, **105**, 674-682.
81. W. S. Karwatowski, T. E. Jeffries, V. C. Duance, J. Albon, A. J. Bailey and D. L. Easty, *Br. J. Ophthalmol*, 1995, **79**, 944-952.
82. J. W. Crabb, M. Miyagi, X. Gu, K. Shadrach, K. A. West, H. Sakaguchi, M. Kamei, A. Hasan, L. Yan, M. E. Rayborn, R. G. Salomon and J. G. Hollyfield, *Proc. Natl. Acad. Sci*., 2002, **99**, 14682-14687.
83. R. Fisher, *Eye*, 1987, **1**, 184-189.
84. N. Barzegar-Befroei, T. Peto, A. Bergen and I. Lengyel, *Retinal Physician*, 2012, **1**, 1-9.
85. R. F. Spaide, D. Armstrong and R. Browne, *Retina*, 2003, **23**, 595-614.

86. P. Turowski, P. Adamson, J. Sathia, J. J. Zhang, S. E. Moss, G. W. Aylward, M. J. Hayes, N. Kanuga and J. Greenwood, *Invest. Ophthalmol. Vis. Sci.*, 2004, **45**, 2786-2794.
87. B. P. Chan and K. W. Leong, *Eur. Spine J*., 2008, **17**, 467-479.
88. R. Langer and J. P. Vacanti, *Science*, 1993, **260,** 920–926.
89. L. L. Hench, *J. Am. Ceram. Soc*., 1998, **81**, 1705-1728.
90. A. M. Ambrosio, J. S. Sahota, Y. Khan and C. T. Laurencin, *J. Biomed. Mater. Res.*, 2001, **58**, 295-301.
91. F. O'Brien, *Materials Today*, 2011, **14**, 88-95.
92. B. D. Ratner, A. S. Hoffman, F. J. Schoen and J. E. Lemons, *Biomaterials Science—An Introduction to Materials in Medicine*, Elsevier Academic Press, San Diego, 2004, 127–136.
93. P. Gunatillake, R. Mayadunne and R. Adhikari, *Biotechnol. Annu. Rev*., 2006, **12**, 301–347.
94. B. D. Boyan, T. W. Hummert, D. D. Dean, and Z. Schwartz, *Biomaterials*, 1996, **17**, 137–146.
95. K. S. Midwood, L. V. Williams and J. E. Schwarzbauer, *Int. J. Biochem. Cell B.*, 2004, **36**, 1031–1037.
96. K. Nishida, M. Yamato, Y. Hayashida, K. Watanabe, K. Yamamoto, E. Adachi, S. Nagai, A. Kikuchi, N. Maeda, H. Watanabe, T. Okano and Y. Tano, *N. Engl. J. Med*, 2004, **351**, 1187–1196.
97. M. Cabodi, N. W. Choi, J. P. Gleghorn, C. S. D. Lee, L. J. Bonassar and A. D. Stroock, *J. Am. Chem. Soc.*, 2005, **127**, 13788–13789.
98. R. Zhang and P. X. Ma, *J. Biomed. Mater. Res.*, 1999, **45**, 285–293.
99. S. R. Bhattarai, N. Bhattarai, H. K. Yi, P. H. Hwang, D. I. Cha, and H. Y. Kim, *Biomaterials*, 2004, **25**, 2595–2602.
100. H. A. Thomson, A. J. Treharne, L. S. Backholer, F. Cuda, M. C. Grossel, and A. J. Lotery, *J. Biomed. Mater. Res. A,* 2010, **95**, 1233-1243.
101. B. Dhandayuthapani, Y. Yoshida, T. Maekawa and D. S. Kumar, *Int. J. Poly. Sci.*, 2011, DOI:10.1155/2011/290602.
102. S. Binder, *Br. J. Ophthalmol.*, 2011, **95**, 441-442.
103. G. I. Taylor, *Proc. R. Soc.*, 1969, **313**, 453–475.

104. Z. M. Huang, Y. Z. Zhang, M. Kotaki and S. Ramakrishna, *Compos. Sci. Technol*., 2003, **63**, 2223–2253.
105. G. Eda and S. Shivkumar, *J. Appl. Polym. Sci.*, 2007, **106**, 475–487.
106. A. Koski, K. Yim and S. Shivkumar, *Mater. Lett.*, 2004, **58**, 493–497.
107. Q. Yang, Z. Li, Y. Hong, Y. Zhao, S. Qiu, C. Wang and Y. Wei, *J. Polym. Sci. Part B Polym. Phys.*, 2004, **42**, 3721–3726.
108. D. A. Shimko and E. A. Nauman, *J. Biomed. Mater. Res. B Appl. Biomater.*, 2007, **80**, 360-369.
109. Z. Li and C. Wang, *SpringerBriefs in Materials*, 2013, DOI: 10.1007/978-3-642-36427-3_2.
110. C. Zhang, X. Yuan, L. Wu, Y. Han and J. Sheng, *Eur. Polym. J.*, 2005, **41**, 423–432.
111. X. Yuan, Y. Zhang, C. Dong and J. Sheng, *Polym. Int.*, 2004, **53**, 1704–1710.
112. M. M. Demir, I. Yilgor, E. Yilgor and B. Erman, *Polymer*, 2002, **43**, 3303–3309.
113. M. Tomita, E. Lavik, H. Klassen, T. Zahir, R. Langer and M. J. Young, *Stem Cells*, 2005, **23**, 1579–1588.
114. A. T. Christiansen, S. L. Tao, M. Smith, G. E. Wnek, J. U. Prause, M. J. Young, H. Klassen, H. J. Kaplan, M. la Cour and J. F. Kiilgaard, *Stem Cells Int.*, 2012, DOI:10.1155/2012/454295.
115. A. J. Treharne, H. J. Thomson, M. C. Grossel and A. J. Lotery, *J. Biomed. Mater. Res.*, 2012, **100**, 2358-2364.
116. N. Ashammakhi, A. Ndreu, A. M. Piras, L. Nikkola, T. Sindelar, H. Ylikauppila, A. Harlin, M. E. Gomes, N. M. Neves, E. Chiellini, F. Chiellini, V. Hasirci, H. Redl and R. L. Reis, *J. Nanosci. Nanotechnol.*, 2006, **6**, 2693-2711.
117. Z. Liu, N. Yu, F. G. Holz, F. Yang and B. V. Stanzel, *Biomaterials*, 2014, **35**, 2837-2850.
118. K. Sreejalekshimi and P. Nair, *J. Biomed. Mater. Res. A,* 2011, **96**, 477-491.
119. W. P. Daley, S. B. Peters and M. Larsen, *J. Cell. Sci.*, 2008, **121**, 255-264.
120. E. S. Place, N. D. Evans and M. M. Stevens, *Nature Materials*, 2009, **8**, 457-470.

121. X. Niu, Y. Wang, Y. Luo, J. Xin and Y. Li, *J. Mater. Sci. Technol.*, 2005, **21**, 571-576.
122. M. J. Cooke, S. R. Phillips, D. S. H. Shah, D. Athey, J. H. Lakey and S. A. Przyborsk, *Cytotechnology*, 2008, **56**, 71–79.
123. H. K. Kleinman, L. Luckenbill-Edds, F. W. Cannon and G. C. Sephel, *Anal. Biochem.*, 1987, **166**, 1–13.
124. B. Lu, M. R. Smyth and R. O'Kennedy, *Analyst*, 1996, **121**, 29–32.
125. M. Pierschbacher and E. Ruoslahti, *Nature*, 1984, **81**, 5985-5988.
126. P. A. Underwood, F. A. Bennett, A. Kirkpatrick, P. A. Bean and B. A Moss, *Biochem. J.*, 1995, **308**, 765-771.
127. W. Comisar, N. Kazmers, D. Mooney and J. Linderman, *Biomaterials*, 2007, **26**, 4409-4417.
128. J. Yewdell and J. Bennink, *Curr. Opin. Immunol*., 2001, **13**, 13-18.
129. K. Tashiro, G. Sephel, B. Weeks, M. Sasaki, G. Martin, H. Kleinman and Y. Yamada, *J. Biol. Chem*., 1989, **264**, 1671-1682.
130. H. Fittkau, P. Zilla, D. Bezuidenhout, M.P Lutolf, P. Human, J. A. Hubbell and N. Davies, *Biomaterials*, 2005, **26**, 167-174.
131. F. Danhier, B. Vroman, N. Lecouturier, N. Crokart, V. Pourcelle, H. Freichels, C. Jérôme, J. Marchand-Brynaert, O. Feron and V. Préa, *J. Controlled Release*, 2009, **140**, 166–173.
132. L. Perlin, S. Macneil and S. Rimmer, *Soft Matter*, 2008, **4**, 2331-2349.
133. A. Ripka and D. Rich, *Curr. Opin. Chem. Biol.*, 1998, **2**, 441-452.
134. J. Beer and K. Springer, B. Coller, *Blood*, 1992, **79**, 117-128.
135. U. Hersel, C. Dahmen and H. Kessler, *Biomaterials*, 2003, **24**, 4385-4415.
136. R. S. Bohacek and C. McMartin, *Curr. Opin. Chem. Biol*., 1997, **1**, 157-161.
137. W. H. Miller, R. M. Keenan, R. N. Willette and M. W. Lark, *Drug Discovery Today*, 2000, **5**, 397-408.
138. J. Xiong, T. Stehle, R. Zhang, A. Joachimiak, M. Frech, S. L. Goodman and M. Arnaout, *Science*, 2002, **296**, 151-155.
139. P. Banerjee, C. Brunce and D. G. Chatenis, *Trails*, 2013, **147**, 358-366.
140. N. K. Varde and D. W. Pack, *Expert Opin. Biol. Ther.*, 2004, **4**, 35-51.
141. R. Jalil and J. R. Nixon, *J. Microencap*., 1990, **7**, 297-325.
142. M. Chauba, *Drug Delivery Technology*, 2002, **2**, 34-36.

143. L. S. Nair and C. T. Laurencin, *Prog. Polym. Sci.*, 2007, **32**, 762-798.
144. J. M. Anderson and M. S. Shive, *Adv. Drug Deliv. Rev.*, 2012, **64**, 72-82.
145. J. L. Cleland, E. T. Duenas, A. Park, A. Daugherty, J. Kahn, J. Kowalski and A. Cuthbertson, *J. Controlled Release*, 2001, **72**, 13-24.
146. R. Robinson, J. P. Bertram, J. L. Reiter and E. B. Lavik, *J. Microencapsulation*, 2010, **27**, 263-271.
147. S. Brunauer, P. H. Emmett and E. Teller, *J. Am. Chem. Soc*., 1938, **60**, 309-319.
148. S. Jung Liu, C. Hsueh, S. W. Ueng, S. Su Lin and J. Chen, *Asia Pac. J. Chem. Eng*., 2009, **4**, 154-160.
149. I. O. Smith, X. H. Liu, L. A. Smith and P. X. Ma, *WIREs Nanomed. Nanobiotechnol*., 2009, **1**, 226-236.
150. A. Treharne, PhD Thesis, University of Southampton, 2012.
151. A. R. Zehbe, M. Kazubek, K. Grzeschik, N. Sternberg, H. Bäumler, H. Schubert, M. Sittinger and J. Ringe, *Acta Biomater.*, 2011, **7**, 1485–1495.
152. A. M. Sophocleous, Y. Zhang and S. P. Schwendeman, *J. Control Release*, 2009, **137**, 179-184.
153. D. Klose, F. Siepmann, K. Elkharraz, S. Krenzlin and J. Siepmann, *Int. J. Pharm*., 2006, **314**, 198-206.
154. A. Brunner, K. Mäder and A. Gopferich, *Pharm. Res*., 1999, **16**, 847-853.
155. J. Siepmann, K. Elkharraz, F. Siepmann and D. Klose, *Biomacromolecules*, 2005, **6**, 2312-2319.
156. R. Herrero-Vanrell and M. F. Refojo, *Adv. Drug Deliv. Rev.*, 2001, **52**, 5-16.
157. H. C. Kang, J. E. Lee and Y. H. Bae, *J. Control Release*, 2012, **28**, 440-450.
158. S. M. Kelly, T. J. Jess and N. C. Price, *Biochim. Biophys. Acta*, 2005, **1751**, 119-139.
159. Y. Zhu, Z. W. Mao, H. Y. Shi and C. Y. Gao, *Sci. China Chem*, 2012, **55**, 2419-2427.
160. H. Schlaad and R. Hoogenboom, *Macromol. Rapid Commun*., 2012, **33**, 1595-1599.
161. S. Zargham, S. Bazgir, A. Tavakoli, A. S. Rashidi and R. Damerchely, *J. Eng. Fiber. Fabr.*, 2012, **7**, 42-49.

162. R. Hoogenboom, H. M. Thijs, M. J. Jochems, B. M. van Lankvelt, M. W. Fijten and U. S. Schubert, *Chem. Commun.*, 2008, **44**, 5758-5760.
163. R. Hoogenboom, *Angew. Chem. Int. Ed.*, 2009, **48**, 7978-7994.
164. C. Diab, Y. Akiyama, K. Kataoka and F. M. Winnik, *Macromolecules*, 2004, **37**, 2556-2562.
165. M.C. Woodle, C. M. Engbers and S. Zalipsky, *Bioconjugate Chem*., 1994, **5**, 493-496.
166. M. Bauer, C. Lautenschlaeger, K. Kempe, L. Tauhardt, U. S. Schubert and D. Fischer, *Macromol. Biosci*., 2012, **12**, 986-998.
167. W. Bartlett, J. A. Skinner, C. R. Gooding, R. W. J. Carrington, A. M. Flanagan, T. W. R. Briggs and G. Bentley, *J. Bone Joint Surg. Br*., 2005, **5**, 640-645.
168. J. Kopeček, *J. Polym. Sci. A Polym. Chem.*, 2009, **47**, 5929-5946.
169. D. W. Pitt, A. J. Treharne, H. A. Thomson, J. A. Scott, A. J. Lotery and M. C. Grossel, *J. Mater. Chem. B*, 2013, **1**, 6627-6633.
170. S-K. Min, H. K. Kang, D. H. Jang, S. Y. Jung, O. B. Kim, B-M. Min and I-S. Yeo, *Biomed. Res. Int.*, 2013, DOI: 10.1155/2013/638348.
171. R. Vasita and D. Katti, *Int. J. Nanomedicine*, 2006, **1**, 15-30.
172. P. Situ, T. L. Simpson, L. W. Jones and D. Fonn, *Invest. Ophthalmol. Vis. Sci.*, 2010, **51**, 6111-6117.
173. S. Ji, Z. Zhu, T. R. Hoye and C. W. Macosko, *Macromol. Chem. Phys*., 2009, **210**, 823–831.
174. N. T. K. Thanha and L. A. W. Green, *Nano Today*, 2010, **5**, 213-230.
175. C. Wang, Y. Gong, Y. Lin, J. Shen and D. A. Wang, *Acta Biomater.*, 2008, **4**, 1226–1234.
176. L. Lu, M. J. Yaszemski and A. G. Mikos, *Biomaterials*, 2001, **22**, 3345–3355.
177. A. E. Hudson, N. Carmean and J. A. Bassuk, *Tissue Eng.*, 2007, **9**, 2219-2225.
178. R. Karki, P. Thapa, M. J. Kang, T. C. Jeong, J. M. Nam, H-L. Kim, Y. Na, W-J. Cho, Y. Kwon and E-S Lee, *Bioorg. Med. Chem.*, 2010, **18**, 3066–3077.
179. D. Batovska, S. Parushev, A. Slavova, V. Bankova, I. Tsvetkova, M. Ninova and H. Najdenski, *Eur. J. Med. Chem.*, 2007, **42**, 87–92.

180. A. Stroba, F. Schaeffer, V. Hindie, L. Lopez-Garcia, I. Adrian, W. FroÃàhner, R. W. Hartmann, R. M. Biondi and M. Engel, *J. Med. Chem.*, 2009, **52**, 4683-4693.
181. J. Mason, *Future Med. Chem.*, 2010, **2**, 1813–1822.
182. S. Biltresse, M. Attolini, G. Dive, A. Cordi, G. Tucker and A. Marchand-Brynaert, *Bioorg. Med. Chem*., 2004, **12**, 5379-5393.
183. O. Cavalleri, G. Gonella, S. Terreni, M. Vignolo, P. Pelori, L. Floreano, A. Morgante, M. Canepa and R. Rolandi, *J. Phys. Condens. Matter.*, 2004, DOI: 10.1088/0953-8984/16/26/021.
184. J. Marchand-Brynaert , E. Detrait, O. Noiset, T. Boxus, Y-J. Schneider and C. Remacle, *Biomaterials*, 1999, **20**, 1773-1782.
185. Y. Qian, H. J. Zhang, P. C. Lv and H. L. Zhu, *Bioorganic & Medicinal Chemistry*, 2010, **18**, 8218-8225.
186. M. Cabrera, M. Simoens, G. Falchi, M. L. Lavaggi, O. E. Piro, E. E. Castellano, A. Vidal, A. Azqueta, A. Monge, A. L. de Cerain, G. Sagrera, G. Seoane, H. Cerecetto and M. Gonzalez, *Bioorg. Med. Chem*., 2007, **15**, 3356-336.
187. US pat., US4757079 A1, 1988.
188. R. B. Basani, G. D'Andrea, N. Mitra, G. Vilaire, M. Richberg, M. A. Kowalska, J. S. Bennett and M. Poncz, *J. Biol. Chem*, 2001, **276**, 13975-13981.
189. D.M. Haverstick, J. F. Cowan, K.M. Yamada and S.A. Santoro, *Blood*, 1985, **66**, 946-952.
190. Sigma-Aldrich, Product Information Sheet, Retrieved from URL www.sigmaaldrich.com/content/dam/sigma.../f7250pis.
191. S. Noel, B. Liberelle, L. Robitaille and G. De Crescenzo, *Bioconjug. Chem.*, 2011, **22**, 1690-1699.
192. J. S. Koo, M. C. Grossel, M. J. Whitcombe, P. G. R. Smith and R. B. Williams, *Chem. Mater.*, 2002, **14**, 5030-5036.
193. E. Malmström, R. D. Miller and C. J. Hawker, *Tetrahedron*, 1997, **53**, 15225-15236.
194. M. Pozo, R. Pulido and V. Gotor, *Tetrahedron*, 1992, **48**, 6477-6484.
195. K. Ishihara, K. Moriyama, K. Kamiya and M. Hatano, *Org. Lett.*, 2011, **13**,

430-433.

196. I. Zlatev, F. Giraut, A. Morvan, P. Herdewijn and J. Vasseur, *Bioorg. Med. Chem.,* 2009, **17**, 7008-7014.
197. A. Fisher, MRes Thesis, University of Southampton, 2011.
198. W. Eschweiler, *Berichte der deutschen chemischen Gesellschaft*, 1905, **38**, 880–882.
199. H. T. Clarke, H. B. Gillespie and S. Z. Weisshaus, *J. Am. Chem. Soc*., 1933, **55**, 4571–4587.
200. Merk Index. 14th ed. Merck, Whitehouse Station, NJ, 2007